

BIOFABRICATION OF IMPLANTS FOR ARTICULAR JOINT REPAIR

Cartilage regeneration in reinforced gelatin-based hydrogels

Jetze Visser

2015

Promotor

Prof. dr. W.J.A. Dhert

Copromotoren

Dr. ir. J. Malda

Dr. ir. D. Gawlitta

Biofabrication of implants for articular joint repair: Cartilage regeneration in reinforced gelatin-based hydrogels

Jetze Visser

PhD thesis, Utrecht University, University Medical Center Utrecht, Utrecht, the Netherlands

Copyright © J. Visser 2015. All rights reserved. No parts of this thesis may be reproduced, stored in a retrieval system of any nature or transmitted in any form or by any means, without prior written consent of the author. The copyright of the articles that have been published has been transferred to the respective journals.

Financial support for the printing of this thesis was generously provided by: De Nederlandse Orthopaedische Vereniging, the Dutch society for Biomaterials and Tissue Engineering, Anna Fonds te Leiden, Livit Orthopedie MRI Centrum and Chipsoft.

The research in this thesis was financially supported by: the Netherlands Institute for Regenerative Medicine, the European Community's Seventh Framework Programme (FP7/2007-2013) under grant agreement n309962 (HydroZONES) and the Dutch Arthritis Foundation.

ISBN 978-94-6169-706-6

Layout and printing: Optima Grafische Communicatie, Rotterdam, the Netherlands

Cover design: Marco Bot

Biofabrication of implants for articular joint repair
Cartilage regeneration in reinforced gelatin-based hydrogels

Bioprinten van implantaten voor het herstel van gewrichtsschade
Kraakbeenregeneratie in versterkte gelatine hydrogel

(met een samenvatting in het Nederlands)

Proefschrift

ter verkrijging van de graad van doctor aan de Universiteit Utrecht
op gezag van de rector magnificus, prof. dr. G.J. van der Zwaan,
ingevolge het besluit van het college voor promoties
in het openbaar te verdedigen op dinsdag 25 augustus 2015 des avonds te 6.00 uur

door

Jetze Visser
geboren op 6 januari 1985 te Gaasterland

THIS THESIS IS BASED UPON THE FOLLOWING PUBLICATIONS:

Reinforcement of hydrogels using three-dimensionally printed microfibrils.

Visser J, Melchels FPW, Jeon JE, van Bussel EM, Kimpton LS, Byrne HM, Dhert WJA, Dalton PD, Hutmacher DW, Malda J.

Nature Communications. 2015;6:6933 doi: 10.1038/ncomms7933

Crosslinkable Hydrogels derived from Cartilage, Meniscus and Tendon Tissue.

Visser J, Levett PA, Te Moller NC, Besems J, Boere KW, Van Rijen MH, de Grauw JC, Dhert WJA, van Weeren PR, Malda J.

Tissue Engineering Part A. 2015 Apr;21(7-8):1195-206

Endochondral bone formation in gelatin methacrylamide hydrogel with embedded cartilage-derived matrix particles.

Visser J, Gawlitta D, Benders KE, Toma SM, Pouran B, van Weeren PR, Dhert WJA, Malda J.

Biomaterials. 2015 Jan;37:174-182

Biofabrication of tissue constructs by 3D bioprinting of cell-laden microcarriers.

Levato R, Visser J, Planell JA, Engel E, Malda J, Mateos-Timoneda MA.

Biofabrication. 2014 Sep;6(3):035020

Covalent attachment of a three-dimensionally printed thermoplast to a gelatin hydrogel for mechanically enhanced cartilage constructs.

Boere KW*, Visser J*, Seyednejad H, Rahimian S, Gawlitta D, van Steenberghe MJ, Dhert WJA, Hennink WE, Vermonden T, Malda J.

Acta Biomaterialia. 2014 Jun;10(6):2602-11

*Authors contributed equally to this manuscript

Weefsel uit de printer: de mogelijkheden van 3D-printen in de geneeskunde.

Visser J, Melchels FP, Dhert WJ, Malda J.

Nederlands Tijdschrift voor Geneeskunde. 2013;157(52):A7043

Engineering hydrogels for biofabrication.

Malda J, Visser J, Melchels FP, Jüngst T, Hennink WE, Dhert WJA, Groll J, Hutmacher DW.

Advanced Materials. 2013 Sep;25(36):5011-28

Biofabrication of multi-material anatomically shaped tissue constructs.

Visser J, Peters B, Burger TJ, Boomstra J, Dhert WJ, Melchels FP, Malda J.

Biofabrication. 2013 Sep;5(3):035007

TABLE OF CONTENTS

	Introduction	
Chapter 1	General introduction, outline and research questions	9
Chapter 2	Engineering hydrogels for biofabrication	27
Part I	Biological improvement of GelMA hydrogel with tissue-derived matrices	
Chapter 3	Crosslinkable hydrogels derived from cartilage, meniscus and tendon tissue	61
Chapter 4	Endochondral bone formation in gelatin methacrylamide hydrogel with embedded cartilage-derived matrix particles	81
Part II	Mechanical improvement of GelMA hydrogel constructs with 3D-printed scaffolds	
Chapter 5	Covalent attachment of a three-dimensionally printed thermoplast to a gelatin hydrogel for mechanically enhanced cartilage constructs	103
Chapter 6	Reinforcement of hydrogels with three-dimensionally printed microfibres	127
Chapter 7	<i>Preliminary results of a translational animal model</i> Cartilage repair with a combination of chondrons and MSCs in gelatin methacrylamide hydrogel: the establishment of an equine model	153
Part III	Biofabrication of complex shaped constructs from GelMA for osteochondral tissue repair	
Chapter 8	Biofabrication of multi-material anatomically shaped tissue constructs	171
Chapter 9	Biofabrication of tissue constructs by 3D bioprinting of cell-laden microcarriers	187
Chapter 10	<i>Preliminary results of a translational animal model</i> Biofabrication of anatomically shaped implants for regeneration of the rabbit humeral head	207
	Discussion and summary	
Chapter 11	General discussion and future perspectives	221
	References	237
	List of abbreviations	265
	Summary and answers to the research questions	271
	Nederlandse samenvatting	281
	Papers not included in this thesis	289
	Acknowledgements/Dankwoord	291
	Curriculum Vitae	295

Chapter 1

General Introduction, Outline and Research Questions

This introduction was partially based on the following publication:

Visser J, Melchels FP, Dhert WJ, Malda J. Weefsel uit de printer: de mogelijkheden van 3D-printen in de geneeskunde. [Tissue printing: the potential application of 3D printing in medicine]. *Nederlands Tijdschrift voor Geneeskunde*. 2013;157(52):A7043.

INTRODUCTION

Regenerative medicine

The acute or chronic degeneration of tissues in the human body can be regarded as the fundamental cause for morbidity and mortality¹. All tissues degenerate over time, only some regenerate (heal) better than others. For example, a small skin laceration or stable bone fracture is likely to heal spontaneously. In contrast, heart and brain tissue have poor regenerative capacities, which becomes clinically evident by organ failure after hypoxia^{2,3}. Cartilage is another tissue with very limited healing capacities, as no nerves and blood vessels are present to initiate regeneration⁴. Therefore, cartilage defects can occur already in young patients, usually as a result of acute degeneration^{5,6}. Chronic degeneration of cartilage is a common problem in middle-aged and older patients: a disease known as osteoarthritis⁷.

The field of regenerative medicine aims to assist the body to restore the function of an injured tissue. Traditionally, the development of regenerative therapies relies on the engineering of tissues by a combination of cells, growth factors and biomaterials^{8,9}. Based on these principles, the first regenerative therapies for the repair of focal cartilage defects have already been implemented in health care⁶.

Multiple disciplines contribute to further development of regenerative medicine. Advances in stem cell research offer increasing knowledge on the differentiation of multipotent mesenchymal stromal cells (MSCs) as the cellular component of regenerative therapies¹⁰. In addition, advances in the field of biomaterials and bioengineering have yielded materials and techniques to potentially create implants with biological and mechanical compatibility for the regeneration of tissues^{11,12}.

This chapter is an introduction to cartilage tissue, its acute and chronic degeneration and the current options and challenges in treatment. Next, biofabrication is introduced as a tool for the engineering of implants in regenerative medicine. This chapter concludes with research questions that focus on the biofabrication of implants for articular joint repair.

Articular cartilage tissue

In every articulating joint, the long bones are covered by a layer of cartilage that provides smooth articulation and shock absorption. Cartilage is avascular and aneural, and separated from the underlying bone by a calcified cartilage zone and a tidemark layer¹³. Therefore, nutrition of the cartilage tissue predominantly depends on the synovial fluid. The unique mechanical properties of cartilage can be ascribed to its specific extracellular matrix (ECM) composition, being water (70%), within a network of collagen type II and proteoglycans¹³. Chondrocytes are the only residing cells. A superficial, transitional

and bottom zone can be identified in cartilage, based on its ECM composition, collagen alignment and chondrocyte subtype¹⁴.

For example, collagen type II fibers form an organized matrix with an arching alignment, resulting in fibers perpendicular to the articulating surface in the bottom layer and parallel to the surface in the superficial layer (Fig. 1)¹⁵. The superficial collagen fibers provide the highest stiffness and tensile strength, which gradually decreases in the transitional and bottom layer¹⁴. The compressive strength of cartilage tissue is mainly provided by the fluid pressurization of the proteoglycan matrix¹⁶. Proteoglycans are large proteins with attached glycosaminoglycans (GAGs), which surround the collagen matrix. As GAGs are negatively charged, they attract positive ions, which in turn resorb and retain water in the cartilage tissue¹³. This osmotic pressure mechanism puts the collagen fibers under tension, and causes cartilage to have a high resilience to axial compression. The combined network of collagens and proteoglycans thus results in a stiff, yet elastic tissue. These properties are essential for resisting both shear and compressive stresses that are regularly applied to the cartilage during the load-bearing movement of joints.

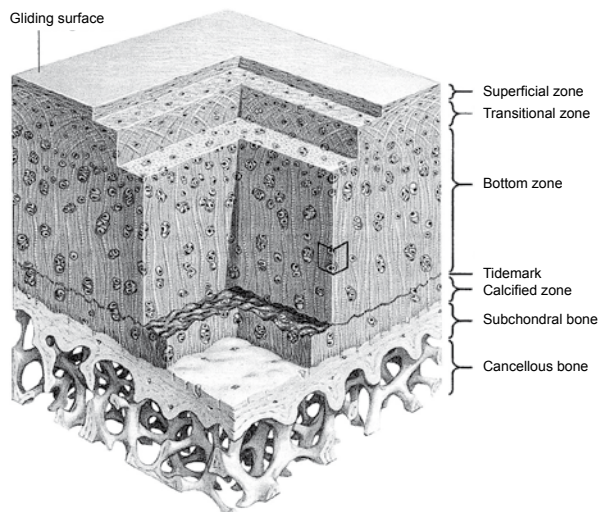


Figure 1. The structure of articular cartilage. Collagen fibers are oriented parallel to the articular surface in the superficial zone, and perpendicular to the surface in the bottom zone. The cartilage is separated from the underlying bone by a tidemark and the calcified cartilage. Image was adapted from James et al.⁸⁴

Cartilage defects

Pathology

Focal cartilage defects are often seen in adults^{5,6}. Partial thickness cartilage defects heal poorly⁴, whereas full-thickness cartilage defects that disrupt the subchondral plate will trigger a healing response by the bone marrow¹⁷. Cells invade the defect in a hematoma and will typically produce a “scar tissue” that consists of predominantly collagen type I¹⁸. This fibrocartilage has inferior resilience, stiffness and wear resistance compared to hyaline cartilage that was originally produced by chondrocytes¹⁷. Focal cartilage defects can predispose for the development of osteoarthritis by the inferior quality of the repair tissue, along with the catabolic effects that are triggered^{6,17}. Cartilage defects (non-healed or fibrocartilaginous tissue) can result in pain and swelling of the joint and hence decreased mobility. Moreover, it was found that full-thickness defects in the knee give an equal reduction in quality of life compared to osteoarthritis¹⁹. Thus, the focal cartilage defect can be symptomatic and predispose to further cartilage degeneration.

Treatment

The treatment of cartilage defects historically relies on debridement and microfracture of the subchondral plate in order to allow cells from the bone marrow to invade the defect¹⁷. As these therapies resulted in a fibrocartilaginous fill of the defect, regenerative cell-based therapies for cartilage repair started in the '90s⁶. In the first generation of autologous chondrocyte implantation (ACI), expanded chondrocytes were placed in the cartilage defect and covered with a periosteal flap. Patients with a 2-year follow up after this first-generation ACI showed good results when femoral condyle lesions were repaired²⁰. In a later technique, a synthetic collagen sheet was used to cover the implanted cells. In the third generation ACI, the cells were cultured in a porous collagen matrix, which was subsequently implanted in the defect. The introduction of this cell/biomaterial unit omitted the need for a sutured cover flap and allowed for arthroscopic delivery^{21,22}.

The focus for the next generation of cell therapy for cartilage repair is three-fold:

- 1) The use of alternative and selected cell sources, such as a co-culture of chondrocytes and MSCs^{23,24}. In this specific procedure, chondrons – chondrocytes with their pericellular matrix intact – or chondrocytes are harvested from the cartilage defect site and reimplanted in a co-culture with allogeneic MSCs. With this combination of cell types, chondrocytes do not need to be expanded before implantation, allowing a one-stage procedure²⁵. Alternatively, cell-free scaffolds could be implanted in a single surgical session, which will have large practical and regulatory advantages over cell products. Unfortunately, their efficacy in cartilage repair has not been proven yet⁹.

2) The development of strong, stiff and instructive biomaterials for the delivery of cells. Biomaterials serve as a scaffold for the cells and usually consist of hydrated polymer networks, known as hydrogels. Fibrin glue is currently used as a cell delivery vehicle, because of its availability in clinical grade and surgical applicability^{6,9}. However, fibrin glue was not designed for application in regenerative medicine: it holds no specific biochemical cues and the crosslinked fibrin polymer network is soft and has a high degradation rate²⁶⁻²⁸. A large effort is made for development of more instructive and strong gels with a controlled degradation rate that balances with tissue regeneration^{9,29,30}.

3) Improving the surgical workflow and techniques for implantation of cells and biomaterials in the cartilage defects. Examples are a one-stage procedure by the implantation of cell-free scaffolds or allogeneic cells, and the arthroscopic delivery of cells by spraying of the hydrogel³¹.

Osteochondral defects

Pathology

Osteochondral lesions involve the cartilage and the underlying bone. The etiology is proposed to be multifactorial, including trauma, both acute and repetitive, and genetic factors^{32,33}. Osteochondral defects are often seen in young patients.

Treatment

As debridement and microfracture were found not to result in the regeneration of durable repair tissue, several replacement therapies with autografts and allografts were developed¹⁷. Another valid treatment option for large osteochondral defects is the combination of autologous bone implantation and ACI³⁴. This procedure - known as the 'sandwich technique' - is performed in two surgical sessions.

The most popular replacement technique is the transfer of autologous osteochondral grafts: a procedure usually referred to as 'mosaicplasty'^{18,35}. Plugs consisting of viable bone with hyaline cartilage are transferred into the defect from a non weight-bearing location in the joint. The surgical procedure is done in one session and patients can quickly rehabilitate. However, there is limited availability of tissue, a chance of donor site morbidity and a poor defect fill in between the transferred plugs¹⁸. Nevertheless, the short-term clinical outcomes for mosaicplasty are superior to a commercially available cell-free collagen scaffold (TruFit)³⁶. In addition to TruFit, numerous biphasic scaffolds were engineered, with distinct matrix, cells and/or growth factor compositions for the cartilage and bone component³⁵. These products have not yet successfully found their way to clinical application.

Osteoarthritis

Pathology

A quarter of people above 55 years of age suffer from frequent knee pain and half of this population has osteoarthritic features of the knee on X-ray⁷. The diagnosis in this group is symptomatic osteoarthritis. Moreover, on examination with MRI, nearly 90% of middle aged and elder people have osteoarthritic changes in the knee joint³⁷. Risk factors include obesity, occupational overloading and a previous knee injury. Osteoarthritis is a disease of the whole joint, involving the cartilage, but also the subchondral bone, the synovium, ligaments and the periarticular muscles. Inflammation that can potentially be located in all of these structures contributes to pain and further degeneration³⁸. Future therapies will specifically target the inflammation and degeneration process^{6,38}.

Treatment

Current pharmacologic therapies rely on paracetamol and nonsteroidal anti-inflammatory drugs (NSAIDs)³⁹. Operative treatments include osteotomies for alignment of the knee joint in order to unload the most affected side⁴⁰ and distraction of the joint to allow regeneration of the cartilage tissue⁴¹. Replacement of the joint with a prosthesis is the ultimate solution for end-stage osteoarthritis⁴². Arthroplasty leads to long-term improvement of the quality of life and reduction of pain, as proven in particular for the replacement of the knee⁴³ and hip joint⁴⁴.

3D printing

New printing techniques enable the production of three-dimensional objects from a digital model that can be either designed, or derived from 3D-scanning data. Because of its constructive nature, 3D printing is an additive manufacturing technique. The development was based on inkjet printing that started in the 1950s, followed by stereolithography in the '80s and fused deposition modeling (FDM) in 1990 (Fig. 2)¹¹. Nowadays, 3D printing is able to produce complex tools from plastic or metals, such as bike or car components, machine parts but also electrical elements¹². In fact, every material with a reasonable stiffness that retains its shape after deposition has a potential in 3D printing. For example, real-size houses we recently printed from concrete. This digitization of manufacturing was recently termed 'the third industrial revolution' by The Economist⁴⁵.

The exploration of the clinical potential of 3D printing has just started by generating customized objects based on CT or MRI scans of patients. Currently, the technique is clinically applied for the production of:

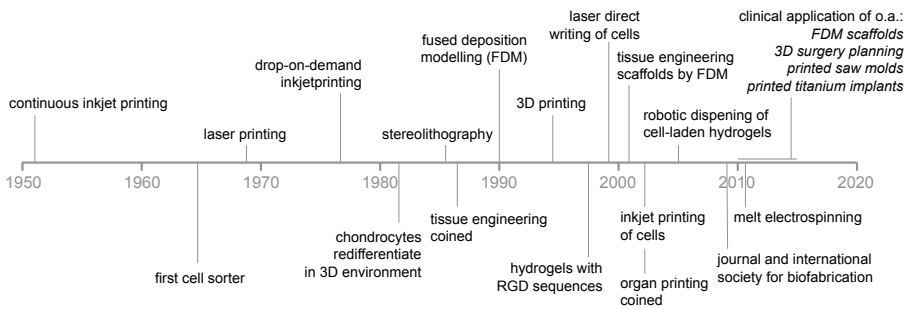


Figure 2. Chronological development of 3D printing and biofabrication. Figure adapted from Melchels et al.¹¹

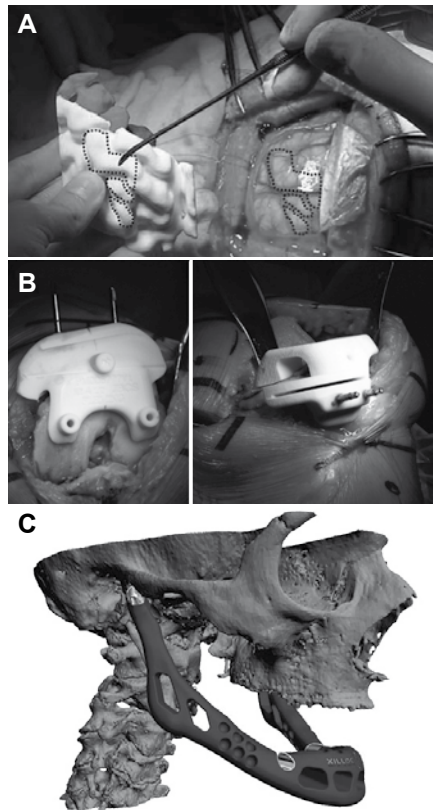


Figure 3. Clinical applications of 3D printing based on patient-specific 3D-scans. (a) Models of anatomical structures for the 3D-planning of complex surgery⁴⁷; (b) a customized saw mold for knee arthroplasty⁴⁸; (c) a laser-sintered titanium implant for replacement of the jaw (layerwise.com).

1) Models of anatomical structures for 3D-planning of complex surgery (Fig. 3a). The specific location of surgery, being the brain, heart, jaw or joint, can sometimes better be visualized with a model than on a screen^{45,46}. 3D-models are usually printed from thermoplastic polymers, and used for the preparation of a surgical procedure. Moreover, when printed from softer materials, the 3D-model can be subject of practice for surgeons. In addition, the models aid in explanation to the patient and can even visualize their facial appearance after reconstructive maxillofacial surgery^{46,47}.

2) Surgical tools, such as custom-made saw molds for knee arthroplasty⁴⁸ or a drill guide for reducing the error in the placement of pedicle screws in spine surgery (Fig. 3b).

3) Prostheses and implants, such as laser-sintered titanium implants for maxillofacial surgery⁴⁹ or for surgical reconstruction of the pelvis after tumor or trauma (Fig. 3c). Recent developments include 3D-printed casts for the external fixation of fractures.

Biodegradable thermoplastic polymer scaffolds

The 3D printing of scaffolds from biodegradable materials is often referred to as FDM, as filaments of a thermoplastic polymer are stacked and fused into a porous scaffold (Fig. 4a)⁵⁰. Polycaprolactone (PCL) is the most versatile polymer for FDM because of its physicochemical properties⁵¹. PCL is available in a clinical grade and 3D-printed scaffolds from PCL mixed with tricalcium phosphate (TCP) have been shown to guide bone regeneration in calvarial defects in rodents⁵¹ and segmental bone defects in sheep⁵². In

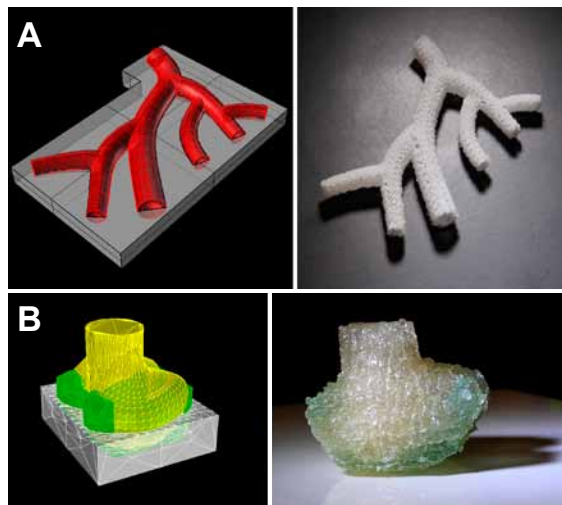


Figure 4. 3D printing in regenerative medicine. (a) Scaffolds for matrix produced by cells are fabrication by a fused deposition modeling process with thermoplastic polymers, such as polycaprolactone; (b) Inks for biofabrication are typically hydrogels, such as gelatin methacrylamide, in which cells and bioactive components can be encapsulated (left: computer design, right; printed object).

addition, a porous shoulder 'prosthesis' based on PCL was demonstrated a promising scaffold for cell infiltration and subsequent articular cartilage regeneration in a rabbit model⁵³. Melt electrospinning constitutes a new form of FDM. By establishment of an electrostatic field between the printer needle and the collecting platform, filaments with a diameter of a few micrometers can be deposited in a controlled architecture⁵⁴. These filaments have the potential to better resemble the natural fibrous ECM than the thicker, yet stronger, filaments produced with traditional FDM^{55,56}, although natural extracellular matrix polymers are within the nanometer scale.

Biofabrication

Biofabrication is the construction of well-defined biological products from raw materials, such as cells, molecules, extracellular matrices and biomaterials^{57,58}. The printing of cells started in home-transformed inkjet printers, with the advent of tissue engineering in the '90s. Today, biofabrication is a 'trending' additive manufacturing technique that is also referred to as (3D) bioprinting^{11,12}. Gartner, Inc., a leading information technology research and advisory company, located both 3D bioprinting systems and 3D printing on their hype cycle (Fig. 5). 3D Bioprinting systems was considered a young, upcoming technology, whereas consumer 3D printing was placed just over the top of the hype cycle, at the peak of inflated expectations. This hype cycle illustrates that a realistic picture of

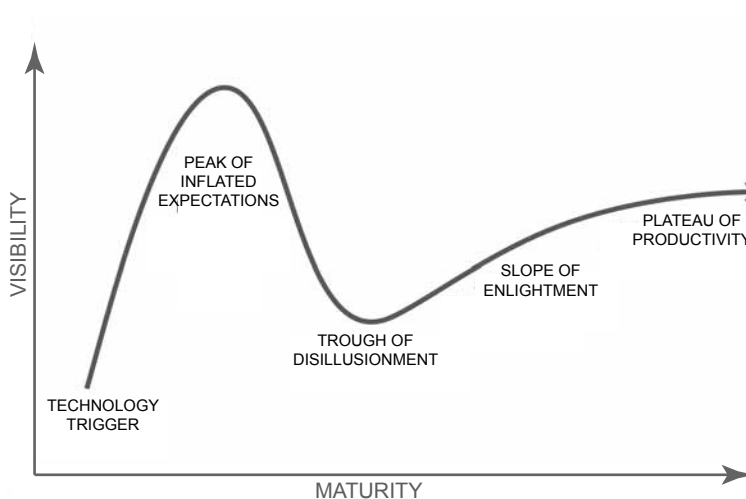


Figure 5. The generic hype cycle by Gartner Inc. 3D Bioprinting Systems was placed as a technology trigger with increasing visibility. Consumer 3D printing was located over the peak of inflated expectations. (www.gartner.com). Attribution: Gartner, generic Hype Cycle. Gartner, Hype Cycle for 3D Printing, 2014, Pete Basiliere, Michael Shanler, 21 July 2014

biofabrication should be presented to society in order to prevent inflated expectations and soften the subsequent 'trough of disillusionment'.

Materials for biofabrication are referred to as "bioinks"⁵⁹. Hydrogels are typical bioinks, as they allow the encapsulation of cells and bioactive components (Fig. 4b). Gelatin methacrylamide (GelMA) is a hydrogel that was recently developed as a versatile bioink, in terms of the biological and physical properties^{60,61}. GelMA is a natural polymer derived from collagen type I, and is enzymatically degradable⁶². The polymer concentration and the degree of methacrylation, hence crosslink density, are tunable for the engineering of specific tissues, such as cartilage^{60,63} or vascular tissue⁶⁴. In chapter 2 of this thesis, the development status of bioinks is outlined, along with its current and future applications in biofabrication. The full arsenal of biofabrication techniques and applications have been presented in recent review articles^{35,36}.

Biofabrication techniques have the potential to produce tissue-mimicking constructs, by the spatially controlled deposition of molecules, cells, matrix and biomaterials. These constructs could possibly act as tissue replacements in patients with end-stage organ failure. However, there are major challenges in the field of biofabrication for medical applications:

1) The fabrication of stiff tissue constructs with well-defined internal and external architectures. The techniques for the printing of complex objects are available, only these are focused on construction with metals and plastics. Building objects layer-by-layer from hydrogels, that are composed of circa 90% water and include viable biological components, is obviously more challenging. The current limitation in object geometry in biofabrication can be ascribed to the lack of suitable bioinks, as highlighted in chapter 2 of this thesis. In chapter 2, strategies are introduced to improve bioinks by tailoring their physicochemical properties. In addition, the reinforcement of hydrogel constructs with a stiff, printed scaffold is discussed. This reinforcement can be achieved with a multi-material printing technique that was recently developed, in order to improve the architecture and overall stiffness of printed hydrogel constructs⁶⁵.

2) The maturation of a printed construct into functional tissue. Hydrogel objects with an outer contour resembling anatomical structures such as an ear, aortic valve or kidney have been printed recently¹². Once, hypothetically, all cell types in these structures have been deposited in a desired anatomical order, the large challenge remains to have them interact and collectively exert the specific function of the target tissue or organ. A fundamental prerequisite for tissue function is the production of tissue-specific ECM within the construct. Larger constructs also require vascularization and innervation. Matrix formation and tissue function are, therefore, a major focus of tissue engineering research.

3) General challenges that come with tissue engineering, such as the selection of the most available and effective cell sources (autologous, allogeneic, stem cells or somatic

cells); a sterile and standardized workflow from the engineering stage to the bedside; the certification of custom-made tools, prostheses and advanced therapy medicinal products (ATMPs) and a reduction of the manufacturing costs.

Tissue-derived matrices

All tissues and organs consist of an organized collection of cells and ECM. The complex interaction between cells and ECM regulates the specific function of the tissue. As the field of regenerative medicine aims to restore tissue function, ECM is a scaffold material worthwhile exploring for the engineering of tissues. The architecture and the biochemical cues in the ECM could potentially guide seeded cells in the regeneration of new tissue⁶⁶. Before ECM can be used in tissue engineering, cells need to be removed from the original tissue by chemical and/or mechanical processes, to reduce its antigenicity⁶⁷. In this fashion, several tissue-derived matrices (TDM), *e.g.* derived from the heart, liver and the trachea were acquired. These TDMs were shown useful substrates for tissue regeneration in clinical proof of principle studies⁶⁸.

Preliminary research demonstrates that TDM also forms a potential scaffold biomaterial for bone and cartilage engineering⁶⁹. However, it is not known which specific growth factors and signaling molecules of the TDM are responsible for guiding cell differentiation. As a consequence, it is unclear which tissue the matrix should be derived from and which decellularization process should be applied. For example, is decellularized bone tissue the best scaffold for bone regeneration, or do cells just as well produce bone matrix on a scaffold derived from fat tissue?

There are several options to produce TDM from native tissues, *e.g.*: leaving the original tissue structure intact; molding or printing of freeze-dried, particulated TDM into a porous scaffold or enzymatically digest TDM into a collagenous hydrogel^{70,71}. The TDM can be subsequently implanted as a cell-free biomaterial, or be recellularized *in vitro* prior to implantation. A challenge in the production of TDM is to remove the resident cells from the tissues, while retaining any bioactive cues.

The most abundant polymer in TDM is collagen, as collagen is the major ECM component of most tissues. TDM gels, therefore, have physical properties similar to collagen gels, and may form an instructive cell-carrier for cartilage repair and/or biofabrication.

OUTLINE AND RESEARCH QUESTIONS

Biofabrication is a potential tool for joint repair, especially for large (osteo)chondral defects. The regenerative treatment options for large joint defects are currently limited, as biomaterials for the delivery of cells and/or bioactive factors have biological and mechanical shortcomings. For example, osteochondral defects require the repair of two

distinctive tissue types and the larger they are, the more they are exposed to mechanical forces in the joint. Here, biofabrication offers potential control over the strength and stiffness of constructs, their internal organization and external architecture.

Bioinks for the fabrication of such constructs require specific biological signals, in order to differentiate cells into the line of the target tissue. These biological signals can potentially be provided by hydrogels based on native, decellularized matrices.

The overall aim of this thesis is to deploy biofabrication techniques to improve cartilage and osteochondral tissue repair. GelMA hydrogel was selected as a cell carrier across all chapters of this thesis, because its potential for biofabrication^{60,61,72} and *in vitro* cartilage regeneration^{63,73} was yet demonstrated. Three specific aims can be identified:

- Part I) Biological improvement of GelMA hydrogel with tissue-derived matrices (Chapters 3 and 4)
- Part II) Mechanical improvement of GelMA hydrogel constructs with 3D-printed scaffolds (Chapters 5, 6 and 7)
- Part III) Biofabrication of complex shaped constructs from GelMA for osteochondral tissue repair (Chapter 8, 9 and 10)

Specific research questions to be addressed in this thesis:

Chapter 2. What is the current status of hydrogels as a bioink for biofabrication and what are the opportunities in this field?

Hydrogels with suspended biological components, such as growth factors or cells, can serve as bioinks for the fabrication of three-dimensional structures^{11,12}. However, the printability of hydrogels is usually poor, and bioinks have been insufficiently developed to simultaneously meet the biological and mechanical demands for tissue implants. This review of the literature highlights the current status of bioink development and also presents several approaches to modify bioinks and biofabrication approaches to make the next step in this field.

Part I) Biological improvement of GelMA hydrogel with tissue-derived matrices

Chapter 3. Can stable hydrogels be derived from natural tissues, such as cartilage, meniscus and tendon? Does the addition of such tissue-derived matrices to GelMA hydrogel enhance chondrogenic differentiation of chondrocytes and MSCs in vitro?

Tissue-derived matrices have been shown able to guide cell fate⁶⁸. Also, the addition of small amounts of hyaluronic acid and chondroitin sulfate to GelMA were shown to

improve differentiation of embedded chondrocytes^{63,73}. Can we further improve cellular differentiation in GelMA by the addition of cartilage, tendon and meniscus matrices, which were decellularized, but still contained limited amounts of GAGs?

Chapter 4. What is the effect of cartilage-derived matrix particles in GelMA on the differentiation of chondrocytes and MSCs? Can osteochondral tissue be regenerated in bilayered hydrogel constructs with chondrocytes and MSCs?

Scaffolds composed of cartilage-derived matrix (CDM) particles have been shown beneficial for cartilage matrix production by MSCs⁷⁴. In contrast, they seemed to trigger a counterproductive effect on seeded chondrocytes. Here, we aimed for CDM to improve the differentiation of both cell types, when suspended with the cells in GelMA hydrogel. Tissue formation in these hydrogel constructs is evaluated *in vitro* and *in vivo* in a subcutaneous rat model. In addition, bilayered hydrogel constructs consisting of a separate chondrocyte and MSC layer are implanted. These two adjacent cell types can potentially reproduce osteochondral tissue.

Part II) Mechanical improvement of GelMA hydrogel constructs with 3D-printed scaffolds

Chapter 5. Does the covalent attachment of a 3D-printed scaffold as reinforcement to GelMA gel lead to stronger constructs?

Hydrogels can serve as a temporary carrier for cells to secrete tissue-specific extracellular matrix and remodel tissue. However, hydrogels are too soft to withstand the forces acting in large weight-bearing tissue defects. Therefore, porous scaffolds fabricated from thermoplastic polymers, such as PCL, were used to reinforce hydrogels^{65,75-77}. Both materials can be printed in one session. Still, the hydrogel and PCL have a poor physical connection. In this chapter we aim to chemically modify the PCL for covalent attachment to GelMA hydrogels. In addition, we investigate if human chondrocytes suspended in the hydrogel component of such constructs produce cartilage matrix *in vitro* and *in vivo*.

*Chapter 6. Could the mechanical properties of articular cartilage be approached with composite constructs consisting of a hydrogel reinforced with 3D-printed microfibers? How do chondrocytes embedded in these constructs respond to dynamic loading in an *in vitro* bioreactor culture?*

Traditional 3D-printed scaffolds can successfully reinforce hydrogels. Because these scaffolds were constructed from thick fibers, they have a relatively large polymer mass, are stiffer than articular cartilage, and have low elasticity^{65,75,76}. In this chapter we aim to overcome these issues by reinforcing hydrogels with microfiber scaffolds that are 3D-printed with a new technique termed *melt electrospinning*⁵⁴. The differentiation of

human chondrocytes embedded in these constructs is extensively tested in response to a repetitive mechanical loading regime in a bioreactor.

Chapter 7. How can (reinforced) GelMA hydrogel be applied in an equine model for the repair of focal cartilage defects?

Cell therapies for the repair of focal cartilage defects currently rely on rapidly degrading cell carriers, such as fibrin glue^{21,23,78}. These vehicles contrast with hydrogels that have been specifically engineered for use in regenerative medicine, which have a lower degradation rate to balance with new tissue formation by embedded cells^{29,30,79}. Now GelMA has proven its role in supporting cartilage tissue formation by embedded cells *in vitro*^{60,63,73}, we here set out to translate (reinforced) GelMA to clinical application. The International Cartilage Repair Society has recognized that equine chondral defect models form a valuable pre-clinical evaluation method for cartilage repair therapies⁸⁰. This chapter describes the *in vitro* work, cadaveric and pilot studies leading to the establishment of a cartilage defect model in equine stifle joints. Furthermore, a long-term study for the evaluation of cell-carriers for cartilage repair in ponies is outlined.

Part III) Biofabrication of complex shaped constructs for osteochondral tissue repair

Chapter 8. Which support and construction materials can best be combined to establish the complex geometry of anatomical structures in a multi-material 3D printing setting?

So far, printed objects for regenerative medicine had relatively simple geometries, because of limitations in biofabrication materials and techniques. In this chapter, we set out to print more complex shapes by deposition of the construction material, such as PCL or a bioink, in one session with a temporary support material. Support materials are specifically selected to be compatible with the construction material.

Chapter 9. Can GelMA bioinks be improved for bone regeneration by the incorporation of microcarriers?

One challenge in the engineering of functional tissue grafts is to obtain a sufficient amount of cells. Microcarriers (MCs) can serve as an expansion vehicle for *in vitro* cultured cells^{81,82}. Cell types, such as chondrocytes and osteoblasts, cultured on these MCs have shown to retain their matrix forming capacities⁸³. In this chapter, the biofabrication and bone regeneration properties were evaluated of a GelMA bioink with MSC-seeded MCs.

Chapter 10. Can both bone and cartilage tissue be regenerated in a shoulder replacement model in rabbits with an anatomically shaped, biphasic implant?

One of the advantages of biofabrication over other tissue engineering methods is the generation of implants with a complex hierarchy. Here we aimed to fabricate a

biodegradable, porous implant based on PCL and GelMA for the replacement of an articular joint. Such implants have once been shown to successfully regenerate cartilage tissue in a shoulder replacement model in rabbits⁵³. In this chapter, the next generation biodegradable joint implant was biofabricated consisting of a bone and a cartilage component, with specific biological and mechanical properties. A pilot study on the feasibility of the model is ongoing in three rabbits. A study comparing three different cartilage components of the implant was outlined.

Chapter 2

Engineering Hydrogels for Biofabrication

Jos Malda

Jetze Visser

Ferry P. Melchels

Tomasz Jüngst

Wim E. Hennink

Wouter J.A. Dhert

Jürgen Groll

Dietmar W. Hutmacher

Advanced Materials. 2013 Sep;25(36):5011-28

ABSTRACT

With advances in tissue engineering, the possibility of regenerating injured tissue or failing organs has become a realistic prospect for the first time in medical history. Tissue engineering – the combination of bioactive materials with cells to generate engineered constructs that functionally replace lost and/or damaged tissue – is a major strategy to achieve this goal. One facet of tissue engineering is biofabrication, where three-dimensional tissue-like structures composed of biomaterials and cells in a single manufacturing procedure are generated. Cell-laden hydrogels are commonly used in biofabrication and are termed “bioinks”. Hydrogels are particularly attractive for biofabrication as they recapitulate several features of the natural extracellular matrix and allow cell encapsulation in a highly hydrated mechanically supportive three-dimensional environment. Additionally, they allow for efficient and homogeneous cell seeding, can provide biologically-relevant chemical and physical signals and can be formed in various shapes and biomechanical characteristics. However, while advances in modifying hydrogels for enhanced bioactivation, cell survival and tissue formation, little attention has so far been paid to optimize hydrogels for the physico-chemical demands of the biofabrication process. The resulting lack of hydrogel bioinks have been identified as one major hurdle for a more rapid progress of the field. In this review we summarize and focus on the deposition process, the parameters and demands of hydrogels in biofabrication, with special attention to robotic dispensing as an approach that generates constructs of clinically relevant dimensions. We aim to highlight this current lack of effective hydrogels within biofabrication and initiate new ideas and developments in the design and tailoring of hydrogels. The successful development of a “printable” hydrogel that support cell adhesion, migration and differentiation will significantly advance this exciting and promising approach for tissue engineering.

INTRODUCTION

Tissue engineering (TE) aims for the full restoration of damaged or degenerated tissues and organs through the use of TE, cell and growth factor delivery. Tissue-engineered constructs will have to mimic a certain degree of the native complexity of the tissue in order to assist in restoration of the full structure and functionality of the tissue. Traditionally, the three main components of TE are cells, scaffolds and growth factors and they are combined to form a construct that can be immediately implanted or incubated *in vitro* prior to implantation. A scaffold can successfully deliver cells and/or growth factors to a damaged or degenerated tissue or organ, while simultaneously providing temporal mechanical support for the period the newly formed tissue matures. However, the three-dimensional (3D) constructs that have been generated for these scaffold-based or scaffold-guided TE approaches are typically based on the random distribution of cells, matrix, and bioactive cues, since their manufacturing does not allow the control of specific distribution. Mimicking the biological and functional organizational complexity of native tissues is now regarded as the next challenge in the full regeneration of tissues.

To address this challenge, additive manufacturing (AM) technology has been employed to generate bio-engineered 3D structures to replicate the complex nature of tissue¹¹. In this approach, termed "biofabrication"^{57,85}, biological structures for TE, pharmacokinetic or basic cell biology studies (including disease models) are created by a computer-aided manufacturing process for patterning and assembling living and non-living materials with a prescribed 3D organization⁸⁶. The resulting shape can be customized, and include open inner structures that improve the supply of nutrients towards embedded cells⁸⁷. Moreover, the fabricated structures can be used to study interactions between different cells and/or bioactive compounds⁸⁸⁻⁹², but could also lead to functional tissue equivalents⁹³, and potentially, to whole functioning organs.⁹⁴ Recent investigations have, for example, adopted biofabrication for the engineering of 3D constructs with the organizational features of different tissues, including skin^{95,96}, meniscus⁹⁷, aortic valves⁹⁸, cartilage^{99,100}, bone¹⁰¹, and blood vessels¹⁰².

Whilst AM technologies, as applied in the processing of metals, ceramics and thermoplastic polymers have inspired the field of biofabrication, these "classic" AM approaches generally involve the use of organic solvents, high temperatures or crosslinking agents that are not compatible with living cells and/or bioactive proteins. Hydrogels can be processed under more cell friendly conditions and often classified in the biofabrication field as "bioinks". From a biological point of view, high water content hydrogels are attractive candidates for the incorporation of cells and bioactive compounds, because they can provide an instructive, aqueous 3D environment, simulating the natural extracellular matrix.¹⁰¹

Historically, hydrogels used in tissue engineering applications are predominantly based on naturally derived polymers, including alginate, gelatin, collagen, chitosan, fibrin and hyaluronic acid^{29,30,103}. Cells benefit from the abundance of chemical signals present in these hydrogels, resulting in high viability and proliferation rates^{29,104}. These signals can also be used to induce the formation of specific neo-tissues^{29,30}, however, due to batch-to-batch variation and the sensitivity of cells (especially stem cells) to these variations, reproducibility of constructs often remains complicated. In addition, implementation of these materials in biofabrication can be challenging due to their variable printability.

In contrast to hydrogels based on natural polymers, 3D printed structures with high shape fidelity can be obtained with polymers based on synthetic networks, like poly(ethylene glycol)¹⁰⁵ and pluronics¹⁰⁶⁻¹⁰⁸. However, these hydrogels provide embedded cells with an inert environment without active binding sites⁷⁹, often resulting in low cell viability¹⁰⁶⁻¹⁰⁸. In order to improve control over cellular differentiation in these gels, bioactive compounds have to be added or grafted to the network, like peptide sequences¹⁰⁹ and growth factors^{30,110,111}. Peptide sequences can modulate cellular behavior by providing binding sites in otherwise inert hydrogels¹¹², whereas growth factors can further direct cellular differentiation in order to regenerate a specific tissue type. There already are a number of reviews on the mandatory biological characteristics of hydrogels for biomedical applications and this goes beyond the scope of this review. For further reading we recommend recent reviews by Seliktar¹⁰⁴ and by DeForest and Anseth⁷⁹.

The present review will focus on the physicochemical aspects important for the development and characterization of hydrogels for biofabrication. Despite the fact that photocuring methods, such as two-photon polymerization¹¹³ and stereolithography¹¹⁴ can also yield organized 3D cell-laden hydrogel structures, their working principles do not involve deposition of gels and cells and hence pose different demands regarding hydrogel properties. Therefore, these techniques fall outside the scope of the current review. Here, we guide the reader in making choices regarding available approaches to tailor existing hydrogel platforms by means of physicochemical modification. Finally, current developments in hydrogels that could impact on the composition and properties of future hydrogel bioinks will be discussed.

The Biofabrication Window

Although major progress has been made with both natural and synthetic hydrogels in biofabrication¹¹⁵, bioinks have some significant complications regarding the required physical and biological properties. The central problem is that the fabrication of complex, tissue-like structures with high resolution dictates narrow boundaries for the physical properties of the hydrogels. Additionally, the hydrogel construct should

facilitate migration, proliferation and differentiation of the embedded and endogenous cells. Thereby, biofabrication imposes opposing requirements on the properties of materials and specifically the lack of such versatile hydrogel systems has been coined as an important factor restraining further progress in this field^{11,116-120}. The traditional approach to improve printability of hydrogels has been increasing the polymer concentration or crosslink density^{121,122}. Highly crosslinked hydrogels serve as a stiff construction material as represented by the blue fabrication window (Fig. 1). On the contrary, cells thrive best in an aqueous environment, in which their migration and matrix deposition is not limited by a dense polymer network⁷⁹, represented by the yellow cell culture window (Fig. 1). Unfortunately, hydrogels with a low extend of crosslinks lack the ability to maintain their imposed shape on fabrication, resulting in a low shape-fidelity and limited overall mechanical properties. Therefore, most constructs have been fabricated with a moderate degree of hydrogel crosslink densities, represented by the green “traditional” biofabrication window (Fig. 1). However, since hydrogels, which fit in this window compromise on

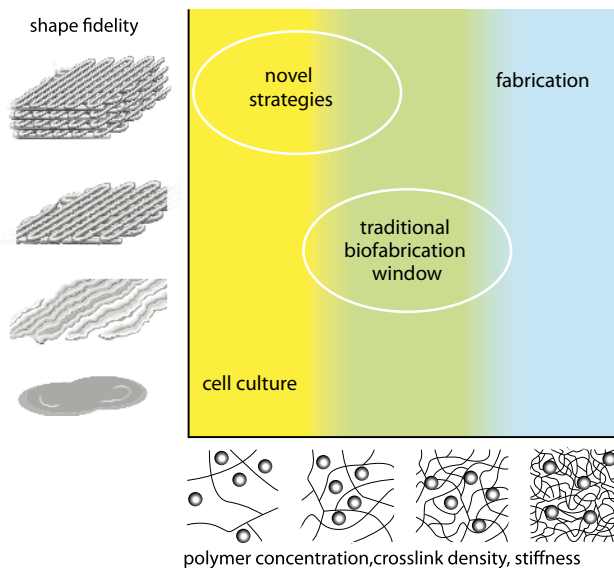


Figure 1. This review advocates a change in the paradigm of biopolymer development by shifting the biofabrication window. Optimal shape fidelity in biofabrication processes can typically be achieved with stiff hydrogels containing high polymer concentrations /or crosslink densities (fabrication window), however, this dense polymer network limits cell migration, growth and differentiation. On the other end of the spectrum, cells thrive best in soft hydrogels (cell culture window), which are too watery to maintain shape for fabrication purposes. Therefore, a biofabrication window exists for medium crosslinked hydrogels,¹²¹ compromising on both biological and fabrication properties. Recently, strategies are applied to shift the bioprinting window, obtaining high shape fidelity with cytocompatible hydrogels.

biological, as well as fabrication properties, there is a need to shift this biofabrication window in order to achieve high shape-fidelity with hydrogels that facilitate maximal cell and tissue compatibility (“novel strategies” (Fig. 1)).

Hydrogels for biofabrication should allow the translation of the computer-aided design (CAD) to a tissue construct that potentially contains intricate internal and/or external organizational structures. This requires a high degree of control over the deposition process, which is closely associated with the printability of the hydrogel. The printing of inks on paper is well documented with various available tests that are taking in account surface and structural properties of the paper, however quantification of printability of ink on paper remains difficult¹²³. Standardized tests to evaluate the capacity of hydrogels to be printed do not yet exist. Obviously, an important outcome parameter from a physical point of view would be the geometric accuracy or shape fidelity of the generated constructs. As such, there is a strong need for methods of geometry comparison of tissue-engineered constructs that go beyond simple visual inspection, manual measurements using rulers or calipers¹²⁴ and photographs^{97,122,125,126}. Optical methods have been developed to assess the geometric fidelities of tissue constructs using laser triangulation.¹²⁴ Although this yields valuable data on the outer contours of homogeneous solid tissue replacements, such as for the meniscus, this technique will not visualize the potentially more intricate internal geometry. More recently, Murphy *et al.*⁹⁶ evaluated properties relevant to bioprinting, including printability, of a range of available hydrogels. In an attempt to quantify the printability, deviation of a 1.0 x 1.0 cm printed square area was determined. Although the authors were challenged by the fact that not all hydrogels could be reproducibly processed by the printer, this allowed for an, albeit rough, quantification, of the printability. Nevertheless, the fabrication of tissue structures is likely to require a significantly higher resolution than what could be evaluated in this approach. In view of this, the visualization of the difference between a computer design and a μ CT generated image of a tissue construct, as represented in a heat map¹²⁷, is a promising development, despite the fact that this will not discriminate between different hydrogels in a single generated tissue blueprint.

HYDROGEL BASED BIOFABRICATION SYSTEMS

The use of hydrogels as a carrier for cells and/or bioactive compounds has been described for many deposition-based biofabrication approaches^{101,118}. Briefly, these can be divided in methods based on laser-induced forward transfer, inkjet printing (both thermal and piezoelectric) and robotic dispensing (Fig. 2). Each technique demanding very specific requirements for characteristics of the hydrogel-based bioinks, with regards to their rheology and post-curing rate in order to achieve reliable fabrication of 3D constructs.

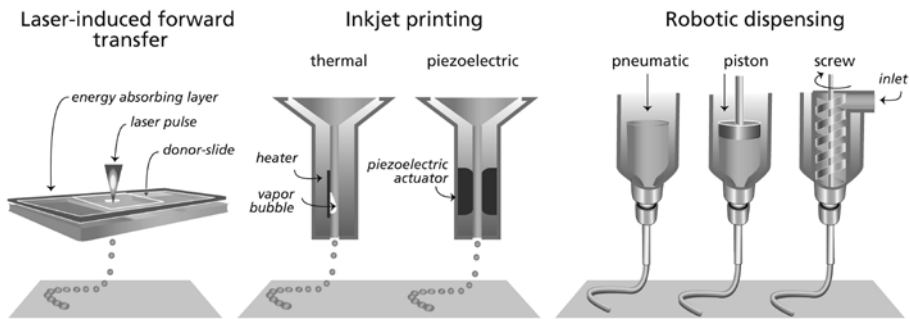


Figure 2. Selected biofabrication approaches involving the use of hydrogels in form of a so-called “bioink”.

Laser-Induced Forward Transfer

Laser-induced forward transfer technology refers to the use of a donor slide covered with a laser energy absorbing layer and a layer of cell-containing bioink¹²⁸. The focused laser pulses cause local evaporation of the absorbing layer that, in turn, generates a high gas pressure propelling the bioink compound towards the collector slide (Fig. 2). This technology allows for the precise deposition of materials and (high densities of) cells in relatively small 3D structures without negatively affecting viability or cellular function^{128,129}. It is a nozzle-free approach and is therefore not affected by clogging issues. It has successfully been used with bioinks with a wide range of viscosities (1-300 mPa/s). Nevertheless, the high resolution of this process complicates even distribution of cells over the ejected drops, requires rapid gelation kinetics to achieve high shape fidelity and does result in a relatively low overall flow rate (Fig. 2). Consequently, the generation of larger and thus clinically relevant 3D constructs is time-consuming, hampering the successful translation towards widespread application.

Inkjet Printing

Usually, inkjet printing in the biofabrication field is defined as the dispensing through a small orifice and precise positioning of very small volumes (1-100 picolitres) of bioink (PBS, cell culture media and/or hydrogel) on a substrate⁵⁷. For the inkjet printing of cells thermal and piezo-electric inkjet printing are the two most commonly adopted approaches. For thermal inkjet printing (Fig. 2), small volumes of the printing fluid are vaporized by a micro-heater to create the pulse that expels droplets from the print head¹³⁰. The generated heat and resulting evaporation do result in stress for the deposited cells¹¹⁷ and causes transient pores in the cell membrane¹³¹. In piezoelectric inkjet printing (Fig. 2), on the other hand, no heating is used, but a direct mechanical pulse is

Table 1. Typical characteristics of three key dispensing approaches in biofabrication.

	Laser-induced forward transfer	Inkjet printing	Robotic dispensing
Resolution	++	+	+/-
Fabrication speed	-	+/-	++
Hydrogel viscosity	+/-	-	+
Gelation speed	++	++	+/-

applied to the fluid in the nozzle by a piezoelectric actuator, which causes a shock wave that forces the bioink through the nozzle.

Inkjet printing has successfully been applied for accurate deposition of cells¹³² and even allows for the generation of, albeit small, 3D structures¹³³. One of the main restrictions of the inkjet technology is perhaps the low upper limit of the viscosity for the ink (Table 1), which is in the order of 0.1 Pa/s¹³⁴, complicating the deposition of higher viscous natural extracellular matrix materials¹³⁵. As small droplets of this ink are deposited onto a substrate with high velocity, the low viscosity will facilitate spreading of the droplet on the surface upon impact. This impedes building up 3D constructs, for which inkjet technology originally was not developed. Moreover, most researchers in this area have been using commercially available inkjet printers, which are designed for dispensing low-viscous inks -not containing particles measuring over 1 μm - at high resolution. Since this involves channels and orifices measuring not much larger than the diameter of a cell, challenges regarding both cell viability and inkjet system reliability result¹³⁶. In summary, as a consequence of the small droplet size and the diffusion-dependent gelation of inkjet printers results in a challenge to translate this technology to larger, more clinically relevant, sizes.

Robotic Dispensing

An alternative approach for the design and fabrication of organized 3D hydrogel constructs is based on dispensing systems. For this method, hydrogels with suspended cells are generally inserted in disposable plastic syringes and dispensed, either pneumatic, piston- or screw-driven, on a building platform (Fig. 2). Rather than single droplets, robotic dispensing yields larger hydrogel strands. In order to maintain the shape of the constructs after printing, hydrogels with higher viscosities are often used. Resolution that can be achieved with robotic dispensing is in the order of 200 μm , which is considerably lower compared to laser- or inkjet-based systems. Nevertheless, fabrication speed using robotic dispensing is consequently significantly higher (Table 1) and anatomically shaped constructs have successfully been generated (Fig. 3). Piston-driven deposition generally provides more direct control over the flow of the hydrogel from the nozzle,

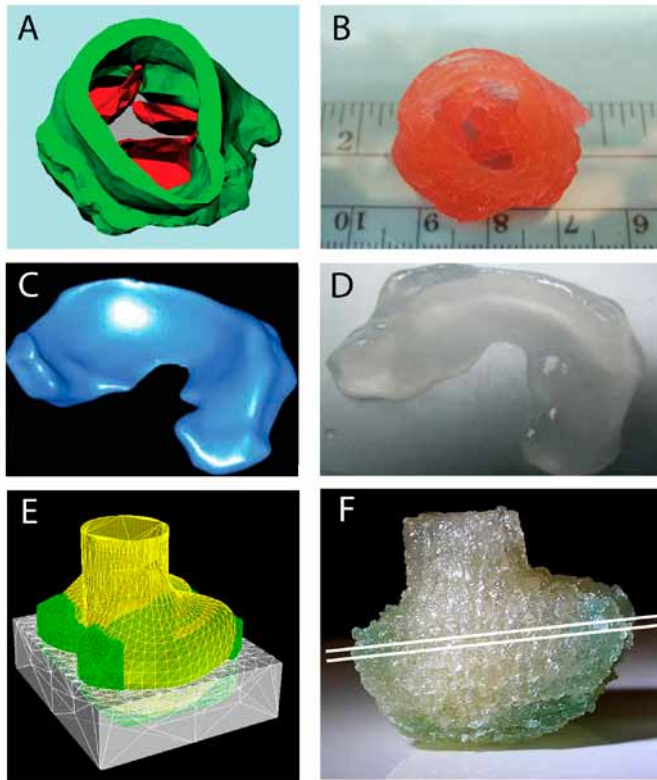


Figure 3. Biofabrication examples - Aortic valve model reconstructed from micro-CT images (a). The root and leaflet regions rendered separately into 3D geometries (green color indicates valve root and red color indicates valve leaflets) and printed (b). An ovine meniscus reconstructed from micro-CT images (c) and printed (d). A miniaturized distal femur from a human knee designed using Rhino Software LxWxH: 40x35x-32mm containing a cartilage layer (green) and a bone component (yellow) and a support structure (white) (e) and printed after manual removal of the support structure (f). Reproduced with permission from Duan et al.⁹⁸ and Wiley (a, b), Cohen et al.²¹⁶ Liebert (c, d), and Visser et al.¹⁹⁰ (e, f).

due to the delay of the compressed gas volume in the pneumatic systems. On the other hand, screw-based systems may give more spatial control and are beneficial for the dispensing of hydrogels with higher viscosities. To further improve the printing quality of the 3D constructs, deposition within high viscous crosslinking solutions has been explored^{137,138}. Cells have been deposited with high viability and no notable effects on differentiation capacity using both pneumatic and piston driven systems (see Table 2). Screw extrusion can generate larger pressure drops at the nozzle, which can potentially be harmful for embedded cells. Thus, the screw design needs to be specifically designed to accommodate biofabrication, rather than using off-the-shelf screws designed for oth-

Table 2. Hydrogels applied for fabricating 3D-structures.

hydrogel	fabrication technique	polymer concentration (w/v)	gelation method	printing quality	cytocompatibility	reference
	<u>laser-induced forward transfer</u>					
alginate		2%	ionic	2	intermediate, day 10	217
		1%	ionic	a*	high, day 7	203
		1%	ionic	3	high, day 1	218
		2%/8%	ionic	1/2	not studied	219
	<u>inkjet</u>					
alginate	thermal	2%	ionic	2	not reported	220
	piezo	0.8%	ionic	2	high, day 0	133
alginate/collagen type 1	thermal	1%/0.3%	ionic	2	90%, day 7	221
collagen type 1	not reported	0.1%	thermal	1	migrating cells	222
fibrinogen/collagen type 1	thermal	1%/0.15%	enzymatic	a*	82%, day 7	201
poly(ethylene glycol) dimethacrylate	thermal	10%; 20%	photo (during print)	2	89%, day 1	99
	<u>robotic dispensing</u>					
agar	pneumatic	5%	thermal	2	not studied	156,223
agarose	piston-driven	1.5%	thermal	3b*	95%, day 21	137
	piston-driven	5%	thermal	1	95%, day 7	106
	piston-driven	not reported	thermal (cooling of strand in needle)	3 d*	not studied	224
agarose	pneumatic	4%	thermal	2*b	not studied	138
alginate	piston-driven	10%	ionic	2	89%, day 1	148

Table 2. Hydrogels applied for fabricating 3D-structures. (continued)

hydrogel	fabrication technique	polymer concentration (w/v)	gelation method	printing quality	cytocompatibility	reference
	laser-induced forward transfer					
	piston-driven	2%	ionic	2	82%, day 3	106
	piston-driven	2%	ionic	2	75-94%, day 0	179,216,225
	pneumatic	1.5% - 3%	ionic	2 (3%)	85%, day 0 (1.5%)	226
	piston-driven	4%	ionic	2	not studied	122
	piston-driven	2%	ionic	c*	70%, day 3	65
	pneumatic	3.5%	ionic	c*	84%, day 0	76
	piston-driven	4%	ionic	c*	94%, day 7	75
	pneumatic	5%	ionic	1*b	not studied	138
	piston-driven	1%	ionic	2	not studied	227
	Piston	4%	ionic	2	95%, day 7	228
alginate/fibrin	pneumatic	6.3%/7%	ionic/enzymatic	1	not studied	223
alginate/gelatin	piston-driven	7.5%/5%	thermal/ionic/chemical	2	95%, day 0	229
atelocollagen	pneumatic	3%	thermal	c*	95%, day10	202
collagen type 1	pneumatic	0.3%	thermal	2	86%, day 1	108,230
	pneumatic	0.223%	pH (sodium bicarbonate)	2*e	not studied	231
	piston-driven	0.1%	thermal	1	migrating cells	222
gelatin	piston-driven	20%	thermal/chemical	2	95%, month 1	232
	piston-driven	20%	thermal/chemical	2/3	poor cell differentiation	233

Table 2. Hydrogels applied for fabricating 3D-structures. (continued)

hydrogel	fabrication technique	polymer concentration (w/v)	gelation method	printing quality	cytocompatibility	reference
laser-induced forward transfer						
	pneumatic	7%	thermal	2*d	not studied	231
	pneumatic	2%	extruded in gel phase at 20°C	2	not studied	138
gelatin methacrylamide	piston-driven	20%	thermal/photo	1	73%	60
gelatin/alginate	piston-driven	6%/5%	thermal/ionic	3	82%, day 7	98
gelatin/alginate/chitosan	piston-driven	15%/1.25%/2.5	enzymatic/ionic/chemical	2	proliferating cells, day 7	
gelatin/alginate/fibrinogen	piston-driven	15%/1.25%/0.5%	thermal/enzymatic/ionic/chemical	2	proliferating cells, day 7	234
gelatin/alginate/fibrinogen	piston-driven	2:1:1	thermal/ionic/enzymatic	2	differentiating cells	235
gelatin/chitosan	piston-driven	5%/0.5%	ionic/chemical	2	98%, month 2	236
gelatin/chitosan	piston-driven	4.6%/0.4%	thermal	1	Not reported	237
gelatin/chitosan	piston-driven	9%/1%	thermal	2	85-97%	237
gelatin/fibrinogen	piston-driven	13.3%/3.3% 10%/5% 6.6%/6.6%	enzymatic	2	98%, day 0	238
gelatin/Hyaluronan	piston-driven	10%/0.5%	thermal/chemical	2/3	poor cell differentiation	233
gelatin methacrylamide/hyaluronic acid	piston-driven	20%/2.4%	thermal/photo	3	82%, day 3	60

Table 2. Hydrogels applied for fabricating 3D-structures. (continued)

hydrogel	fabrication technique	polymer concentration (w/v)	gelation method	printing quality	cytocompatibility	reference
gelatin methacrylamide/gellan	piston-driven	10%/1.1%	ionic/ thermal/photo	3 e*	80%, day 3	61,190
hyaluronic acid/ hydroxyethyl- methacrylate- derivatized- dextran (dex-HEMA)	piston-driven	10%	photo	2	75%, day 3	183
hyaluronic acid methacrylate (HA-MA)/ gelatin methacrylate (GE-MA)	piston-driven	1.2%/0.3%	photo (during print)	1	proliferating cells, day 7	178
hyaluronic acid methacrylate (HA-MA)	piston-driven	1.5%	photo (during print)	1	not studied	178
Lutrol F127	piston-driven	25%	thermal	3	2%, day 7	106
	pneumatic	30%	thermal	3	60%, day 0	108
	piston-driven	40%	thermal	3d*	not applicable	158
Lutrol	piston-driven	25%	thermal/photo	3	50%, day 3	179,216
Matrigel	piston-driven	not reported	thermal	1	High viability	239
methylcellulose	piston-driven	4%	thermal	1	not reported	106
N- isopropylamid and polyethylene glycol)	pneumatic	10%	thermal	2	not studied	240
poly(ethylene glycol) diacrylate	pneumatic	25%	photo	1	not studied	138

Table 2. Hydrogels applied for fabricating 3D-structures. (continued)

hydrogel	fabrication technique	polymer concentration (w/v)	gelation method	printing quality	cytocompatibility	reference
	laser-induced forward transfer					
poly(ethylene glycol) diacrylate/alginate	piston-driven	20%/12.5%	photo (during print)	3	near 100%, day 21	127
p(HPMAm-lactate)-PEG	piston-driven	25-35%	thermal /photo	3	94%, day 1	105
tetraPac	piston-driven	1-2%	michael addition	2e*	high, day 28	241

Printing quality rated on shape-fidelity scale.1 = **low** undefined structure2 = **intermediate** irregular pattern/fiber, 3D potential3 = **high** well-defined building material

*a = reinforced with solution electrospun fibers

*b = submerged fabrication technique

*c = reinforced with co-deposited thermoplastic polymer scaffold

*d = hydrogel is sacrificial component, no aim for direct cell encapsulation

*e = support component used

er applications. Taken together, robotic dispensing allows the fabrication of organized constructs of clinically-relevant sizes within a realistic time frame, hence this technology is often regarded as the most promising^{118,120}.

KEY HYDROGEL PROPERTIES IN BIOFABRICATION

The suitability of a hydrogel for a specific biofabrication process mainly depends on its physicochemical properties under the conditions imparted by the specific biofabrication instrument. The development of robust hydrogel systems for biofabrication, *i.e.*, hydrogels that are suitable for both fabrication and cell culture, remains a challenge (Fig. 1). The major physicochemical parameters that determine the printability of a hydrogel are its rheological properties and crosslinking mechanisms (Fig. 4). However, the specific

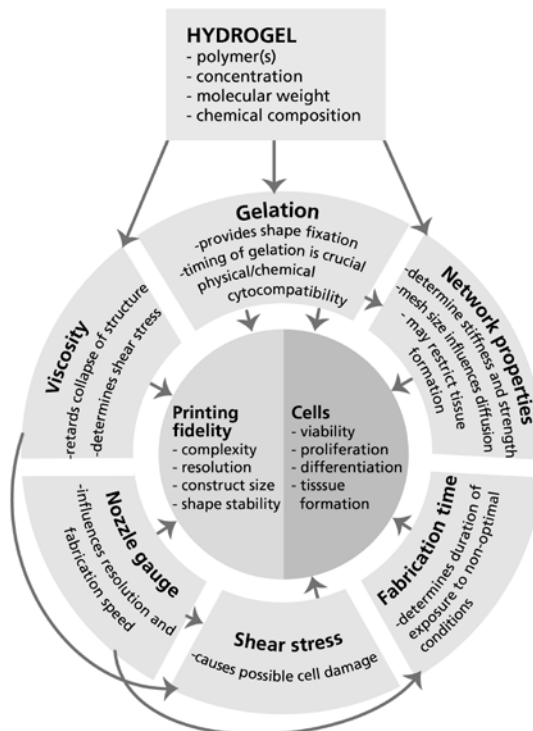


Figure 4. Concept map of variables and relations critical to biofabrication. The hydrogel (polymer type(s), concentration, molecular weight and chemical composition) directly determines the viscosity, gelation mechanism and speed, and mechanical properties of the final gel. This -in combination with processing parameters, such as nozzle gauge and fabrication time- influence the main outcomes Printing fidelity and Cell viability and function.

processing parameters, such as nozzle gauge (Fig. 4), will consequently determine the shear stress the embedded cells are exposed to, as well as the maximal time required for fabrication of a clinically relevant size (cm^3 -scale) construct (Fig. 4). Finally, once the hydrogel precursors have been printed and the cells have survived, the printed construct has to possess, develop or be endowed with shape fidelity and sufficient mechanical stability, for example by (post-processing) gelation as a result of crosslinking.

These parameters are interlinked and important for the different biofabrication technologies, however, absolute numbers can be considerably different given the nature of the deposition process. For example, inkjet printing is generally limited to low maximum viscosities, while with robotic dispensing bioinks with higher viscosities can be processed. Accordingly, inkjet printing requires rapid gelation to allow fabrication of an intricate 3D structure. On the other hand, robotic dispensing will facilitate the maintenance of the initial shape after deposition of highly viscous liquids allowing for gelation (crosslinking) of the generated structures post-fabrication, as well as building large constructs in the x, y, z directions. This illustrates how the viscosity of the hydrogel forming solution dictates how quickly it needs to solidify. In addition, swelling or contraction characteristics of hydrogels must also be considered and taken in account when designing a biofabricated tissue construct of particular size. Moreover, care should be taken when applying different bioinks with dissimilar swelling behaviour, since this can be complicated due to limited grafting of the layers and deformation of the final construct.

Rheology

Rheology is the study of the flow of matter under application of an external force, and is therefore highly relevant to biofabrication. Nevertheless, its importance is underestimated, given the high number of investigations that do not take rheology into account when developing or evaluating hydrogels for biofabrication. In the instances that rheological data is presented, it often lacks the clear correlation to the results of the deposition processes, underscoring the complexity of field of rheology and its poorly understood role in biofabrication. Here, we discuss the influence of number of rheological parameters on the biofabrication process.

Viscosity

Viscosity is the resistance of a fluid to flow upon application of a stress. In biofabrication, a high viscosity impedes both surface tension-driven droplet formation (particularly important for filament-based deposition techniques) and the collapse of deposited structures. The viscosity of a polymer solution, such as a hydrogel precursor, is predominantly determined by the polymer concentration and molecular weight. This is illustrated in Table 3 for a number of hydrogel forming polymers, including sodium alginate (typical molecular weight 200 kDa) and Lutrol F127 (molecular weight 12 kDa). As hydrogels of

Table 3. Viscosities of some hydrogel precursor solutions used for printing.

polymer	concentration % w/v	viscosity (Pa·s)	shear rate (s ⁻¹)	molecular weight (kDa)	reference
sodium alginate	2	0.9	100	100-500 (typical)	150
	3	2.0			
	5	6.4			
Lutrol F127	25	0.03	-	12	158
	30	1.5			
	35	26 600			
	40	>600 000			
PEG	10	0.008	200-1300	3.35	99,242
	20	0.017			
Hyaluronic acid	1.5	22	1	950	241
Collagen type I	0.3	10	0.1-100	115+230	108,230,243

high polymer concentrations can be restrictive environments for cell proliferation, migration and tissue formation^{139,140}, it seems logical to opt for low concentrations of high molecular weight polymers. This (besides the before mentioned inherent biofunctionality) may explain the popularity and success of naturally derived polymers in the field, as many have high molecular weights that have not been matched by the same extend by synthetic biodegradable alternatives so far. Viscosity of the bioink directly influences shape fidelity after deposition (Fig. 5). Low-viscous 20% gelatin methacrylamide (GelMA) solution forms droplets at the needle tip, resulting in the deposition of strands that spread out on the surface, while the increase in viscosity by orders of magnitude upon addition of 2.4% high molecular weight hyaluronic acid (HA), allows the formation of a filament rather than a droplet⁶⁰. Consequently, high-fidelity 3D structures could be deposited in which horizontal pores exist in addition to the vertical pores.

Printing fidelity, thus, generally increases with increasing viscosity, and this is the major underlying reason why hydrogels are usually printed with lower accuracies and resolutions than thermoplastic polymers. However, an increase in viscosity implies an increase of the applied shear stress, which may be harmful for the suspended cells¹⁴¹. A plethora of long-term studies on the influence of intermediate shear stress levels on cell attachment and behavior has been performed (e.g., on endothelial cells¹⁴²⁻¹⁴⁴). For example, at levels in the order of 1Pa endothelial cells may detach from a surface¹⁴⁵ and the morphology and metabolic activity of articular chondrocytes is significantly changed¹⁴⁶. Much less is known about short-term exposure to very high shear stresses that may arise in printing nozzles and orifices, but cells appear quite resilient in this respect¹⁴⁷ as the viability of printed endothelial cells have been shown to not decrease for shear stress

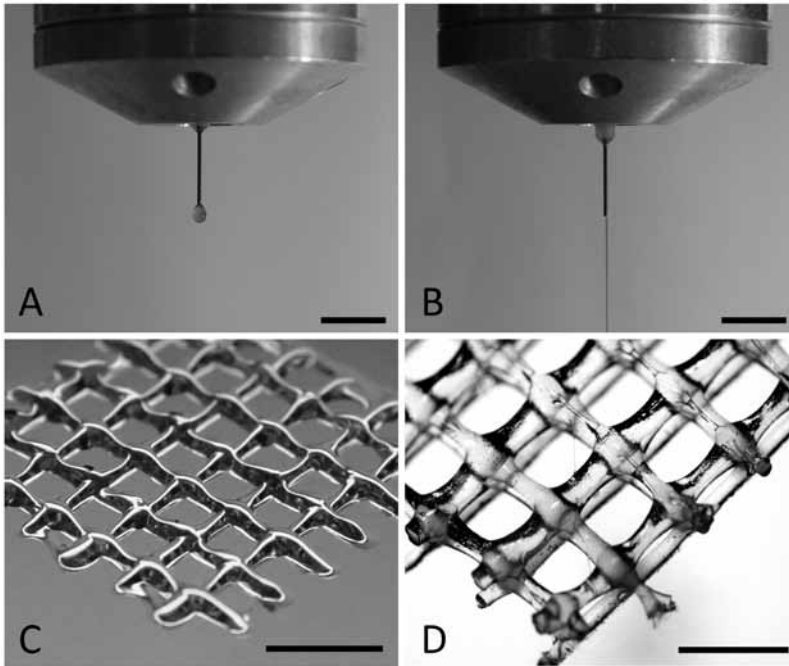


Figure 5. Illustration of the role of viscosity in bioprinting. Gelatin methacrylamide (GelMA) on its own (20%) forms droplets at the nozzle (**a**) and deposits in flat lines that spread out on the surface (**c**). When 2.4% hyaluronic acid (HA) is added, strands can be deposited from the nozzle (**b**), resulting in a construct of four layers (**d**). The scale bars in a-c represent 5 mm; the scale bar in **d** is 2 mm. Reproduced with permission from Schuurman et al.⁶⁰ and Wiley.

levels up to 1150 kPa¹²¹, which is 6 orders of magnitude higher than typical values for detaching cells from a surface or influencing cell morphology and metabolism. Within the range of systems, hydrogels and cells used so far, cell viability was generally not severely affected although a (negative) influence of shear stress (higher speeds and thinner nozzles) has been observed for robotic dispensing based systems¹⁴⁸. In inkjet printing, transient pores have been observed in the cell membrane of printed Chinese hamster ovary cells¹³¹. These pores, measuring approximately 10 nm, did not negatively affect viability or apoptosis and were self-repaired within 2 hours. Their presence was even used to the benefit of allowing gene transfer through the pores. Besides viscosity, the geometry of the dispensing setup (dimensions of channels, nozzles and/or orifices) and flow rates are additional factors that influence shear stress. In other words, shear stresses may be reduced at the cost of loss of resolution (larger nozzles/orifices) or at the cost of flow rate.

In addition to polymer concentration and molecular weight (as main contributors), viscosity further depends on the solubility parameter (influencing the polymer coil's hy-

hydrodynamic radius), shear rate, temperature and other specific interactions. This means more sophisticated adaptations, which are more likely to ensure proper cellular behavior, are available for improving the rheological behavior of hydrogels for biofabrication.

Shear Thinning

Shear thinning (also pseudo-plasticity) refers to the non-Newtonian behavior in which the viscosity decreases as shear rate increases¹⁴⁹. It is caused by shear-induced reorganization of the polymer chains to a more stretched conformation, which leads to decreased entanglement and, therefore, viscosity. This phenomenon is, to a variable extent, exhibited by most polymeric systems. Particularly, shear thinning is observed for solution of polymers with high molecular weight. Sodium alginate is an example of a polymer that shows strong shear thinning behavior (Fig. 6)¹⁵⁰. At shear rates relevant for 3DF of hydrogels ($100\text{--}500\text{ s}^{-1}$), the viscosity is approximately an order of magnitude lower than the plateau value at low shear rates. For higher concentrations, the relative reduction in viscosity induced by shear is even greater. This implies a decreased shear stress at the high shear rates that are present inside a nozzle or orifice during biofabrica-

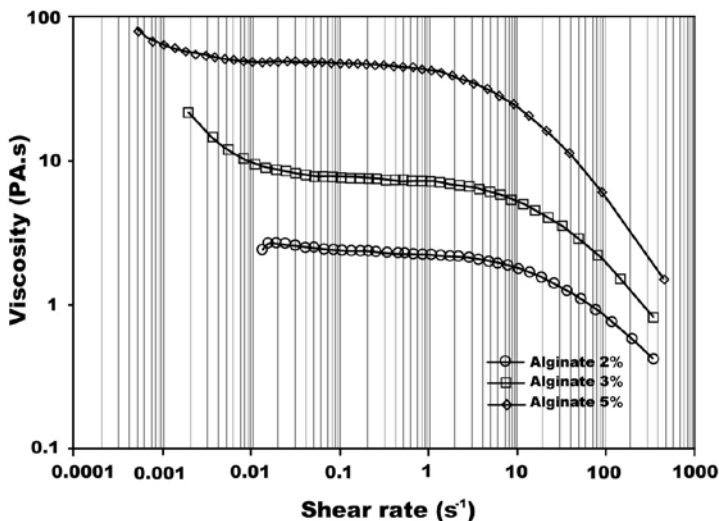


Figure 6. Viscosity variation as a function of shear rate for different alginate solutions. Shear thinning is demonstrated by the rapid decline in viscosity as the shear rate is increased, with higher concentration alginate having the greatest reduction in shear viscosity. Reproduced with permission from Rezende et al.¹⁵⁰ and Wiley.

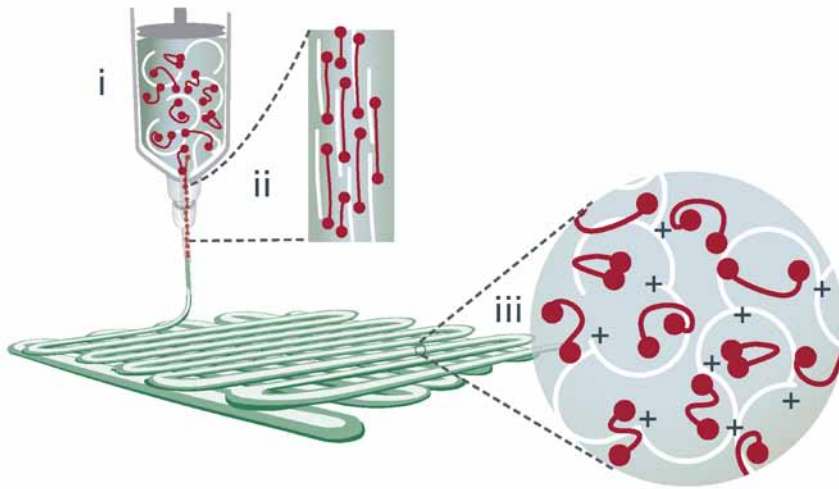


Figure 7. Schematic representation of shear thinning and yield stress in plotting gelatin methacrylamide (GelMA)/gellan gum. In the syringe the gellan chains (in white) form a temporary network and induce gel-like viscosity (**i**). Upon dispensing through a needle, the temporary network is broken up by shear and all polymer chains align, reducing the viscosity by orders of magnitude (**ii**). Directly after removal of shear stress, the temporary network is restored and the plotted filament solidifies instantly (**iii**).

tion, followed by a sharp increase in viscosity (resulting in a high printing fidelity) upon deposition (Fig. 7).

Yield Stress

Yield stress is a stress that must be overcome to initiate flow. Generally interactions between polymer chains result in the formation of a fragile, physically crosslinked network, which is broken by shear forces (above the yield stress) and (slowly) reforms when the shear is removed. Where high viscosity only delays collapse of a deposited 3D structure, the presence of a yield stress can potentially prevent flow and collapse. For example, gellan gum is an anionic polysaccharide that can be crosslinked by cations to form physical networks¹⁵¹. When added to GelMA at tailored salt concentrations it forms a gel suitable for robotic dispensing as it exhibits strong yield stress behavior (Fig. 7)⁶¹. Besides improving printing fidelity, the presence of a yield stress also prevents cell settling in the hydrogel precursor reservoir. Other hydrogel systems that exhibit yield stress and shear-thinning have been developed more specifically for delivering cells or bioactive molecules into the body by injection from a syringe¹⁴⁹. Among these systems are self-assembling peptide based hydrogels¹⁵², recombinant protein hydrogels¹⁵³, colloidal systems¹⁵⁴, gels based on cyclodextrin inclusion complexes and block copolymers¹⁵⁵.

CROSSLINKING MECHANISMS FOR HYDROGELS

Gelation of a printed hydrogel structure is necessary to preserve its shape; even structures constructed from the most viscous precursor solution will change shape due to shape and collapse at some point. The gelation can either be physical (based on reversible interaction), chemical (based on formation of covalent chemical bonds) (Table 4), or a subsequent cascade and combination of both processes (Fig. 8).

Table 4. Advantages and disadvantages of different crosslinking strategies for biofabrication.

Crosslinking		Advantages	Disadvantages
Physical	Ionic	<ul style="list-style-type: none"> - Reversible interactions ensure constant viscosity during printing - Excellent compatibility with biological systems 	<ul style="list-style-type: none"> - Requires additional crosslinking agent and / or post-processing crosslinking - Mechanically weak constructs
	Stereocomplex	<ul style="list-style-type: none"> - Reversible interactions ensure constant viscosity during printing - Excellent compatibility with biological systems 	<ul style="list-style-type: none"> - Relatively slow gelation - Relatively high viscosity of the building blocks - Requires additional crosslinking agent and / or post-processing crosslinking - Mechanically weak constructs
	Thermal	<ul style="list-style-type: none"> - Reversible interactions ensure constant viscosity during printing - Rapid reassembly to gels after printing - Excellent compatibility with biological systems 	<ul style="list-style-type: none"> - Requires post-processing crosslinking
Chemical	UV	<ul style="list-style-type: none"> - Polymerisation through irradiation during printing does not affect viscosity during printing in the nozzle - Allows for post-processing crosslinking (stabilization) of mechanically weak physically crosslinked hydrogel constructs 	<ul style="list-style-type: none"> - High reaction rates necessary as polymerisation needs to be completed between nozzle and deposition - May involve exposure of constructs to irradiation - Irradiation may affect embedded cells
	Wet-chemical	<ul style="list-style-type: none"> - No need for irradiation or other further stabilization - Mechanically stable constructs 	<ul style="list-style-type: none"> - May require (potentially harmful) crosslinking agent - A trigger for chemical reactivity with required stringent control of crosslinking kinetics is needed to avoid viscosity change in the nozzle throughout printing time but ensure crosslinking between nozzle and deposition

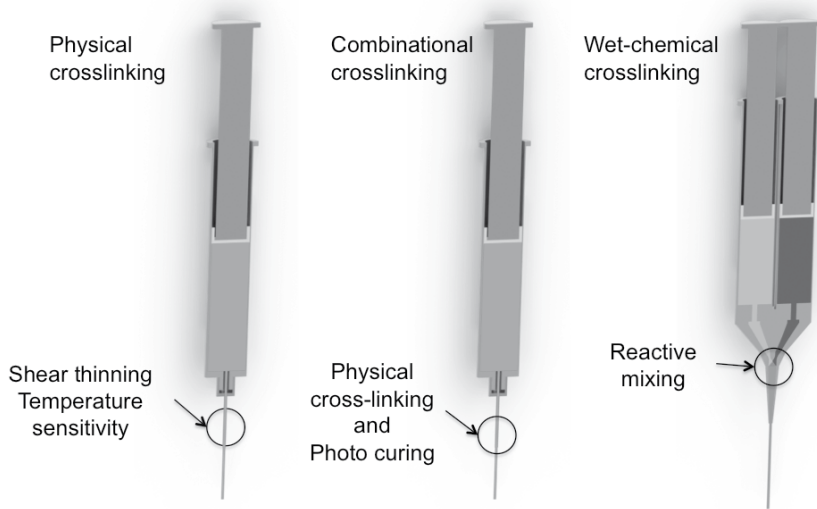


Figure 8. Graphical illustration of physical, combinational and wet-chemical crosslinking mechanisms for extrusion-based biofabrication.

Physical Crosslinking

Physical crosslinking mechanisms rely on non-chemical interactions based on entanglements of high molecular polymer chains, ionic interactions, hydrogen bridges or hydrophobic interactions. Physically crosslinked hydrogels are the most prominent hydrogel class used for biofabrication processes. For example, the first robotic dispensing approach, as described by Landers *et al.*¹⁵⁶, involved printing a physically crosslinked hydrogel into a liquid. Due to the buoyancy of the hydrogels in the liquid, printed constructs are supported, facilitating the generation of porosity in the x-, y-, and z-directions. Gelation is predominantly based on ionic-crosslinking or on a thermally-induced property change and it has been demonstrated that printing into a liquids can also be combined with chemical crosslinking¹⁵⁷. This strategy is still being applied, for example by the printing of hydrogels into perfluorinated hydrocarbon-liquids¹³⁷.

One reason for the popularity of physically crosslinked gels is that they have excellent compatibility with fragile molecules (*e.g.* growth factors) and with living cells, because potentially harmful chemical crosslinking agents are avoided. With physically crosslinked hydrogels, as the name implies, non-covalent physical interactions between hydrophilic polymer chains exist that prevent the gel from (immediate) dissolution in an aqueous environment. Many physical interactions have been exploited to design such physically

crosslinked hydrogels, these interactions include hydrogen bonding, ionic interactions (polyelectrolyte hydrogels), stereocomplex formation of polymers or polymer fragments of opposite chirality, and hydrophobic interactions (e.g. self-assembly peptides)^{158,159}.

Ionic Crosslinking

Ionic crosslinking is therefore an important mechanism in biofabrication, particularly for biopolymers. For example, alginate is a polysaccharide that consists of mannuronic and glucuronic acid residues and that is highly soluble in water as Na-salt. However, upon addition of Ca^{2+} ions (or other di/trivalent cations) rapid gelation of alginate occurs. Since this crosslinking occurs under mild and physiological conditions, alginate gels have been studied as system for the controlled release of pharmaceutical proteins and for the entrapment of living cells for TE applications¹⁶⁰⁻¹⁶². As a consequence alginate has been widely applied in biofabrication approaches (Table 2). In recent years, hydrogels have also been developed exploiting electrostatic interactions between particles (nano and or micro) of opposite charge dispersed in an aqueous systems. These gels are rapidly formed upon mixing of the particles of opposite charge, but become fluid above a certain shear stress, sufficient to break the interactions between the charged particles, making them suitable as injectable drug delivery system and likely also for bioprinting^{163,164}.

Stereocomplex Crosslinking

Stereocomplex formation occurs, for example, between poly(D-lactic acid) (PDLA) and poly(L-lactic acid) (PLLA), homopolymers of D- and L-lactic acid, respectively. When oligomers of D- and L-lactic acid are coupled to water-soluble polymers like dextran or polyethylene glycol, hydrogels are formed which are crosslinked by stereocomplexes composed of oligomers of opposite chirality. Stereocomplexation does not occur immediately upon mixing of the hydrogel building blocks, allowing their use as injectable systems for controlled drug/protein release and as scaffolds for entrapment of cells¹⁶⁵⁻¹⁶⁷. An additional form of complexation mechanisms is the formation of inclusion complexes. For example, cyclodextrins, cyclic oligosaccharides composed of R-1,4-coupled D-glucose units contain a hydrophobic internal cavity that can accommodate lipophilic guest molecules. Cyclodextrins have therefore been investigated for the solubilization of hydrophobic drugs, but also used for the design of super-molecular materials, including hydrogels. In this approach, hydrophilic polymers are derivatized with cyclodextrin units, which, upon mixing with a guest molecule-derivatized polymer, result in the formation of a hydrogel structure. These systems can be readily loaded with bioactive proteins and used as injectable sustained release system¹⁶⁸⁻¹⁷⁰.

Thermal Crosslinking

Mechanisms described above may be exploited for biofabrication in combination with sensitiveness to changes in external stimuli, especially shear force to yield shear-thinning systems^{149,171}. Of particular interest are systems that are liquid at room temperature, allowing their formulation with bioactive molecules and/or cells, but that gel at body temperature after their administration. Such hydrogels comprise of thermosensitive polymers which have a good aqueous solubility at room temperature but are insoluble at body temperature. A main representative of thermosensitive polymers is poly(N-isopropylacryl amide) (PNIPAm) which is characterized by a cloud point in water of 32 °C. This polymer has been combined in different architectures with a great variety of water-soluble polymers to yield injectable hydrogels¹⁷²⁻¹⁷⁴. PNIPAm is, however, not biodegradable and therefore in recent years a number of biodegradable thermosensitive polymers have been described, which were subsequently investigated for TE^{60,105}, as well as for pharmaceutical applications¹⁷⁵⁻¹⁷⁷.

Chemical Crosslinking

A significant drawback of the physically crosslinked hydrogels is their poor mechanical properties, which may raise stability problems of a printed construct and be associated with difficulties in handling and its overall performance. Therefore, increasing attention has been given to hydrogels that are hold together by weak (reversible) physical interactions that enable good printability, but that can further be stabilized by chemical crosslinking post-processing. Chemical crosslinking, which comprises all methods that lead to hydrogel formation by connection of gel precursors (low molecular weight monomers or polymeric building blocks) through newly formed covalent bonds, may be tuned to provide hydrogels with good handling properties and high mechanical strength. Chemical crosslinking is usually achieved by mixing of two low viscous solutions with gel precursors (*e.g.* monomers and initiator, complementarily reactive gel precursors), which initiates the crosslinking reaction. This results in a constant increase of viscosity until the gel-point is reached and a 3D polymer network develops. A major drawback of this strategy for biofabrication is the need for very stringent control of crosslinking kinetics from low viscosity printable precursor solutions to the crosslinked hydrogels without blocking the nozzle during the continuous printing process. Yet, shape fidelity of the printed construct has to be guaranteed. One possibility to exploit chemical crosslinking for biofabrication is the use of reactive mixing heads (Fig. 8). Importantly, these technologies should be developed in such a way that the crosslinking can be done under mild/physiological conditions using chemistry compatible with bioactive proteins and living cells. Hence, chemical crosslinking methods have to be designed in such a way that toxic reaction by products or non-cytocompatible monomers and hydrogel precursors are avoided.

In order to increase the viscosity of the bioprinted gel, hydrogels have also been partially pre-crosslinked prior to deposition¹⁷⁸. As in the crosslinking process covalent bonds are formed and beyond the gel point the shape is irreversibly fixed, it will be particularly challenging to achieve the desired degree of crosslinking when employing this strategy. Others have ensured high viscosities and fast gelation by initiation of the crosslinking prior to the printing¹⁷⁹. The continuous development of rheological properties over time during the printing process will likely affect the final shape fidelity. Consequently, chemical crosslinking is mainly used for post-processing fixation and stabilization of printed structures. This approach includes post-stabilizing freshly printed hydrogel constructs, usually weakly stabilized through physical crosslinks, by exposure to radiation, temperature, or by post-processing reaction of complementary chemical groups (e.g. by Michael addition reaction¹⁸⁰, click chemistry¹⁸¹ or enzymatic reactions¹⁸²). Thus, often a cascade of gelation mechanisms and triggers are involved in such systems. For example, the printing of warm GelMA-based solutions that form physical gels upon cooling on the collector, is followed by UV-curing to obtain an irreversibly crosslinked gel⁶⁰. This post-processing photo-polymerization step can lead to very fast crosslinking of the hydrogel and, hence, facilitates the maintenance of shape directly after dispensing^{105,183}. However, UV light has potentially deleterious effects on the embedded cells, and hence its use in biofabrication must take this into account.

CONVERGING BIOFABRICATION STRATEGIES

For the fabrication of customized tissue equivalents in tissue engineering, complex anatomical architectures with a certain degree of stiffness may need to be fabricated. Convergence of biofabrication approaches allows for the production of more complex architectures that include overhangs and internal porosity by using sacrificial materials as temporal support during fabrication. Moreover, reinforcing the hydrogel constructs with thermoplastic polymers provides strength, allowing these implants to withstand the mechanical forces they are potentially exposed to within the musculoskeletal system.

Sacrificial Materials

The CAM-models of complex anatomical structures could easily be derived from a 3D-scan of the part of interest of the human body¹¹. Such models often involve overhang geometries due to internal cavities, or due to the outer contour of complex anatomical structures. Through smart rotation of the 3D design, the number of overhangs can be minimized for the AM process. Nevertheless, the remaining overhang geometries need

to be temporarily supported, as the deposition of material above an empty cavity will be difficult. Preferably, the temporary support material can be washed away from the target structure serving as a sacrificial component^{184,185}. Sacrificial materials have been implemented in molding processes for creating microchannels in chips^{184,186,187}. Since these chips were fabricated from inorganic materials the sacrificial components could be removed with a broad spectrum of chemical substances. However, when support materials are a component of viable hydrogel constructs the sacrificial procedure should be cytocompatible. Therefore, sacrificial materials have been applied for realizing channel networks within hydrogel constructs, either by casting^{188,189} or by combining printing and casting^{158,185}. In the latter approach, Miller *et al.*¹⁸⁵ printed a vascular network from carbohydrate glass, a solution of sucrose, glucose and dextran. Subsequently, a hydrogel was cast and crosslinked around this network and the construct was placed in culture medium allowing the printed carbohydrate glass to dissolve. Although this approach provides exceptional control over the shape of the internal vascular network, with such casting control over the architecture of the surrounding hydrogel construct remains limited. In order to control deposition of different cell types or bioactive substances, the sacrificial material could be applied in a bottom-up AM approach. However, this limits the number of suitable biomaterials. For example, a wide range of water-soluble materials, including carbohydrate glass¹⁸⁵ and polyvinyl alcohol (PVA) are stiff enough to carry their own weight, but form unstable interfaces with the surrounding hydrogel target structures due to their hygroscopic properties. Alternatively, a thermoplastic polymer (e.g. polycaprolactone (PCL)) can be co-deposited as a sacrificial component that forms a stable interface with the hydrogel construct¹⁹⁰, yet such thermoplastic polymers require physical removal from the target structure, since dissolution using organic solvents would be detrimental to the embedded cells. As such, the printed thermoplastic structure serves as a mold and only supports the outer contours¹⁹¹. Co-deposition of two stable hydrogels, on the other hand, allows for temporary support of internal cavities, as is the case for tubular structures^{178,190}. In order to dissolve the sacrificial component the target structure needs to be selectively crosslinked¹⁹⁰.

Combination with thermoplastic polymers

Biofabricated hydrogel constructs for implantation usually have a lower stiffness than their target tissue, especially for use in the musculoskeletal system^{60,192}. A stiff and coherent hydrogel construct will be required to withstand such challenging environments in the human body. Pre-culturing cells in these constructs can increase stiffness due to specific tissue matrix deposition.¹⁹³ Yet, this demands high cell concentrations and a substantial preculturing period. Disregarding the influence of incorporated cells, improving stiffness of the hydrogel itself could be achieved by increasing hydrogel crosslink density. Unfortunately, this compromises formation of new tissue partly due

to impaired diffusion coefficients of nutrients and waste products through the hydrogel system^{104,121,193,194}.

In order to combine favorable biological and mechanical hydrogel properties, reinforcement of hydrogels has been achieved at different levels. Hydrogels have been reinforced by use of double networks (DN)¹⁹⁵ and interpenetrating polymer networks (IPN),^{196,197} as well as by incorporation of nanoparticles¹⁹⁸, nanotubes^{192,199,200} or electrospun fibers^{55,56,201}. In these approaches the crosslink density of the hydrogel could remain relatively low allowing for adequate tissue formation. However, most of these approaches will not be compatible with AM processes, since fabrication requires casting or a two-step crosslinking reaction. Therefore, recently multiple-tool biofabrication has been developed in which hydrogel constructs are reinforced by co-deposited thermoplastic polymer fibers (Fig. 9)^{65,76,190,202}. Specifically, this has been achieved by combining hydrogel and PCL in robotic dispensing^{65,76,202} and by combining electrospinning techniques with inkjet printing²⁰¹ or laser-induced forward transfer printing²⁰³. In this way, hydrogels can be processed at low polymer concentrations while shape and strength of the overall construct are secured by the thermoplastic polymer network. Moreover, it can be used in order to fabricate more complex shaped tissue constructs¹⁹⁰ and the Young's

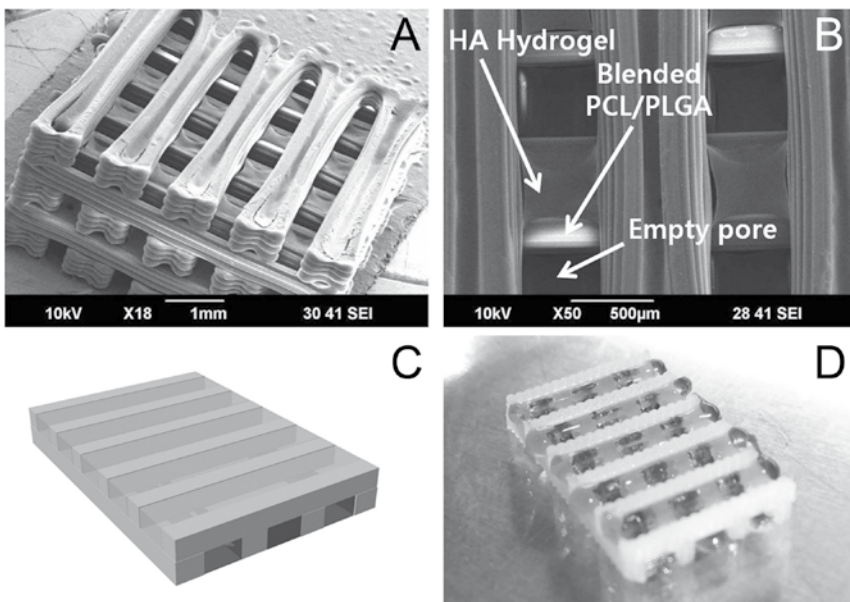


Figure 9. Examples of combined deposition of thermoplastic polymers and hydrogels. Scanning electron microscope images of a hybrid printed polycaprolactone (PCL)/ poly(lactic-co-glycolic acid) (PLGA) scaffold with infused HA hydrogel (a, b). A three-dimensional design (c) is translated to a deposition protocol, which uses (thermoplastic) PCL and alginate hydrogels (d). Reproduced with permission from Shim et al.²⁰² (a, b), Schuurman et al.⁶⁵ (C, D) and IOP Publishing. All rights reserved.

modulus of the target construct can be tailored by adjusting the thermoplastic polymer network.^{65,76} Electrospinning produces a higher resolution of PCL fibers^{201,203} compared to robotic dispensing, and results in a network that better approaches the structure of natural ECM. However, the current solution electrospinning techniques are not able to control fiber deposition and the small pore size of the resulting random meshes limits cell migration²⁰⁴. Recently developed melt electrospinning writing techniques^{205,206} address both these limitations⁵⁴, since fibers can be deposited with high spatial resolution and orientation. Combining this technique with hydrogel deposition approaches will allow for the generation of reinforced hydrogel constructs with high control over the intricate spatial organization, although grafting between fibers and the hydrogel needs to be addressed in order to biofabricate truly integrated constructs. In addition, degradation kinetics of these hybrid structures should be understood and controlled. The hydrogel scaffold acts as a temporary environment and degrades as the embedded cells secrete proteases and subsequently produce extracellular matrix proteins that defines the new tissue. In contrast, the polymeric reinforcement material should degrade in a significant slower rate, providing strength to the developing construct until the tissue has matured and at least once remodeled.

CONCLUDING REMARKS AND FUTURE PERSPECTIVES

Current deposition and fabrication technologies allow researchers to design and build structures with increasingly intricate architectures. However, in achieving this, many concessions were made with regards to the biological aspects of the hydrogels. The overall lack of suitable bioinks for the generation of larger 3D constructs that replicate a certain degree of tissue organization is hampering both the progress in the field of biofabrication and its translation towards clinical application. In part, this may be due to the current lack of comprehensive and systematic studies that focus on the characterization of the potential bioinks from a physical and rheological point of view. The fact that these physical and rheological properties of hydrogel precursors will interact with its biological performance, highlights the need for novel (semi-) high throughput screening assays since new or altered materials will have to be re-evaluated.

Maintaining high shape fidelity may compromise the biological competence and the clinical potential of the generated structures, due to the physicochemical demands of the hydrogel and the extensive fabrication times. Optimization of the environmental conditions during biofabrication, *e.g.*, printing into a culture medium, may allow for longer fabrication times without negatively affecting the embedded cell viability. Reproduction of the tissues with minute detail is most likely not required^{129,207}, although, this is a relatively unexplored topic in the field and a deeper understanding is urgently needed

to which degree the directed organization will contribute to the ultimate organization of the regenerated tissue. A collection of deposited cells and matrix within a 3D structure is not yet a functional tissue and following the biofabrication, extracellular matrix deposition and remodeling are important processes to form functional tissue structures that will determine the ultimate success of the generated tissue replacement. It will take time to actually achieve the required reorganization and to realize functional interaction of the neo-tissue. Besides this, it remains also to be determined if this reorganization should fully take place after implantation or that an *in vitro* conditioning period, e.g., in a bioreactor with mechanical loading regimes or ectopically in the human body, should be incorporated in the approach. The inclusion of more rigid thermoplastic polymer fibers within hydrogel constructs, either generated by fiber deposition modeling⁶⁵ or electrospinning^{54,55}, may assist in taking some of the initial load-bearing, potentially decreasing the bioreactor culture required.

For polymer chemists and material scientists, it remains a challenge to develop unique bioinks, taking in account the required biological competence, the physical requirements dictated by the biofabrication process, as well as the relative toxicity of crosslinking²⁰⁸ and photo-initiator²⁰⁹ agents. Promising developments are the generation of IPNs for biomedical applications, including those based on gelatin methacrylamide and gellan gum methacrylate^{118,195}, which demonstrated to have improved mechanical properties while allowing cellular survival. In addition, double-network (DN) hydrogels^{210,211} are an example of hydrogels that have, despite their high water content (~90 wt%), unsurpassed mechanical strength and toughness and are, therefore, suggested as potential full tissue (cartilage) replacements²¹². However, care should be taken in this instance since compression resistance is lost after repeated compression due to breakage of the primary polymer network. Novel DN hydrogels have recently been developed that show partial healing capacity of the primary network²¹³. Incorporation of cells in these hydrogel systems will still remain a challenge due to the limited cytocompatibility of the crosslinking agents, as well as to the two-step synthesis procedure required to create these IPNs^{118,214}, although incorporation as a reinforcing component of a biofabricated construct can be envisioned.

The range of biomaterials that could be applied as bioinks could be extended through the further development of biofabrication methods that can process hydrogel precursor solutions that rely on the addition of a crosslinking agent. Obviously, processing pre-mixed components is problematic due to the increasing viscosity as a result of the initiation of the crosslinking reaction. To avoid crosslinking within the nozzle it is very important to synchronize feed rate and crosslinking kinetics.

An additional important challenge is the scale-up and speed of biofabrication, in order to manufacture constructs of clinically relevant sizes. Approaches to potentially improve production speed include the further convergence of biofabrication technolo-

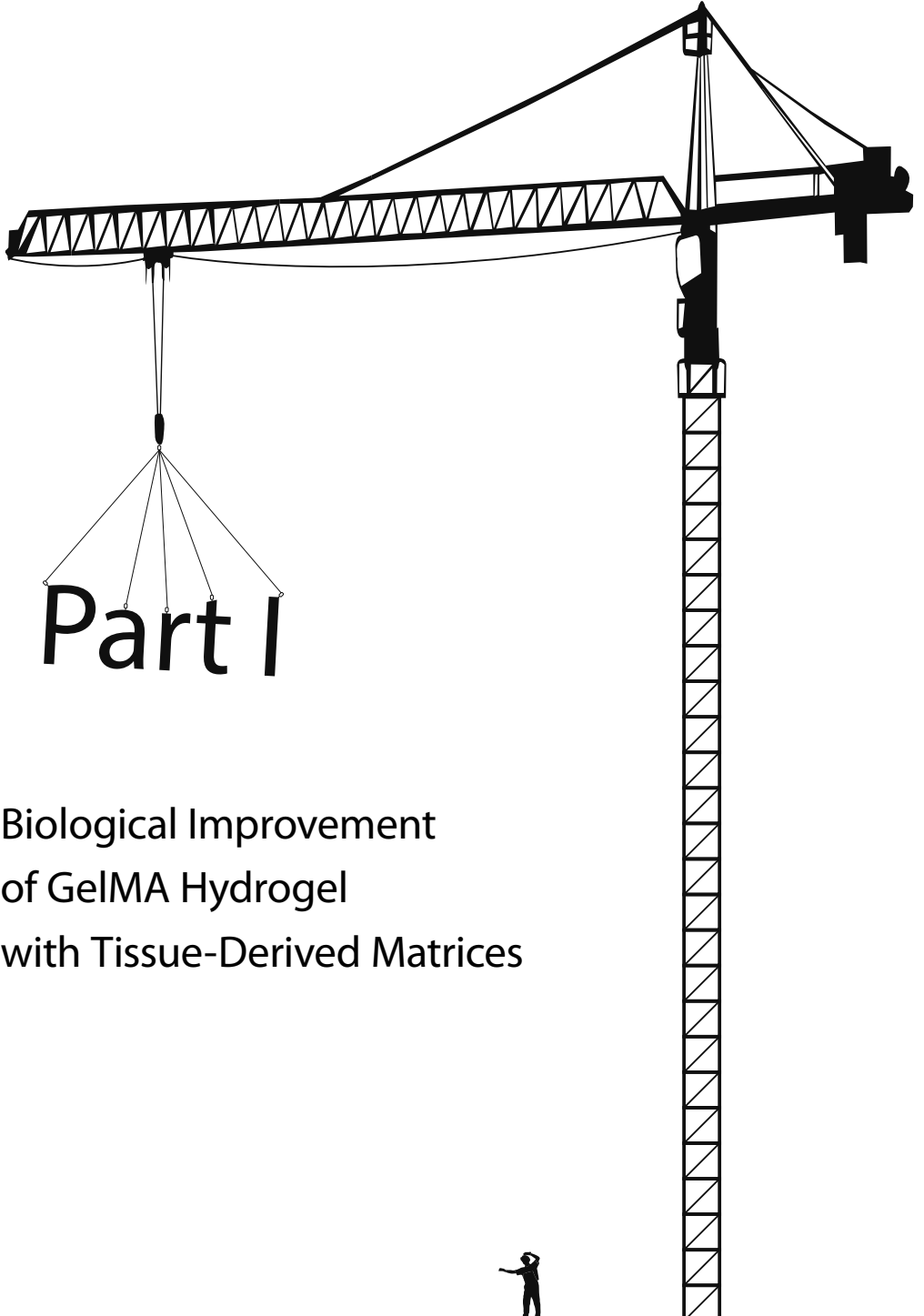
gies, combining approaches with different scales of resolution (e.g., laser-based and robotic dispensing approaches), as well as high throughput production of smaller organized units²¹⁵ that can subsequently be assembled in the laboratory or *in situ* in to larger structures¹²⁹. Still often a trade-off between resolution and speed has to be made. While relatively large constructs can be manufactured with robotic dispensing, scale-up issues should be considered for both laser- and inkjet-based systems¹²⁹. With respect to inkjet printing, if systems were to be redesigned specifically for bioprinting with respect to dimensions, the process may become more reliable and of less impact on cell viability and function. Moreover, higher viscosities may be permitted as larger channels and orifices imply lower pressure drops and shear stresses, thereby widening the range of processable hydrogels and facilitating 3D construction. Even at a tenfold decrease in printing resolution (e.g. from 1200 dpi to 120 dpi), the minimum feature size (200 μm) may still be acceptable for many bioprinting applications. Although inkjet printers applied for bioprinting purposes were designed to print in 2D, 3D inkjet printers have recently become commercially available. 3D inkjet printing works by jetting a photo curable resin in thin layers (typically 28 μm) onto a tray, followed immediately by UV curing to prevent spreading of the droplets. In this way, polymer parts of up to 150 μm in height have been fabricated. These developments clearly illustrate the enormous, yet unexplored, potential of inkjet technology.

Taken together, biofabrication potentially allows for further automation, standardization and control of the generation of customized implants, despite remaining regulatory challenges that still need to be overcome in the translation towards clinical application. However, with the suitable bioinks, supported by advanced biofabrication technologies this technology will allow us to study how cells interact with their surrounding matrix and cells. In addition, this can provide *in vitro* screening models for toxicity screening, drug testing, as well as models of diseased tissue.

ACKNOWLEDGEMENTS

We extend our thanks to Dr. Paul Dalton for proof reading the manuscript. The research leading to these results has received funding from the European Community's Seventh Framework Programme (FP7/2007-2013) under grant agreements n°309962 (HydroZONES) and n°272286 (PrintCART). Jetze Visser was supported by a grant from the Dutch government to the Netherlands Institute for Regenerative Medicine (NIRM, grant n°FES0908), Jos Malda was supported by the Dutch Arthritis Foundation and Dietmar W Hutmacher by the Hans Fischer Senior Fellowship, Institute for Advanced Studies, Technical University Munich.





Part I

Biological Improvement
of GelMA Hydrogel
with Tissue-Derived Matrices

Chapter 3

Crosslinkable Hydrogels derived from Cartilage, Meniscus and Tendon Tissue

Jetze Visser
Peter A. Levett
Nikae C.R. te Moller
Jeremy Besems
Kristel W.M. Boere
Mattie H.P. van Rijen
Janny C. de Grauw
Wouter J.A. Dhert
P. René van Weeren
Jos Malda

*This chapter is also published in the doctoral thesis of Peter. A
Levett*

Tissue Engineering Part A. 2015 Apr;21(7-8):1195-206

ABSTRACT

Decellularized tissues have proven to be versatile matrices for the engineering of tissues and organs. These matrices usually consist of collagens, matrix-specific proteins, and a set of largely undefined growth factors and signaling molecules. Although several decellularized tissues have found their way to clinical applications, their use in the engineering of cartilage tissue has only been explored to a limited extent. We set out to generate hydrogels from several tissue-derived matrices, as hydrogels are the current preferred cell carriers for cartilage repair. Equine cartilage, meniscus and tendon tissue was harvested, decellularized, enzymatically digested and functionalized with methacrylamide groups. After photo-crosslinking, these tissue digests were mechanically characterized. Next, gelatin methacrylamide hydrogel (GelMA) was functionalized with these methacrylated tissue digests. Equine chondrocytes and MSCs (Mesenchymal stromal cells) (both from 3 donors) were encapsulated and cultured *in vitro* up to 6 weeks. Gene expression (COL1A1, COL2A1, ACAN, MMP3, 13 and 14), cartilage-specific matrix formation and hydrogel stiffness were analyzed after culture. The cartilage, meniscus and tendon digests were successfully photo-crosslinked into hydrogels. The addition of the tissue-derived matrices to GelMA affected chondrogenic differentiation of MSCs, although no consequent improvement was demonstrated. For chondrocytes, the tissue-derived matrix gels performed worse compared to GelMA alone. This work demonstrates for the first time that native tissues can be processed into crosslinkable hydrogels for the engineering of tissues. Moreover, the differentiation of encapsulated cells can be influenced in these stable, decellularized matrix hydrogels.

INTRODUCTION

In tissue engineering, there is a rationale for designing biomimetic materials that re-create the native cell niche^{68,79}. Tissue-derived matrices for example can provide structural and biological support for matrix formation by embedded or invading cells⁶⁶. Native tissues that have been decellularized while maintaining the natural growth factors and signaling molecules, may thus provide the ultimate biomimetic environment²⁴⁴. Despite the clinical translation of decellularized materials for the repair of skin, bone, heart valves etc., the application in the field of cartilage regeneration has only been explored to a limited extent^{67,69}.

There is a strong need for novel biomaterials for cartilage tissue engineering^{30,245}. Hydrogels are good potential candidates, since they can support the chondrogenic morphology and simultaneously serve as a temporary scaffold for matrix formation. Moreover, hydrogels are easily delivered to a cartilage defect and allow for engineering of advanced cartilage constructs²⁴⁶.

Currently, fibrin glue is the clinical standard for cell delivery to cartilage defects⁶. However, this gel is relatively unstable with a high degradation rate and is thus a delivery vehicle rather than a support structure for cartilage matrix formation^{26,27}. Therefore, several new hydrogels are being designed, in which ideally the degradation rate is balanced with active cartilage matrix formation, and biochemical cues are incorporated to direct the behavior of encapsulated cells^{247,248}. Hydrogels derived from natural tissues are interesting candidates to meet these requirements, as they may form a potential scaffold for cells and include the appropriate biochemical cues. To this end, native matrix gels have been acquired from several tissues through digestion with pepsin enzymes^{70,71,77,249}. These hydrogels allowed for the invasion of cells and subsequent matrix deposition. However, tissue-derived matrix gels so far have only been physically crosslinked resulting in low shape stability, which is a serious drawback.

In the current study, decellularized matrices were derived from cartilage, meniscus and tendon tissues. Cartilage has a high level of collagen II and GAGs; meniscus has an intermediate level of GAGs, and a mixture of collagen types I and II, whereas tendon is predominantly composed of collagen type I and a small amount of GAGs²⁵⁰. Decellularized cartilage tissue may contain the biochemical cues that are present in the native chondrocyte niche. Whereas intuitively a collagen type II scaffold would be the scaffold of choice for cartilage engineering, there are indications that this type of collagen induces catabolic pathways in cultured chondrocytes^{74,251,252}. On the other hand, collagen type I scaffolds have proven efficacy in the regeneration of cartilage tissue^{253,254}. Therefore, both types of collagen and a mixed composition (meniscus tissue) were evaluated here. The tissue-derived matrices were used for the functionalization of Gelatin Methacrylamide (GelMA) hydrogels. GelMA has been identified as a stable, versatile hydrogel for

tissue regeneration²⁵⁵⁻²⁵⁷. It can be synthesized at low cost and gelatin is widely available as a substrate; cell adhesion sites are abundant and cells are allowed to migrate through the hydrogel and remodel the newly formed tissue. We previously showed that functionalizing GelMA with glycosaminoglycans (GAGs) can substantially improve cartilage matrix formation in *in vitro* models⁶³. In the current study, cartilage, meniscus and tendon tissues were processed into hydrogels that were covalently crosslinked to GelMA hydrogel. The potential of these matrices to enhance cartilage tissue formation by chondrocytes and mesenchymal stromal cells (MSCs) *in vitro* was evaluated.

MATERIALS AND METHODS

Development of crosslinkable tissue-derived matrix hydrogels

Stifle joints (n=8; age 3-10 years) were obtained from horses that had died or were euthanized due to non-orthopaedic ailments. Consent was obtained from the owner prior to tissue harvest and tissue was only obtained from macroscopically healthy joints. The stifle joints were dissected and the full-thickness cartilage was harvested from the entire femoral condyles. Also both complete menisci and the patellar tendons were harvested, 0.5 cm from their anchoring site in the bone. The tissues were dissected into small pieces (ca. 5x5x5 mm for meniscus and tendon, and ca. 5x5x2 mm for cartilage tissue) and all donors were pooled. Three random samples were taken from each tissue type to measure the GAG and DNA content. The obtained values will thus reflect the variability between donors and sample location (e.g. cartilage from the medial or lateral condyle). Then the tissues were separately milled in liquid nitrogen (A11 basic analytical mill, IKA, Staufen, Germany). The cartilage fragments were subsequently sieved through pores of 710 μm . Cells were removed from the tissues by treatment with 10 mM Tris / 1% triton on a roller bench for 24 hours; sonication for 2 hours at 55 \pm 10 kHz and a nuclease solution consisting of 1 U/ml desoxyribonuclease and 1 U/ml ribonuclease in PBS on a roller bench for 72 hours at 37°C. The resulting matrices (from cartilage, meniscus and tendon tissue) were freeze-dried and digested with pepsin (Sigma-Aldrich, St. Louis, Missouri, USA) in a 0.01M hydrochloric acid solution at 37°C on a roller bench, until clear suspensions were obtained. The pH of the solutions was raised to 9.0 for one hour (using 1 M NaOH), in order to irreversibly inactivate the remaining pepsin enzymes²⁵⁸, before adjustment to 7.5 (using 1 M HCl). Next, methacrylic anhydride (Sigma) was added dropwise (2.5 ml per gram matrix) and was allowed to react with the matrices under constant stirring for one hour. The methacrylated tissue-derived matrices (CartMA, MenMA and TendMA) were dialyzed against distilled water for 7 days at 40°C to remove unreacted methacrylic acid and anhydride. After freeze-drying, the tissue digests were dissolved in PBS 10% (w/v),

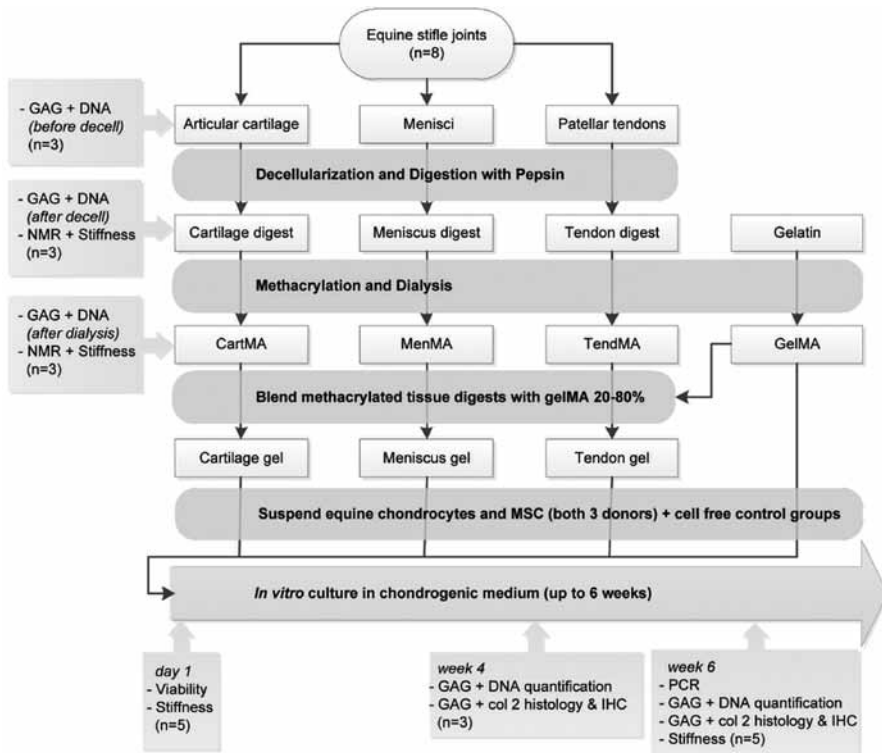


Figure 1. Experimental set-up of the study. n = the number of analyzed samples per donor. GAG = glycosaminoglycans; Col = Collagen; NMR = Nuclear Magnetic Resonance; IHC = Immunohistochemistry.

containing photoinitiator Irgacure 2959 (0.1% (w/v), Ciba, BASF, Ludwigshafen am Rhein, Germany). A schematic overview of the experimental set-up is presented in Figure 1.

Characterization of tissue-derived matrices

Collagen type I (rat tail, BD Biosciences, Bedford, MA, USA), collagen type II (from chicken sternal cartilage, Sigma), meniscus, tendon and cartilage digests (not methacrylated) were electrophoresed on a Bolt 4-12% Bis-Tris Plus gel (Novex, life technologies) under reducing conditions (1.25% 2-mercaptoethanol). The proteins were visualized with Page Blue (Thermo Scientific) and compared to a Multicolor High Range protein ladder (Thermo Scientific). Images were recorded using a Epson perfection 4490 Photo scanner.

The success of the methacrylation procedure was evaluated using proton nuclear magnetic resonance (^1H NMR). ^1H NMR spectra of 10 mg/mL solutions of decellularized cartilage, meniscus and tendon tissue digests, and their methacrylated equivalents (respectively cartMA, menMA and tendMA), were recorded on a Mercury 300 MHz instrument (Varian Associates Inc., NMR Instruments, Palo Alto, CA). Chemical shifts were recorded in ppm with reference to the solvent peak ($\delta = 4.8$ ppm for D_2O).

Blending of tissue digests with GelMA

For cellular differentiation experiments, the methacrylated tissue digests (cartMA, menMA and tendMA), were separately blended with GelMA at 37°C, and will be referred to as the cartilage, meniscus and tendon group, respectively. GelMA was synthesized by reaction of type A gelatin (Sigma) with methacrylic anhydride as described previously^{60,62}. The final composition of the hydrogels was 8% GelMA and 2% tissue digest in 1x PBS (Phosphate-Buffered Saline) with 0.1% photoinitiator (all w/v). GelMA (10% w/v) was used as a control.

Photo-crosslinking of hydrogels

Photo-crosslinking of all hydrogels was performed for 15 minutes in a custom-made Teflon mold (width x height = 4 mm x 2 mm) using 365 nm UV light in a UVP CL-1000L crosslinker (UVP, Upland, California, USA). The crosslinked samples were stored overnight at 37°C in PBS before analyzing the compressive modulus.

Compressive mechanical testing

The compressive modulus of all three uncrosslinked and crosslinked (-MA) tissue digests was measured, and compared to crosslinked GelMA gels (all n=5). The compressive modulus was also measured at day 1 and week 6 of *in vitro* culture for all experimental groups (crosslinked cartilage, meniscus, tendon and GelMA gels, all n=5). Measurements were performed by uniaxial unconfined compression in air at room temperature. Hydrogels and hydrogel-cell constructs were compressed to approximately 20% strain in 2 minutes using a Dynamic Mechanical Analyzer (DMA 2980, TA Instruments, New Castle, DE, USA). The compressive modulus was calculated from the linear derivative of the stress/strain curve at 10-15% strain.

Isolation of equine chondrocytes and MSCs

Full-thickness cartilage was harvested under sterile conditions from the stifle joint of fresh equine cadavers (n=3, age 3-10 years) with macroscopically healthy cartilage and with consent of the owners. After overnight digestion in 0.15% type II collagenase (Worthington Biochemical Corp) at 37°C, the suspension was filtered, stored at -196°C and encapsulated in the hydrogels at passage 1, according to a previously described protocol²⁵⁵.

With approval of the institutional animal ethical committee, bone marrow aspirates were obtained from the iliac crest of healthy horses under general anesthesia (n=3). The mononuclear fraction (MNF) was isolated according to a previously described protocol²⁵⁹. The cells were stored at -196 °C and encapsulated in the hydrogels at passage 3-4. The multilineage potential of cells cultured from the bone marrow aspirates was confirmed by a three-way differentiation assay as previously described^{259,260}.

Viability assay

To evaluate the effect of the addition of the methacrylated tissue digests to GelMA on embedded cells, the viability of chondrocytes and MSCs (both 3 donors) was analyzed on day 1. The cells had been encapsulated in the cartilage, meniscus, tendon and GelMA hydrogels at a concentration of 5×10^6 cells/ml. A LIVE/DEAD Viability Assay (Molecular Probes MP03224, Eugene, USA) was performed according to the manufacturer's instructions. Live and dead cells were counted for 3 samples per time point, at four locations within each construct. Viability was calculated as: (live cells / total cells) x 100.

Cellular differentiation experiments

Equine chondrocytes and MSCs (both 3 donors, 15×10^6 cells/ml) were embedded in the cartilage, meniscus, tendon and GelMA groups. The gels were cultured *in vitro* for up to 6 weeks in chondrogenic differentiation medium. For chondrocyte-laden hydrogels this consisted of DMEM (41965, Invitrogen) supplemented with 0.2 mM L-ascorbic acid 2-phosphate, 0.5% human serum albumin (SeraCare Life Sciences), 1x ITS-X (Invitrogen), 100 units/ml penicillin, 100 µg/ml streptomycin, 25 mM 4-(2-hydroxyethyl)-1-piperazineethanesulfonic acid (HEPES) (Invitrogen) and 5 ng/ml TGFβ-2. MSC-laden samples were cultured in DMEM (31966, Invitrogen) supplemented with 0.2 mM L-ascorbic acid 2-phosphate, 1x ITS+ premix (BD Biosciences, USA), 0.1 µM dexamethasone, 100 units/ml penicillin and 100 µg/ml streptomycin, and 10 ng/ml TGFβ-2 (R&D Systems). Cell free hydrogels cultured for six weeks served as a negative control group.

Histology, immunohistochemistry and biochemistry

After 4 and 6 weeks of culture (3 and 5 replicates respectively), the DNA and glycosaminoglycan (GAG) content was quantified for all donors and groups. To this end, the samples were digested overnight in papain solution (200 µl per sample (0.01 M cysteine, 250 µg/ml papain, 0.2 M NaH₂PO₄ and 0.01 M EDTA) at 60 °C). Total DNA was quantified using the Picogreen DNA assay (Invitrogen) according to the manufacturer's instructions. Total GAG content was determined by photospectrometry at 525 and 595 nm, after reaction with dimethyl-methylene blue using a microplate reader (Biorad). The ratio of both absorbances was calculated and the GAG content was quantified using a chondroitin sulphate (Sigma) standard. The concentrations of GAG and DNA in each papain digest were normalized per donor to the 4-week GelMA control group. GAG/DNA was calculated to display the single cell synthetic activity for the production of cartilage specific matrix.

After 6 weeks of culture, 3 samples from each donor were taken for histology and immunohistochemistry. Samples were dehydrated through a graded ethanol series, cleared in xylene and embedded in paraffin. The samples were sectioned into 5 µm slices and a triple stain of hematoxylin (Klinipath BV, Duiven, The Netherlands) fast green, and

Safranin-O (Merck) was applied to identify GAG deposition. The stained sections were examined using a light microscope (Olympus BX51).

Collagen type II was stained by immunohistochemistry after deparaffinization and rehydration of the sections, according to a previously described protocol²⁵⁵ (primary antibody: 1:100, monoclonal mouse, II-II6B3, Developmental Studies Hybridoma Bank (DSHB); secondary antibody: 1:200, Po447, Dako). Isotype controls were performed by using mouse isotype IgG1 monoclonal antibody at concentrations similar to those used for the stainings.

Gene expression

After six weeks of culture, the samples were homogenized in TRIzol reagent (Invitrogen). The best-performing chondrocyte and MSC donors were selected for PCR-analysis, based on a safranin-O staining of the GelMA control groups at week six. The RNA was isolated according to the manufacturer's guidelines (chloroform was substituted by 3-bromo-chloropropane²⁶¹). RNA was cleared of any DNA contamination by DNase digestion. Total RNA yield was determined spectrophotometrically (NanoDrop ND1000, Isogen Life Science, De Meern, The Netherlands) and 500 ng total RNA per sample was reverse transcribed into complementary DNA (cDNA) using Superscript III (Invitrogen) and random primers. SybrGreenTM quantitative real-time PCR was subsequently performed on an iQ-5 real time PCR detection system (Bio-rad laboratories, Hercules, CA, USA). Each sample was run in duplicate and a three-fold serial dilution of pooled cDNA was used as a standard curve.

Primers were designed using computer software (primer BLAST, <http://www.ncbi.nlm.nih.gov/tools/primer-blast>) and obtained from Eurogentec (Maastricht, The Netherlands). The specific genes of interest were collagen type IA₁ (COL1A1), collagen type IIA₁ (COL2A1), aggrecan (ACAN), matrix metalloproteinases -3 (MMP-3), -13 (MMP-13) and -14 (MMP-14). Hypoxanthine-guanine-phosphoribosyltransferase 1 (HPRT-1) and signal recognition particle 14 kDa (SRP-14) were selected as reference genes. Following fold-change calculation using the standard curve method, the geometric mean of these two reference genes was used to calculate the normalised mRNA expression of each target gene. Primer sequences of selected genes are provided in Supp. Table 1.

Statistical analysis

An independent samples T-test, assuming unequal variances, was performed to compare the DNA and GAG content of the tissues before and after the decellularization protocol and also to compare the stiffness of crosslinked and uncrosslinked cell-free hydrogels. A Univariate Analysis of Variance with a Tukey HSD post-hoc test was performed to compare GAG, DNA, GAG/DNA and the compressive modulus between the groups of the cell culture experiments. Because the level of matrix formation differed

significantly between the cell donors, a randomized block design was used, correcting for donor effects. GAG and DNA were normalized to the GelMA control group at week 4 for each separate cell donor; the compressive modulus was normalized to GelMA day 1. The statistical analyses were done using SPSS statistics (IBM, version 20). For the PCR data, Kruskal Wallis and Dunn's multiple comparison post-hoc tests were used to test differences between experimental conditions for each primer pair using Graphpad software (Graphpad Prism version 5.2 for Windows). Differences were considered significant when $P < 0.05$ for all tests.

RESULTS

Decellularization procedure

The DNA content of the cartilage, meniscus and tendon tissues decreased significantly after decellularization, to values below $50 \mu\text{g}/\text{mg}$ dry weight (Fig. 2a). The DNA content was unaltered by the subsequent dialysis. The GAG content of all three tissues showed large variations between donors and/or sample location (Fig. 2b). Yet, the variation, as well as the absolute GAG content decreased considerably after the decellularization procedure and remained unaltered after dialysis. $58 \pm 10\%$ of methacrylated and decellularized material could be obtained from the original tissues (expressed in dry weight).

Characterization of tissue-derived matrices

The decellularized cartilage, meniscus and tendon matrices were successfully digested with pepsin enzymes until clear or close to clear solutions were obtained. Short treatment of the tissue particles (cartilage) or fibers (meniscus and tendon) with pepsin resulted in viscous substances, whereas overnight treatment resulted in low-viscosity solutions. Overnight digestion was used to facilitate the methacrylation procedure. Gel electrophoresis showed that all digested tissues consisted of polymers with a molecular weight predominantly in the range of 130-300 kiloDaltons (kDa) (Fig. 3a). The profile of the collagen I solution reflects the collagen monomers (two subunits), dimers (two subunits) and trimers. This typical profile can also be observed in the tendon and meniscus digests. The collagen type II control only displays monomers with one subunit. This single unit monomer can also be found in the cartilage digest. Successful methacrylation of the solutions was confirmed with NMR by the double peak that emerged between 5 and 6 ppm after methacrylation of all three tissue digests (Fig. 3b-g). Comparing the stiffness of methacrylated tissue digests (cartMA, menMA and tendMA) with GelMA and non-methacrylated tissue digests revealed significant variations (Fig. 4). CartMA was stiffer than all other groups ($66.2 \pm 11.9 \text{ kPa}$, $P < 0.05$) and GelMA was stiffer ($33.8 \pm 6.5 \text{ kPa}$, $P < 0.05$) compared to menMA ($15.1 \pm 5.4 \text{ kPa}$) and tendMA ($11.4 \pm 0.6 \text{ kPa}$). The

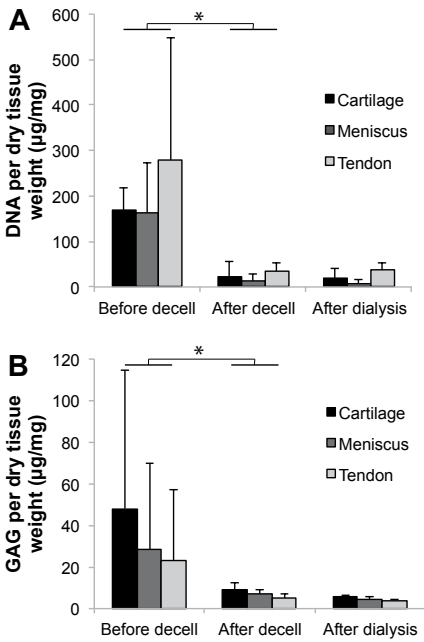


Figure 2. The effect of the decellularization protocol on DNA and glycosaminoglycan (GAG) content of equine cartilage, meniscus and tendon tissues. (a) The DNA content of all tissues was significantly reduced by the decellularization protocol. **(b)** The GAG content of all tissues directly after harvesting from the knee joint (before decell) shows large standard deviations, caused by donor and location variations. The subsequent decellularization procedure significantly reduced and standardized the GAG contents.

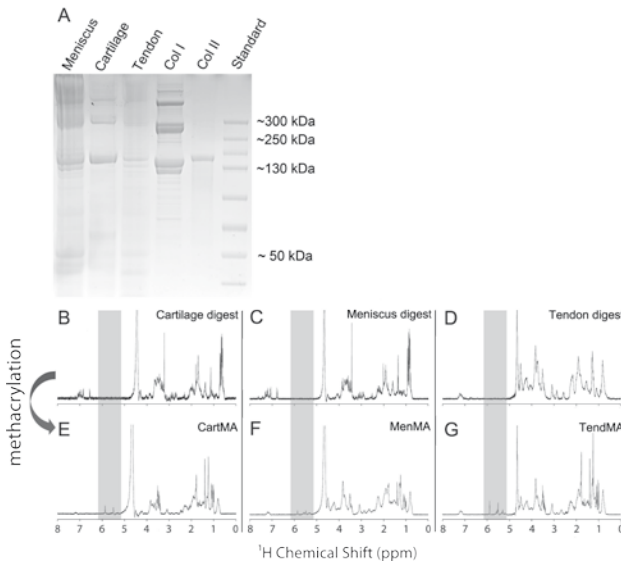


Figure 3. Characterization of tissue-derived matrices. (a) Protein gel of tissue digests, collagen type I and II. **(b-d)** Nuclear Magnetic Resonance (NMR) of the tissue digests shows an inhomogeneous tissue profile after the decellularization procedure, reflecting the natural polymers. **(e-g)** The two peaks that appeared after methacrylation (shaded area, between 5-6 ppm) show the presence of vinyl protons, and confirm the success of the methacrylation procedure.

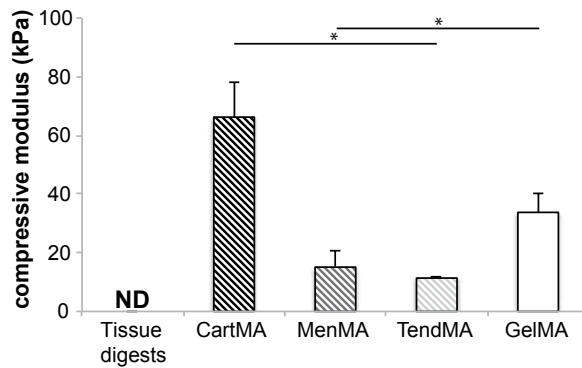


Figure 4. Compressive modulus of photocrosslinked 10% hydrogels. Non-methacrylated tissue digests were not crosslinkable and hence their compressive modulus could not be determined (ND). The compressive modulus of crosslinked tissue digests (cartMA, menMA and tendMA) and GelMA varied significantly.

non-methacrylated tissue digests remained low-viscosity solutions after treatment with UV-light and, therefore, their stiffness could not be determined. Considering the variable degree of stiffness and in order to functionalize the existing GelMA hydrogel platform, the methacrylated tissue digests were blended with GelMA for the cellular differentiation experiments.

Viability and cartilage matrix formation by embedded chondrocytes

Encapsulation of chondrocytes resulted in high viability at day 1 in all tissue derived matrix hydrogels (Fig 5a). During *in vitro* culture, the tendon samples rapidly disintegrated for all chondrocyte donors and could, therefore, not be included in the differentiation analysis. GelMA gels had a higher stiffness 1 day after cell encapsulation compared to the cartilage, meniscus and tendon groups (Fig 5b). A comparable pattern was observed after 6 weeks of culture. The DNA and GAG content and GAG/DNA of hydrogels was comparable for all groups after 4 weeks, but was significantly higher in the GelMA group compared to cartilage and meniscus after 6 weeks (Fig 5c-e). The absolute GAG content in the GelMA control samples was $1.17 \pm 0.28 \mu\text{g}/\text{mg}$ wet weight after 4 weeks and increased to $2.73 \pm 2.13 \mu\text{g}/\text{mg}$ after 6 weeks of culture. GAG and DNA in all experimental groups were significantly higher than the cell free control samples. The superior cartilage-specific matrix formation after 6 weeks in the GelMA group was confirmed by histology for GAGs (Fig. 5f) and immunohistochemistry for collagen type II (Fig 5g). The differences between the experimental groups at week 4 were comparable to week 6. Therefore only week 6 data were presented for both cell types. The cell free cartilage gels contained no significant traces of GAGs and collagen type II after 6 weeks.

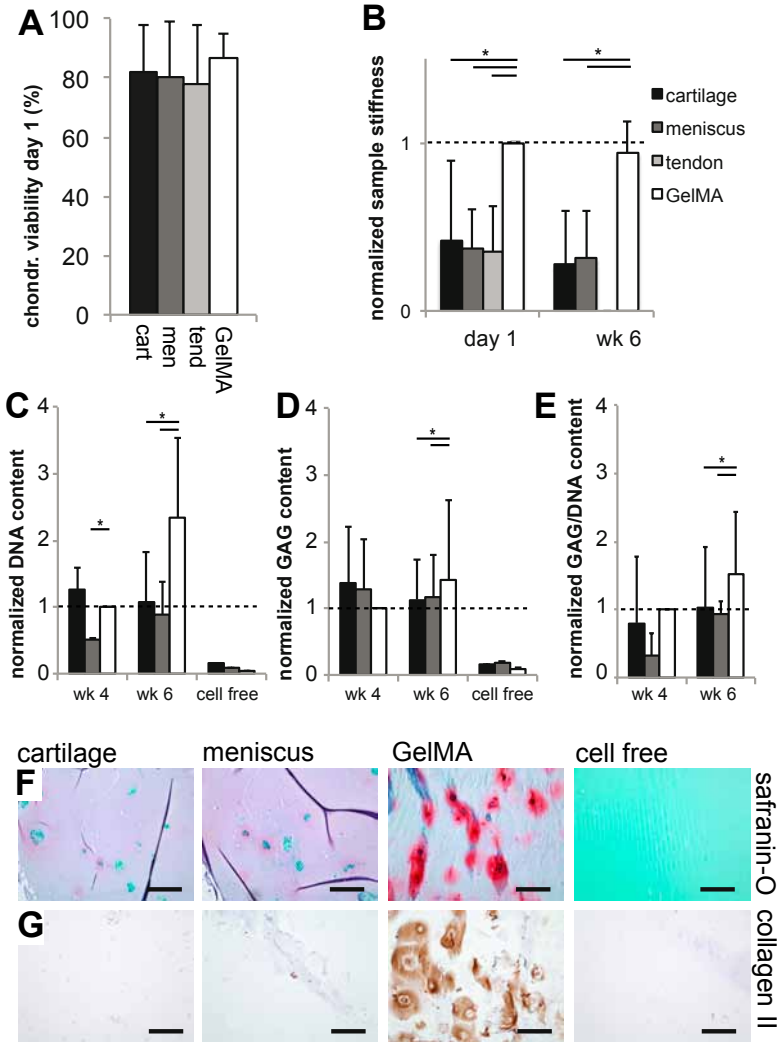


Figure 5. Survival and chondrogenic differentiation of chondrocytes embedded in the tissue-derived matrix gels. (a) The cartilage, meniscus and tendon gels were not cytotoxic for embedded chondrocytes; (b) the stiffness of the tissue-derived hydrogels was lower than GelMA directly after encapsulation (day 1) and after 6 weeks of culture; (c-e) the DNA, GAG and GAG/DNA values after 6 weeks of culture were lower in both experimental groups compared to the GelMA group; (f) GAG formation (red) and (g) collagen type II content (brown) were superior in the GelMA group after 6 weeks. The tendon group disintegrated during culture of chondrocytes and is therefore not displayed for GAG and DNA content. The DNA, GAG and GAG/DNA content were normalized per donor to GelMA week 4; sample stiffness was normalized to GelMA day 1. All scale bars are 200 μm ; "cell free" sample is cartilage gel.

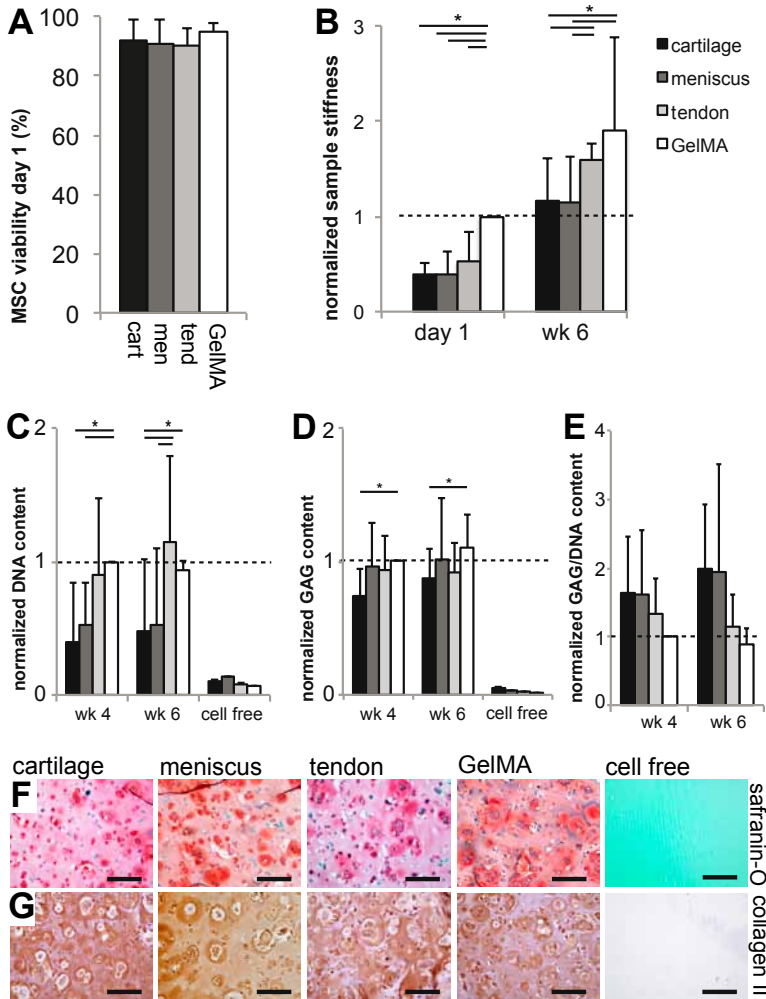


Figure 6. Survival and chondrogenic differentiation of MSCs embedded in the tissue-derived matrix gels. (a) The cartilage, meniscus and tendon gels were not cytotoxic for embedded MSCs; (b) directly after encapsulation of the MSCs (day 1), the stiffness of GelMA samples was highest; after 6 weeks of culture, GelMA as well as the tendon group were stiffer; (c-d) differences were observed in the DNA and GAG content of the experimental groups; (e) GAG/DNA content was higher in the cartilage and meniscus gels, although this difference was not statistically significant; (f) GAGs (red) and (g) collagen type II (brown) localization in all groups after 6 weeks. The DNA and GAG content were normalized per donor to GelMA week 4; sample stiffness was normalized to GelMA day 1. All scale bars are 200 μ m; "cell free" sample is cartilage gel.

Viability and cartilage matrix formation by embedded MSCs

MSCs in all experimental groups retained a high viability one day after encapsulation in the hydrogels (Fig. 6a). The stiffness of GelMA gels was highest one day after encapsulation of the MSCs (Fig. 6b). GelMA and tendon gels showed superior stiffness after 6 weeks of cell culture. The DNA content was higher in the tendon and GelMA gels compared to the cartilage and meniscus gels, both after 4 and 6 weeks of culture (Fig. 6c). A comparable amount of GAG was measured for all groups; only the cartilage gels had a statistically lower amount than the GelMA group (Fig. 6d). The absolute GAG content in the GelMA control samples was $3.48 \pm 3.62 \mu\text{g}/\text{mg}$ wet weight after 4 weeks and $3.82 \pm 4.38 \mu\text{g}/\text{mg}$ after 6 weeks of culture. The GAG/DNA values for the cartilage and meniscus gels were larger than found in the GelMA group (due to a lower DNA content in cartilage and meniscus gels), although these differences were not statistically significant. Staining of GAGs and collagen type II showed abundant cartilage-specific matrix formation by MSCs in all groups (Fig. 6f, g).

Gene expression levels

The poor interaction of the chondrocytes with the various tissue cultures (Fig. 5) led to insufficient RNA yields in the cartilage and meniscus groups (the tendon group having disintegrated and not being available for that reason), so that the chondrocytes were

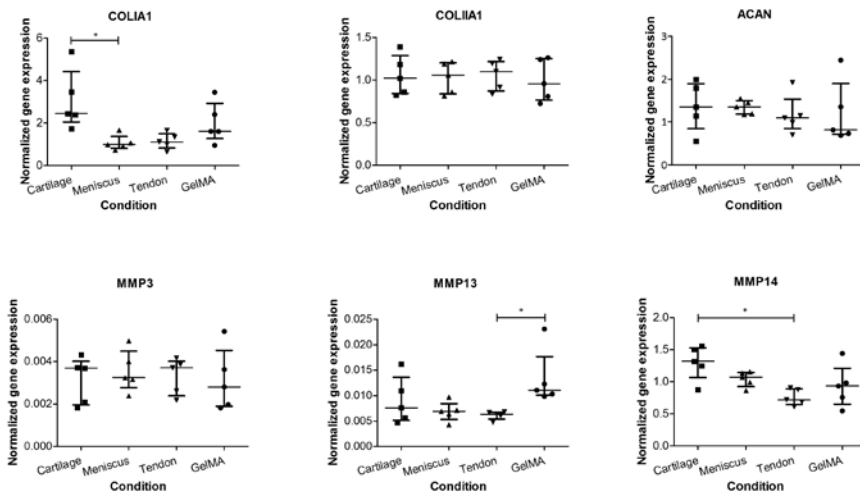


Figure 7. Gene expression by MSCs in tissue-derived matrix gels. Gene expressions for aggrecan and collagen type II were similar in all hydrogels cultured with MSCs. Collagen I expression was higher in the cartilage hydrogel compared to meniscus. MMP-3 expression was similar in all cultures, whereas expression of MMP-13 and MMP-14 was lower in tendon gels compared to GelMA and cartilage respectively. Separate data points were presented ($n=5$) including the median and interquartile range.

excluded from the gene expression analysis. In contrast, the RNA yields of MSCs were sufficient for all samples. ACAN, as well as COL2 expression was similar for all experimental groups (Fig. 7). The expression of COL1A1 was significantly lower in meniscus than in cartilage gels. Catabolic enzyme MMP-13 and MMP-14 expression was significantly lower in the tendon group compared to GelMA and the cartilage group respectively. These were the only target genes for which a significant difference existed between the experimental conditions.

DISCUSSION

In this study, crosslinkable hydrogels were created, based on matrix derived from cartilage, meniscus and tendon tissues. These substrates allowed for the biological functionalization of the existing GelMA hydrogel system, in which they influenced the quantity and quality of matrix produced by embedded cells. All tissue types negatively influenced outcomes for chondrocytes, whereas encapsulated MSCs exhibited variable differentiation patterns, depending of the type of tissue the matrix gel was derived from.

To our knowledge, this is the first report in which decellularized tissues are covalently crosslinked into stable hydrogels. Previously, the Badylak group has derived hydrogels from the extracellular matrix of the dermis, urinary bladder and the central nervous system^{70,71,249}. These hydrogels allowed for the infiltration and adhesion of cells and influenced their differentiation. In addition, hydrogels derived from heart, cartilage and adipose were recently shown capable of supporting tissue formation by embedded cells⁷⁷. Analogous to our work, the hydrogels were obtained by pepsin digestion of the respective tissues. However, only physical crosslinking of the natural polymers was accomplished, resulting in considerable contraction of the hydrogel constructs during culture. This behavior is comparable to other natural polymer networks like collagen gels and fibrin glue^{27,262,263}. The resulting shape instability, however, is unfavorable for the sustainable filling and regeneration of a tissue defect, especially for load-bearing tissues such as cartilage. We have now successfully overcome this issue by covalent crosslinking of the matrix-derived hydrogels through the addition of methacrylamide groups. These substrates were subsequently incorporated into GelMA hydrogel, because we aimed to further develop this versatile hydrogel, which was proven efficient for cartilage matrix formation by embedded cells^{60,63,255}. The methacrylation procedure resulted in a very substantial increase in the compressive modulus, which was largest in the cartilage-derived matrix and of the same order of magnitude as occurring in the GelMA reference matrix. The methacrylation procedure can hence be considered as an important asset in the production of extracellular matrices for tissues that have to withstand biomechanical forces.

The chondrogenic potential of MSCs in extracellular matrix gels was greater than that of chondrocytes. MSCs have previously shown capable of forming a cartilage specific matrix in 3D-hydrogel systems²⁶⁴. The quality and quantity of cartilaginous tissue formed by MSCs was found comparable to that of chondrocytes, although dependent of the type of hydrogel²⁶⁵. From our work we can conclude that equine MSCs thrive relatively well in GelMA gels. Nevertheless, chondrocytes from the different donors did show less donor variation than the MSCs, which is a known phenomenon for the latter cell type²⁶⁶. Still, MSCs are of great interest as an allogeneic cell source for the single-stage repair of cartilage tissue²⁴. A limitation for the application of MSCs *in vivo* is that they require the addition of growth factors to be directed toward the chondrogenic lineage²⁶⁰. Recently, chondrocytes have shown capable of guiding MSC differentiation, and therefore, a co-culture of MSCs and chondrocytes holds promise for the repair of cartilage tissue²⁴.

The absolute GAG production by chondrocytes embedded in the GelMA hydrogels is similar to the amounts reported in previous *in vitro* studies^{60,63}. However, a consistent negative effect of the incorporation of all three tissue-derived components was observed on the differentiation of chondrocytes. This is in line with previous reports on the culture of chondrocytes on collagen matrices^{74,251,252}. Collagen type II matrix induces catabolic pathways in cultured articular chondrocytes, including the upregulation of MMP-3, -13 and -14^{251,252}. In addition, earlier work from our group showed poor GAG production of chondrocytes cultured on decellularized cartilage matrix scaffolds (collagen type II) and even accelerated degradation of the scaffolds⁷⁴. In the current work, scaffold (*i.e.* hydrogel) disintegration was observed only for the tendon hydrogels (collagen type I), which may be a result of the catabolic activities of the chondrocytes, analogous to those observed in osteoarthritis^{267,268}. Unfortunately, we were unable to analyze MMP expression by chondrocytes, since the tendon gels had disintegrated and RNA yield was too low in the cartilage and meniscus groups. In contradiction to these findings, successful cultures of chondrocytes were shown on synthetic collagen type I and II matrices²⁶⁹⁻²⁷². The literature is thus inconclusive about the effect of collagen matrices on chondrocyte behavior, although the upregulation of inflammatory pathways has been clearly indicated.

In interpreting cell-matrix interactions, the difference between pure collagen scaffolds and tissue-derived matrices should be taken into account. In the latter, other matrix components, growth factors and/or signaling molecules may contribute to effects on cell behavior^{68,244}. For example, it was shown that several growth factors were retained in decellularized bladder submucosa matrix²⁷³ and small intestinal submucosa matrix²⁷⁴. The decellularization protocol in the current study was relatively mild compared to previous studies⁶⁷. Therefore, a panel of growth factors is likely to be retained within the matrix, although this was not specifically studied here. The main components of the tissue-derived matrices were shown to be collagens type I and II, the proportions

depending on the original tissue. However, the exact biochemical composition of the polymers, for example the amount of available reactive amines to be methacrylated, remains unknown. As a result, the degree of methacrylation of the tissue-derived matrices was not controlled, and will hence vary between tissue types and tissue donors. This limitation should be taken into account during the interpretation of the responses of embedded cells.

The absence of trypsin as a protein-cleaving enzyme in the current protocol lead to the preservation of some of the GAGs (ca. 10%, compared to 0% when treated with trypsin⁷⁴) while the DNA content could be decreased to acceptable standards, *i.e.* below 50 µg/mg dry tissue⁶⁷. Chondrocytes probably benefit more from GAG- than collagen components in hydrogel cultures^{60,63}. Therefore, the current outcomes could be improved by a modified decellularization protocol, preserving still more GAGs.

For the chondrogenic differentiation of MSCs, our results show a slight preference for a collagen type I rich matrix (tendon gels) over collagen type II (cartilage gels). For example, MSCs proliferated more in tendon and GelMA gels and the sample stiffness was higher after culture, compared to meniscus and cartilage gels. In addition, MSCs in the tendon gels showed reduced expression of MMP-13 and -14, although gene expression of cartilage-specific matrix genes was similar. Recently, Yang *et al.* also analyzed the effects of tendon-derived matrix on MSCs and found a reduced expression of collagen type I, which is considered a marker for inferior fibrocartilage formation²⁶³. The lowest GAG production by MSCs was observed in the cartilage matrix gels, along with a higher gene expression of collagen type I. Previous research however revealed a stimulatory effect of cartilage matrix on the chondrogenic differentiation of MSCs *in vivo*^{275,276}. In addition, other work showed that chondrogenesis of bovine MSCs was slightly enhanced in collagen type II compared to collagen type I gels²⁷⁷. It appears that certainly collagens influence the differentiation of MSCs, yet the optimal collagen composition still needs to be unraveled and will require specific tailoring for the target tissue to be engineered.

Further research should identify the specific biological cues in native tissues that are favorable to cells in tissue engineering. Unfortunately, the specific factors responsible for the cell behavior in decellularized tissues are still largely unknown. A better understanding of the native cell niche can guide the process of producing biomimetic materials.

CONCLUSION

Crosslinkable hydrogels were created from cartilage, meniscus and tendon tissue through a process that included enzymatic digestion and methacrylation. The methacrylation procedure successfully increased the stiffness of these matrices, which is a critical factor in the manufacturing of scaffolds for use in musculoskeletal tissue repair.

Moreover, a stable hydrogel platform was created by covalent incorporation of these tissue-derived matrices in versatile GelMA hydrogels. The response of embedded cells to these matrices depended on the cell type and the matrix components. Chondrocytes performed relatively poor in the tissue-derived matrix gels compared to the GelMA control group. The chondrogenic differentiation capacity of MSCs was comparable across all hydrogels.

ACKNOWLEDGEMENTS

The authors would like to thank Karin van Leersum and Trudy van Ruiten for their assistance in the experimental work. The antibody against collagen type II (II-II6B3), developed by T.F Linsenmayer, was obtained from the DSHB developed under the auspices of the NICHD and maintained by The University of Iowa, Department of Biology, Iowa City, IA 52242. Jetze Visser was supported by a grant from the Dutch government to the Netherlands Institute for Regenerative Medicine (NIRM, grant n°FES0908) and Jos Malda was supported by the Dutch Arthritis Foundation.

Supplementary Table 1. Names, symbols and primer sequences of selected genes for qRT-PCR analysis. For each primer pair, the top sequence denotes the forward primer and the bottom sequence the reverse.

Gene name	Gene symbol	Primer sequence
Collagen type I A1	COL1A1	5'-AGCCAGCAAGATCGAGAACAT-3' 5'-CGTCTCCATGTTGAGAAGA-3'
Collagen type II A1	COL2A1	5'-GGCAATAGCAGTTACGTACA-3' 5'-CGATAACAGTCTTGCCCCACTT-3'
Aggrecan	ACAN	5'-AAGACAGGGTCTCGCTGCCAA-3' 5'-ATGCCGTGCATCACCTCGCA-3'
Matrix metalloproteinase-3	MMP-3	5'-TTTTGGCCATCTTCTTCA-3' 5'-TGTGGATGCCTTTGGGTATC-3'
Matrix Metalloproteinase-13	MMP-13	5'-CAAGGGATCCAGTCTCTATGGT-3' 5'-GGATAAGGAAGGGTCACATTTGTC-3'
Matrix Metalloproteinase-14	MMP-14	5'-GGACTGTCCGGAATGAGGATCT-3' 5'-TTGGAATGCTCAAGGCCCA-3'
Hypoxanthine-guanine-phosphoribosyltransferase 1	HPRT-1	5'-TGGACAGGACTGAACGGCTTGC-3' 5'-GCAGGTCAGCAAAGAATTTATAGCCCC-3'
Signal recognition particle 14 kDa	SRP-14	5'-TGCTGGAGAGCGAGCAGTTCT-3' 5'-AGCCCTCCACGGAACCTTTCCT-3'

Chapter 4

Endochondral Bone Formation in Gelatin Methacrylamide Hydrogel with embedded Cartilage-Derived Matrix Particles

Jetze Visser
Debby Gawlitta
Kim E.M. Benders
Selynda M.H. Toma
Behdad Pouran
P. René van Weeren
Wouter J.A. Dhert
Jos Malda

Biomaterials. 2015 Jan;37:174-182

ABSTRACT

The natural process of endochondral bone formation in the growing skeletal system is increasingly inspiring the field of bone tissue engineering. However, in order to create relevant-size bone grafts, a cell carrier is required that ensures a high diffusion rate and facilitates matrix formation, balanced by its degradation. Therefore, we set out to engineer endochondral bone in gelatin methacrylamide (GelMA) hydrogels with embedded multipotent stromal cells (MSCs) and cartilage-derived matrix (CDM) particles. CDM particles were found to stimulate the formation of a cartilage template by MSCs in the GelMA hydrogel *in vitro*. In a subcutaneous rat model, this template was subsequently remodeled into mineralized bone tissue, including bone-marrow cavities. The GelMA was almost fully degraded during this process. There was no significant difference in the degree of calcification in GelMA with or without CDM particles: $42.5 \pm 2.5\%$ vs. $39.5 \pm 8.3\%$ (mean \pm standard deviation), respectively. Interestingly, in an osteochondral setting, the presence of chondrocytes in one half of the constructs fully impeded bone formation in the other half by MSCs. This work offers a new avenue for the engineering of relevant-size bone grafts, by the formation of endochondral bone within a degradable hydrogel.

INTRODUCTION

Engineering bone through the endochondral pathway has gained increased attention over recent years²⁵⁹. This approach is based on our growing knowledge on the formation of long bones in the developing embryo²⁷⁸ and on the bone fracture healing process²⁷⁹. The formation of long bones starts with the condensation of mesenchymal stromal cells (MSCs), which then differentiate into chondrocytes. These chondrocytes secrete a cartilage-specific matrix, rich in collagen type II and glycosaminoglycans (GAGs). In a terminal hypertrophic differentiation process, the chondrocytes subsequently recruit a mixture of cells that is responsible for the ossification and vascularization of the cartilage template²⁸⁰. Thus, the hypertrophic chondrocyte is the director of the development of long bones in the human body.

Bone tissue engineering, however, has traditionally focused on mimicking the intramembranous pathway^{281,282}. This process is more straightforward than endochondral ossification and naturally occurs in, for example, the formation of the flat bones of the skull²⁷⁸. A major drawback to this approach for the repair of large bone defects is the limited size of the engineered tissues²⁸¹. Large engineered bone constructs require rapid vascularization in order to provide cells in the core of the construct with sufficient oxygen and nutrients. A co-culture of osteogenic and vascular progenitor cells or the engineering of advanced prevascularized constructs may offer solutions^{185,281,283}. Alternatively, the endochondral approach could overcome this limitation as chondrocytes thrive well in hypoxic conditions^{284,285}. Also, the natural healing of bone fractures relies on endochondral ossification within the fracture callus²⁷⁹. In this context, chondrogenically pre-differentiated MSC aggregate cultures have shown capable of recapitulating the process of endochondral bone formation *in vivo*²⁸⁶⁻²⁸⁸. Moreover, these hypertrophic cell aggregates and cartilage grafts stimulated endochondral bone formation in segmental bone defects^{289,290}.

To increase the size of the endochondral bone forming constructs, a scaffold may be required as a carrier for cells or cell aggregates, as recently shown for biodegradable polymer or organic scaffold materials^{288,291,292}. We additionally developed cartilage-derived matrix (CDM), obtained by the decellularization of cartilage tissue^{69,74}. Following this process, CDM consists of predominantly collagen type II, in the absence of GAGs and cells. Biochemical cues are supposedly retained in this decellularized biomaterial that can direct the differentiation of cells⁶⁹. We have recently shown that these CDM scaffolds are suitable templates for *in vitro* cartilage matrix formation by seeding MSCs⁷⁴. Nevertheless, hydrogels may be preferred over dry, (in)organic scaffolds, since their degradation profile is tailorable, biochemical cues can easily be incorporated to direct cell fate⁷⁹ and they allow for the fabrication of multiphasic constructs^{246,293}.

Ideally, the hydrogel facilitates the proliferation and condensation of cells, the formation of a cartilage template and subsequent remodeling into bone. Gelatin methacrylamide (GelMA) hydrogel could be a suitable substrate, given the extensive cartilage matrix formation we previously observed in this gel^{60,63}. GelMA hydrogels are enzymatically degradable and tunable for specific regenerative applications through modification of the degree of methacrylation and the polymer concentration^{60,257,294}. For example, besides cartilage regeneration, functional vascular networks could be established in GelMA gels⁶⁴.

The objective of this study was to engineer relevant-size bone tissue equivalents via the endochondral pathway in a composite of GelMA hydrogel with CDM particles. This composite biomaterial was created in order to benefit from the biological activity of the CDM, while retaining the versatility of the GelMA system. We evaluated *in vitro* cartilage matrix formation by MSCs embedded in GelMA/CDM and subsequent *in vivo* endochondral bone formation in an ectopic rat model. Chondrocytes in GelMA with and without CDM particles served as a control group. In addition, bone formation by MSCs was studied in bilayered constructs with chondrocytes in the cartilage layer to evaluate the potential of GelMA for osteochondral tissue formation.

MATERIALS AND METHODS

Experimental set-up

The objective was to evaluate endochondral bone formation in GelMA hydrogel with embedded equine CDM particles. To determine the optimal concentration of equine CDM particles in the hydrogel, the effect of various concentrations of CDM particles

Sample	CDM	<i>In vitro</i> 3 donors; replicates (n)	<i>In vivo</i> 1 donor; replicates (n)
GelMA	-	-	3
GelMA	+	-	3
GelMA + chondrocytes	-	3	6
GelMA + chondrocytes	+	3	-
GelMA + MSCs	-	3	6
GelMA + MSCs	+	3	6
GelMA bilayered: chondrocytes/MSCs	-	-	6

Table 1. Experimental set-up. The chondrogenic differentiation capacity of chondrocytes and MSCs, and the effect of CDM particles in GelMA were tested *in vitro*. Subsequently, chondrogenesis and endochondral bone formation were evaluated subcutaneously in rats. Samples were implanted for eight weeks.

on the GelMA mechanical properties was tested. Chondrogenesis was assessed as the cartilage-specific matrix formation by equine chondrocytes and MSCs in *in vitro* cultures for up to six weeks (Table 1). Both cell types were incorporated in GelMA with and without CDM particles (CDM + and CDM - respectively). After eight weeks of subcutaneous implantation in rats, the same groups were evaluated for chondrogenesis and endochondral bone formation *in vivo*. In addition, bilayered samples were implanted to assess the effect of chondrocytes on the endochondral bone forming capacity by MSCs.

Production of CDM particles

Full-thickness cartilage was harvested from cadaveric stifle joints (knee) of healthy equine donors (age 3-10 years) that had been euthanized for reasons other than joint disease, with consent of the owners. The cartilage was pooled and decellularized according to a protocol adapted from Benders *et al.*⁷⁴. In short, after washing the cartilage slices in phosphate-buffered saline (PBS), they were snap-frozen in liquid nitrogen and lyophilized overnight. Then, cartilage was milled in liquid nitrogen (A11 basic analytical mill, IKA, Staufen, Germany) for a few minutes in order to increase exposure to the following chemical treatments, which were all performed on a shaker plate at 2,000 rpm. The cartilage particles were treated with six cycles of 0.25% trypsin-EDTA (Invitrogen) at 37°C for 48 hours in total. The particles were then washed in PBS and underwent a 4-hour treatment with a nuclease solution of 50 U/ml deoxyribonuclease (Sigma) and 1 U/ml ribonuclease A (Sigma) in 10 mM Tris-HCl (pH 7.5), at 37°C. Next, the particles were treated with 10 mM hypotonic Tris-HCl for 20 hours followed by 1% (v/v) Triton X-100 in PBS for 24 hours, both at room temperature. The particles were thoroughly washed in PBS in 6 cycles for 48 hours in total, in order to remove all enzymatic agents. The suspension of cartilage particles in PBS was lyophilized overnight and the pellet was milled again in liquid nitrogen and sieved through pores of 300 µm. The length and width of the CDM particles was measured from 2D light microscope images with ImageJ software (1.46r, National Institutes of Health, USA).

Isolation of equine chondrocytes and multipotent stromal cells

Macroscopically healthy full-thickness cartilage was harvested under sterile conditions from the stifle joint of fresh equine cadavers (n=3, age 3-10 years) with consent of the owners. After fragmentation and overnight digestion in type II collagenase (Worthington Biochemical Corp) at 37°C, the suspension was filtered through a 100 µm cell strainer, washed in PBS and stored in liquid nitrogen at -196°C in culture medium (Dulbecco's Modified Eagle Medium (DMEM) 41965, Invitrogen) supplemented with 20% heat-inactivated fetal bovine serum (FBS, Biowhittaker) and 10% dimethylsulfoxide (DMSO (Merck, Darmstadt, Germany)). Upon thawing, the chondrocytes were seeded at a density of 5×10^3 cells/cm² and expanded for 10-12 days in a monolayer culture in chondrocyte

expansion medium consisting of DMEM, 10% FBS, 100 units/ml penicillin and 100 µg/ml streptomycin (Invitrogen), and 10 ng/ml FGF-2 (R&D Systems) and embedded in GelMA at passage 1.

With approval of the local animal ethical committee, a bone marrow aspirate from the sternum was obtained from healthy, living equine donors (n=3, age 3-10 years). The mononuclear fraction (MNF) was isolated by centrifuging the sample on Ficoll-Paque (Sigma). The MNF was seeded at a density of 2.5×10^5 cells/cm² and expanded in a monolayer culture till sub-confluency in MSC expansion medium containing α -MEM (22561, Invitrogen) complemented with 10% heat-inactivated FBS, 0.2 mM L-ascorbic acid 2-phosphate (Sigma), 100 units/ml penicillin and 100 µg/ml streptomycin, and 1 ng/ml FGF-2 and embedded in GelMA in passages 3-4.

The multilineage potential of the cells that were cultured from the bone marrow aspirate was investigated by a three-way differentiation assay as previously described^{174,260,295}.

Preparation of GelMA with CDM particles and cells

GelMA was synthesized by reaction of porcine type A gelatin (Sigma-Aldrich, St. Louis, Missouri, USA) with methacrylic anhydride (Sigma-Aldrich) at 50 °C for one hour, as previously described^{60,62}. In short, methacrylic anhydride was added dropwise to a 10% solution of gelatin in PBS under constant stirring. To achieve a high degree of functionalization, 0.6 g of methacrylic anhydride was added per gram of gelatin. The functionalized polymer was dialyzed against distilled water for 7 days at 40 °C to remove methacrylic acid and anhydride, neutralized to pH 7.4 with 10% sodium bicarbonate (Merck, Darmstadt, Germany), freeze-dried and stored at -20 °C until use. This protocol results in a degree of functionalization of circa 75%⁶⁰.

Defrosted GelMA was dissolved in PBS at 70°C at a concentration of 10% (w/v) containing a photoinitiator Irgacure 2959 (Ciba, BASF, Ludwigshafen am Rhein, Germany) at a final concentration of 0.1% (w/v). The CDM particles were mixed (in various concentrations, see section 2.5) in the GelMA with a positive displacement pipet. Then chondrocytes or MSCs were suspended in the hydrogel at a concentration of 5×10^6 cells/ml for the viability assay and at a concentration of 20×10^6 cells/ml for the *in vitro* and *in vivo* differentiation analyses. For mechanical analyses, cylindrical GelMA samples of 1.3 mm height and 8-9 mm diameter were UV-crosslinked at an intensity of 180 mW/cm² (350-450 nm, Höppler UV technology, Munich, Germany). For all other assays, the cell- and CDM-laden GelMA was crosslinked for 15 minutes in a custom-made air-sealed Teflon mold (sample size ca. 8x8x2 mm) using 365nm light in a UVP CL-1000L crosslinker (UVP, Upland, California, USA).

Chondrocyte-laden samples were cultured *in vitro* in chondrogenic differentiation medium (DMEM (41965, Invitrogen) supplemented with 0.2 mM L-ascorbic acid 2-phosphate, 0.5% human serum albumin (SeraCare Life Sciences), 1x ITS-X (Invitrogen), 100

units/ml penicillin and 100 µg/ml streptomycin, 25 mM 4-(2-hydroxyethyl)-1-piperazineethanesulfonic acid (HEPES) (Invitrogen) and 5 ng/ml TGF-β2) and MSC-laden samples were cultured in MSC chondrogenic differentiation medium (DMEM (31966, Invitrogen) supplemented with 0.2 mM L-ascorbic acid 2-phosphate, 1x ITS+ premix (BD Biosciences, USA), 0.1 µM dexamethasone (Sigma-Aldrich), 100 units/ml penicillin and 100 µg/ml streptomycin, and 10 ng/ml TGFβ-2 (R&D Systems)). *In vitro* culture was done in three replicates per donor for 1 and 14 days for the viability assay and for four and six weeks for *in vitro* differentiation. Two weeks pre-culturing was performed for the *in vivo* differentiation study for chondrocytes and MSCs (each 1 donor). Bilayered GelMA samples were created by crosslinking a layer with chondrocytes onto a layer with MSCs in a double molding process (height: 2+2 mm), and pre-cultured for two weeks in 50/50 chondrocyte/MSChondrogenic differentiation medium. This was done to assess the influence of chondrocytes on bone formation by MSCs *in vivo*.

Sample stability and compression modulus

In order to find the maximum amount of CDM particles that can be incorporated in GelMA while maintaining a stable, crosslinked construct, CDM particles were mixed in the GelMA in concentrations of 1%, 1.5%, 2%, 3%, 4% and 5% (w/v). 100 µL GelMA/CDM mixtures without cells were photocrosslinked and maintained in chondrocyte differentiation medium at 37°C for 1 week, after which sample integrity was macroscopically assessed. In addition, the stiffness of these samples was measured at room temperature by unconfined compression with a dynamic mechanical analyzer (TA instruments, DMA 2980). A force increasing from 0-5 Newton at a rate of 0.5 N/min was applied to the surface of the samples (8-9 mm diameter). The displacement and applied force were recorded during the compression and converted to stress and strain based on the initial specimen dimensions. The stress-strain curve was plotted and the compression modulus was calculated from the slope of the linear part of this curve. Failure of a sample was defined as the sudden disintegration with a concomitant drop in stress.

Viability assay

To visualize cell viability, a LIVE/DEAD Viability Assay (Molecular Probes MP03224, Eugene, USA) was performed according to the manufacturer's instructions. The samples were examined using an Olympus BX51 microscope and photomicrographs taken with an Olympus DP70 camera (both Olympus, The Netherlands). The excitation/emission filters were set at 488/530 nm to observe living (green) cells and at 530/580 nm to detect dead (red) cells. Live and dead cells were counted in 3 samples per time point, at four locations within each construct (chondrocytes and MSCs, both 1 donor). Viability was calculated as (alive cells / total cells counted) x 100 %.

***In vitro* culture: histology, immunohistochemistry and biochemistry**

One half of each sample was processed for histology and immunohistochemistry and the other half was used for biochemistry. Therefore, one part was dehydrated through a graded ethanol series, cleared in xylene and embedded in paraffin. The samples were sectioned into 5 μm slices and stained with hematoxylin and eosin for cell detection. A triple stain of hematoxylin, fast green, and Safranin-O (all from Sigma) was applied to identify the presence of GAGs. The stained sections were examined using a light microscope (Olympus BX51).

Collagens types I and II were stained by immunohistochemistry after deparaffinization and rehydration of the sections. All sections were blocked in 5% bovine serum albumin and 0.3% H_2O_2 following antigen retrieval. Rat collagen type I was retrieved by boiling the sections for 10 minutes in 10 mM citrate buffer, pH 6. Antigen retrieval for collagen type II was performed by incubation with 1 mg/mL pronase (Sigma) and 10 mg/mL hyaluronidase (Sigma) at 37 degrees for half an hour each. Next, sections were incubated with the primary antibodies for collagen type I (rabbit anti-rat collagen type I Antibody, ABT123, Millipore) or collagen type II (1:100, monoclonal mouse, II-II6B3, DSHB) both at 4°C overnight. Subsequently, collagen type II sections were incubated with GAM-HRP (1:200, Po447, Dako) at room temperature for an hour. Collagen type I sections were treated with secondary biotinylated goat anti-rabbit antibody 1:200 (Eo432, Dako) at (60 min at RT) and tertiary streptavidin-HRP antibody 1:400 (60 min at RT). Both collagen types were detected by a 10-minute conversion of 3,3'-diaminobenzidine solution (Sigma). Nuclei were counterstained with 50% Mayer's hematoxylin. Isotype control stainings were carried out with either a murine IgG1 monoclonal antibody (Dako) at concentrations matching those used for the primary antibodies or by incubation without primary antibody. The reactivity of the applied antibodies for collagen type I and II have been tested in our lab. It was found that both were specific for the type of collagen and reacted with both rat and equine collagens.

The other half of the *in vitro* cultured samples was used for DNA and GAG quantification. For this purpose, the samples were digested overnight in papain solution, 200 μl per sample (0.01 M cysteine, 250 $\mu\text{g}/\text{ml}$ papain, 0.2 M NaH_2PO_4 and 0.01 M EDTA) at 60°C. Total DNA was quantified on the papain digests using a Picogreen DNA assay (Invitrogen) according to the manufacturer's instructions. Total GAG content was determined by photospectrometry at 540 and 595 nm after reaction with dimethylmethylene blue using a microplate reader (Biorad). The ratio of both absorbances was calculated and the GAG content was quantified using a chondroitin sulphate (Sigma) standard. Calculated concentrations in each digested sample were expressed as GAG/DNA.

Implantation and evaluation of samples in rats

The animal study was approved by the local Ethics Committee for Animal Experimentation and was in compliance with the Institutional Guidelines on the Use of Laboratory Animals. Six 10 to 11-weeks old male athymic rats (Hsd:RH-Foxn1^{tmu} Harlan Laboratories B.V., The Netherlands) were anesthetized with 1.5% isoflurane in oxygen. One dorsal pocket was created for each sample on the rats, in which the sample was placed with a forceps. Six pockets per animal were created and not more than one sample from a group was implanted per animal according to a randomized scheme. The skin was closed in one layer using Vicryl 4.0 sutures. Preoperatively and postoperatively, the animals received 0.05 mg/kg buprenorphine subcutaneously. The rats were housed solitary for one day postoperatively and afterwards in groups at the Central Laboratory Animal Institute of Utrecht University. The replicates in the experimental groups were divided over different rats (table 1). Three and six weeks after implantation, the animals received subcutaneously administered fluorochromes to monitor bone formation: 100 mg/kg xylene orange and 10 mg/kg calcein green, respectively (both from Sigma)²⁹⁶. Eight weeks after implantation, the rats were killed; the tibial bones from three rats and all subcutaneous samples were harvested and fixed in formalin.

Rat study: X-ray and micro-CT

To screen for the existence of calcified tissue in different explants, the samples were imaged in a Faxitron® X-ray system, while immersed in formalin in a 24-Wells plate. A dose of 22 kV was applied for 12 seconds and the femur of the rats was taken along as a positive control. In order to quantify the degree of calcification accurately, the explants underwent micro-CT scans (Quantum FX- Perkin Elmer). The scan parameters were 90 kV tube voltage, 180 μ A tube current, 40 μ m resolution and 3 min scan time. Reconstruction of 2D projections was automatically performed using the in-built software of the micro-CT while pre-processing (image calibration and noise reduction) of the images was undertaken with the aid of an Analyze-11.0 package. Local bone segmentation was performed to yield the total amount of calcified tissue for subsequent calculation of bone volume per total sample volume (BV/TV), *i.e.* degree of calcification. Redundant rat tissue in the images was manually eliminated prior to the segmentation step.

Rat study: histology and immunohistochemistry

After 3D-imaging, the explants were split in two parts; one half of each sample was embedded in polymethylmethacrylate (MMA) and the other half was decalcified in ethylenediamine tetraacetic acid (EDTA) and embedded in paraffin. The paraffin samples underwent a safranin-O triple staining and collagen type I and II localization. In addition, a double staining of alcian blue and picosirius red was performed to detect aligned collagenous structures. Tartrate-resistant acid phosphatase (TRAP) was stained to detect

osteoclasts and macrophages. Slides were therefore incubated with 0.2 M acetate buffer – tartaric acid pH 5.0 for 20 minutes at room temperature. Then 25 mg Naphtol AS-MX phosphate (final concentration 0.5 mg/ml) and 55 mg fast red TR salt (final concentration 1.1 mg/ml) were added and incubation was continued until the osteoclasts were bright red (all products from Sigma). Samples were counterstained with Mayer's hematoxylin.

MMA embedded samples were cut in 20-30 μm sections with a Leica 4 SP1600 Saw Microtome system (Leica, Germany). The sections were stained with methylene blue / basic fuchsine and evaluated with light microscopy. In addition, the presence of fluorochromes was assessed from unstained sections.

Statistical Analysis

The stiffness of GelMA constructs with various concentrations of CDM particles was analyzed with an ANOVA followed by Bonferroni *post-hoc* correction (SPSS statistics (IBM software)). To evaluate the *in vitro* differentiation of MSCs and chondrocytes separately, a one-way ANOVA was performed in a randomized block design to correct for donor variability. A Bonferroni *post-hoc* test was applied. An independent T-test, assuming unequal variances, was performed to compare the degree of calcification *in vivo* between GelMA with and without CDM particles. A p -value < 0.05 was considered significant.

RESULTS

Characterization of GelMA with CDM particles

The size of the generated CDM particles as measured in a 2D plane was 400 ± 167 by 179 ± 62 μm . GelMA samples with a concentration of 2% or more (w/v) of these CDM particles disintegrated in culture medium after a week. In addition, a maximum stiffness of the CDM/GelMA samples, without cells, was found when a concentration of 1 to 1.5% of CDM particles was incorporated (Fig. 1a). These samples exhibited a higher compressive modulus compared to the GelMA samples without particles ($p = 0.000$) and compared to higher concentrations of 2-4% CDM particles ($p = 0.002$). All samples with 0-4% CDM particles remained intact during compression, only samples with 5% (w/v) CDM particles disintegrated at a force of 2.8 ± 0.4 N. A concentration of 1.5 % CDM particles was chosen for cellular differentiation experiments in order to achieve a maximal biologic effect of the particles on the encapsulated cells without sample disintegration over the course of culture. The particles were equally distributed throughout the GelMA as observed with stereomicroscopy (Fig. 1b). Histology on cross-sections of these samples showed that CDM particles consisted predominantly of collagen type II (Fig. 1c) and did not contain any residual cells (as confirmed by H&E-staining; Fig. 1d) nor GAGs (as observed in the safranin-O stained sections; Fig. 1e).

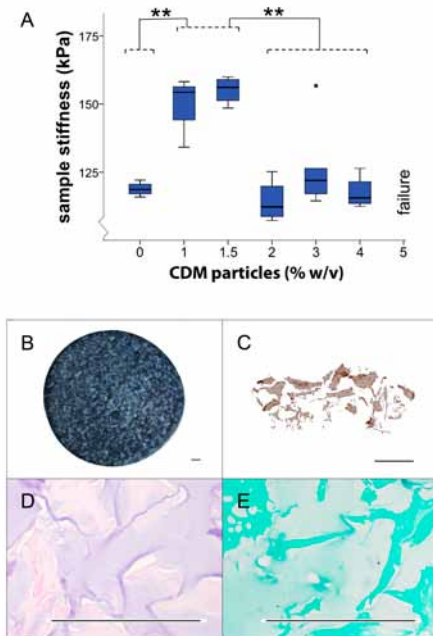


Figure 1. Mechanical testing and imaging of GelMA hydrogel with embedded CDM particles. (a) A significant increase of GelMA stiffness was observed when 1-1.5% CDM particles were incorporated vs. no CDM particles or a higher particle concentration (** $p < 0.01$). Samples with 5% CDM particles disintegrated during the compression test. (b) CDM particles (1.5% (w/v)) were divided equally through the GelMA sample as observed with stereomicroscopy; (c) all CDM particles were positive for collagen type II; (d) no remaining cells (H&E staining) or (e) GAGs (Safranin-O staining) were detected. All scale bars represent 500 μm .

Viability of MSCs and chondrocytes

The viability of equine chondrocytes and MSCs in GelMA ranged between 71-96% after 1 and 14 days of culture and was not significantly affected by the co-incorporation of 1.5% CDM particles (Fig. 2a).

In vitro cartilage tissue formation

MSCs produced significantly more GAG/DNA in GelMA with CDM particles compared to without after 6 weeks of *in vitro* culture (15.7 ± 3.5 vs. 11.3 ± 3.6 mg/mg ($p = 0.010$)) (Fig. 2b). Chondrocytes and MSCs produced a comparable amount of GAG/DNA in GelMA without CDM after 6 weeks. Noteworthy, GAG production by chondrocytes was negatively affected by co-embedding of CDM particles in GelMA after 4 weeks (4.8 ± 1.9 vs. 8.2 ± 1.7 mg/mg ($p = 0.011$)) and 6 weeks (5.2 ± 3.9 vs. 12.1 ± 6.0 mg/mg ($p = 0.000$)). Histological observations confirmed these quantitative findings by showing superior GAG and collagen type II matrix formation by chondrocytes in GelMA/CDM- (Fig. 2c, d) compared to GelMA/CDM+ (Fig. 2e, f). MSCs formed abundant cartilage-specific matrix in GelMA/CDM- (Fig. 2g, h) and GelMA/CDM+ samples (Fig. 2i, j). GAG deposition in GelMA by MSCs was more clustered compared to a homogeneously spread matrix produced by chondrocytes.

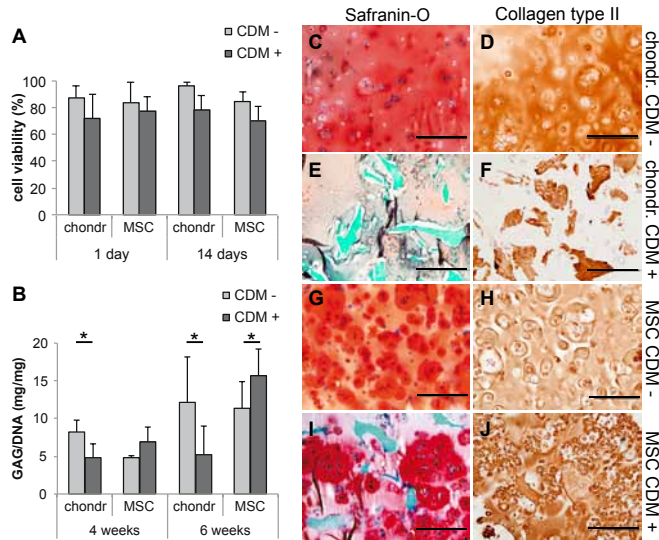


Figure 2. Viability and chondrogenic differentiation of chondrocytes and MSCs in GelMA hydrogels *in vitro*. (a) the viability of equine chondrocytes and MSCs in GelMA hydrogel was high, and not affected by 1.5% co-embedded cartilage-derived matrix particles (CDM); (b) CDM particles positively influenced the formation of glycosaminoglycans (GAGs) by MSCs after six weeks and negatively affected GAG formation by chondrocytes, both after four and six weeks of *in vitro* culture (* $p < 0.05$); (c-j) an interconnected cartilage-specific matrix was formed by both cell types, except for chondrocytes in combination with CDM particles. This matrix contained GAGs (safranin-O in red, fast green and hematoxylin counterstain) and collagen type II (stained in brown, hematoxylin counterstain). All scale bars represent 200 μm .

***In vivo* cartilage tissue formation by chondrocytes and MSCs**

Both chondrocytes and MSCs had produced GAGs in the GelMA hydrogel after two weeks of *in vitro* pre-culture (Fig. 3a, e). After eight weeks of subcutaneous implantation of these constructs in rats, the chondrocyte-laden hydrogels had a transparent or milky hydrogel-like appearance. Conversely, samples containing MSCs were opaque and solid. The GAG content for chondrocyte-laden samples was lower than before implantation, irrespective of the presence of CDM particles (Fig. 3b). Pericellular collagen depositions by the chondrocytes were observed within the intact GelMA matrix, more pronounced for type II collagen than for type I (Fig. 3c, d). MSC-laden constructs showed hypertrophic cells within GAG clusters (Fig. 3f), adjacent to cell-containing collagenous areas with the morphology of woven bone and areas containing fatty bone marrow. The clusters with hypertrophic MSCs also contained collagen type II (Fig. 3g). The collagen bundles surrounding the cartilage clusters were composed of collagen type I (Fig. 3h). Only scarce remnants of GelMA were observed in the MSC constructs. The implanted GelMA gels without cells remained intact and were peripherally infiltrated with fibrous tissue (Fig 3i, j).

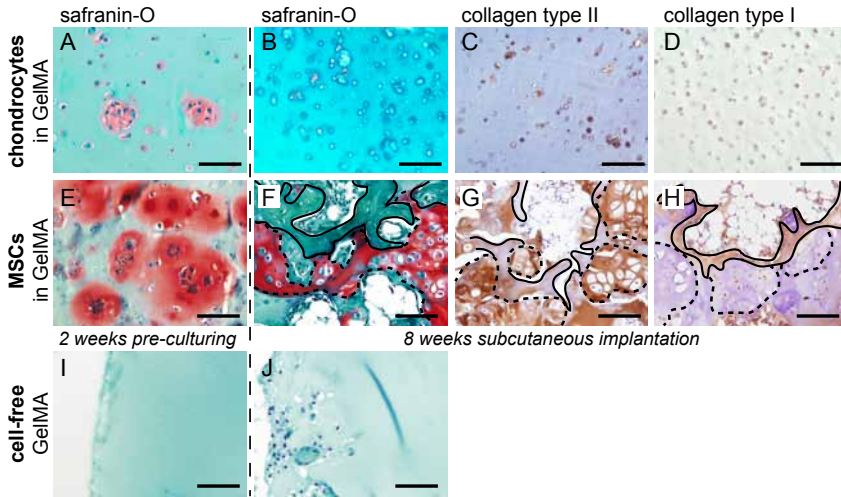


Figure 3. *In vitro* and *in vivo* chondrogenic differentiation of chondrocytes and MSCs in GelMA hydrogels. **a)** chondrocytes secreted glycosaminoglycans (GAGs: red) after 2 weeks of *in vitro* pre-culture; **b)** the content of GAGs was lower after eight weeks of subsequent subcutaneous implantation in rats; pericellular deposition of collagen types II (**c**) and I (**d**) were observed. **(e)** Abundant GAG production by MSCs before implantation; **(f)** hypertrophic cells were observed within GAG clusters (red, dashed line) after implantation, adjacent to fatty bone marrow (white), hematopoietic bone marrow, and bone (intense green, black line); **(g)** hypertrophic cells were located within collagen type II clusters (brown, dashed line); **(h)** collagen type I (brown, black line) was located between the hypertrophic cell clusters (dashed line) and the fatty bone marrow. No effect of the presence of CDM particles on histological outcome was observed after implantation. Therefore, only the groups without CDM particles are presented. **(i,j)** GelMA samples without cells remained intact *in vivo* with peripheral infiltration of host tissue. All scale bars represent 100 µm.

***In vivo* endochondral bone formation by MSCs: histology and IHC**

Endochondral bone formation in the gels containing MSCs was more specifically studied. Complete cross-sections of the samples revealed central GAG clusters that co-localized with collagen type II positive areas (Fig. 4a, b); remnants of CDM particles were not detected. Collagen type I positive areas were located peripherally to the central cartilage clusters (Fig. 4c). A comparable localization of woven bone was revealed by basic fuchsin on MMA embedded samples (Fig. 4d). Collagen (type I) bundles were identified throughout the constructs with polarized light on picro-sirius red stained slides (Fig. 4e, f). Fluorescent dyes were retained in the samples in a diffuse pattern and there was no uniform direction of bone growth (i.e. inward or outward) (Fig. 4g). A clear outward, appositional bone growth was observed in the rat tibia that was taken along as a control (Fig. 4h). Multinucleated, TRAP-positive osteoclasts (red) were found adjacent to areas rich in collagen type I (Fig. 4i).

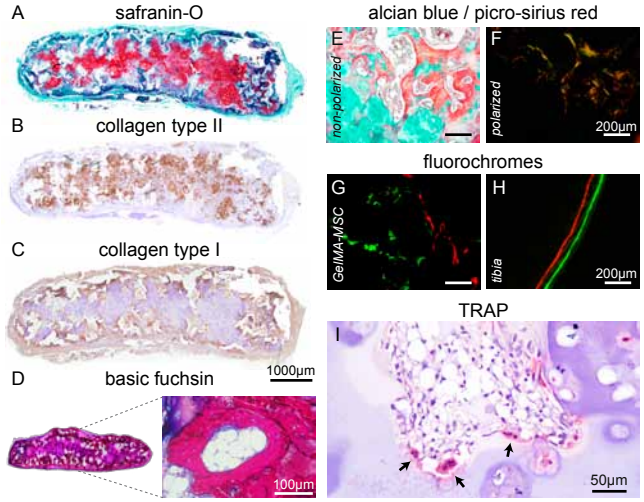


Figure 4. Endochondral bone formation in MSC-laden GelMA *in vivo*. Cross-sections of complete samples show: **(a)** central glycosaminoglycan (GAG) clusters (red) that **(b)** co-localized with collagen II areas (brown); **(c)** peripheral collagen type I deposition (brown) including an outer layer of fibrous rat tissue; **(d)** central GAG clusters (purple), fatty bone marrow (white) and woven bone (pink); **(e)** GAG clusters (blue) and collagens bundles (red) that **(f)** are positive on polarized light imaging; **(g)** diffuse incorporation of fluorochromes in the GelMA samples compared to **(h)** appositional bone growth in the rat tibia; **(i)** multi-nucleated, TRAP positive cells (arrows, red) predominantly align bone areas.

	schematic	X-ray	MicroCT	calcified volume (%)
A. MSC/CDM -				39.5 ± 8.3
B. MSC/CDM +				43.5 ± 2.5
C. bilayered chondrocytes MSCs				0
	<div style="display: flex; justify-content: space-around;"> <div style="text-align: center;"> <p><i>pre-implant</i> safranin-O</p> </div> <div style="text-align: center;"> <p>safranin-O</p> </div> <div style="text-align: center;"> <p><i>post-implant</i> collagen type I</p> </div> <div style="text-align: center;"> <p>basic fuchsin</p> </div> </div>			

Figure 5. Bone formation in GelMA hydrogels with MSCs and in bilayered constructs with MSCs and chondrocytes. Analysis of explanted tissues following eight weeks of subcutaneous implantation. **(a)** Subcutaneous implantation of GelMA/MSCs constructs resulted in consistent mineralized tissue formation as expressed by the calcified volume-%. **(b)** There was no significant effect of CDM particles on mineralization of constructs. **(c)** No calcification occurred when GelMA with MSCs were combined with a layer of GelMA/chondrocytes. Histology on bilayered constructs revealed that MSCs still cluster and form glycosaminoglycans; however, there was very limited hypertrophy and no bone deposition.

***In vivo* endochondral bone formation by MSCs: X-ray and micro-CT**

Radiographic examination revealed a high degree of calcification in all MSC samples with and without CDM particles in a 2D plane (Fig. 5a and b). The calcified volume fraction in the MSC-containing samples, as calculated from the 3D micro-CT images, was 39.5 ± 8.3 for CDM- and 42.5 ± 2.5 for CDM+ ($p = 0.503$). Mineral depositions were most abundant in the periphery of the samples, although scattered calcifications could be observed in the central regions. No calcifications were detected in any of the chondrocyte or the bilayered MSC/chondrocyte samples (Fig. 5c). The MSCs in the bilayered constructs did form GAG clusters, however, there was a very limited degree of hypertrophy and a complete absence of bone and bone marrow formation.

DISCUSSION

MSCs have previously been shown capable of mimicking the natural process of endochondral bone formation²⁸⁶⁻²⁹². In several of these studies, aggregated MSCs were cultured and subsequently implanted. Cell aggregates constitute an attractive culture model as the condensation of cells, as a first step in endochondral bone formation, is per definition achieved. Also, cartilage grafts that are derived from fracture callus have shown to be a successful matrix for bone formation in orthotopic locations²⁹⁰. Engineering of larger tissues, however, requires a scaffold to carry cartilage grafts, cell aggregates or separate cells. Recent work showed that pre-differentiated MSCs seeded on a porous copolymer scaffold were capable of bridging large bone defects in rats²⁹¹. However, the exclusiveness of the endochondral route to bone formation was not evident in these experiments, and was likely combined with intramembranous bone regeneration.

Alternatively, choosing a biomaterial that more closely mimics the properties of the natural (starting) tissue may favor endochondral bone regeneration. GelMA hydrogel is a suitable scaffold for the formation of a cartilage matrix by embedded cell^{60,63}. In the present study, the aqueous hydrogel environment allowed for clustering of MSCs and chondrogenic matrix production. In comparison, a more homogeneous distribution of cells and matrix was observed in chondrocyte-laden gels. Prior to subcutaneous implantation, the constructs were cultured in chondrogenic medium for two weeks, which is short compared to previous studies on *in vivo* endochondral bone formation^{286-288,292}. The cartilage matrix clusters formed by MSCs in GelMA appear to be an attractive template for endochondral bone formation in a subcutaneous rat model. The newly formed matrix accounted for the integrity of the constructs, since the GelMA was almost fully degraded. This confirmed the unique degradation behavior of GelMA as a cell carrier in regenerative medicine, for which the degradation of the biomaterial should be balanced to the formation of neo-tissue.

The process of endochondral bone formation involves intensive remodeling of cartilage and bone tissue²⁸⁶. This active remodeling process was here indicated by the presence of osteoclasts and/or macrophages (TRAP-positive cells) throughout the GelMA constructs. Active remodeling can explain the diffuse incorporation pattern of fluorochromes. This pattern was similar to the alignment of collagen bundles that was observed with polarized light. Conversely, during intramembranous bone formation in tissue engineering, the fluorochromes are incorporated in a more appositional fashion²⁹⁶, comparable to our observation in the rat tibia.

The total calcified volume (including the cortical layer) after eight weeks was roughly 40%. This is high compared to natural human cancellous bone, which was reported between 29.3 and 37.8%, depending on the location in the body²⁹⁷. Abundant bone was thus formed in GelMA via the endochondral pathway. Further, most calcified bone in the present work was located in the periphery of the constructs, although unmineralized bone tissue, or osteoid, was located more towards the construct center, surrounding the hypertrophic cartilage clusters. A similar progression of bone formation was previously observed in an ectopic goat model. There, bone was formed via the intramembranous route by MSCs starting at the periphery of the implanted calcium phosphate scaffolds after three weeks, while more bone was formed in the center of the scaffold after nine weeks^{298,299}.

Although CDM positively stimulated the formation of GAGs by MSCs *in vitro*, no significant difference was observed in endochondral bone formation *in vivo*. Decellularized tissues, such as CDM, have been used in regenerative medicine both for their biochemical and structural characteristics^{66,69,244}. The Badylak group has indicated that growth factors and signaling molecules in native tissues can be retained after the decellularization process^{273,274}. Therefore, these matrices can potentially direct cell behavior in tissue-engineered constructs. CDM scaffolds have previously been reported to be beneficial for the chondrogenic differentiation of MSCs^{275,276}. The present study gives a further insight in the performance of MSCs and chondrocytes in relation to CDM. Earlier work by our group revealed that MSCs outperform chondrocytes when cultured directly on scaffolds composed of CDM⁷⁴. Here, a similar effect was observed when the cells were co-embedded in GelMA with CDM particles *in vitro*, suggesting the involvement of a biologically active component in the cell-matrix interaction.

The specific regulatory pathways that are involved in the interaction between decellularized matrices and cells remain elusive. Nevertheless, for primary chondrocytes, it is known that collagen type II can trigger a negative feedback loop, inducing the formation of pro-inflammatory cytokines and matrix metalloproteinases^{251,252}. This negative interaction is in line with the effect of CDM on matrix production by chondrocytes in the current work, as well as with previous findings of *in vitro* cultured chondrocytes on CDM scaffolds⁷⁴. Still, this specific cell-matrix interaction in tissue engineering remains

a remarkable phenomenon, since chondrocytes naturally reside in a collagen type II matrix in articular cartilage. Chondrocytes may require their natural pericellular collagen type VI matrix for differentiation in decellularized cartilage matrices³⁰⁰, or the collagen type II is too degraded for the cells to consider it a healthy template to form cartilage, whereas MSCs with a more regenerative nature might in fact be triggered to remodel and deposit new healthy tissue.

We showed that endochondral bone formation in MSC-seeded GelMA was fully suppressed in layered GelMA constructs with chondrocytes in the adjacent layer. This was a more rigorous effect compared to bi-layered cultures in agarose gels, in which partial suppression of mineralization was found²⁹³. The proposed underlying mechanism is the production of parathyroid hormone-related protein by chondrocytes, which inhibits hypertrophy of MSCs³⁰¹. Although this finding is unsatisfactory for osteochondral tissue engineering, the suppression of bone formation is encouraging for the field of cartilage tissue engineering, which explores MSCs as an allogeneic cell source for the single-stage repair of articular cartilage⁶. To this end, co-cultures of bone marrow-derived MSCs and articular chondrocytes have been shown beneficial for cartilage matrix formation²⁴. In this light, GelMA would be a potential carrier for a co-culture of MSCs and chondrocytes, regarding the abundant matrix formation by both cell types separately and the fact that chondrocytes in this hydrogel can prevent bone formation by MSCs.

Future work will evaluate the bone forming capacities of the current constructs in orthotopic locations. The construct size displayed here is large enough for the repair of segmental bone defects in rodents; however, scale-up is required to reach relevant dimensions for clinical application in humans. Therefore, it should be investigated what is the upper size limit for the solid GelMA constructs, regarding diffusion limitations. Alternatively, large, porous MSC-laden constructs can be 3D-printed, as GelMA is a proven effective bio-ink for 3D bioprinting of cartilaginous constructs^{72,190}. In addition, GelMA may serve as a carrier for hypertrophic cell aggregates, since these have demonstrated capable of forming a bony bridge in segmental bone defects in rats²⁸⁹. However, encapsulation of single MSCs in the GelMA/CDM constructs, as was done in the current work, may be a more straightforward approach to the repair of bone defects.

CONCLUSION

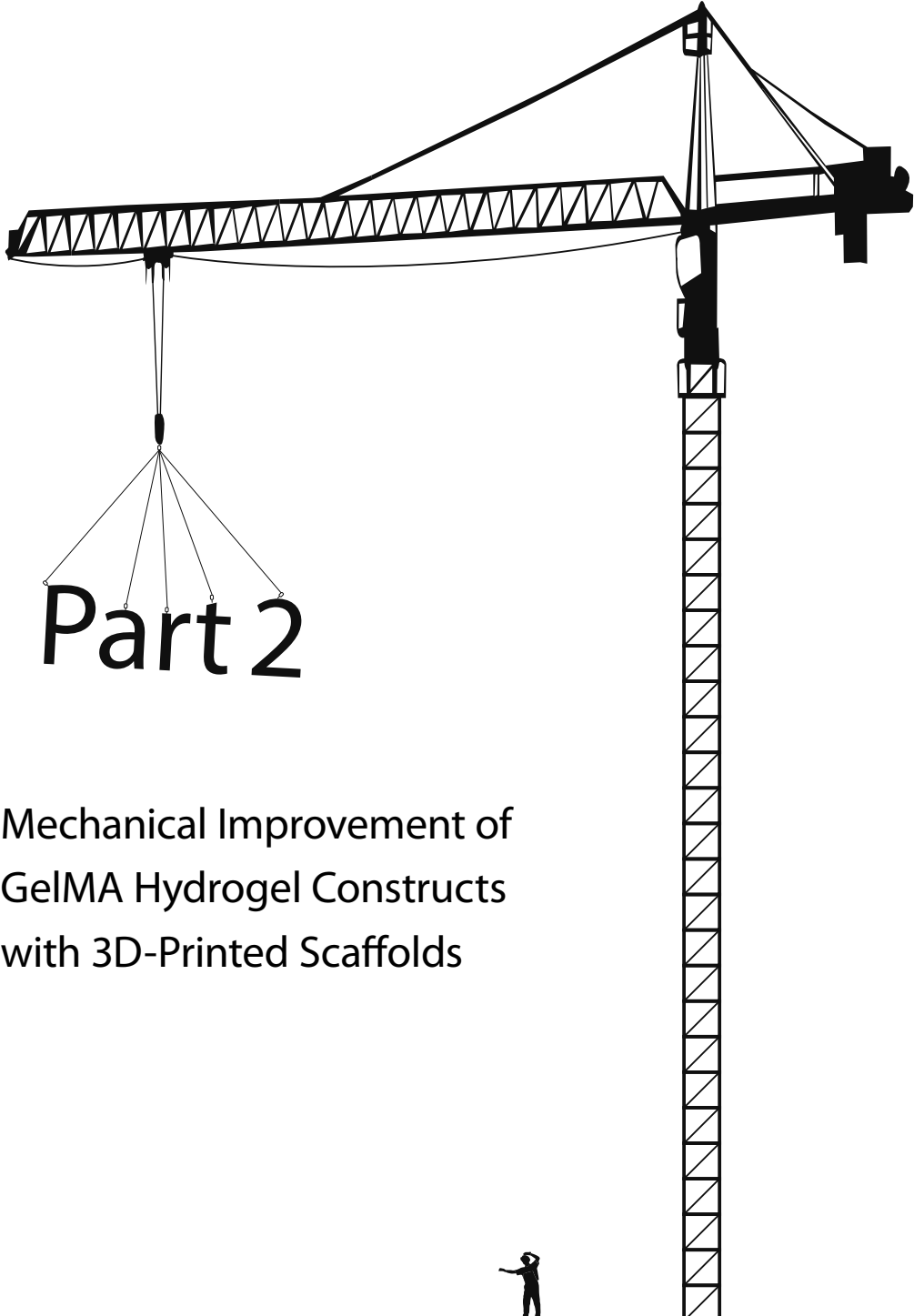
The process of endochondral bone formation was recapitulated by MSCs in GelMA hydrogels in an ectopic rat model, irrespective of the co-incorporation of CDM particles. The formation of bone was based on a cartilage template in the hydrogel that was formed by the MSCs *in vitro* within two weeks. A large amount of mineralized bone including bone marrow cavities was subsequently formed *in vivo*, surrounding hyper-

trophic cartilage clusters. A major fraction of the GelMA hydrogel carrier was degraded in this process. Chondrocytes fully inhibited *in vivo* bone formation by MSCs in bilayered GelMA constructs. The current work forms a good starting point for the engineering of relevant-size endochondral bone constructs in the versatile GelMA hydrogel system.

ACKNOWLEDGEMENTS

The authors would like to thank Kristel Boere for her assistance with the mechanical testing and Mattie van Rijen for his assistance in fluorescent microscope imaging. The antibody against collagen type II (II-II6B3), developed by T.F Linsenmayer, was obtained from the DSHB developed under the auspices of the NICHD and maintained by The University of Iowa, Department of Biology, Iowa City, IA 52242. Jetze Visser was supported by a grant from the Dutch government to the Netherlands Institute for Regenerative Medicine (NIRM, grant n°FES0908); DG was supported by a VENI fellowship (11208) from the Dutch Technology Foundation, STW, Applied Science Division of NWO and the Technology Program of the Ministry of Economic Affairs. Kim Benders received an Alexandre Suerman Stipendium from the University Medical Center Utrecht and Jos Malda was supported by the Dutch Arthritis Foundation.





Part 2

Mechanical Improvement of
GelMA Hydrogel Constructs
with 3D-Printed Scaffolds

Chapter 5

Covalent Attachment of a Three-Dimensionally Printed Thermoplast to a Gelatin Hydrogel for Mechanically Enhanced Cartilage Constructs

Kristel W.M. Boere*

Jetze Visser*

Hajar Seyednejad

Sima Rahimian

Debby Gawlitta

Mies J. van Steenbergen

Wouter J.A. Dhert

Wim E. Hennink

Tina Vermonden

Jos Malda

*Authors contributed equally to this manuscript

Acta Biomaterialia. 2014 Jun;10(6):2602-11

ABSTRACT

Hydrogels can provide a suitable environment for tissue formation by embedded cells, allowing its application in regenerative medicine. However, hydrogels only possess limited mechanical strength and have therefore been reinforced for application in load-bearing conditions. In most approaches the reinforcing component and the hydrogel network have poor interactions and the synergetic effect of both materials on the mechanical properties is not effective. Therefore, in the present study, a thermoplastic polymer blend of poly(hydroxymethylglycolide-co- ϵ -caprolactone)/poly(ϵ -caprolactone) (pHMGCL/PCL) was functionalized with methacrylate groups (pMHMGCL/PCL) and covalently grafted to gelatin methacrylamide (GelMA) hydrogel through photopolymerization. The grafting resulted in an at least 5x increased interface-binding strength between the hydrogel and thermoplastic polymer material. GelMA constructs were reinforced with 3D printed pHMGCL/PCL and pMHMGCL/PCL scaffolds and tested in a model for a focal articular cartilage defect. In this model, covalent bonds at the interface of both materials resulted in constructs with an improved resistance to repeated axial and rotational forces. Moreover, chondrocytes embedded within the constructs were able to form cartilage-specific matrix both *in vitro* and *in vivo*. Thus, by grafting the interface of different materials, stronger hybrid cartilage constructs can be engineered.

INTRODUCTION

Hydrogels consist of hydrophilic polymer networks that are able to hold large amounts of water in a three-dimensional (3D) structure, while maintaining their shape^{104,302}. Thereby they can provide a 3D aqueous environment to embedded cells, analogous to the extracellular matrix of natural tissues^{29,303}. For tissue engineering purposes, stem cells^{304,305}, tissue specific cells³⁰⁶ and/or bioactive factors^{111,231,304} can be incorporated in the temporary hydrogel scaffold to direct specific tissue regeneration^{29,293}. By doing so, hydrogel systems have already been clinically applied for regeneration of a range of tissue types including skin, blood vessels, neural tissues and cartilage^{11,29}. Unfortunately, hydrogels have limited mechanical strength due to their high water content^{115,307}, which may result in construct failure of the hydrogel under mechanically challenging conditions, as found in the load-bearing bone and cartilage tissues. One approach to overcome this limitation is by stimulation of extracellular matrix formation of the cells prior to implantation, resulting in a stiffer implant⁶⁰. However, this requires long *in vitro* preconditioning periods, limiting clinical translation. The most straightforward approach to directly enhance the stiffness and strength of a hydrogel is by increasing its polymer concentration and crosslinking density^{171,246}. Nevertheless, this also impacts the diffusion rates of bioactive factors, nutrients and cell metabolites through the hydrogel, thereby most likely also the regenerative capacities of embedded cells^{104,121,246}. Therefore, alternative strategies have been explored to increase the strength of hydrogel constructs, e.g. through creation of interpenetrating polymer networks (IPNs)^{183,195-197,308} or incorporation of solid particles³⁰⁹⁻³¹¹ and nanofibers/nanotubes³¹²⁻³¹⁴. Mechanical properties of hydrogels can also be improved by integrating a secondary scaffold material, such as fiber mats³¹⁵⁻³¹⁷, randomly organized porous polylactic acid scaffolds^{318,319} non-woven meshes³²⁰ or electrospun polymer networks^{55,56,203,321,322}. Moreover, with advances in biofabrication techniques, a rigid thermoplastic polymer network can be fabricated layer-by-layer, along with the hydrogel construct^{65,75,76,190,201,323} allowing for a tailored reinforcement of hydrogels. In addition, when mechanical stability is provided by this secondary rigid network, hydrogels with a lower crosslink density can be processed⁶⁵, which is beneficial for the viability and proliferation capacity of embedded cells^{79,104,121,246}. Besides, reinforcing the cell-laden hydrogel with a secondary scaffold material may also reduce the often-experienced swelling or shrinking of the hydrogel-based implant that can lead to imperfect filling of the tissue defect³²⁴.

In the present generation of constructs, however, the reinforcing network and the hydrogel show insufficient adhesion, mostly because of their different physicochemical properties^{76,325}, which leads to construct disintegration upon application of mechanical stresses. Hence, the introduction of chemical bonds between both components may

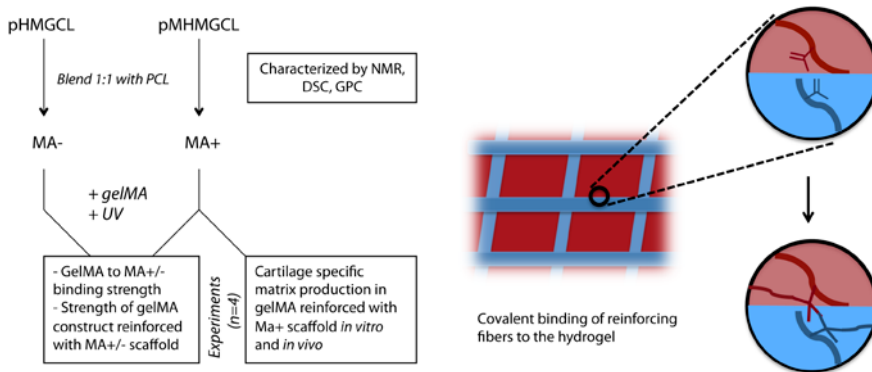


Figure 1. Overview of the performed experiments in the present study. Poly(hydroxymethylglycolide-co- ϵ -caprolactone) pHMGCL, methacrylate-functionalized pHMGCL (pMHMGCL) and their corresponding blends with poly- ϵ caprolactone (MA- and MA+ respectively) were characterized with NMR, DSC and GPC. Reinforced constructs of MA- and MA+ with methacrylated gelatin (GelMA) were UV-irradiated and the interface-binding strength and strength of the reinforced construct was tested. Constructs of MA+/GelMA were further tested *in vitro* and *in vivo* for cartilage specific matrix production. All mechanical, *in vitro* and *in vivo* experiments were performed in quadruplicate.

improve the construct strength to withstand the challenging mechanical conditions in the musculoskeletal system.

Therefore, this study aims to mechanically enhance cartilage implants by grafting a hydrogel to a 3D-fabricated biodegradable thermoplastic polymer network. To achieve this, the polyester poly(hydroxymethylglycolide-co- ϵ -caprolactone) (pHMGCL³²⁶) was functionalized with methacryl groups coupled to the hydroxyl side groups of this polymer. In previous studies, we have shown that pHMGCL is more hydrophilic than e.g. poly- ϵ caprolactone (PCL) due to the presence of the pendant hydroxyl groups³²⁶, facilitating cell attachment, matrix deposition³²⁷ and resulting in an increased degradation rate³²⁸. Thereby, pHMGCL is more likely to balance its degradation to the formation of neo-tissue⁵⁰, compared to PCL^{65,75,76}. However, pHMGCL containing more than 20% HMG is an amorphous polymer with a low glass transition temperature (T_g) and therefore has low dimensional stability. PCL, on the other hand, is semi-crystalline, which is beneficial for dimensional stability, but has no reactive groups to allow for example surface grafting. To increase the dimensional stability of pHMGCL, it can be blended with PCL³²⁹. The blending also improves the physical properties of the material for scaffold fabrication techniques such as electrospinning³³⁰ and 3D fiber deposition (3DF)³²⁷.

In the present study, covalent binding between methacrylated pHMGCL (pMHMGCL) blended with PCL and a methacrylated gelatin hydrogel (GelMA) through photopolymerization was investigated. The interface-binding strength between GelMA and pMHMGCL/PCL was studied and reinforced constructs as fabricated with 3DF were tested

with a repetitive loading regime. Finally, the *in vitro* and *in vivo* regenerative capacities of human chondrocytes within these fiber-reinforced constructs were analyzed.

MATERIALS AND METHODS

Materials

All reagents and solvents were purchased from Sigma-Aldrich (Zwijndrecht, the Netherlands) and used without purification, unless stated otherwise. Benzyl alcohol, acetone, triethylamine (TEA) and dimethyl sulfoxide (DMSO) were obtained from Merck (Darmstadt, Germany). Peptide grade dichloromethane (DCM) and tetrahydrofuran (THF) were obtained from Biosolve (Valkenswaard, the Netherlands). *N,N'*-dimethyl amino pyridine (DMAP) was purchased from Fluka (Zwijndrecht, the Netherlands). Irgacure 2959 was obtained from Ciba Specialty Chemicals Inc (Basel, Switzerland). Type II collagenase was purchased from Worthington Biochemical Corp, (Lakewood, New Jersey). Phosphate-buffered saline (PBS), Dulbecco's Modified Eagle Medium (DMEM), ITS-X, penicillin, streptomycin and Picogreen DNA assay were provided by Invitrogen (Carlsbad, California). Fetal bovine serum (FBS) was purchased from Biowhittaker (Walkersville, Maryland). FGF-2 and TGF- β 2 were obtained from R&D Systems (Minneapolis, Minnesota). Human serum albumin was provided by SeraCare Life Sciences (Milford, Massachusetts). Histoclear II was obtained from BiozymTC, the Netherlands. Buprenorphine (Temgesic) was purchased from Schering-Plough/Merck (USA). Antibody against collagen type II (1:100; II-6B3II) was obtained from Developmental Studies Hybridoma Bank, USA. Polylactic acid (PLA) filament for 3D printing was obtained from Ultimaker LTD, Geldermalsen, The Netherlands.

Synthesis of poly- ϵ caprolactone (PCL)

Poly- ϵ caprolactone (PCL) was synthesized by ring opening polymerization of ϵ -caprolactone (CL) using benzyl alcohol (BnOH) and stannous octoate (SnOct_2) as initiator and catalyst, respectively, according to a previously described method³²⁶. The molar ratio of CL/BnOH was 300/1 in the feed. The obtained PCL was characterized by ^1H NMR, GPC and DSC.

Synthesis of methacrylated poly(hydroxymethylglycolide-co- ϵ -caprolactone) (pMHMGCL)

Poly(hydroxymethylglycolide-co- ϵ -caprolactone) (pMHMGCL) was synthesized as described before by ring opening polymerization of 3S-benzyloxymethyl-1,4-dioxane-2,5-dione (benzyl protected hydroxymethyl glycolide (BMG)) and ϵ -caprolactone in the melt using BnOH and SnOct_2 as initiator and catalyst, respectively, followed by removal of

the protecting benzyl groups by catalytic hydrogenation³²⁶. pHMGCL was synthesized by melt polymerization in a 40/60 molar ratio of HMG/CL and the monomer to initiator molar ratio was 300. These random copolymers were further functionalized aiming for derivatization of 50% of the available hydroxyl groups of pHMGCL with methacrylate groups (Fig. 2). In a typical reaction, pHMGCL (4.2 g, 13.2 mmol OH groups) was dissolved in freshly distilled THF (40 mL), in an aluminum foil covered, dry round-bottom flask. After dissolution, DMAP (39.3 mg, 0.32 mmol) and TEA (897 μ L, 6.4 mmol) were added as catalyst and base, a combination that has shown to efficiently functionalize hydroxyl groups with methacryloyl groups with methacryloyl groups³³¹. Next, methacrylic anhydride (960 μ L, 6.4 mmol, feed ratio methacrylic anhydride/OH_{polymer} = 0.5) was added. To prevent premature crosslinking, hydroquinone monomethyl ether (84 mg, 0.67 mmol) was added and the reaction proceeded overnight under N₂ atmosphere in an ice-cooled flask. After 16 hours, the polymer was purified by three times precipitation in ice-cold water, followed by centrifugation and removal of the supernatant. The precipitate was re-dissolved in DCM and dried using anhydrous Na₂SO₄. The salts were filtered off, DCM was evaporated

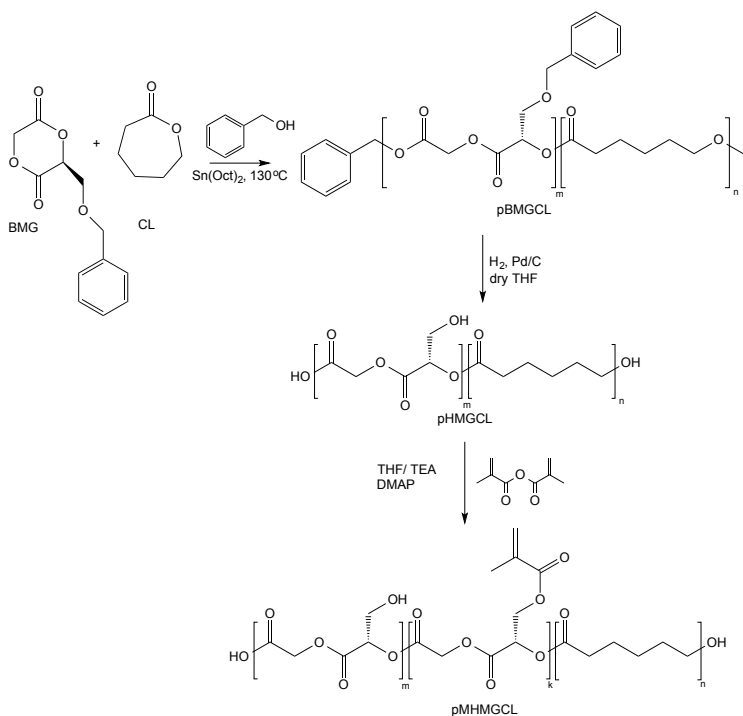


Figure 2. Synthesis of poly(benzylmethacrylate-co- ϵ -caprolactone) pBMGCL, poly(hydroxymethylglycolide-co- ϵ -caprolactone) pHMGCL, and methacrylate-functionalized pHMGCL (pMHMGCL).

and the polymer was dried under vacuum at room temperature for several days. The obtained methacrylated pHMGCL (pMHMGCL) was characterized by ^1H NMR, DSC, and GPC.

Synthesis and gel preparation of gelatin methacrylamide (GelMA)

GelMA was synthesized by reaction of type A gelatin with methacrylic anhydride at 50 °C for one hour as previously described⁶². GelMA was dissolved in demineralized H₂O at 70 °C in a concentration of 10% (w/v). The solution also contained Irgacure 2959 (0.1% w/v), a photoinitiator that has shown to be well compatible with living cells^{332,333}. When a clear solution was obtained, the osmolarity of the gel was adjusted to physiologic levels (1x PBS) by adding 50 μl concentrated PBS (disodium hydrogen phosphate 60 g/L, sodium dihydrogen phosphate 6.6 g/L and sodium chloride 164 g/L) to 1 ml of methacrylated gelatin.

Preparation of p(M)HMGCL/PCL blends

pHMGCL or pMHMGCL was dissolved in DCM and mixed with PCL in a 1:1 weight ratio at a concentration of 0.2 g/mL DCM (total volume was 5 ml). The mixture was concentrated by blowing air for 10 minutes and next, the viscous polymer solution (~3 ml) was pipetted on a petri dish. DCM was allowed to evaporate overnight at room temperature and a white solid was obtained, which was subsequently analysed by differential scanning calorimetry (DSC). For sake of readability, the pMHMGCL/PCL blend and pHMGCL/PCL blend are abbreviated as MA+ blend and MA- blend respectively.

Nuclear magnetic resonance (NMR)

^1H NMR spectra of the obtained polymers and blends were recorded on a Mercury 300 MHz instrument (Varian Associates Inc., NMR Instruments, Palo Alto, CA). Chemical shifts are recorded in ppm with reference to the solvent peak ($\delta = 7.26$ ppm for CDCl₃ in ^1H NMR).

Differential scanning calorimetry (DSC)

Thermal properties of polymers and blends were measured using a DSC Q2000 apparatus (TA Instruments, New Castle, DE, USA). Scans of polymer samples (approximately 5 mg, loaded into Tzero aluminum pans (TA Instruments)) were taken from -80 °C to 100 °C with a heating rate of 10 °C/min and a cooling rate of 0.5 °C/min under nitrogen flow of 50 mL/min. The glass transition temperature (T_g) was recorded as the midpoint of heat capacity change in the second heating run. Melting temperature (T_m) and heat of fusion (ΔH_f) were determined from the onset of the endothermic peak position and integration of the endothermic area, respectively. The thermal transitions of PCL, pHMGCL

and pMHMGCL are reported for the second heating run; the thermal transitions of the blends for the first heating run.

Gel permeation chromatography (GPC)

Molecular weights (M_w and M_n) of the different polymers were measured by GPC analysis using a 2695 Waters Alliance system and a Waters 2414 refractive index detector. Two PL-gel 5 μm mixed-D columns fitted with a guard column (Polymer Labs, M_w range 0.2-400 kDa) were used. The columns were calibrated with polystyrene standards of known molecular weights using AR grade THF, eluting at 1 mL/min flow rate at 30 °C. The concentration of samples was 5 mg/mL and the injection volume was 50 μL .

Creep-recovery test: interface-grafting strength

To investigate grafting strength between GelMA and the MA+ blend and to compare this with GelMA and the MA- blend, creep-recovery tests were performed with an AR G-2 rheometer (TA-instruments), equipped with a UV light guide connected to a BluePoint lamp 4 (350-450 nm, Hönle UV technology (Munich, Germany) at 37°C. Flat discs (surface area 80 mm², thickness 0.1 mm) of MA+ or MA- were prepared as described in section 2.5. GelMA solutions were prepared at a concentration of 20% w/v in deionized water

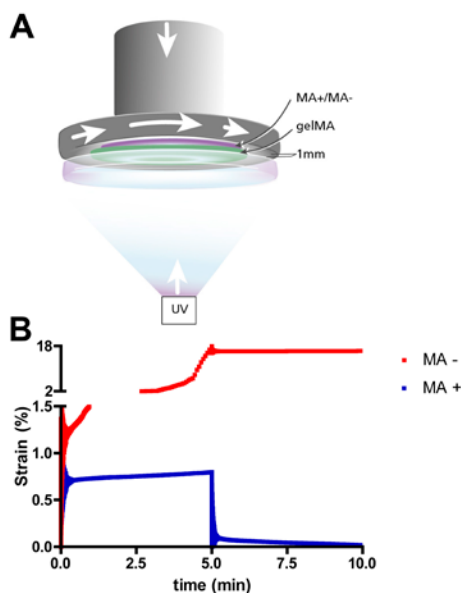


Figure 3. (a) samples of 100 μL GelMA hydrogel were placed at the bottom glass plate of a rheometer and sheets of MA- or MA+ were attached to the top metal plate which was lowered onto the GelMA sample with a 1 mm gap. The two components were UV-illuminated through the bottom glass plate. Subsequently, torque forces were exerted over the construct for 5 minutes followed by a recovery period of 5 minutes; (b) Strain and recovery as a function of time at a torque force of 400 μNm .

containing 0.1 w/v% Irgacure 2959. For each sample, measurements were performed in triplicate. The MA+ and MA- discs were attached with a photosticker (HEMA, Groningen, the Netherlands) to the upper 20 mm diameter plate of the geometry (Fig. 3a). 100 μ L of GelMA solution (20% w/v, also containing 0.1% w/v Irgacure) was pipetted at the bottom plate before lowering the top plate to a gap of 1.0 mm: the level at which GelMA and MA+ or MA- had a standardized surface interface of $100 \pm 10 \text{ mm}^2$ (Fig. 3a). Then, the construct was UV-illuminated for 10 minutes (light intensity of 180 mW/cm^2). Next, the obtained constructs were mechanically deformed at different torque values ranging from 50 to 1500 μ Nm consisting of 5 minutes creep followed by 5 minutes recovery, while keeping the temperature at 37°C . In the creep step, a constant torque force was exerted on the top MA+/- layer that was connected to the GelMA sheet and the observed strain or deformation of the material was recorded over time. In the recovery step, the applied force was released, allowing the (grafted) materials to recover to their starting position, representing the elastic properties of the material. The percentage of recovery was calculated as follows:

$$\frac{\text{strain (5 min)} - \text{strain (10 min)}}{\text{strain (5 min)}} \times 100\%.$$

Three-dimensional fiber deposition

Printing of PCL, MA+ and MA- was performed using a Bioscaffolder (SYS+ENG, Salzgitter-Bad, Germany)⁶⁵. Constructs were designed with Rhino 3D software (McNeel, Seattle, WA, USA) and the Standard Tessellation Language (STL) files of these models were translated to the Bioscaffolder through computer-aided manufacturing (CAM) software (PrimCAM, Einsiedeln, Switzerland). 1) A semi-open hollow cuboid was printed (LxWxH: 12x4x2mm), which was filled with GelMA for measuring construct strength; 2) a dome-shaped scaffold (diameter: 15 mm, height 3 mm, strand spacing 1.5 mm, 27 layers) was fabricated for mechanical testing in a model representing an articular chondral defect; 3) a cylindrical scaffold (diameter: 10 mm, height: 0.9 mm, strand spacing 2 mm, 5 layers) was fabricated as a reinforcing framework to GelMA loaded with chondrocytes for *in vitro* and *in vivo* evaluation. Optimal printing was achieved by melting PCL at 160°C and MA+ and MA- at 140°C for extrusion with a 25G metal needle (DL Technology LLC, Haverhill, MA, USA), at a pressure of 0.5 MPa, and a deposition speed of 250 mm/min, producing fibers with a mean thickness of 0.26 mm. Air (20°C) was blown over the construct to facilitate rapid solidification of the printed fibers. A shape inspired by the femoral condyles of a knee joint was fabricated from PLA with an Ultimakertm (Ultimaker LTD, Geldermalsen, The Netherlands) filament-extrusion machine. An indentation was

included (diameter: 15 mm, depth 1 mm) to mimic a chondral defect. The dome-shaped scaffolds were fabricated to tightly fit in this holder for mechanical testing.

Fabrication of reinforced GelMA constructs

GelMA solution (10% w/v, containing 0.1% w/v Irgacure 2959) was added to the MA+ or MA- framework to create fiber-reinforced constructs. First, a mold was printed from PVA with the Ultimaker™ machine in which the frameworks were placed. Then, the GelMA solution was infused at the periphery of the frameworks using a positive displacement pipet, until all pores were completely filled. The constructs were UV-irradiated for 10 minutes with a UV intensity of 120 mW/cm². After photopolymerization, the constructs were taken from the molds and any excess of GelMA at the outside of the constructs was removed.

Integrity of constructs on axial loading

To investigate whether interface grafting of pMHMGCL to GelMA results in a stronger construct, two approaches were used to investigate construct failure.

1) The semi-open cuboids filled with GelMA were UV-irradiated for 10 minutes at 120 mW/cm² and placed in unconfined position between the parallel plates (upper plate 6 mm in diameter) using a DMA 2980 Dynamic Mechanical Analyzer (TA Instruments, New Castle, DE, USA). A force ramp of 0-15 N, with incremental steps of 1.5 N/min was applied at the centre of the construct. Construct failure was defined as the force at which GelMA was squeezed out of the MA+ or MA- cuboid. The force and displacement were recorded throughout compression. Measurements were performed in triplicate and the results were analysed using Thermal Advantage (v. 1.1A) and Microsoft® Excel software.

2) Cylindrical dome-shaped scaffolds, consisting of MA+/GelMA or MA-/GelMA were UV irradiated for 10 min (120 mW/cm²) and were then press-fit in a holder inspired by a knee chondral defect. Because the indentation was 1 mm deep, and the top of the dome was 3 mm in height, the implant raised maximally 2 mm from the defect ridge, matching the curvature of the joint model. In this semi-confined environment the constructs were axially loaded with 20 N (using an AR G-2 rheometer (TA-instruments)) and the change in height of the scaffold was recorded during the compression. Next, 100 creep-recovery cycles were applied onto the construct, each consisting of a 10-second creep step with a torque of 0.01 Nm followed by a 10-second recovery step. The construct was axially compressed for approximately 1 mm, so that the mechanical properties of the PLA holder would not disturb the measurements. The construct strain, resistance to compression and recovery during the creep-recovery cycles were analysed and the constructs were visually inspected after the mechanical loading for signs of structural damage. Supplementary Figure 4 shows the experimental set-up.

Harvest of human chondrocytes

Macroscopically healthy human cartilage from a discarded talus bone was obtained immediately after resection from a 7-years old patient, undergoing an orthopaedic intervention for an ankle disease, according to the institutional code of conduct regarding the use of discarded tissues in the University Medical Center Utrecht. The cartilage was sectioned into small slices under sterile conditions and washed three times with PBS supplemented with penicillin and streptomycin. The full-thickness cartilage was digested overnight using 0.15% type II collagenase at 37 °C and the obtained cell suspension was filtered (100 µm cell strainer) and washed three times with phosphate-buffered saline (disodium hydrogen phosphate 3 g/L, sodium dihydrogen phosphate 0.33 g/L and sodium chloride 8.2 g/L). Cells were then resuspended in chondrocyte expansion medium: DMEM supplemented with 10% heat-inactivated FBS, 100 units/mL penicillin and 100 µg/mL streptomycin, and 10 ng/mL FGF-2 and expanded for 10 days in monolayer cultures (seeding density 5,000 cells/cm²) for use in passage 2.

In vitro redifferentiation of chondrocytes in a fiber reinforced GelMA construct

Chondrocytes were resuspended in 10% GelMA (also containing Irgacure 0.1% (w/v)) at a concentration of 20×10^6 cells/mL. As a negative control group to histological stainings, a sample of chondrocytes was mortalized through a 2-hour trypsin treatment (0.25% trypsin-EDTA, life technologies Europe, Bleiswijk, the Netherlands) before suspension in the hydrogel. The pores of the printed cylindrical MA+ constructs (described in section 2.10) were infused with the cell-laden GelMA solution and UV-irradiated for 5 minutes. For *in vitro* redifferentiation, these samples (n=4) were cultured for 6 weeks in chondrocyte differentiation medium: DMEM supplemented with 0.2 mM ascorbic acid 2-phosphate, 0.5% human serum albumin, 1x ITS-X, 100 units/mL penicillin and 100 µg/mL streptomycin, and 5 ng/mL TGF-β₂, with biweekly medium change.

In vivo redifferentiation of chondrocytes in a fiber reinforced GelMA construct

For *in vivo* redifferentiation, the fiber-reinforced samples (n=4) described in the previous paragraph were pre-cultured for 2 weeks in chondrocyte differentiation medium before subcutaneous implantation. This study was approved by the local Ethics Committee for Animal Experimentation and was in compliance with the Institutional Guidelines on the Use of Laboratory Animals. Four 11-weeks old male athymic rats (Hsd:RH-Foxn1^{tmu} Harlan Laboratories B.V., The Netherlands) were anesthetized with 1.5% isoflurane. A dorsal pocket was created on each rat in which the 10-mm diameter cylindrical construct was placed with a forceps. The skin was closed using Vicryl 4.0 sutures. Preoperatively and postoperatively, the animals received 0.05 mg/kg buprenorphine subcutaneously. The rats were housed in groups at the Central Laboratory Animal Institute of Utrecht University. The rats were sacrificed and the samples were harvested 8 weeks after implantation.

Scaffold morphology and cellular differentiation was investigated and a quarter of each explant was analysed with ^1H NMR to assess degradation of the MA+ component.

Histological, immunohistochemical and biochemical analysis

After the *in vitro* and *in vivo* differentiation experiments, the samples were split and processed for histology, immunohistochemistry and biochemistry. Therefore, one part of the samples was dehydrated through a graded ethanol series, cleared in Histoclear and embedded in paraffin. The samples were sectioned into 5 μm slices and a triple stain of Weigert's hematoxylin, fast green, and Safranin-O was applied to detect tissue formation and deposition of glycosaminoglycans (GAGs).

Immunolocalization of collagen type II involved dewaxing and rehydration through graded alcohol series, washing in PBS/Tween (0.1%), followed by antigen retrieval with 1 mg/mL pronase (30 min) and 10 mg/mL hyaluronidase (30 min). Next, samples were blocked with 0.3% H_2O_2 and 5% BSA (bovine serum albumin) in PBS for 30 minutes and then incubated overnight at 4 °C with antibodies against collagen type II (1:100 from ascites, II-Il6B3, Developmental Studies Hybridoma Bank). Then, samples were washed and incubated for 60 minutes with a horseradish peroxidase-conjugated goat anti-mouse antibody. Antibody-binding was visualized using 3,3'-diaminobenzidine (DAB) solution for 10 minutes and counterstaining was performed with Mayer's hematoxylin. Isotype control stainings were performed by using mouse isotype IgG1 monoclonal antibody at concentrations similar to those used for the primary antibodies. All stained sections were examined using a light microscope (Olympus BX51).

For DNA and GAG quantification, a part of the *in vitro* samples was digested overnight in 20 μl papain solution per mg construct (0.01 M cysteine, 250 $\mu\text{g}/\text{ml}$ papain, 0.2 M NaH_2PO_4 and 0.01 M EDTA) at 60 °C. Total DNA was quantified using a Quant-iT Pico-green dsDNA kit (Invitrogen) according to the manufacturer's instructions. Total GAG content was determined by photospectrometry at 540 and 595 nm after reaction with 1,9-dimethyl-methylene blue (DMMB, 341088; Sigma) using a microplate reader (Biorad)³³⁴. The ratio of both absorbances was calculated and the GAG content was quantified using chondroitin sulphate C (C4384; Sigma). Concentrations in the papain digest were expressed as GAG/DNA.

Statistics

A Mann-Whitney-U test for independent samples was used for comparing construct failure between the two groups. Raw data were processed in SPSS version 18 (IBM software, USA) and $p < 0.05$ was considered significant. All data are represented as means \pm standard deviations.

RESULTS AND DISCUSSION

Poly(hydroxymethylglycolide-co- ϵ -caprolactone) (pHMGCL) was methacrylated (pHMGCL) and blended with poly- ϵ caprolactone (PCL) (1:1) to obtain the thermoplastic polymer blends pHMGCL/PCL (abbreviated as MA-) and pMHMGCL/PCL (abbreviated as MA+). In addition, a hydrogel was produced from methacrylated gelatin (GelMA). Figure 1 shows an overview of the performed experiments to characterize the polymers and blends and to investigate interface-binding strength between both materials and the cartilage specific matrix production in hydrogel constructs reinforced with a MA+ scaffold.

Polymer synthesis and characterization

Poly(benzyloxymethylglycolide-co- ϵ -caprolactone), pBMGCL, was synthesized via ring opening polymerization (ROP) of benzyl protected hydroxymethyl glycolide (BMG) and ϵ -caprolactone in the melt at 130 °C for 16 hours using benzyl alcohol (BnOH) and stannous octoate (SnOct₂) as initiator and catalyst, respectively, and obtained in a high yield (Table 1). The synthesized polymer was deprotected to yield poly(hydroxymethylglycolide-co- ϵ -caprolactone), pHMGCL (Fig. 2). The molar ratio of HMG/CL was calculated using ¹H-NMR by comparing the integrals of peaks belonging to methylene protons of HMG units (3.7-4.0 ppm) and those of CL units (1.3-4.2 ppm) and was found to be very close to the feed ratio, as expected for polymers obtained in high yield (Table 1). The thermal properties of pBMGCL and pHMGCL were investigated by DSC and no melting endotherms were detected showing that these polymers were completely amorphous as can be expected for a random copolymer³³⁵. DSC analysis also showed that removal of the bulky benzyl rings resulted in a decrease in T_g (Table 1).

	HMG/CL molar ratio*	Degree of methacrylation****	Yield (%)	M _w (kDa)	PDI	T _g (°C)	T _m (°C)	ΔH (J/g)
PCL	N.A	0	87	79.1	2.0	-61	57	71
pBMGCL		0	96	36.6	2.3	-25	-	-
pHMGCL	39/61	0	95	31.9	1.8	-38	-	-
pMHMGCL	39/61	44	74	32.4	2.2	-22	-	-
MA-**						-44	56	40
MA+***						-47	52	37

Table 1. Overview of the polymer characteristics

* HMG/CL ratio based on ¹H NMR analysis

** 1:1 pHMGCL/PCL

*** 1:1 pMHMGCL/PCL

**** Measured by ¹H NMR

Subsequently, pHMGCL was functionalized with methacrylate groups aimed at a degree of methacrylation of 50% using methacrylic anhydride, 4-dimethylamine (DMAP) and triethylamine (TEA) as the reactant, catalyst and base (Fig. 2) to yield pMHMGCL. A degree of methacrylation of 50% was chosen because it allows for sufficient bonding after photopolymerization without losing the beneficial properties of the pendant hydroxyl groups³²⁶. The structural analysis of the obtained polymer by ¹H NMR (Supporting Information (SI) Fig. 1) showed the presence of methacrylate groups at 1.9-2.0 ppm and 5.6- 6.4 ppm (peaks j and i). The degree of substitution (DS) was calculated by comparison of the average integrals of peaks at 1.9-2.0 ppm and those of protons attributed to non-functionalized HMG units (4.0-4.3 ppm) and found to be 44%.

After introduction of the methacrylate groups, the molecular weight of the polymer as determined by GPC showed a very slight increase from 31.9 kDa for pHMGCL to 32.4 kDa for pMHMGCL indicating that neither premature cross-linking nor chain scission had occurred. DSC analysis showed that after methacrylation the T_g increased from -38°C to -22°C, which indicates a lower mobility of pMHMGCL chains with rather bulky methacrylate side groups compared to polymers bearing only hydroxyl groups.

PCL was synthesized via ring opening polymerization following the procedures for the synthesis of pBMGCL. DSC analysis showed a melting temperature of PCL of 57°C and a heat of fusion (ΔH) of 71 J/g, similar to other reported PCLs³³⁶. GPC analysis showed a molecular weight (M_w) of 79.1 kDa and polydispersity of 2.0.

Since p(M)HMGCL is fully amorphous with a low T_g , it was blended with PCL to introduce crystallinity and allowing the preparation of scaffolds of suitable dimensional stability. DSC thermograms of the blends pMGMGCL and PHMGCL with PCL (MA+ and MA-, blend ratio 1:1) are shown in Supplementary Figure 2. The melting temperatures of MA+ and MA-, were slightly lower than that of PCL (Table 1). The heat of fusion (ΔH) of the blends was lower compared to PCL (37 and 40 J/g, for MA+ and MA- respectively, compared to 71 J/g for PCL). The reduction in ΔH is in agreement with the percentage of PCL in the scaffolds, which is in line with previously obtained results of blends from PCL/pHMGCL³²⁹. Also, a single T_g was found between the T_g of PCL and p(M)HMGCL, showing that p(M)HMGCL and PCL are fully miscible.

Binding strength of MA+ or MA- to GelMA

To determine the binding strength of MA+ or MA- to GelMA, creep recovery experiments were performed. A schematic representation of the experimental set-up is shown in Figure 3a. Torque forces ranging from 50 to 1500 μNm were applied to measure the resistance over the interface between MA+ or MA- and GelMA. A torque force up to 300 μNm over the grafted MA+ or MA- with GelMA yielded a strain between 0.5 and 0.8% for both groups and subsequently; after removal of the torque, 95-100% recovery was observed (data not shown). These numbers are similar to creep-recovery tests for GelMA

alone (data not shown), reflecting the elastic properties of GelMA. At a torque force of 400 μNm , the MA- / GelMA samples showed a high strain (12-100%) with a negligible recovery of only 0-3% (Fig. 3b). This indicates complete loosening of the material interface, which was macroscopically confirmed. The high variation in the maximal reported strain is due to the early disintegration of the MA-/GelMA constructs. Importantly, at torque forces of 400-1500 μNm the interface of MA+ with GelMA remained intact as confirmed by a low strain and recovery of 94-99%. When the torque force was further increased, the test samples detached from the machine, but leaving the material interface intact. Therefore it can be concluded that the binding strength between MA+ and GelMA is at least 5 times higher than that between MA- and GelMA. This indicates that upon UV-polymerization, reaction between the two methacrylate-functionalized materials had occurred, resulting in a higher mechanical resistance after applied rotational forces.

Construct integrity on axial loading

In a second mechanical experiment, the construct integrity of MA+/MA- with GelMA was tested by axial loading (Fig. 4). The semi-open cuboids printed from MA+ and MA- that were filled with GelMA were loaded with increasing axial compressive forces till construct failure occurred. Construct failure was defined as the moment at which GelMA was pushed out of the thermoplastic cuboid frame, accompanied by an abrupt drop in measured height of the construct as recorded in force-displacement graph (Supplementary Figure 3). Fig. 4d shows that the MA+ construct with GelMA could withstand a significantly higher ($p < 0.05$) axial mechanical force before construct failure occurred (7.7 ± 2.4 N) as compared to the MA- construct (2.7 ± 0.5 N). This experiment confirmed that

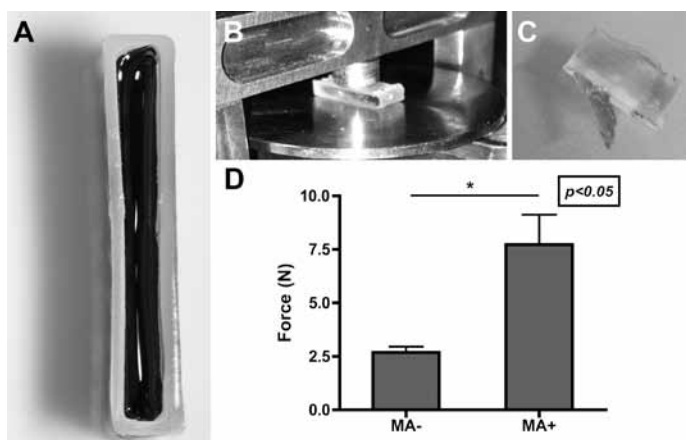


Figure 4. (a) hollow cuboids (LxWxH: 12x4x2mm) were printed from MA- and MA+ and filled with GelMA (stained blue); (b) compression was performed till (c) the construct failed as defined by GelMA being squeezed out of the construct; (d) force at construct failure.

photopolymerization between MA+ and GelMA had occurred, resulting in a three-fold higher mechanical resistance during axial compression.

Mechanical testing of fiber-reinforced constructs in a model mimicking an articular joint

Reinforced constructs were studied in a model resembling an articular cartilage defect (Fig. 5a). The experimental set-up is shown in Supplementary Figure 4. The constructs were first axially loaded followed by 100 cycles of rotational forces in order to simulate repeated movement of a joint. A typical creep-recovery registration by the rheometer is shown in Fig. 5b. During these repetitive rotational forces, a significantly higher deformation, as reflected in the percentage strain, was found for MA-/GelMA constructs compared to the MA+/GelMA constructs. Table 2 shows that loading 20 N on the constructs compressed the MA-/GelMA scaffolds to a higher extent than the MA+/GelMA scaffolds ($71 \pm 4\%$ for MA-/GelMA compared to $43 \pm 5\%$ for MA+/GelMA). In addition, after the repetitive rotational forces, the residual loading on the MA-/GelMA scaffolds was only 7.4 ± 0.4 N whereas for the MA+/GelMA scaffolds 14.1 ± 0.5 N of compressive

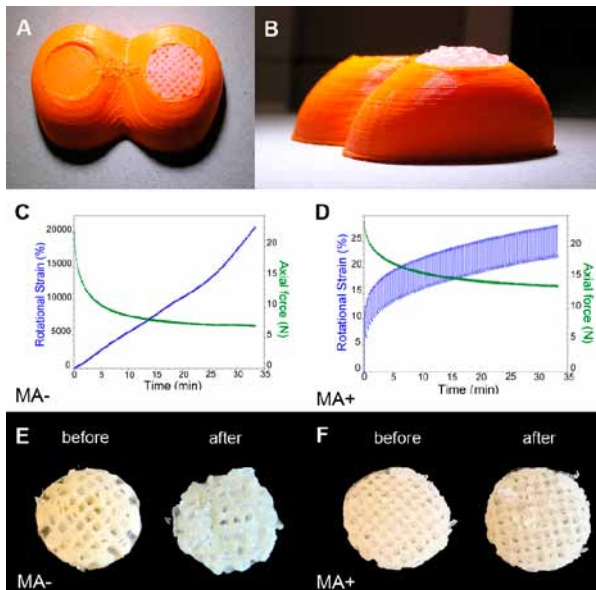


Figure 5. (a) a model representing the femoral condyles of the human knee was fabricated from poly lactic acid (orange). Fiber reinforced constructs were press-fit in a designed indentation in the condyle (diameter 15 mm, depth 2 mm); (b) side view of a femoral condyle model; (c) effect of 100 cycles of rotational forces (0.01Nm creep of 10 sec, followed by 10 sec recovery) on the rotational strain and axial force of MA- scaffolds and (d) MA+ scaffolds; (e) photographs of the MA- scaffolds before and after the applied forces; (f) photographs of the MA+ scaffolds before and after the applied forces.

	Axial compression/strain*	Residual compression strength**
MA-/gelMA	71 ± 4 %	7.4 ± 0.4 N
MA+/gelMA	43 ± 5 %	14.1 ± 0.5 N

Table 2. Construct strain following axial compression of 20 N and residual compression strength after 100 cycles of 0.01 Nm creep-recovery.

* Height of construct after 20 N axial loading divided by original height of construct * 100%

** Remaining axial loading after 100 creep-recovery cycles (axial loading at start =20 N)

strength remained. The lack of recovery after repeated rotational forces and the low values of residual compressive strength for MA-/GelMA constructs demonstrate the lack of integration of both materials. On macroscopical assessment after the loading regime the shape of the MA+/GelMA constructs appeared to be unchanged, but the MA-/GelMA constructs showed an irreversible structural damage (Fig. 5c). GelMA without a reinforcing scaffold was tested under the same loading regime and was found to disintegrate completely, showing that reinforcement is necessary to use these constructs in load-bearing applications. It should be noticed that 20 N is only a fraction of a full load-bearing situation in which forces lay typically in the range of 1700-2700 N in an average weight person³³⁷. Yet in this model GelMA reinforced with a MA+ scaffold showed a superior mechanical strength, compared to reinforcement with a MA- scaffold and GelMA alone.

Chondrogenic differentiation in a fiber-reinforced construct *in vitro*

After six weeks of *in vitro* culture, human chondrocytes in MA+ reinforced GelMA constructs had produced a network of GAGs and collagen type II (Fig. 6), which are the main cartilage-specific extracellular matrix components³³⁸. GAGs were deposited and had diffused throughout the whole hydrogel compartment as is indicated by the red staining (Fig. 6a), compared to the negative control samples (Fig. 6b). Also, chondrocytes and GAGs were present at the interface with the MA+ network (Fig. 6c). The formation of such an interconnected matrix is essential in order to achieve an adequate cartilage-like function of the construct^{60,63}. The amount of GAGs that was produced in the constructs after six weeks was found to be 10.5 ± 2.7 mg GAG / mg DNA, which is in line with earlier reports of chondrocytes in GelMA-based scaffolds^{60,63}. In addition, immunohistochemistry revealed the presence of a pericellular matrix of cartilage specific collagen type II (Fig. 6d).

Chondrogenic differentiation in a fiber-reinforced construct *in vivo*

The MA+/GelMA constructs were implanted in rats and it was shown that a network of GAGs was present eight weeks after subcutaneous implantation (Fig. 6e). Here, GAGs were not quantified because normalization to DNA of implanted cells was impossible due to infiltration of host cells and their DNA in the implanted constructs. Collagen type II production was more pronounced *in vivo* compared to *in vitro* results as shown by the

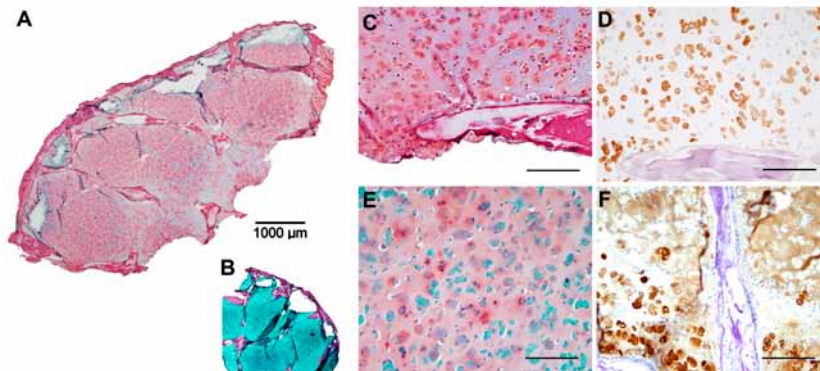


Figure 6. Human articular chondrocytes produced cartilage-specific matrix components in MA+ reinforced GelMA constructs after 6 weeks *in vitro* culture as shown by positive safranin-O staining (**a, c**; red) for glycosaminoglycans (GAGs) produced by chondrocytes in GelMA. The MA+ scaffold architecture is visible in dark red. In negative control samples (**b**), GelMA stains green and the MA+ stains dark red by the safranin-O triple staining. Staining collagen type II staining is visible in the pericellular matrix of the chondrocytes (**d**), MA+ scaffold in purple. After 8 weeks *in vivo* with 2 weeks pre-culturing there was production of GAGs (**e**), although less extensive compared to *in vitro* cultures (**c**). An interconnected collagen type II network was formed *in vivo* (**f**). Scale bar C-F = 200 µm.

extensive network formation reflected by the immunohistochemical stainings (Fig. 6f). Also, collagen type II was deposited at the interface of the MA+ scaffold, contributing to the integration of neo-tissue with the polyester scaffold. This is important, since the neo-tissue together with the MA+ scaffold will determine the mechanical properties of the construct after the hydrogel component has been degraded⁵⁰.

Degradation of pMHMGCL *in vivo*

Degradation of the explanted MA+ component was shown with ¹H NMR by the disappearance of HMG units (Supplementary Figure 5), which is in line with previous observations^{328,339}. Furthermore, NMR shows a reduction in the methacrylate signals at 5.6 and 6.4 ppm. This is most likely caused by both crosslinking of pMHMGCL with GelMA and hydrolysis of the ester groups connecting the methacrylate groups of pMHMGCL. Since no photoinitiator was incorporated in the polyester, it was to be expected that not all methacrylate groups in pMHMGCL had photopolymerized. Degradation of these constructs will therefore lead to the formation of methacrylic acid. As is shown before for methacrylated dextran-based hydrogels^{340,341}, methacrylic acid does not cause cytotoxicity and therefore does not affect the suitability of these materials for tissue engineering purposes.

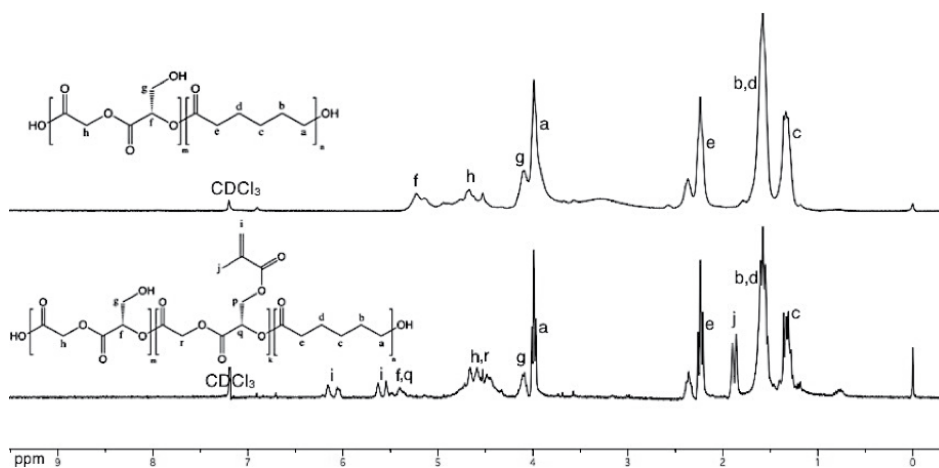
CONCLUSIONS

This study showed that a 3D-fabricated pMHMGCL/PCL thermoplastic polymer scaffold could be covalently linked to a chondrocyte-laden GelMA hydrogel. Covalently grafting both materials significantly improved the binding strength between the materials and consequently resulted in an enhanced mechanical integrity of reinforced hydrogel constructs. Embedded chondrocytes showed significant cartilage-specific matrix deposition in these constructs both *in vitro* and *in vivo*. Moreover, since both materials have shown their ability to support matrix formation and both can be applied in additive manufacturing techniques, the current work allows for the fabrication of mechanically enhanced, patient-specific cartilage implants.

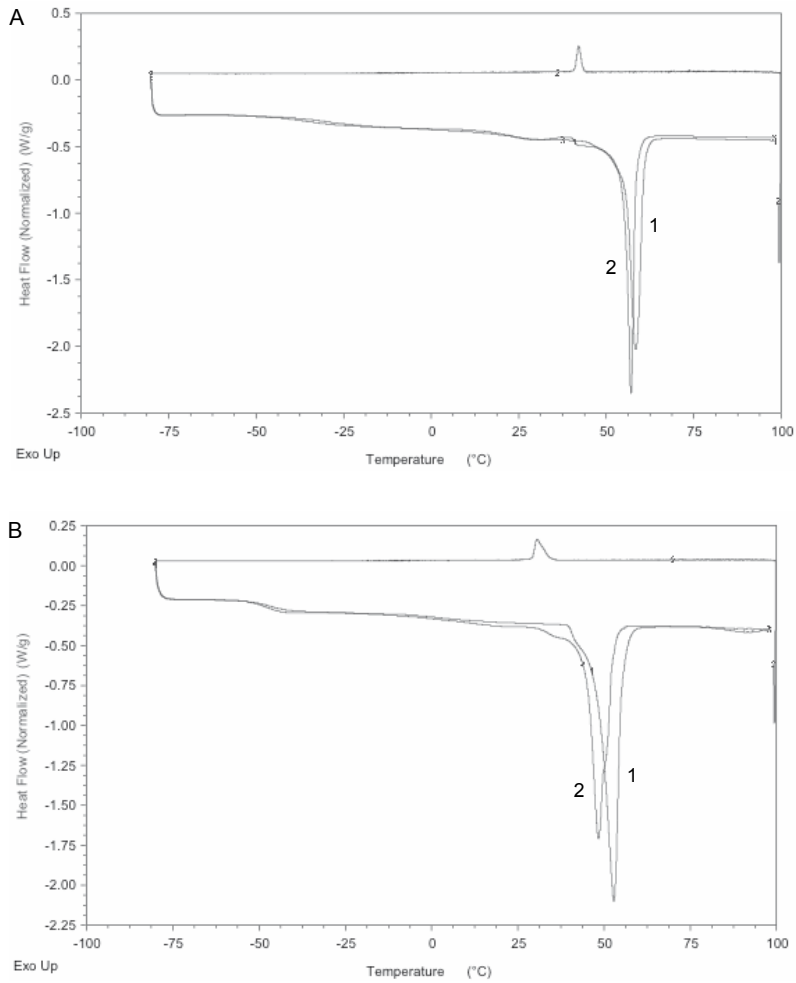
ACKNOWLEDGEMENTS

The authors would like to thank Kim Benders for her assistance in isolating human chondrocytes. Also we would like to thank Marco Raaben for optimizing printing parameters for MA+/MA-, Ben Peters for designing the knee implant model and Jeremy Besems for assisting in the histology analyses. The collagen type II monoclonal antibody (developed by T.F. Linsenmayer) was obtained from the Developmental Studies Hybridoma Bank. Jos Malda was supported by the Dutch Arthritis Association, Kristel Boere and Jetze Visser were supported by Netherlands Institute of Regenerative Medicine (NIRM). Debby Gawlitta was supported by the Dutch Technology Foundation, STW (Veni 11208).

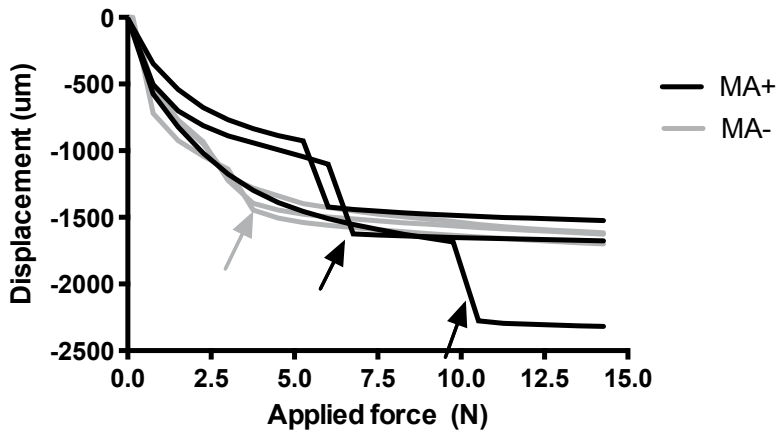
SUPPLEMENTARY INFORMATION



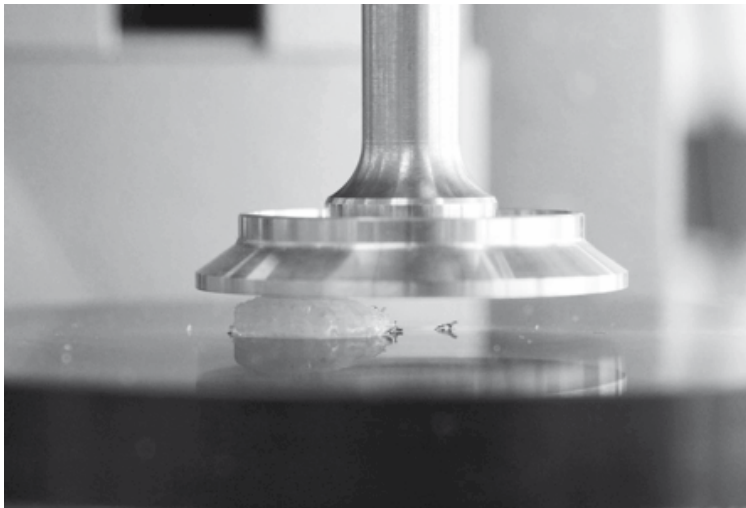
Supplementary Figure 1. ¹H NMR spectra of (above) pHMGCL, and (below) pMHMGCL in CDCl₃. Methacrylate peaks of pMHMGCL are shown at 1.9-2.0 ppm (peak j) and 5.6-6.4 ppm (peaks i).



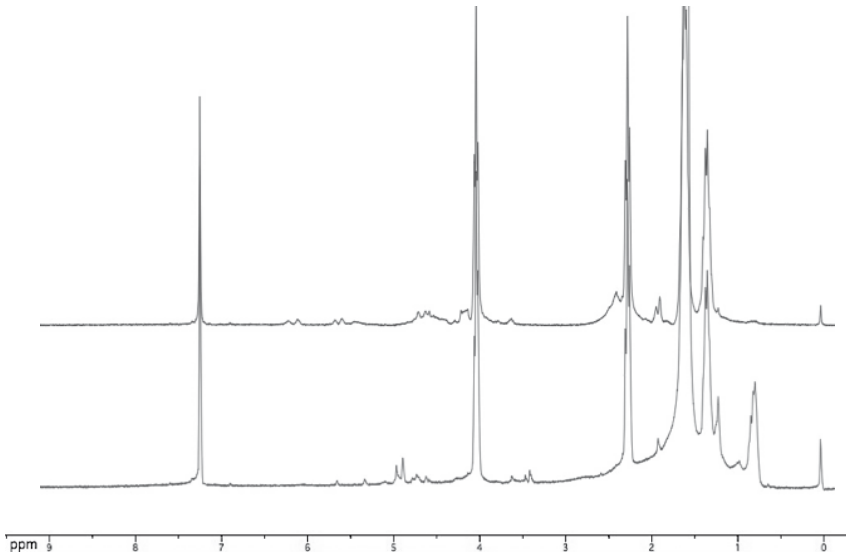
Supplementary Figure 2. DSC thermograms of the blends (a) MA- (1:1 PCL:pHMGCL) and (b) MA+ (1:1 PCL: pHMGCL). 1 and 2 show thermograms of the 1st and 2nd heating run respectively.



Supplementary Figure 3. Force-displacement graph of rectangle fiber reinforced constructs. A drop in displacement was visible when the hydrogel was squeezed out from the reinforced construct.



Supplementary Figure 4. Experimental set-up of the mechanical integrity test for constructs used in a knee chondral defect. Mechanical tests were performed with a rheometer, set at an initial axial loading of 20N, followed by 100 creep-recovery cycles of 0.01Nm.



Supplementary Figure 5. ¹H NMR spectrum in CDCl₃ of MA+ before (above) and after (below) 8 weeks implantation in rats. Degradation was confirmed by the disappearance of the peak at 4.2 ppm (HMG peak).

Chapter 6

Reinforcement of Hydrogels using Three-Dimensionally Printed Microfibres

Jetze Visser
Ferry P.W. Melchels
June E. Jeon
Erik M. van Bussel
Laura S. Kimpton
Helen M. Byrne
Wouter J.A. Dhert
Paul D. Dalton
Dietmar W. Hutmacher
Jos Malda

*Nature Communications. 2015;6:6933 doi: 10.1038/
ncomms7933*

ABSTRACT

Despite intensive research, hydrogels currently available for tissue repair in the musculoskeletal system are unable to meet the mechanical, as well as the biological, requirements for successful outcomes. Here, we reinforce soft hydrogels with highly organised, high-porosity microfibre networks that are 3D-printed with a technique termed *melt electrospinning writing*. We show that the stiffness of the gel/scaffold composites increases synergistically (up to 54-fold), compared to hydrogels or microfibre scaffolds alone. Modelling affirms that reinforcement with defined microscale structures is applicable to numerous hydrogels. The stiffness and elasticity of the composites approach that of articular cartilage tissue. Human chondrocytes embedded in the composites are viable, retain their round morphology and are responsive to an *in vitro* physiological loading regime in terms of gene expression and matrix production. The current approach of reinforcing hydrogels with 3D-printed microfibres offers a fundament for producing tissue constructs with biological and mechanical compatibility.

INTRODUCTION

Hydrogels are an important class of biomaterials with many applications, including as cell carriers for the engineering of tissues^{104,246}. In this respect, hydrogels are designed to provide the cells with a fully hydrated three-dimensional (3D) environment comparable to the extracellular matrix of native tissues^{29,79}. When embedded within hydrogels, cells need to form a tissue-specific matrix that is capable of repairing or regenerating the damaged tissue. However, hydrogels often have inadequate mechanical properties, which are either unfavourable to embedded cells or make them too weak for application in the musculoskeletal system^{6,307,342}.

The performance of hydrogel implants is expected to be superior when they closely match the mechanical properties of their target tissue^{56,343}. This is based on the principle that cells in native tissues are responsive to different types of mechanical stresses, such as compression, tension, and shear³⁴⁴⁻³⁴⁶. These properties, *e.g.* stiffness, can be improved by increasing the hydrogel polymer concentration or crosslink density^{79,246,347} or by the formation of tissue-specific extracellular matrix prior to implantation of the graft^{63,246,348}. However, this generally compromises the biological performance of the hydrogel^{79,246} or requires a long and costly period of pre-culture.

Tissue engineers have, therefore, been inspired by the architecture of native tissues, which derive their unique mechanical properties from a fibrous protein framework that supports the aqueous component, forming a complex composite³⁰³. For example, hydrogels have been reinforced with nanofibres^{192,200,349}, microfibres³⁵⁰ and woven^{316,343,351}

or non-woven³⁵² scaffolds. The mechanical properties of hydrogels in such composites are less demanding, so they can be processed with a low crosslink density, which is beneficial for cell migration and the formation of neo-tissue^{79,246}. Recent composite systems include non-woven scaffolds, manufactured via solution electrospinning techniques^{55,56,201,321,322} and scaffolds fabricated via 3D printing^{65,76,77,255,353,354}. Due to the small fibre diameters that can be obtained, electrospun meshes have the potential to mimic native tissue extracellular matrix structures, including its mechanical properties. However, a disadvantage of traditional solution electrospinning techniques is the limited control over network architecture. Recently, melt electrospinning has been used in a direct writing mode, and may overcome this limitation, with the layer-by-layer assembly of the low diameter fibres, permitting tight control over the network architecture^{54,206}.

This study aims to mechanically reinforce gelatin methacrylamide (GelMA) hydrogels with organized, high-porosity poly(ϵ -caprolactone) (PCL) fibre scaffolds. GelMA is a hydrogel platform with recent use that allows for matrix deposition by embedded cells, e.g. vascular networks or cartilage matrix^{60,63,64}. Reinforcing scaffolds with different porosities were fabricated from medical-grade PCL by melt electrospinning in a direct writing mode⁵⁴. Fibrous hydrogel composites were then fabricated by infusing and crosslinking GelMA within the PCL scaffolds. The stiffness and recovery under cyclic compression of these composites were analysed depending on PCL scaffold porosity and the degree of crosslinking of the GelMA. A mathematical model was developed using the scaffold parameters, and subsequently used to simulate and predict the degree of hydrogel reinforcement. Finally, human primary chondrocytes were encapsulated in the composite constructs and their viability, morphology, and chondrogenic differentiation were investigated in an *in vitro* culture assay under physiological compressive loading.

We demonstrate that hydrogels are reinforced in a synergistic fashion with high-porosity microfibre scaffolds. The stiffness of the composites approaches that of articular cartilage, while maintaining a relevant elasticity. Chondrocytes embedded in the composite constructs respond positively to a repetitive mechanical loading regime in a bioreactor culture, in terms of cartilage gene expression and matrix formation. These hydrogel/microfiber composites thus offer a mechanically and biologically favourable environment for the engineering of tissues.

METHODS

Fabrication of PCL microfibre scaffolds

Several scaffolds were 3D-printed from medical-grade PCL (PURAC, Gorinchem, the Netherlands) with a custom-made melt electrospinning device⁵⁴. PCL was heated to 103°C in a 2 ml polypropylene syringe and extruded at a rate of 18 μ l/hour using a syringe

pump. In combination with an electrostatic field of 8-10 kV between the syringe needle tip (23G) and the collector plate (3 cm distance), a stable PCL jet was obtained. Defined scaffold architectures, with dimensions up to 120x120x1 mm, were realized through computer-aided movement of the aluminium collector plate at a speed of 1400 mm/min, using Mach3 motion control software (Artsoft, USA). A predefined 0-90° architecture was imposed, with a fibre spacing of 0.2, 0.4, 0.6, 0.8 or 1.0 mm. The melt electrospinning writing was terminated when scaffolds reached a height of 1.0 mm, to ensure maximum quality of the architecture. To investigate the effect of PCL flow rate on fibre diameter and scaffold porosity, we printed constructs at 4x and 10x flow rate, with a fibre spacing of 0.4 mm and 1.0 mm respectively. Cylindrical samples were extracted from the scaffolds with a 5 mm diameter biopsy punch. Two scaffolds were stacked in order to achieve a height of 2 mm, which is comparable to the thickness of human cartilage in the knee joint³⁵⁵. The porosity and mechanical properties of the melt electrospun scaffolds were compared to scaffolds fabricated with traditional 3D printing technologies. To this end, scaffolds were 3D-printed from PCL with a BioScaffolder system (SYS+ENG, Salzgitter-Bad, Germany) as described previously¹⁹⁰. Briefly, PCL was heated till 70 °C and extruded with an Auger screw through a 27 gauge needle. Scaffolds measuring 40x40x2 mm were fabricated with a fibre spacing of 0.75, 1.0, 1.25, 1.5 and 1.75 mm. The quality of the scaffolds was imaged both with stereomicroscopy and Scanning Electron Microscopy (Hitachi TM3000, Japan and Quanta 200, FEI, Milton, Australia). The fibre diameter was measured with ImageJ software (National Institutes of Health, USA). The porosity of the PCL scaffolds was determined gravimetrically.

Etching of PCL microfibre scaffolds

PCL scaffolds were etched in order to increase its hydrophilicity and surface area, which could potentially contribute to the stiffness of reinforced GelMA constructs. Cylindrical PCL scaffolds with a porosity of 94% were treated with 70% ethanol and subsequently etched with 5M sodium hydroxide for 0, 1, 2, 4, 8 and 16 hours. After etching, the scaffolds were washed in deionized H₂O until the pH reached 7.4, and then air-dried. The effect of etching was evaluated by measuring the fibre diameter (ImageJ) from SEM images, and by assessing the weight from 2 x 5 mm diameter scaffolds (expressed in relative weight loss). Since mild etching will increase hydrophilicity and may facilitate perfusion of GelMA through the PCL scaffold, 2 hours of etching was performed for all other experiments presented.

Preparation of gelatin methacrylamide and alginate gels

GelMA was synthesized by reaction of type A gelatin (Sigma-Aldrich, St. Louis, Missouri, USA) with methacrylic anhydride at 50 °C for one hour as previously described⁶³. GelMA was dissolved in Phosphate Buffered Saline (PBS) at 60 °C at a concentration of 10% (w/v)

containing 12.5 or 25 mM ammonium persulfate (APS). 12.5 or 25 mM tetramethylethylenediamide (TEMED) was added followed by 5 seconds vortexing in order to initiate crosslinking of the GelMA. Alginate (IMCD, Amersfoort, The Netherlands) was dissolved in PBS at 3% (w/v), and used as a control gel to GelMA for the mechanical analyses.

Preparation of reinforced hydrogel constructs

The scaffolds were placed in an injection mold that was custom made from polymethylmethacrylate in order to fit 10 cylinders with a diameter of 5 mm and a height of 2 mm. All cylindrical voids in the mold were interconnected so that gel could be serially perfused. The mold was sealed with a sheet of polyethylene that was fixed between two glass histology slides. Directly after mixing in the TEMED, the GelMA solution as described above was injected in the mold until all PCL scaffolds were fully infused. Crosslinking of the GelMA was allowed in this mold at 37° C for 1 hour. Cell-free samples were then stored in PBS at 37° C. Chondrocyte-laden samples were kept in chondrocyte expansion medium. In order to evaluate the effect of etching time of the scaffolds on construct stiffness, GelMA was reinforced with scaffolds etched for 0-16 hours (all n=5) and crosslinked with 25 mM APS/TEMED. In addition, 93-98% porosity PCL scaffolds (all n=5) were infused with alginate in the mold. The alginate composite constructs were then crosslinked by immersion in a 102 mmol calciumchloride solution for 30 minutes.

Harvest of equine cartilage

Full-thickness cartilage was harvested from the knee joint from one equine donor (10 years old) with macroscopically healthy cartilage. This was done after consent of the horse owner and according to the ethical guidelines of Utrecht University. Equine cartilage was used because of the availability and its similarities to human cartilage³⁵⁵. Cylindrical samples with a diameter of 5 mm and a height of 2 mm (n=8) were taken with a biopsy punch from the medial patellofemoral groove and stored in PBS for up to 3 hours.

Mechanical analyses

The stiffness (or compressive modulus) of GelMA and alginate hydrogels, PCL scaffolds, the composite constructs and articular cartilage (all n=5) was measured by single uniaxial unconfined compression in air at room temperature, after 1-3 days submersion in PBS from their preparation. We confirmed that for single cycle compression testing, the absence of a PBS immersion bath does not influence the stress responses of hydrogel samples. The effect of crosslinking with 12.5 or 25 mM APS/TEMED was tested. The stress/strain curves of (reinforced) GelMA that was crosslinked with 12.5 mM APS/TEMED were compared with cartilage samples. Over a period of two minutes, a force ramp (axial strain rate ca. 25%/min) was applied to the samples employing a microtester (Instron,

Melbourne, Australia) or a Dynamic Mechanical Analyser (DMA 2980, TA Instruments, New Castle, DE, USA). The stiffness was calculated from the linear derivative of the stress/strain curve at 12-15% strain. In the low-porosity scaffolds that were fabricated with traditional 3D printing, the 6-9% strain region was taken, as these constructs often disintegrated when strained beyond 10%. The compression cycle of GelMA reinforced with 97% and 82% porosity scaffolds was captured from the side (hand-held digital microscope 1.3 MP, Meade instruments, Europe GmbH & Co, Rhede, Germany) in order to analyse the lateral expansion of both components of the composite construct. In addition, images from the top of these constructs were taken with a stereomicroscope, when uncompressed and at 30% strain between two glass slides.

In order to test the time-dependent stress response, GelMA, GelMA reinforced with 93% porosity scaffolds and articular cartilage samples, were subjected to a series of isostrain steps³⁵⁶. Samples were 2% pre-strained for 5 minutes, followed by strains of 6%, 9% and 13% that were consecutively applied for 15 minutes each. The experiments were performed in PBS and the stress response of all samples was recorded. The modulus on fast initial loading and the equilibrium modulus were extracted and the stress decay rate was estimated by fitting to a bi-exponential function.

The resistance to axial deformation of GelMA and GelMA reinforced with PCL constructs (porosity 93% and 97%) was measured after a cyclic (20x) axial strain of 20% (All-round-line Zo20, Zwick Roell, Germany). In addition, the resistance after 20 cycles of axial deformation of 50% was measured for GelMA constructs. The recovery measurements were performed in PBS and constructs were allowed to recover for 1 minute after every cycle. GelMA constructs reinforced with a 93% porous scaffold underwent compression with incremental maximum strains of 20-40% (with 5% increments) in order to analyse the maximal strain that could be exerted before irreversible damage would occur.

Modelling the fibre reinforcement of hydrogels

A mathematical model was constructed to investigate further the mechanisms by which the 3D-printed scaffolds reinforce the hydrogels. There is an extensive literature on the modelling of fibre reinforced biological materials, with recent cartilage-focussed examples^{357,358}. Fibre reinforced materials are often modelled by assuming it is reasonable to define a continuously varying fibre density and orientation and then making the material properties a function of these. In this instance, given that we know the arrangement and approximate number of fibres in each plane of the material, we take the more direct approach of considering how each fibre stretches as the scaffold deforms. Our model takes into account the number of fibres in the scaffold and the fibre diameter; the Young's modulus of PCL and the construct dimensions. In the model, the composite construct was viewed as an elastic solid, in which the PCL fibres are placed under tension by the hydrogel on axial compression.

Harvest of human chondrocytes

Macroscopically healthy cartilage was harvested either from a discarded talus bone that was resected from a 7-year old patient undergoing an orthopaedic intervention, or from the femoral condyles of knee replacement surgery patients (age: 71.0 ± 4.1 ; $n = 6$) with consent. This was in concordance with the institutional code of conduct regarding the use of discarded tissues in the University Medical Center Utrecht, and ethics approval was also obtained from Queensland University of Technology and Prince Charles hospital prior to sample collection. Cartilage was cut into small slices and washed with PBS supplemented with penicillin and streptomycin. The cartilage was digested overnight in 0.15% type II collagenase at 37°C. The resulting cell suspension was filtered (100 μm cell strainer) and washed three times with phosphate-buffered saline. Then cells were resuspended in chondrocyte expansion medium (DMEM supplemented with 10% FBS (Fetal Bovine Serum), 100 units/mL penicillin and 100 $\mu\text{g}/\text{mL}$ streptomycin, and 10 ng/mL FGF-2) and expanded for 10 days in monolayer cultures (seeding density 5,000 cells/ cm^2). For the short-term study (7 day), chondrocytes from the talus bone were used at passage 2, and for the long-term study (28 day), chondrocytes obtained from the femoral condyles of the different donors were pooled and used at passage 1.

Cell viability

Chondrocytes were mixed in the GelMA/APS solution at a concentration of 10 million/ml. Crosslinking was done with different proportions of APS/TEMED (12.5/12.5 and 25/25 mM) in order to evaluate cytotoxicity of the redox crosslinking process. The viability of the chondrocytes was measured 4 hours (day 1) and 7 days after embedding and crosslinking of the GelMA constructs. To visualize cell viability, a LIVE/DEAD Viability Assay (Molecular Probes MP03224, Eugene, USA) was performed according to the manufacturer's instructions. The samples were examined using a light microscope with the excitation/emission filters set at 488/530 nm to observe living (green) cells and at 530/580 nm to detect dead (red) cells. Photographs were taken with an Olympus DP70 camera. The ratio dead/alive was measured by assessing multiple parts of the sample.

Cell morphology

The morphology and location of chondrocytes in the reinforced GelMA constructs was assessed 7 days after encapsulation. Reinforced GelMA constructs with chondrocytes ($n=3$, 93% porosity) were dehydrated through a graded ethanol series, cleared in xylene and embedded in paraffin. The samples were sectioned into 10 μm slices and stained with hematoxyline and eosine for the detection of GelMA, the PCL scaffold and the cells. In addition, the location of chondrocytes and their relation to the PCL fibres were assessed at days 1 and 7 by fluorescent staining with 4',6-diamidino-2-phenylindole (DAPI). To this end, constructs from GelMA only and reinforced with a PCL scaffold (93%

porosity) were crosslinked with 12.5 mM APS/TEMED ($n=3$). The GelMA was subsequently permeabilized with 1% Triton/PBS for 15 minutes and incubated with DAPI (0.1 $\mu\text{g}/\text{ml}$ in PBS) for 5 minutes, followed by three washing steps with PBS. Fluorescence microscopy images were taken (with excitation/emission filter 330-385nm) to detect the cell nuclei (blue).

Mechanical stimulation

For the chondrocyte redifferentiation experiment, 0.5% hyaluronic acid was added to 10% GelMA to promote redifferentiation of embedded chondrocytes^{60,63}. Chondrocyte-laden GelMA-HA gels and GelMA-HA-PCL composite gels (PCL scaffold porosity: 93%) were able to swell freely under static conditions during the first 14 days. Following this pre-culture period, the constructs were cultured for another 14 days using a pre-established loading protocol (3 hours/day, 20% strain, 1 Hz sinusoidal loading) in a commercial bioreactor (Cartigen C10-12c, Tissue Growth Technologies, Minnetonka, MN, USA). Constructs were cultured in high glucose DMEM supplemented with 10 ng/mL TGF- β_3 , 1% ITS, 1.25 mg/mL bovine serum albumin, 10⁻⁷ M dexamethasone, and other additives (GlutaMAX-1, 110 mg/L sodium pyruvate, 10 mM HEPES, 0.1 mM nonessential amino acids, 50 U/mL penicillin, 50 $\mu\text{g}/\text{mL}$ streptomycin, 0.5 $\mu\text{g}/\text{mL}$ fungizone and 0.1 mM L-ascorbic acid). Constructs were cultured for a total of 28 days.

qRT-PCR

Gene expression analysis was performed on the GelMA-HA hydrogels and the GelMA-HA hydrogels reinforced with 93% porosity PCL scaffold following 28 days of culture. RNA from the compressed (C) and non-compressed (NC) constructs was purified using the TRIzol reagent ($n=4$). cDNA synthesis was carried out using the SuperScriptTM III first-strand synthesis supermix kit. Gene expression of ACAN (F: 5'-GCCTGCGCTCCAATGACT-3', R: 5'-TAATGGAACACGATGCCTTTCA-3', NM_001135), COL2A1 (F: 5'-GGCAATAGCAGGTTACAGTACA-3', R: 5'-CGATAACAGTCTTGCCCCACTT-3', NM_001844), COL1A1 (F: 5'-CAGCCGCTTACCTACAGC-3', R: 5'-TTTTGTATTCAATCACTGTCTTGCC-3', NM_000088), and COL10A1 (F: 5'-ACCCAACACCAAGACACAGTTCT-3', R: 5'-TCTTACTGCTATACCTTACTCTTTATGGTGTA-3', NM_000493) were analyzed by real-time PCR using the SYBR GreenERTM qPCR supermix universal kit. All reagents and kits were purchased from Life Technologies and samples were processed according to the manufacturer's instructions. The cycle threshold (Ct) value of each gene was normalized to the housekeeping gene β_2 microglobulin (B2M, F: 5'-ATGAGTATGCCTGCCGTGTGA-3', R: 5'-GGCATCTTCAAACCTC-CATGATG-3') using the comparative Ct method ($2^{-\Delta\text{Ct}}$).

Glycosaminoglycan analysis

Samples from the compression experiment were digested in 0.5 mg/mL proteinase K solution overnight at 60°C (n = 5). Digested samples were analyzed for GAG using the 1, 9-dimethylmethylene blue assay at pH 3. GAG measurements for each construct were normalized to its wet weight.

Immunohistochemistry

After 28 days, the reinforced GelMA-HA gels were paraffin-embedded and sectioned at 5 µm. For antigen retrieval, ready-to-use proteinase K solution (Dako) was used for 10 minutes at 37 °C. Sections were blocked with 2% FBS solution prior to exposure to primary antibodies: I-8H5 (MP Biomedicals), dilution 1:300 for collagen type I; II-116B3 (DSHB), dilution 1:200 for collagen type II. Following incubation in fluorescence-labelled goat anti-mouse secondary antibody (Alexa Fluor 488, Invitrogen), sections were mounted with Prolong Gold (Invitrogen) and visualized using a confocal fluorescence microscope (A1R Confocal, Nikon).

Statistics

All data were expressed as mean ± standard deviation of five independent samples, unless stated otherwise. One-way ANOVA with Bonferroni correction was performed to compare the stiffness of the reinforced hydrogels; the effect of scaffold porosity was compared for every hydrogel and the effect of the hydrogel was compared for every scaffold porosity. Two-way ANOVA was used to evaluate the effect of compression and hydrogel types on gene expression, GAG/ww, and stiffness. An independent samples T-test, not assuming equal variances, was performed to evaluate cell viability (SPSS, IBM software, USA). Differences were considered significant when $P < 0.05$.

RESULTS

Fabrication of PCL microfibre scaffolds

PCL scaffolds of 1 mm height were 3D-printed with a reproducible quality using melt electrospinning writing (Fig. 1a and Supplementary Movie 1). Scaffolds were fabricated with fibre spacings between 0.2 mm (Fig. 1b) and 1.0 mm (Fig. 1c). The fibres were well aligned and fused at the 0°-90° oriented junctions (Fig. 1d). The fidelity of fibre deposition decreased for constructs higher than 1 mm, probably because of the electric isolating effect of the scaffold that had already been deposited on the collector plate. Therefore, two scaffolds were stacked in the current study to obtain 2 mm high constructs. The scaffold porosity could be controlled within the range of 93-98% by varying the set fibre spacing between 0.2 and 1.0 mm (Fig. 1e). Flow rates of 18 µL/hr, 72 µL/hr and 180 µL/hr

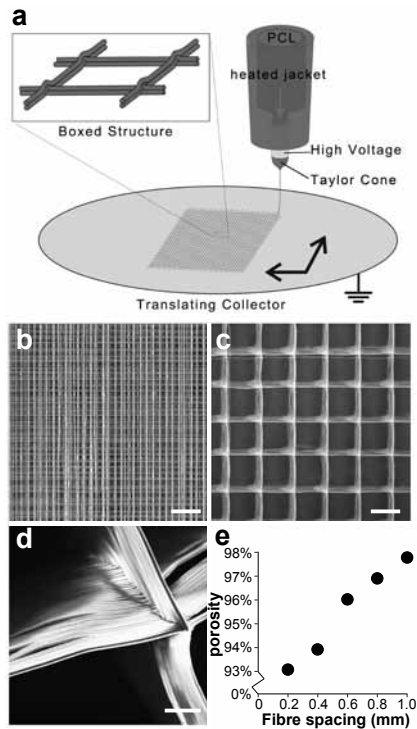


Figure 1. Fabrication of microfibre scaffolds. Three-dimensional scaffolds were fabricated from poly(ϵ -caprolactone) (PCL) by 3D printing, i.e. melt-electrospinning in a direct writing mode. **(a)** Thin PCL fibres were stacked in a 0-90° orientation through combined extrusion and an electrostatic field between the dispensing needle and the translating collector plate. Several fibre spacings were applied ranging from **(b)** 0.2 mm and **(c)** 1.0 mm as visualized with stereomicroscopy (scale bar 1 mm). **(d)** Detailed image of the fibres that fused at the cross-sections (fibre spacing 1.0 mm, scale bar 200 μ m). **(e)** The porosity of the scaffolds varied between 93% and 98% depending on the set fibre spacing.

corresponded to fibre diameters of $19.4 \pm 1.7 \mu\text{m}$, $48.5 \pm 8.2 \mu\text{m}$ and $88.5 \pm 7.6 \mu\text{m}$ respectively. Larger diameter scaffolds of the same polymer were 3D-printed with traditional melt extrusion based methods as a control for the mechanical analyses. These scaffolds had a fibre diameter of 219.7 ± 14.2 and a porosity ranging from 89% to 72%, depending on the set fibre spacing.

Stiffness of reinforced GelMA and alginate hydrogels

A synergistic effect was observed on construct stiffness (strain rate 25%/min) when GelMA and alginate hydrogels were reinforced with the microfibre PCL scaffolds (Fig. 2). The stiffness of PCL scaffolds alone increased from 1.1 ± 0.3 kPa for 98% porosity to 15.2 ± 2.2 kPa for the 93% porosity scaffold (Fig. 2a). The stiffness of the scaffolds was

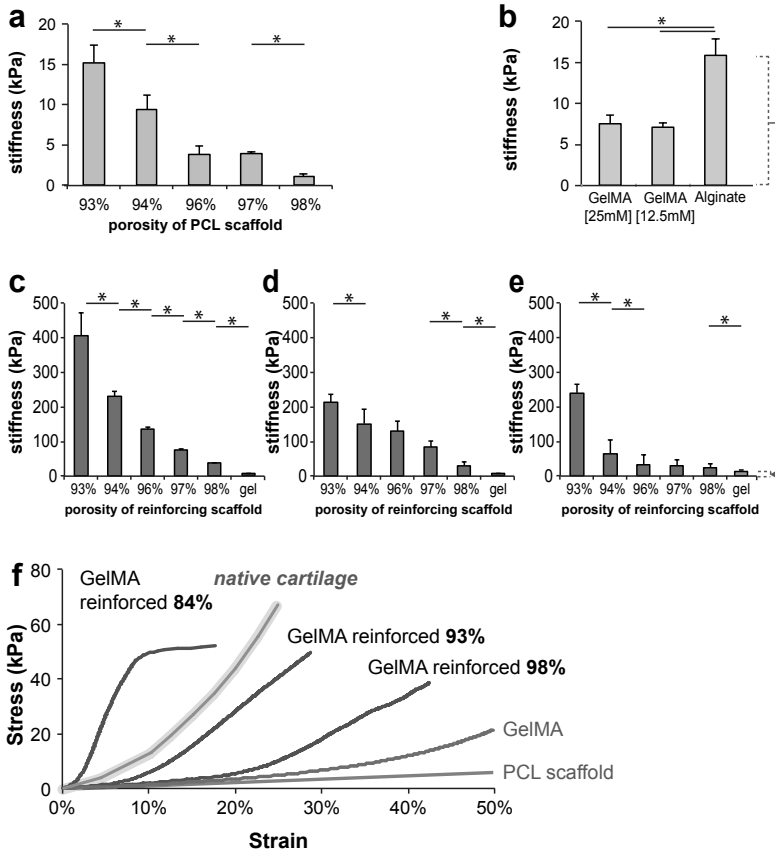


Figure 2. Reinforcing effect of high-porosity 3D-printed PCL scaffolds incorporated into hydrogels.

(a) Compressive moduli of PCL scaffolds were in the same range as those of (b) hydrogels alone. GelMA reinforced with PCL scaffolds and crosslinked with either (c) 25 mM or (d) 12.5 mM APS/TEMED were one order of magnitude stiffer than the scaffolds or gel alone; (e) a comparable degree of reinforcement for reinforced alginate gels (* $P < 0.05$, one-way ANOVA with Bonferroni correction). (f) Stress-strain curves of GelMA, the PCL scaffold and reinforced GelMA, approaching the curve of native cartilage (yellow). Scaffolds fabricated from thick fibres (i.e. 84%) were stiffer than native cartilage, but often disintegrated at a strain of approximately 10% (all groups $n = 5$, mean \pm s.d.; cartilage $n = 8$). Here, GelMA was crosslinked with 12.5 mM APS/TEMED and the strain rate applied was 25%/min.

comparable to that of hydrogels: 7.1 ± 0.5 kPa and 7.5 ± 1.0 kPa for GelMA crosslinked with either 12.5 mM or 25 mM APS/TEMED and 15.8 ± 2.0 kPa for alginate (Fig. 2b). When the compressive strength of the 93% porous PCL/hydrogel composite was investigated, the construct stiffness was increased 30-fold, up to 214 ± 24 kPa for GelMA with 12.5 mM APS/TEMED, and 54-fold, up to 405 ± 68 kPa, when the GelMA was crosslinked with 25 mM APS/TEMED (Fig. 2c,d)-. Alginate hydrogels also showed synergistic reinforcement (15-fold up to 240.7 ± 37.8 kPa) that was comparable to GelMA gels (Fig. 2e). The reinforc-

ing effect in the composites was dependent on the porosity of the PCL scaffold, which ranged from 93 to 98%. Interestingly, increasing the fibre roughness and surface area by etching of the PCL scaffold did not increase the degree of reinforcement (Supplementary Fig. 1). In fact, prolonged etching times resulted in mass loss of PCL, and hence decreased the construct stiffness. Therefore we concluded that the strength increase seen in the composites was not due to hydrogel/fibre bonding.

Comparison of reinforced gels with articular cartilage

The average stress-strain curve of native cartilage samples (strain rate 25%/min) (n=8) that were harvested from the patellofemoral groove of an equine knee joint, was plotted in Figure 2f together with the average (n=5) stress-strain curves for GelMA, high-porosity PCL scaffolds and GelMA reinforced with 98%, 93% and 84% porosity PCL scaffolds. Clearly, GelMA gels were much softer than the cartilage. However, the stiffness and deformation profile (shape of the stress-strain curve) of GelMA could be tailored to that of native cartilage by reinforcement with high-porosity PCL scaffolds. While thick-fibre scaffolds (porosity 72-88%), as fabricated with traditional 3D printing methods, were stiffer than native cartilage, they broke at around 10% strain when large fibre spacings were applied (> 1.25 mm). This sudden loss of integrity was not observed for native cartilage or gels reinforced with high-porosity scaffolds (Fig. 2f).

Time-dependent stress response of reinforced gels and cartilage

The stress response to isostrain showed that GelMA reinforced with a 93% porosity scaffold has a higher modulus on initial loading than cartilage (Fig. 3). However, relaxation is faster, and to a lower equilibrium modulus than cartilage. The modulus of GelMA was much lower during the isostrain at any time. Analysis of the stress curves at isostrain indicated that the reinforced GelMA constructs could not be adequately described within an isotropic poroelastic framework, but that a bi-exponential function:

$$S = S_0 + S_1 e^{-K_1 t} + S_2 e^{-K_2 t}, \quad (1)$$

provided an accurate, phenomenological characterisation of the time-dependent response of the construct, where S is the stress, t is time and the constants S_i and K_i have units of stress and time respectively. A nonlinear least squares fitting algorithm was used to obtain the best fitting parameters for S_i and K_i from the 9% isostrain curves as detailed in Supplementary Fig. 2 and Supplementary Note 1. We report $E_i = S_i / \text{strain}$ as elastic moduli, so that E_0 is the equilibrium modulus and E_1 and E_2 are 'transient' moduli that characterise the time dependent response of the material so that the 'peak' equilibrium modulus is obtained by summing the E_i (Table 1).

	Equilibrium modulus	Fast decay		Slow decay	
	E_0 (kPa)	E_1 (kPa)	k_1 ($\cdot 10^3$ s $^{-1}$)	E_2 (kPa)	k_2 ($\cdot 10^3$ s $^{-1}$)
GelMA	12 \pm 1.7	0.82 \pm 0.11	610 \pm 310	7.8 \pm 0.43	1.5 \pm 0.76
Reinforced GelMA	130 \pm 7.8	2700 \pm 160	180 \pm 9.8	430 \pm 49	28 \pm 1.1
Cartilage	440 \pm 140	300 \pm 160	110 \pm 45	430 \pm 200	4.9 \pm 2

Table 1. Fit of a bi-exponential function to the time-dependent stress response. Estimates of the moduli E_i and the fast and slow decay rates k_i obtained by fitting the stress response at 9% isostrain of GelMA, reinforced GelMA and cartilage to a bi-exponential function ($n = 3$, mean \pm s.d).

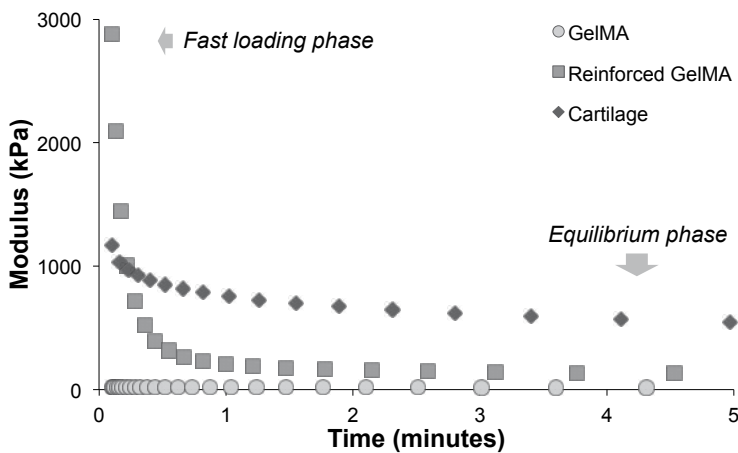


Figure 3. The time-dependent stress response of (reinforced) GelMA gel and articular cartilage at 9% isostrain. Reinforced GelMA displays a high modulus compared to cartilage on direct loading. The modulus of reinforced gels in the equilibrium phase, however, is closer to gel than cartilage. These plots are representative for the series of isostrains that were consecutively performed for 15 minutes.

Modelling the fibre reinforcement of hydrogels

The mechanism we propose to explain the synergistic reinforcement is illustrated in Figure 4a. Hydrogels can be reasonably described as incompressible³⁵⁹, so the volume of the hydrogel is conserved and vertical compression must be accompanied by horizontal expansion. As a composite construct is loaded, each 'semi-confined cell' of hydrogel (right column in Fig. 4a) expands horizontally and places the surrounding fibres under tension. We hypothesise that the fibres' resistance to elongation under compression loading, results in a pre-stress of the scaffold fibres. This resistance leads to the observed increase in stiffness, as the stiffness of bulk PCL is approximately four orders of magnitude higher than that of the gels. In order to confirm our hypothesis, we developed a

mathematical model that enables us to make the following prediction for the construct stiffness, C :

$$C = \frac{\rho^2 E N_f}{2R^2(1-\lambda)^{(3/2)}} \quad (2)$$

where N_f denotes the number of fibres in the construct, E the Young's modulus of the reinforcing polymer, ρ the fibre radius, R the construct radius and λ the axial strain (expressed as a fraction of the initial height). A derivation and more detailed explanation of the model are provided in the Supplementary Table 1 and Supplementary Note 2.

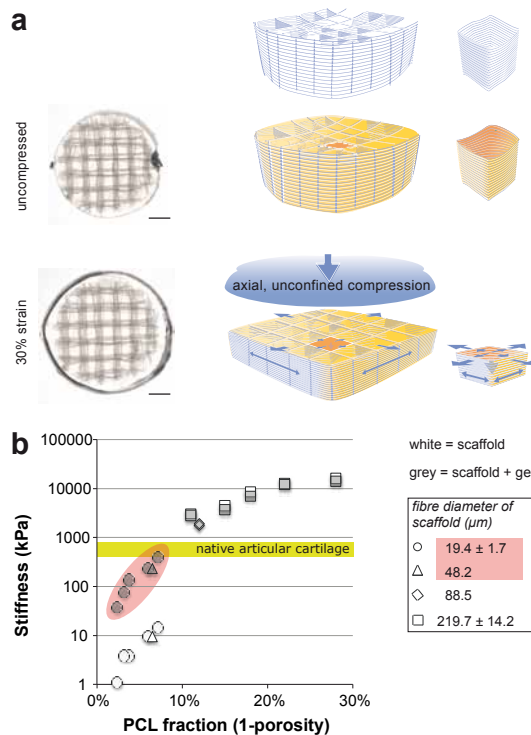


Figure 4. The mechanism of hydrogel reinforcement with organized high-porosity scaffolds. (a) PCL microfibre scaffolds (blue in schematic) serve as a reinforcing component to GelMA hydrogel (yellow in schematic). When axial compression is applied to the reinforced hydrogels, the stiff thin scaffold fibres stretch upon lateral displacement of the hydrogel. This mechanism provides the composites with a high stiffness and elasticity (scale bars represent 1 mm). **(b)** Moduli of scaffolds and scaffold/gel composites as a function of porosity, showing the synergistic increase in stiffness was only observed for thin-fibre scaffolds with a high porosity (polymer fraction 2-7% = porosity 98-93% (highlighted in red)), fabricated with melt-electrospinning writing (MEW). Fused deposition modelling (FDM) scaffolds were fabricated from 10-fold thicker fibres, resulting in a higher stiffness, however, no synergistic reinforcement was observed (mean of $n = 5$).

Video analysis of the compression cycle of reinforced gels

The model was further validated by lateral video imaging of the compression cycle of the GelMA/PCL composites, which revealed elongation (stretching) of PCL microfibres and a concave profile at the sides of the construct due to lateral displacement of water from GelMA (Supplementary Movie 2, 97% porosity scaffold). The microfibres stretched $9 \pm 1\%$ on 30% axial strain. In addition, from a top view it was observed that the PCL scaffold area expanded 17% and the aqueous component expanded 23% (including exudation of water) (Fig. 4a).

Microfibre compared to thick-fibre composites

The reinforcing effect was only observed in high-porosity scaffolds fabricated from thin fibres (diameter $<48.2 \mu\text{m}$), as indicated in Figure 4b. The 3D printing of thicker fibres (diameter $>88.5 \mu\text{m}$) resulted in a significantly lower scaffold porosity, ranging from 88% to 72% (PCL fraction of 12% to 28%, respectively), depending on the fibre thickness and spacing between the fibres. The stiffness of the thick-fibre scaffolds ranged from $1.8 \pm 0.2 \text{ MPa}$ for 88% porosity to $16.1 \pm 1.7 \text{ MPa}$ for 72% porosity. These scaffolds had stiffnesses similar to those of their composite counterparts with crosslinked GelMA. The compression cycle of GelMA reinforced with an 82% porosity scaffold is shown in Supplementary

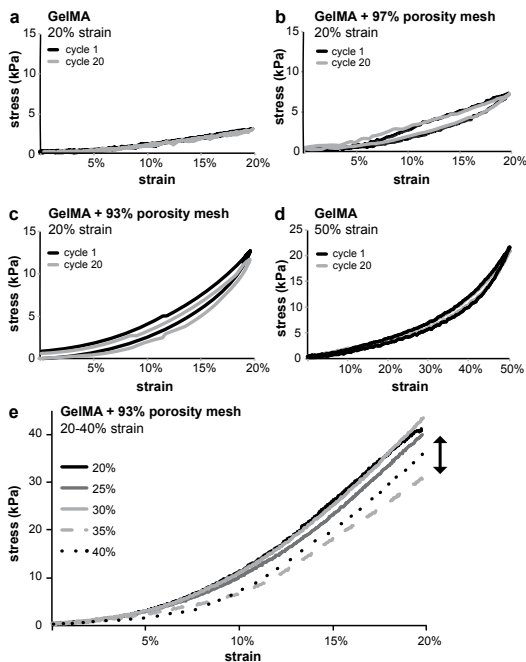


Figure 5. Cyclic compression testing of GelMA and reinforced GelMA constructs.

The stress-strain curves of the first and last of 20 cycles of 20% compression are shown for (a) GelMA alone (b) GelMA reinforced with a 97% porosity PCL scaffold and (c) GelMA reinforced with a 93% porosity PCL scaffold. For all groups no decay in stress was observed. (d) GelMA constructs also recovered after 20 cycles of 50% axial compression, however (e) GelMA reinforced with a 93% porous PCL scaffold required substantially less force to be compressed to 20% strain, after being compressed to over 30% strain (arrow) (mean of $n = 3$).

Movie 3. Exudation of fluid was observed; while the relatively thick scaffold fibres were compressed, they did not elongate.

Recovery of GelMA constructs after compression

The recovery of (reinforced) GelMA constructs after repetitive axial compression was measured. Figure 5a-c show that GelMA, as well as reinforced GelMA constructs are fully elastic after 20 cycles of 20% strain. The stress/strain curves of the initial and final loading cycle are shown. GelMA also fully recovered after repetitive 50% axial strain (Fig. 5d). However, GelMA reinforced with 93% porosity PCL microfibre scaffolds showed significantly decreased resistance when axially deformed by over 35% (Fig. 5e).

Chondrogenic differentiation of embedded human chondrocytes

Haematoxylin and eosin stained sections revealed that chondrocytes retained their spherical morphology within the fibre-reinforced hydrogels after 7 days (Fig. 6c). Chon-

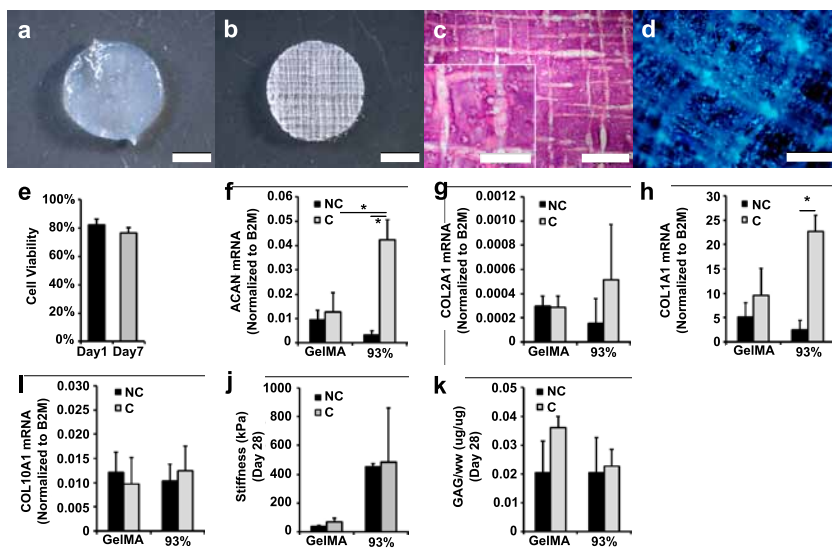


Figure 6. Differentiation of chondrocytes embedded in reinforced gelatin methacrylamide/Hyaluronic Acid-hydrogels. (a) Stereomicroscopy image of a GelMA-HA gel and (b) of a GelMA-HA gel reinforced with a PCL scaffold (93% porosity) on day 1 (scale bars represent 2 mm). (c) Hematoxylin/eosin staining after 7 days of culture shows that chondrocytes remained within the GelMA component and retained a round morphology (scale bar represent 500 μ m, inlay 200 μ m). (d) DAPI staining confirms a homogenous distribution of the cells throughout the construct (scale bar represent 200 μ m). (e) Chondrocytes remained viable over 7 days of culture in the gels. Gene expression analysis for (f) ACAN, (g) COL2A1, (h) COL1A1, and (i) COL10A1 at day 14 for compressed (C) and non-compressed (NC) groups ($n = 4$, mean \pm s.d.; * $P < 0.05$, two-way ANOVA). All gene expression levels were normalized to the housekeeping gene $\beta 2$ microglobulin (B2M). (j) Stiffness of the constructs following long-term culture ($n = 4$). (k) GAG/ww values at day 28 ($n = 5$).

drocytes were also homogeneously distributed throughout the construct as shown by the DAPI-stained cell nuclei (Fig. 6d). Chondrocytes maintained high cell viability at day 1 and day 7 when cross-linked with 12.5 mM APS/TEMED (Fig. 6e). Following 14 days of culture, hydrogels (GelMA with 0.5% hyaluronic acid (Lifecore, USA) (GelMA-HA) for improved chondrogenic differentiation⁶³ and GelMA-HA with 93% porous PCL mesh) were subjected to physiological loading cycles for another 14 days. The stress response to the 1 Hz dynamic loading regime is presented in Supplementary Fig. 3. Analysis of the qRT-PCR data indicated that for chondrocytes within the fibre-reinforced hydrogels, ACAN (gene expression for GAG synthesis) and COL1A1 (gene expression for collagen type I) mRNA levels were significantly up-regulated in the compressed ("C") groups compared to the control, non-compressed groups ("NC") (Fig. 6f-i; $p < 0.05$). Further, chondrocytes in the reinforced gels were more responsive to loading regime than cells in GelMA alone. Stiffness values were ~ 400 kPa in cell-laden fibre-reinforced hydrogels (Fig. 6j). There was no significant effect of reinforcement or compression on construct stiffness and glycosaminoglycan (GAG) content (Fig. 6k). The chondrocytes within the gels exhibited pericellular collagen type I and II deposition in all groups, with no discernible differences between the groups (Supplementary Fig. 4).

DISCUSSION

In this study, high strength composite constructs were fabricated by combining 3D-printed high-porosity scaffolds with a hydrogel. These composite hydrogels can be customized to yield a wide range of mechanical properties and, from a biological point of view, have the capacity to support cell proliferation and extracellular matrix production. The PCL scaffolds were built by micrometre scale fibres that were organized and interconnected through the melt electrospinning writing process. With this unique and new 3D printing technique, pre-set network architectures can be realized in a direct writing mode⁵⁴. This technique allows fibres to be printed well below the limits of classical melt-extrusion based 3D printing technologies such as fused deposition modelling⁵⁰, with filament diameters as small as $5 \mu\text{m}$, instead of $100 \mu\text{m}$ or larger²⁰⁶.

Hydrogels have previously been reinforced with solution electrospun nonwovens^{55,56,201,322}. However, most traditional solution electrospun meshes have disadvantages from both a mechanical and biological point of view, *e.g.* fibres are not fused and hence slide under loading, meshes are usually not thicker than a 100 microns and have a pore size of less than $5 \mu\text{m}$ and are, therefore, too dense for cell infiltration^{201,204,322}. To overcome these issues related to traditional solution electrospinning, fibres have been collected in an earthed ethanol bath, yielding nonwovens with high-porosities^{55,56}. Hydrogel stiffness was increased 4-fold when reinforced with these randomly organized

non-wovens, irrespective of the porosity^{55,201}. Silk microfibrils³⁵⁰ or carbon nanotubes¹⁹² also formed porous reinforcing structures for hydrogels, permitting cellular infiltration and differentiation. However, the stiffness of the gels increased only 1 to 3-fold, as the fibres were not fused. In contrast, in our current composite model consisting of a relatively soft hydrogel (7.1 – 15.8 kPa) and a highly porous and soft PCL scaffold (1.1 - 15.2 kPa), the maximum stiffness obtained was a factor of fifty larger (405 kPa) than that of the hydrogels alone, on a strain rate of 25%/min.

The stiffness of cartilage and (reinforced) hydrogels is strongly strain-rate dependent^{357,358}. We found that the reinforced hydrogels were one order of magnitude stiffer than cartilage on initial fast loading at 9% strain. However, the modulus of reinforced hydrogels displayed a steep decrease to an equilibrium value roughly one-third the equilibrium modulus of cartilage, yet still one order of magnitude larger than the equilibrium modulus of hydrogel alone.

The effect of reinforcement can be explained by the highly organized fibre architecture of the scaffolds. The mathematical model we developed demonstrated that the hydrogel places the PCL fibres under tension on axial compression, and predicts a theoretical upper bound on the attainable stiffness. However, the theoretical stiffness of the reinforced hydrogels is one order of magnitude larger than that observed experimentally. This is reasonable since an idealized construct was considered, in which the fibres are initially taut at zero strain, the hydrogel is purely elastic and there is no slip between the fibres and the hydrogel. In fact, in our experimental set-up, we showed that very little water, or hydrogel, was compressed out of the constructs, so the fibres did not completely lock the hydrogel. The stress relaxation on isostrain (Fig. 3) reflects the exudation of the aqueous component (water or gel) from the reinforcing scaffold. For cartilage we observed a higher equilibrium modulus, which may be a combined effect of the osmotic pressure of fixed charges on proteoglycans and an organised extracellular matrix.

Etching the high-porosity scaffolds did not result in a further increase in stiffness of the composites. This approach was based on our previous finding that covalent attachment of the hydrogel component to a scaffold that was fabricated from modified, methacrylated PCL, resulted in increased construct strength²⁵⁵. It should be noted that etching results in an increase of van de Waals forces but does not establish covalent bonds between the hydrogel and the reinforcing scaffold.

Infiltrating hydrogel into scaffolds that had been fabricated with traditional 3D melt-printing techniques with thick fibres ($\geq 88 \mu\text{m}$)⁵⁰, did not show a significant mechanical effect. Axial loading of these constructs requires compression of the PCL through a strong vertical column of fibre crossings, which is not easily deformed. Video imaging of the compression cycle confirmed that thick fibres were not stretched and water flowed out of these scaffolds without providing a synergistic effect. In contrast, the columns of fine fibre crossings are easily deformed under axial loading, yet they are supported by

the hydrogel component in the composites. Supplementary Movie 2 shows some local distortion of the columns, but no large scale buckling of the columns, so the microfibrils are put under tension. We further note that this axial loading reduces the horizontal pore size, improving gel confinement. To our knowledge we are the first to show the synergistic effect of a well-designed scaffold/hydrogel system; the work shown in this paper could therefore lead to a paradigm shift in the field.

Reinforced GelMA hydrogels possess stress-strain curves that closely resemble those of healthy articular cartilage. Also, in absolute terms, the stiffness of the biodegradable composites was comparable to the stiffness of articular cartilage, which has been reported to range from 400–800 kPa^{360–362}. On the other hand, the stiffness of scaffolds fabricated with traditional 3D printing was one order of magnitude larger than that of articular cartilage, which is consistent with previous reports^{65,76}. The porosity of these scaffolds ranged between 72% and 89%, whereas the porosities reported in the literature range from 28.9% and 91.2%^{50,190,363}. Nevertheless, when aiming to fabricate high-porosity scaffolds (> 80%) from thick fibres, large fibre spacing (> 1.5 mm) is required, which causes scaffold disintegration under strains of approximately 10%. In addition, the thicker fibres occupy a relatively high volume that is inaccessible for tissue formation until the scaffold has degraded.

Hydrogels reinforced with woven scaffolds, composed of either polyglycolic acid³⁴³ or PCL^{316,351} have previously been reported to possess tensile, compressive and shear properties comparable to native cartilage. The porosity of these woven scaffolds was 70–74%, compared to 93–98% in the present study. The stiffness of the woven composites was reported up to 0.2 Mpa (at equilibrium stress), which was twice as stiff as the scaffold without the gel³¹⁶. Both the woven and the melt electrospun composites showed axial recovery after compression for 10% and 20%, respectively. The water that was compressed out of the scaffolds was likely reabsorbed during the relaxation phase, comparable to fluid dynamics in articular cartilage³⁶⁴. Our reinforced hydrogels showed decreased resistance if compressed by 35% or more, which may be due to fractures or delamination in the PCL scaffold junctions. For translational purposes, it is important to realize that native cartilage is exposed to 15–45% axial deformation under long-term static compression³⁶⁵.

Incorporation of organized fibrous PCL scaffolds within a well-characterized hydrogel system makes it possible to culture cells in a customizable, mechanically diversified environment. The hydrogel component of the composite constructs will degrade within months^{63,255}, allowing the regeneration of new tissue, while the PCL component degrades within years⁵¹ forming a temporary reinforcing network to the new tissue. Under physiological compressive loading of 20% strain and 1 Hz, our gene expression data suggest that chondrocyte expression of matrix mRNAs is significantly up-regulated in composite hydrogels compared to non-reinforced, weak hydrogels. These results

highlight the importance of developing cell-culture platforms and tissue engineered constructs that better mimic the *in vivo* mechano-environment of natural articular cartilage. Still, the exact mechanisms of stress-transfer to the cells in fibre-reinforced hydrogels remain to be investigated.

In conclusion, the current work represents a significant step towards developing biomechanically functional tissue constructs. The stiffness of the constructs was significantly enhanced, achieving values similar to those of native articular cartilage, by combining hydrogels with 3D-printed, high-porosity melt electrospun PCL scaffolds. This synergistic effect could be modulated by altering the porosity of the reinforcing scaffolds. The composite constructs have a strong elastic component and recover after physiological axial strains. Finally, human chondrocytes encapsulated in the GelMA/PCL composites were found to be more responsive to mechanical loading, which led to significant changes in gene expression *in vitro*.

ACKNOWLEDGEMENTS

The authors thank dr. Christina Theodoropoulos for her assistance with SEM imaging; Mr. Onur Bas for his assistance with the dynamic bioreactor; Mr. Mies Steenbergen for his assistance with video imaging and Kim Benders MD, for harvesting the human chondrocytes. We are also grateful to prof. Dirk Grijpma and Mrs. Anita Bijsterveld-Podt from the University of Twente for facilitating mechanical testing on their Zwick universal mechanical tester. We thank prof. Harrie Weinans for fruitful discussions on cartilage biomechanics. The II-II6B3 monoclonal antibody developed by T.F. Linsenmayer was obtained from the Developmental Studies Hybridoma Bank developed under the auspices of the NICHD and maintained by The University of Iowa, Department of Biology, Iowa City, IA 52242. Jetze Visser was supported by a grant from the Dutch government to the Netherlands Institute for Regenerative Medicine (NIRM, grant nFES0908); Ferry Melchels was supported by a Marie Curie grant from the European Commission (PIOF-GA-272286) and Jos Malda was supported by the Dutch Arthritis Foundation. This work was also supported by the Australia National Health and Medical Research Council and the European Community's Seventh Framework Programme (FP7/2007-2013) under grant agreement n309962 (HydroZONES).

SUPPLEMENTARY INFORMATION

Supplementary Note 1. Bi-exponential fitting of (reinforced) GelMA and cartilage.

A logscale plot of the reinforced GelMA's stress response at isostrain displayed a near linear response initially and a near linear response at later times, which prompted the use of the bi-exponential function:

$$S = S_0 + S_1 e^{-K_1 t} + S_2 e^{-K_2 t} \quad (1)$$

similar to an approach taken previously to characterize adipose tissue in confined compression³⁶⁶. The inbuilt MATLAB (The MathWorks, Inc., Natick, Massachusetts, United States, 2013) routine `lsqnonlin` was used to fit the biexponential function to the data for each isostrain curve individually, with the maximum stress value on each isostrain curve used to set $t = 0$. This choice is made to combat the uncertainty about when exactly the isostrain is applied, which leads to some error in the fitted values of S_1 and S_2 . The optimisation minimises the sum of the squared error between the data points and the best-fit curve. The fitting procedure was fairly robust to the choice of initialisation, but multiple initialisations were considered to help ensure that the fits we report are global minima. An example fit is shown in Supplementary Figure 2. After fitting, we calculated the average value for each parameter at 9% strain in order to characterise each of the three materials. For each data point we can calculate the error in the fit (the absolute difference in the experimental and fitted stress values) and express this as a percentage of the experimental stress.

Supplementary Note 2. Model of synergistic reinforcement of GelMA constructs with 3D-printed PCL scaffolds.

This model employs classical concepts from elasticity theory³⁶⁷. Firstly we assume that the whole construct deforms uniaxially and uniformly, so that the loaded position (lower case) can be written in terms of the unloaded, reference position (upper case) as follows

$$\begin{pmatrix} x \\ y \\ z \end{pmatrix} = \begin{pmatrix} aX \\ aY \\ (1 - \lambda)Z \end{pmatrix} \quad (2)$$

where λ is the strain (12% strain means $\lambda = 0.12$). Assuming the whole construct is incompressible, we must set $a = 1/\sqrt{1 - \lambda}$. Next we claim that the stiffness of the construct is mostly due to the PCL fibres resisting extension and claim that we can reasonably approximate the force required to compress the construct by instead calculating

the tensile force required to stretch PCL fibres by a factor $1/\sqrt{1-\lambda}$. This neglects any mechanical contribution the GelMA makes to scaffold stiffness, which is reasonable because we know the GelMA is very weak in comparison to the composite scaffolds. In this hypothesis the GelMA is only important for converting vertical load into fibre extension. If we consider one fibre in uniaxial tension then, according to linear elasticity theory, the tensile force in the fibre is given by

$$F_f = \pi\rho^2E\left(\frac{1}{\sqrt{1-\lambda}} - 1\right) \quad (3)$$

where ρ is the fibre radius and E is the Young's modulus of PCL. Our next modelling assumption, that the tensile force in all the fibres can be summed linearly to approximate the force applied to deform the composite scaffold, implies that the stress on the scaffold surface, S , is given by

$$S = \frac{\pi\rho^2EN_f}{\pi R^2}\left(\frac{1}{\sqrt{1-\lambda}} - 1\right) \quad (4)$$

where R is the construct radius and N_f is the number of fibres in the construct. The stiffness is calculated as the derivative of this stress with respect to strain, so that the predicted stiffness of the construct is

$$C = \frac{dS}{d\lambda} = \frac{\rho^2EN_f}{2R^2(1-\lambda)^{3/2}} \quad (5)$$

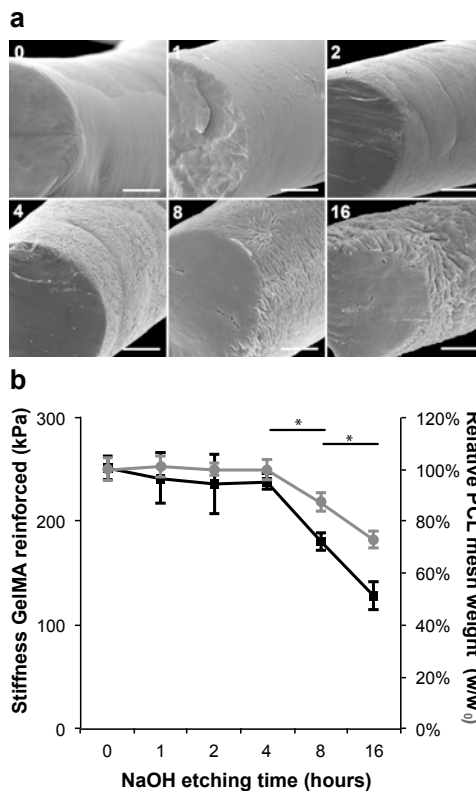
To evaluate this prediction for the construct stiffness we consider the placement of fibres in one layer. This allows us to approximate the length of PCL fibre, L , in a given layer and the number of fibres under tension, N_{fl} , in that layer. Noting that V_{PCL} , the volume of PCL in a construct, is given by

$$V_{PCL} = \pi\rho^2LN_l \quad (6)$$

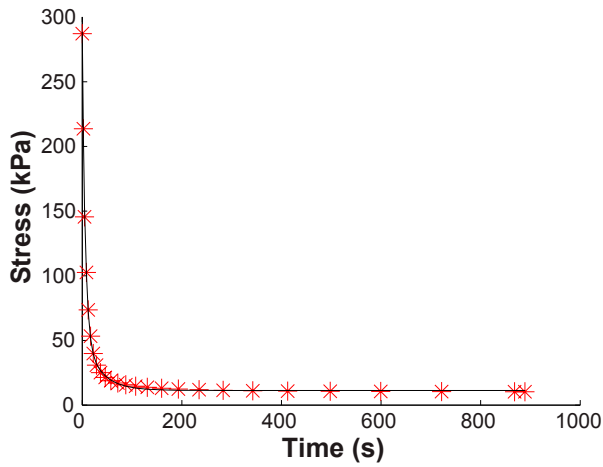
where N_l is the number of layers in a construct, we use the measured PCL volume to estimate ρ^2N_l . Finally we multiply by N_{fl} to obtain an approximation for ρ^2N_f . We take the Young's modulus of PCL to be 310MPa, the construct radius $R=2.5\text{mm}$ and we approximate the stiffness at 12% strain. The numbers used in this section and the predicted stiffnesses are stated in Supplementary Table 1.

Spacing (mm)	L (mm) (2sf)	$V_{PCL}(mm^3)(2sf)$	N_{fl}	C (MPa) (2sf)
0.2	98	2.8	24	6.5
0.4	49	2.6	12	6.0
0.6	33	1.5	8	3.5
0.8	25	1.3	6	2.9
1.0	20	0.93	4	1.8

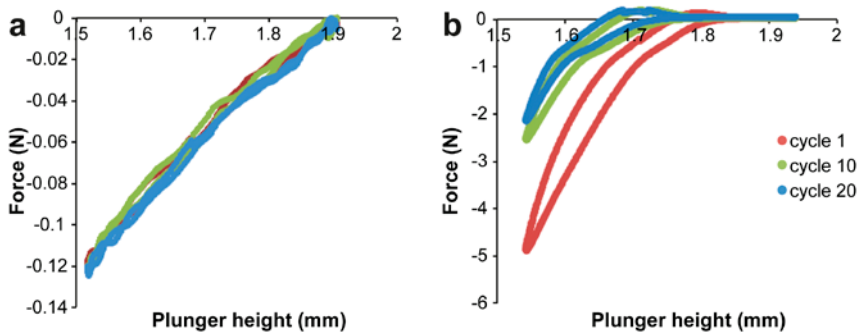
Supplementary Table 1. The predicted stiffness of hydrogel/scaffold composites. The stiffness of the composites increases with a decreased fibre spacing, and thus an increased total fibre length (L) and volume (V_{PCL}). The larger the amount of fibres to be stretched (N_{fl}) on axial compression, the larger the expected stiffness (C) of the composites.



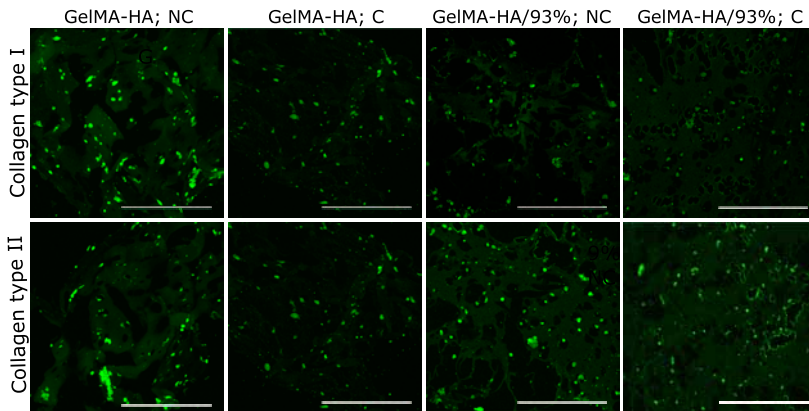
Supplementary Figure 1. Stiffness of hydrogels reinforced with etched PCL scaffolds. (a) Scanning Electron Microscopy images of freeze-fractured 3D-printed scaffold filaments (porosity 94%) etched with sodium hydroxide for 0-16 hours showing an increasing degree of surface roughness of the fibres (scale bar 10 μ m). The fibre diameter decreased significantly ($P < 0.05$) after 16 hours of etching from $48.5 \pm 8.2 \mu$ m to $42.0 \pm 8.0 \mu$ m. (b) Longer etching periods (8 and 16 hours) of the PCL scaffolds resulted in significant weight reduction (grey circles, $*P < 0.05$) and had a negative effect on the stiffness of reinforced GelMA constructs (black squares, $*P < 0.05$), crosslinked with 25 mM APS/TEMED.



Supplementary Figure 2. An example fit for the stress relaxation curve of a fibre reinforced hydrogel at 9% isostrain. The mean percentage error in this fit (black line) to the data points (red) is 5.1%.



Supplementary Figure 3. Load response of the dynamic bioreactor study. The stress response of (a) GelMA and (b) reinforced GelMA to the dynamic loading regime in the bioreactor. A constant, relatively low force was required to axially strain GelMA for 20% with a frequency of 1 Hz. For reinforced GelMA, a larger force was required for compression. The maximum force reduced over time and samples did not fully regain their original height within the 1 Hz time frame.



Supplementary Figure 4. Collagen type I and II secretion by chondrocytes embedded in the gelatin methacrylamide/Hyaluronic Acid-hydrogels. No discernible differences in collagen type I and II expression were observed as a result of either repetitive compression (C) versus non-compression (NC) or reinforcement of the hydrogel constructs with a 93% porosity PCL scaffold.

Chapter 7

Preliminary results of a translational animal model

Cartilage Repair with a Combination of Chondrons and MSCs in Gelatin Methacrylamide Hydrogel: the Establishment of an Equine Model

Jetze Visser
Irina A.D. Mancini
Harold Brommer
Pia H. Puhakka
Lucienne A. Vonk
Imo Hoefler
Wouter J.A. Dhert
Paul D. Dalton
Juha Töyräs
Daniël B.F. Saris
P. René van Weeren
Jos Malda

The results of the 1-year follow-up of ponies in this cartilage repair study are awaited before this manuscript will be submitted for publication

ABSTRACT

Gelatin methacrylamide (GelMA) hydrogel has been shown to support the formation of a cartilage matrix by embedded cells *in vitro*. In addition, when reinforced with a structured microfiber scaffold, GelMA approached the stiffness of articular cartilage, yet the potential of GelMA and reinforced GelMA for the repair of *in vivo* articular cartilage defects remains to be demonstrated. To this end, a surgical technique for implanting and UV-crosslinking GelMA and reinforced GelMA into cartilage defects (10 mm diameter) was developed using cadaveric equine stifle joints (n=3) and applied in one Shetland pony (two defects in one stifle joint) to study surgical feasibility and implant fixation. Next, a mixture of allogeneic chondrons and expanded MSCs was implanted in four different experimental groups in both stifle joints of eight Shetland ponies, comparing three GelMA-based groups with fibrin glue, the clinical standard cell carrier, using two cell concentrations. The groups were 1) GelMA, 2) reinforced GelMA (high cell concentrations), 3) 'GelMA cap' and 4) fibrin glue (low cell concentration). The 'GelMA cap' group consists of cells on the bottom of the defect capped with cell-free GelMA. With this set-up, we aimed to study the mechanism of tissue regeneration – 'bottom-up' or 'substitutive' (within the hydrogel) – depending on the biomaterial and the amount of cells used. The implants were still in place after 50 flexion-extension cycles in cadaveric stifle joints as well as after 2 weeks *in vivo* in a pilot study. Abundant infiltration of fibroblastic cells into the GelMA was found in that animal after 2 weeks. The cohort of eight ponies recovered well from bilateral joint surgery and baseline evaluation of the implants was conducted using optical coherence tomography and ultrasound imaging, confirming the location of the implant and the capturing the quality of the subchondral bone and the surrounding cartilage. In conclusion, a model was developed to study the cartilage repair process in Shetland ponies. GelMA hydrogel, with or without reinforcing microfiber scaffolds, was successfully UV-crosslinked and fixated in cartilage defects in the stifle joint. A study that evaluates the potential of GelMA compared to fibrin glue for the long-term regeneration (12 months) of cartilage is currently ongoing in eight ponies.

INTRODUCTION

Cells for the repair of focal cartilage defects are usually introduced in a hydrogel^{6,9}. Fibrin glue is the standard cell delivery vehicle, because of the availability in clinical grade and its surgical applicability^{6,9}. However, fibrin glue was not specifically developed for application in regenerative medicine as the crosslinked fibrin polymer network is relatively soft and as it has a high degradation rate^{26,27}. Efforts are currently being made to develop more instructive and stronger gels with controlled degradation rates that balances with the process of tissue regeneration^{9,29,30}.

In these tailored hydrogels, the matrix that is formed by embedded cells is meant to be deposited *within* the gel, gradually substituting the volume of the hydrogel^{29,368}. This process was confirmed for chondrocytes and multipotent mesenchymal stromal cells (MSCs) embedded in GelMA hydrogels *in vitro* and *in vivo* in Chapter 3, 4 and 5 of this thesis, as well as in other studies^{60,63,73,257}. In contrast, when cells are implanted in a chondral defect in fibrin³⁶⁹, cartilage tissue formation is likely to occur from the bottom of the defect. Here, we aim to study these different regenerative processes – bottom-up or substitutive - in an orthotopic animal model.

For the purpose of the testing orthopedic interventions or devices, horses have been recognized suitable animals, considering the similarities between equine and human cartilage of the biological and the challenging mechanical environment^{80,355,370}. In this study, a cartilage repair model was established in the stifle joint of Shetland ponies. The Shetland pony was selected because of its robust nature, availability, ease of surgical management and housing, and for having a weight that comes closer to the human situation than that of other horse breeds³⁷¹.

The different tested treatments were GelMA, GelMA reinforced with 3D printed micro-fiber scaffolds (described in Chapter 6), fibrin glue and cell-free GelMA covering the cells ('GelMA cap'). In the 'GelMA cap' group, a low amount of cells is deposited on the bottom of the defect, and subsequently capped with cell-free GelMA. The cap can potentially control the ingrowth of cells from the bottom of the defect. This repair mechanism is also aimed for in recently developed therapies, in which the cartilage defect is covered with a cell-free biomaterial after microfracture^{372,373}.

A cell combination of equine chondrons and MSCs was selected²⁴, inspired by encouraging preliminary results of a study on cartilage repair in humans, using a mixture of autologous chondrons and allogeneic MSCs^{25,374}. Here, two cell concentrations are applied: relative low concentrations as often used for clinical cell therapy (used in the fibrin and 'GelMA cap' group) and higher concentrations, which are more commonly used for hydrogel-based tissue engineering (applied in the GelMA and reinforced GelMA group).

Implantation techniques were first established in cadaveric equine stifle joints and then in a pilot study in a Shetland pony. A comparative study of the treatments was

subsequently initiated in eight Shetland ponies. The one-year follow-up is ongoing, including intensive monitoring featuring repeated arthroscopic assessment with help of advanced imaging techniques of the implant surface and content. At the end point, cartilage matrix formation will be qualified and quantified. In addition, the DNA of the explant will be matched with the implanted cells and the host DNA, to study which source is responsible for matrix formation.

MATERIALS AND METHODS

Experimental set-up

First, we tested the viability and morphology of equine chondrons after storage in liquid nitrogen, for potential use as an allogeneic cell source for the cartilage repair studies in ponies. Next, the effect of various crosslinking periods (ranging from 30-300 seconds) of GelMA with a focused UV-source on cell viability and hydrogel stiffness was assessed. GelMA was implanted and crosslinked in cadaveric stifles ($n=3$) and in the stifle joint of one Shetland pony as a feasibility study for the cartilage repair study with GelMA hydrogels. Finally, the GelMA, reinforced GelMA, 'GelMA cap' and fibrin glue groups with allogeneic chondrons and MSCs were implanted in eight ponies (four defects per animal).

Preparation of GelMA

GelMA was synthesized by reaction of porcine type A gelatin (Sigma-Aldrich, St. Louis, Missouri, USA) with methacrylic anhydride (Sigma-Aldrich) at 50 °C for one hour, as previously described^{60,62}. In short, methacrylic anhydride was added dropwise to a 10% solution of gelatin in PBS under constant stirring. To achieve a high degree of functionalization, 0.6 g of methacrylic anhydride was added per gram of gelatin. The functionalized polymer was dialyzed against distilled water for 4 days at room temperature to remove methacrylic acid and anhydride and was subsequently neutralized to pH 7.4 with 10% sodium bicarbonate (Merck, Darmstadt, Germany). This protocol results in a degree of functionalization of approximately 75%⁶⁰. The dissolved GelMA was filtered (SFCA membrane, 0.2 μm pore size) (Thermo Fisher Nalgene) prior to freeze-drying and storage at -20 °C until use. Upon use, defrosted GelMA was dissolved in PBS at 70°C at a concentration of 10% (w/v) containing a photoinitiator Irgacure 2959 (Ciba, BASF, Ludwigshafen am Rhein, Germany) at a final concentration of 0.1% (w/v).

Preparation of 3D printed microfiber scaffolds

Scaffolds were fabricated with a custom-made melt electrospinning machine in a direct-write mode⁵⁴, according to the protocol extensively described in Chapter 5. Fibers

from polycaprolactone with a thickness of 14 μm were stacked in a 0-90° patterns until a height of 0.5 mm was reached. The scaffolds had a porosity of 92% and were used for reinforcement of GelMA in the *in vivo* experiments. Three scaffold were stacked in the defect and subsequently the GelMA was infused and crosslinked in between the fibers.

Harvest of equine chondrons and mesenchymal stromal cells

Macroscopically healthy full-thickness cartilage was harvested under sterile conditions from the metatarsophalangeal joint of fresh equine cadavers (n=3, age 3-10 years) with consent of the owners. After mincing and digestion in type II collagenase (0.15% w/v) (Worthington Biochemical Corp) at 37°C for 12 hours, the suspension was filtered through a 100 μm cell strainer, washed in PBS and stored in liquid nitrogen in culture medium (Dulbecco's Modified Eagle Medium (DMEM) 41965, Invitrogen) supplemented with 20% heat-inactivated fetal bovine serum (FBS, Biowhittaker) and 10% dimethylsulfoxide (DMSO) (Merck, Darmstadt, Germany).

With approval of the local animal ethical committee, a bone marrow aspirate from the sternum was obtained from a healthy, living equine donor (n=1, age 9 years). The mononuclear fraction (MNF) was isolated by centrifuging the sample on Ficoll-Paque (Sigma). The MNF was seeded at a density of 2.5×10^5 cells/cm² and expanded in monolayer culture till sub-confluency in MSC expansion medium containing α -MEM (22561, Invitrogen) supplemented with 10% heat-inactivated FBS, 0.2 mM L-ascorbic acid 2-phosphate (Sigma), 100 units/ml penicillin and 100 $\mu\text{g}/\text{ml}$ streptomycin, and 1 ng/ml FGF-2 and embedded in hydrogels at passage 4. The multilineage potential of the cells that were cultured from the bone marrow aspirate was investigated by a three-way differentiation assay as previously described²⁵⁹ (data not shown).

Viability of cells

Viability and morphology (collagen type VI) of the cell suspension acquired from cartilage was evaluated directly after digestion and after freeze/thaw, in order to verify the viability after cryopreservation. In addition, the viability of chondrons and MSCs (both one donor) after several UV exposure times was assessed. A LIVE/DEAD Viability Assay (Molecular Probes MP03224, Eugene, USA) was performed according to the manufacturer's instructions. The samples were examined using an Olympus BX51 microscope and photomicrographs taken with an Olympus DP70 camera (both Olympus, The Netherlands). The excitation/emission filters were set at 488/530 nm to observe living (green) cells and at 530/580 nm to detect dead (red) cells. Live and dead cells were counted in three gels or smears per time point, at a minimum of four locations. Viability was calculated as (alive cells / total cells counted) x 100%.

UV-crosslinking protocols

For *in vitro* cultures, the cell-laden GelMA was crosslinked for 15 minutes in a custom-made air-sealed Teflon mold (sample size 5x5x2 mm) using 365 nm light in a UVP CL-1000L crosslinker (UVP, Upland, California, USA). For *in vivo* crosslinking of GelMA in cartilage defects in ponies, a UV beam source (350-450 nm; Hönle UV technology, Munich, Germany) was used with an intensity of 180 mW/cm². Prior to the *in vivo* experiment, the effect of the duration of UV exposure (30-300 sec, n=3 per group) on cell viability was evaluated.

Measurement of stiffness

The stiffness was measured of GelMA constructs with embedded cells that were cross-linked for various periods. Samples (n=3 per group) were subjected to single uniaxial unconfined compression in air at room temperature, after 1 hour submersion in PBS from their preparation. Over a period of two minutes, a force ramp (axial strain rate ca. 20%/min) was applied to the samples employing a Dynamic Mechanical Analyser (DMA 2980, TA Instruments, New Castle, DE, USA). The stiffness was calculated from the linear derivative of the stress/strain curve between 10-15% strain.

Histology, biochemistry and immunohistochemistry

Hydrogel samples for histology and immunohistochemistry were dehydrated through a graded ethanol series, cleared in xylene and embedded in paraffin. The samples were sectioned into 5 µm slices and stained with hematoxylin and eosin for cell detection. A triple stain of hematoxylin, fast green, and Safranin-O (all from Sigma) was applied to identify the presence of GAGs. The stained sections were examined using a light microscope (Olympus BX51).

Collagens of types I, II and VI were stained by immunohistochemistry after deparaffinization and rehydration of the sections. All sections were blocked in 5% bovine serum albumin and 0.3% H₂O₂ following antigen retrieval. Collagen type I was retrieved by boiling the sections for 10 minutes in 10 mM citrate buffer, pH 6. Antigen retrieval for collagen type II was performed by incubation with 1 mg/mL pronase (Sigma) and 10 mg/mL hyaluronidase (Sigma) at 37 degrees for half an hour each. Next, sections were incubated with the primary antibodies for collagen type I (1:250 Col1A1 Santa Cruz, Dallas, Texas, USA) collagen type II (1:100, monoclonal mouse, II-II6B3, DSHB) or type VI collagen (1:10, 5C6, DSHB), all at 4°C overnight. Subsequently, collagen type I sections were treated with Polyclonal Goat Anti-Rabbit Immunoglobulins/HRP (1:200, Dako, Heverlee, Belgium) for 60 min at RT; collagen type II sections were incubated with GAM-HRP (1:200, Po447, Dako) at room temperature for an hour, and type VI collagen sections with anti- mouse horseradish peroxidase (1:100, Po447, Dako). All collagen types were detected by a 10-minute conversion of 3,3'-diaminobenzidine solution (Sigma). Nuclei

were counterstained with 50% Mayer's hematoxylin. Isotype control stainings were carried out with either a murine IgG1 monoclonal antibody (Dako) at concentrations matching those used for the primary antibodies or by incubation without primary antibody.

Cadaveric studies for cartilage repair with GelMA

Three cadaveric equine stifle joints were obtained with consent of the owners. The techniques for making chondral defects in the medial trochlear ridge, and subsequent implantation and UV-crosslinking of (reinforced) GelMA were developed on these cadaveric stifle joint. The fixation of the implants was controlled after closure of the wound and 50 manual flexion-extension cycles.

Pilot study for the cartilage repair model in a Shetland pony

The animal studies were approved by the local Ethics Committee for Animal Experiments and were in compliance with the Institutional Guidelines on the Use of Laboratory Animals. The surgeries were performed under sterile conditions in the surgery theatre at the department of Equine Sciences of Utrecht University. For evaluation of the surgical feasibility and hydrogel fixation, a pilot study was performed in one Shetland pony (age: 24 years, weight: 142 kg). Two chondral defects were made in the medial femoral ridge in the femoropatellar joint, and two experimental groups (reinforced GelMA and GelMA cap) were implanted in a surgical procedure described below. The pony was euthanized after two weeks (for veterinary education purposes) and the presence of GelMA was verified by macroscopic inspection, histology and immunohistochemistry.

Long-term evaluation of cartilage repair in Shetland ponies

Four experimental groups (fibrin glue, GelMA cap, GelMA and reinforced GelMA) were tested in the equine cartilage defect model (Fig. 1). A mixture of allogeneic MSCs and chondrons (80/20% ratio) was implanted in every defect in two concentrations in four groups: a low cell concentration (2 million cells/mL) that is currently used in human cartilage repair was applied in fibrin glue; a 'GelMA cap' implant consisted of 1 million cells in a small volume of GelMA on the bottom of defect, which were covered by a layer of cell-free GelMA. A high cell concentration of 20 million cells/mL was implanted in GelMA gel and GelMA reinforced with a 3D printed scaffold.

Two chondral defects were made in both stifle joints of eight Shetland ponies (age: 7 ± 4 years, weight 191 ± 28 kg, mean \pm SD). The low and high cell concentration groups were paired in every stifle, and their location (proximal or distal) and side (left or right leg) was randomized. A power of 0.94 was set, based on the outcomes of the International Cartilage Repair Society macroscopic scoring system that was performed in a comparable study in goats²³.

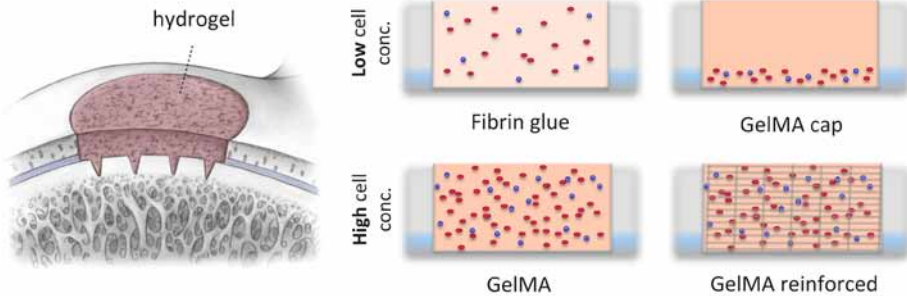


Figure 1. Experimental groups of *in vivo* long-term cartilage repair study. Two cartilage defects with a diameter of 10 mm were made in both stifle joints of Shetland ponies. The subchondral bone was microfractured for anchorage of the hydrogel. An allogeneic mixture of 80% MSCs (red) and 20% chondrons (blue) was implanted in every defect, in low concentrations (Fibrin glue: 2 million cells/mL; 'GelMA cap': 1 million cells on bottom of defect) and high cell concentrations (20 million cells/mL) in the GelMA and reinforced GelMA groups.

General anesthesia was induced with midazolam and ketamine intravenously, after a bolus of detomidine and morphine, and maintained with isoflurane in oxygen with an end tidal concentration of 1.0-1.5 %. The medial trochlear ridge of the stifle joint was exposed via a subpatellar approach, between the medial and middle patellar tendon. Two full-thickness, cylindrical cartilage defects (including the calcified cartilage layer) with a diameter of 10 mm (78 mm²) were created, using a hand-operated drill, guided in a drill sleeve. A sharp surgical spoon was used to remove any remnants of cartilage on the edges and the bottom of the defect. Microfractures (10x, depth ca. 1 mm) were made with a pricker in the subchondral bone in all defects for fixation of the hydrogels. Next, a suspension of chondrons (passage 0) and MSCs (passage 4) was centrifuged in the OR and the resulting cell pellet was suspended in GelMA (ca. 35°C) with a positive displacement pipet. The cell/hydrogel suspension was transferred into a syringe and a 21G needle (both Becton, Dickinson and Company, New Jersey, USA) was mounted. A silicone-based sheet (3x3 cm. Silon-SES, Bio Med Sciences, Allentown, USA, kindly provided by Regentis Biomaterials Ltd., Or-Akiva, Israel) was placed over the cartilage defect, from which the blood was removed with sterile gauze. In the reinforced GelMA group, three scaffolds were placed on top of each other in the cartilage defect. The silicone sheet was fixated over the defect with a custom-made flexible fixation tip with an inner diameter of 15 mm. The sheet was punctured with the needle through an aperture in the fixation tip, and the hydrogel/cell suspension was infused in the defect. The gel was crosslinked with the focused UV beam for 70 seconds, while contained in the defects by compression of the fixation tip onto the silicone sheet and the cartilage. In the 'GelMA cap' group, 1 million cells were infused in the bottom of the defect in 40 µl GelMA and UV-crosslinked for 30 seconds. Subsequently, the defect was filled with cell-free GelMA,

which was UV-crosslinked for 60 seconds. In the fibrin glue group, the cell pellet was suspended in the fibrinogen component after the defects had been made. The glue was then injected in the defect and allowed to crosslink for 3 minutes.

The implanted hydrogels and the surrounding cartilage were scanned with optical coherence tomography (OCT) (Illumien Optis PCI Optimization System, St. Jude Medical, St Paul, MN, USA) and ultrasound (Boston Scientific, San Jose, CA, USA) imaging systems, along the length of three standardized sites of the implant. The stiffness of the cartilage at three standardized sites surrounding the defects was measured (Artscan 200, Artscan Oy, Helsinki, Finland) to obtain baseline values for cartilage. The wound was closed in 4 layers and full weight bearing was allowed after recovery from anesthesia. The ponies received NSAIDs up to 14 days and opiates up to 3 days postoperatively. For antibiotic prophylaxis, ampicillin was administered intravenously once before and procaine penicillin once after surgery.

At 2, 6 and 12 months, biomaterial degradation and tissue regeneration is assessed arthroscopically (Table 1). The surface is imaged with a regular camera and the implant and the subchondral bone are imaged in detail with OCT and ultrasound. The stiffness of the implant and surrounding cartilage is measured. The repair sites are also imaged transcutaneous ultrasound at aforementioned time points, including an early evaluation at 3 weeks. The gait of the ponies is objectively monitored over time by means of pressure/

	<i>Day of surgery</i>	<i>3 weeks</i>	<i>2 months</i>	<i>6 months</i>	<i>12 months</i>
OCT (implant structure)	X		X	X	X
Ultrasound (implant structure and subchondral bone)	X		X	X	X
Mech. Analyser (implant stiffness)			X	X	X
Camera (Implant surface)			X	X	X
Transcutaneous ultrasound		X	X	X	X
Gait Analysis (Force and pressure plate)	<i>Before surgery</i>		X	X	X
GAG/DNA (cartilage matrix quantification)					X
Macro- & Microscopy (cartilage matrix qualification)					X
DNA detection					X

Table 1. Outcome parameters of the long-term cartilage repair study in Shetland ponies. Tissue formation is monitored over time with arthroscopic optical coherence tomography (OCT) and ultrasound. In addition, the stiffness of the repair tissue will be measured with a mechanical analyzer. The study is terminated at 12 months, when final values will be obtained with imaging. The quantity and quality of the newly formed tissue in the defect will be assessed with biochemistry, histology and immunohistochemistry. The DNA in the explanted tissue is compared to the DNA of the implanted cells and the host tissue.

force plate analysis, evaluating the longitudinal changes in ground reaction forces and pressure distribution of the hind hooves. At 12 months, the ponies are euthanized, and the stifle joints are explanted and processed in the laboratory. Macroscopic (ICRS and Mastbergen Score) and histological scoring (O'Driscoll and Mankin) of the implant site are performed²³. GAG and DNA of explanted repair tissue is quantified with biochemistry. Genomic DNA will be isolated from the repair tissue, the horses themselves and from the donor MSCs and donor chondrons. The DNA profiles of the donors, recipients and repair tissue and used for DNA fragment analysis to verify whether there is still DNA from the donors present in the repair tissue³⁷⁵.

RESULTS

Digestion and storage of chondrons

Digestion of chondrons for 12 hours resulted in a mixture of single cells and clustered cells, with predominant positive staining for collagen type VI, which is specific for the pericellular matrix of chondrocytes³⁷⁶. The same morphology was observed when the cells were stored in liquid nitrogen (Fig. 2a). The viability of cells directly after isolation was $80\% \pm 3\%$ and after freeze-thawing $79\% \pm 2\%$ (Fig. 2b).

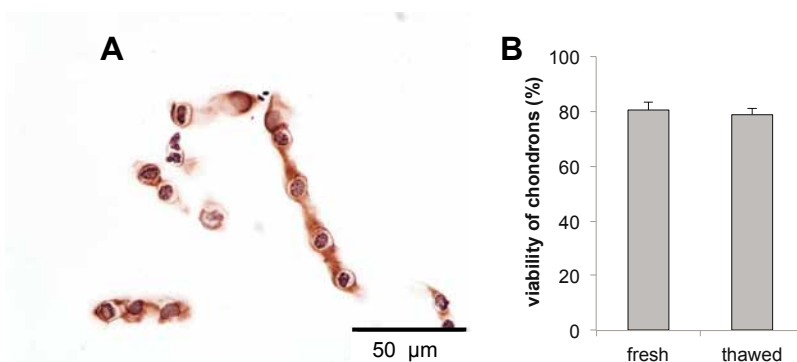


Figure 2. Storage of chondrons in liquid nitrogen for allogeneic implantation. (a) The morphology of chondrons remained intact after the freeze-thaw cycle, as demonstrated with a collagen type VI staining (brown). (b) And the viability of chondrons was unaffected ($n = 3$ donors).

The effect of UV-crosslinking on cell viability and hydrogel stiffness

The stiffness of cell-laden GelMA gels increased with longer UV-exposure times (Fig. 3). The viability of embedded cells was between 79% and 93% after up to 3 minutes of UV-exposure, but decreased to 0%, when exposed for 5 minutes due to the significant amounts of heat generated by the focused UV during longer exposure periods. We also

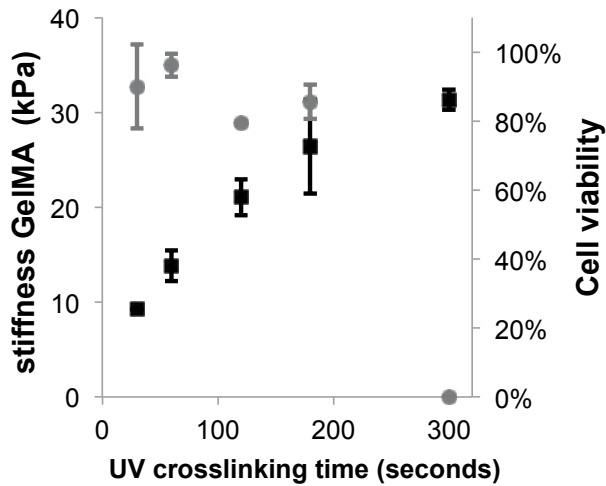


Figure 3. Cell viability and hydrogel stiffness depending on UV exposure times. The viability of chondrocytes and MSCs (both $n=1$) in GelMA decreased after UV exposure for 200 seconds (grey circles). The stiffness of hydrogels increased with longer UV exposure (black squares). GelMA in the equine stifle joints was crosslinked for 70 seconds.

found that the stiffness of the gels decreased, when cells had been suspended in GelMA for over 30 minutes prior to crosslinking, although this observation was not quantified.

Cadaver and pilot study in one Shetland pony

The cadaveric studies showed that the infusion and UV-crosslinking of the GelMA gel in cartilage defects was a feasible procedure. There was full penetration of the gel into the highly porous 3D-printed scaffolds. UV-crosslinking of 70 seconds was sufficient for firm crosslinking of the gel, but without generating too much heat. The crosslinked gels stayed in the defect after repetitive flexion/extension cycles. Furthermore, reinforced and non-reinforced GelMA hydrogels were successfully implanted and crosslinked in chondral defects in the stifle joint of a Shetland pony (Fig. 4a,b). The pony recovered well and the GelMA hydrogel stayed in place in both cartilage defects two weeks after implantation, as observed macroscopically (Fig. 4c), and the GelMA gel was infiltrated with cells of a fibroblastic nature (Fig. 4d). An inflammatory response was observed in the underlying bone, by the presence of fibroblastic cells, neutrophil granulocytes and multinucleated cells (Fig. 3d-f). Bone remodeling was observed under the defect.

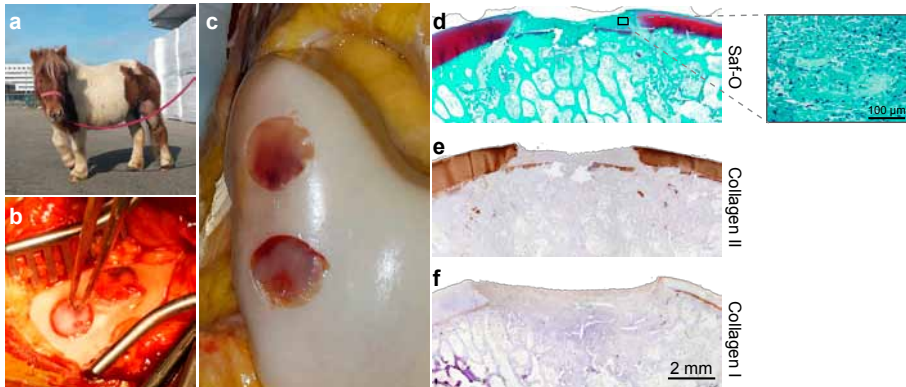


Figure 4. Pilot study in a Shetland pony for fixation of GelMA. (a,b) reinforced GelMA and the ‘GelMA cap’ group were implanted in the stifle joint of one Shetland pony. (c) The gels stayed in the cartilage defect after two weeks. (d-f) Cells migrated into the hydrogel and only scarce remnants of GelMA were observed between the cells (light green in zoom picture).

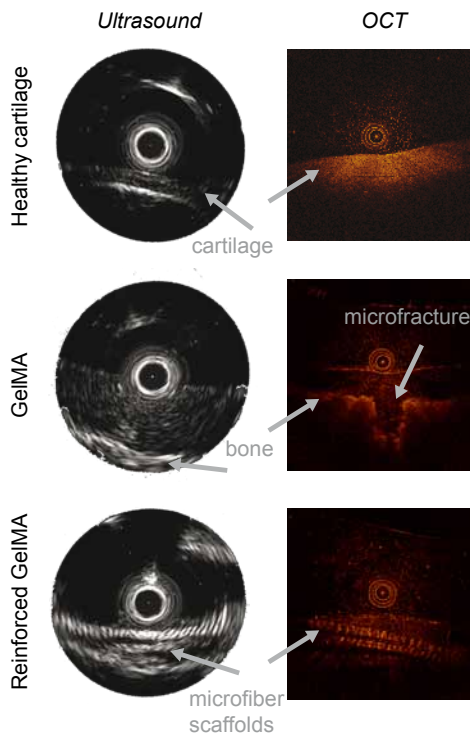


Figure 5. Baseline imaging of implants with OCT and US. Baseline values were obtained of healthy cartilage and of the gels in the defect directly after implantation. The hydrogel, reinforcing scaffolds and the subchondral bone could be clearly identified with OCT and ultrasound.

Long-term evaluation of cartilage repair in Shetland ponies

Two cartilage defects in both stifle joints of eight Shetland ponies were made and repaired in one surgical session. OCT and ultrasound imaging confirmed the depth of the defect, including the microfractures, and the location of the microfiber scaffolds (Fig. 5). All ponies were able to walk unassisted after recovery from anesthesia, with limited stiffness in the hind legs. Walking turned to normal within two weeks postoperatively. No adverse events related to the surgery were observed until one month of follow-up.

DISCUSSION

In this study, a cartilage defect model in the trochlea of Shetland ponies was used. The implantation and *in situ* crosslinking of GelMA gel appeared to be feasible in a pilot study with the gel remaining in the defect site after two weeks of full weight bearing. As a follow-up, a comparative study was initiated in eight ponies, comparing fibrin glue with GelMA and reinforced GelMA as a carrier for allogeneic chondrons and MSCs. Low cell concentrations that are clinically feasible were compared to high cell concentrations, which are often used in *in vitro* tissue engineering to establish an interconnected matrix.

We found that two chondral defects with diameter of 10 mm could be made and repaired on the medial femoral trochlear ridge in both stifle joints of Shetland ponies, followed by a good clinical recovery after surgery. The size of the defect was chosen in order to avoid spontaneous healing that might occur in smaller defects²⁴.

The GelMA that was crosslinked in the defects remained in place after repetitive flexion-extension cycles in cadaveric joint and after two weeks in a pony. No additive fixation techniques were used, except for the application of microfractures in the subchondral bone for anchoring of the gel. However, the gel was fully infiltrated by fibroblastic cells in the Shetland pony after two weeks. The degradation rate of GelMA *in vitro*⁷ and in immunocompromised rats²⁵ has been found to be low^{63,377}, with GelMA serving as a scaffold for matrix formation to embedded cells for at least eight weeks embedded cells. In cell-free gels in nude rats, only limited cell infiltration was observed²⁵. This difference in hydrogel degradation and cellular infiltration can most likely be ascribed to the immunocompetency of the horses, and the abundant presence of cells from the bone marrow that can enzymatically break down the GelMA^{257,377}.

In this study, a mixture of allogeneic chondrons and MSCs was implanted as cell therapy for cartilage repair. This combination of cells was based on two clinical trials on cartilage repair in humans, in which autologous chondrons and allogeneic MSCs^{20,25} or chondrocytes and a bone marrow concentrate²⁶ were implanted in one surgical session. In addition, the presence of chondrocytes in the vicinity of MSCs in GelMA *in vivo* was shown to prevent endochondral bone formation by MSCs³⁷⁷. Allogeneic instead of

autologous chondrons were implanted in the current study, as two experimental groups contained a high cell concentration, which cannot be obtained in a rapid digestion protocol of the autologous cartilage²³. Allogeneic chondrocytes have been applied in the knee joint of horses³⁷⁸ and humans previously^{379,380}. No adverse events were observed, although it remains uncertain whether allogeneic chondrons or chondrocytes have the same regenerative potential as their autologous counterparts.

The mechanism of cartilage formation in a co-culture of chondrocytes (or chondrons) with MSCs is under debate²⁴. Initially, MSCs were thought to contribute primarily to matrix formation, but recent studies suggest that chondrocytes are the major contributors^{381,382}, where MSCs have a trophic role in the co-culture and disappear over time. Preliminary results from the IMPACT trial support this theory, as no allogeneic DNA could be retraced in biopsies from repair cartilage one year after implantation of autologous chondrons and allogeneic MSCs²⁵. Whether the implanted chondrons or homing host cells were responsible for tissue formation remains unclear, however. In the follow-up of the current study, we hope to differentiate between the host cells and implanted chondrons and MSCs (both allogeneic), by comparing the DNA profiles of the donors and recipients to the DNA that is present in the defect site after one year.

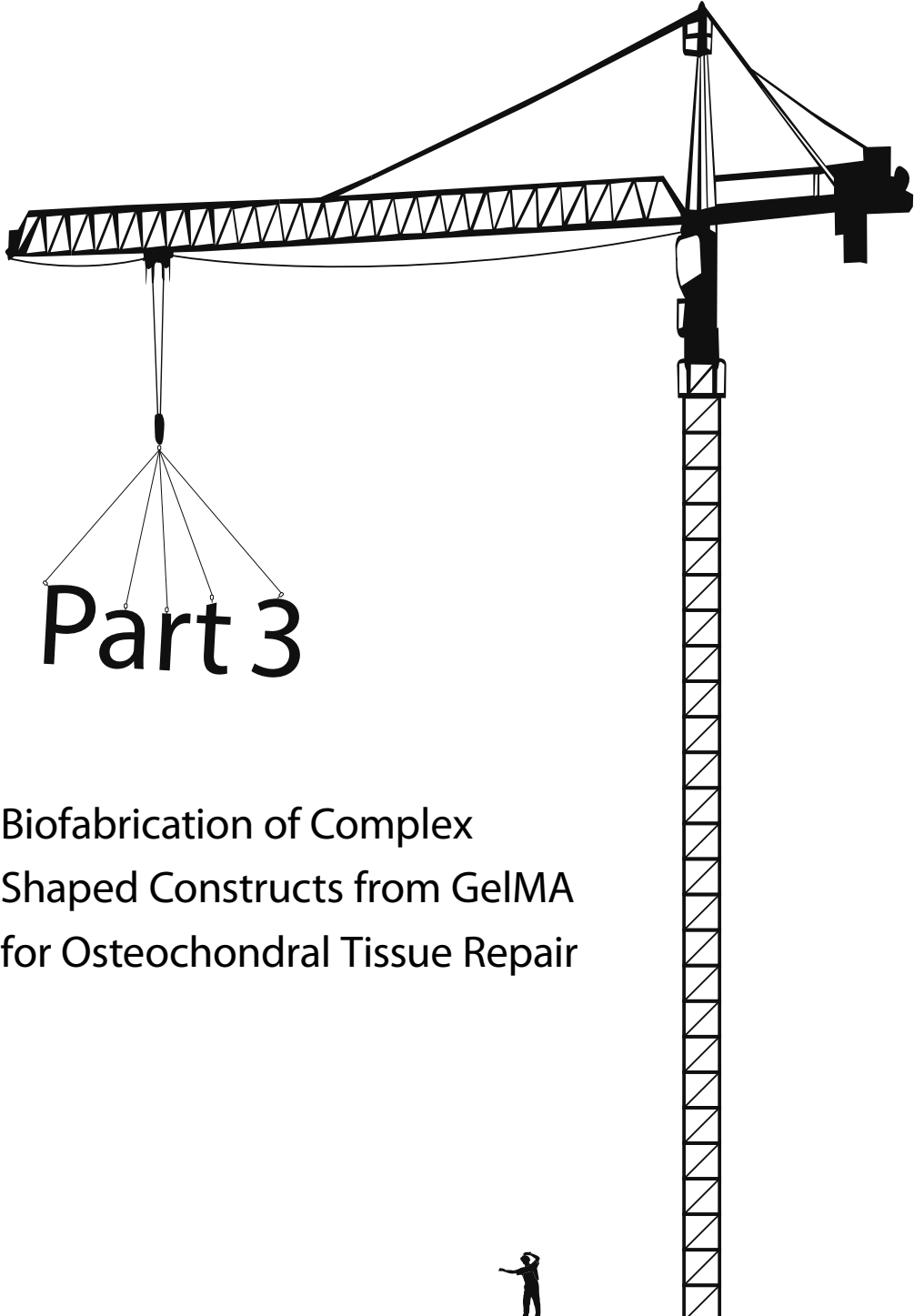
In vitro tissue engineering in GelMA hydrogels has shown that high cell concentrations (20 million cells per mL) are required to form an interconnected matrix within the hydrogel^{63,383,28,73}. In contrast, much lower concentrations (around 2 million cells per mL) are applied in clinical cell therapies, like autologous chondrocyte implantation³⁶⁹. The amount of cells that is required may depend on the options for interaction within the gel. In fibrin glue, the cartilage matrix formation is based on direct cell-cell contact, which is allowed by contraction and rapid degradation of the fibrin glue²⁵. In contrast, cells in low concentrations in slowly degrading hydrogels, like GelMA, may not be able to communicate and form an interconnected matrix. To study the value of GelMA gel combined with a low amount of cells, the 'GelMA cap' group was introduced in the present study.

In conclusion, a model for evaluating cartilage repair in Shetland ponies was established, after preliminary *in vitro*, cadaveric and pilot studies, to monitor cartilage repair by a mixture of allogeneic chondrons and MSCs in several GelMA-based implants. This study is at the moment of writing still ongoing. It is anticipated that this comparative study, in combination with ongoing *in vitro* cultures, will further elucidate the mechanism of cartilage regeneration after the implantation of cell-seeded hydrogels, depending on the biomaterial and the cell concentration. We expect cartilage to regenerate upwards, from the bottom of the defect in the 'GelMA gap' and the fibrin group. In contrast, we hypothesize that cartilage matrix will be deposited *within* the hydrogel in the GelMA groups with high cell concentrations.

ACKNOWLEDGEMENTS

The authors thanks mr. Gernot Hochleitner and mr. Elder Linssen for producing scaffolds with melt-electrospinning. Regentis Biomaterials Ltd., for providing the silicone sheets. Mr. Filipe Serra Braganca and mr. Tsjester Huppkes for assisting in the surgeries. Dr. Janny de Grauw and mr. Thijs van Loon for taking care of anesthesia in the ponies and the complete 'equine cartilage repair team' for logistics around the surgeries. Dr. Guy Grinwis, DVM, veterinary pathologist, for his help in interpreting histology of explants. Dr. Imo Hofer from the experimental cardiology dept. of the UMC Utrecht, for providing the OCT machine. The monoclonal antibodies for the detection of collagens developed by T.F. Linsenmayer were obtained from the Developmental Studies Hybridoma Bank developed under the auspices of the NICHD and maintained by The University of Iowa, Department of Biology, Iowa City, IA 52242. This work was supported by the European Community's Seventh Framework Programme (FP7/2007-2013) under grant agreement n309962 (HydroZONES). Jetze Visser was supported by a grant from the Dutch government to the Netherlands Institute for Regenerative Medicine





Part 3

Biofabrication of Complex
Shaped Constructs from GelMA
for Osteochondral Tissue Repair

Chapter 8

Biofabrication of Multi-Material Anatomically Shaped Tissue Constructs

Jetze Visser
Benjamin Peters
Thijs Burger
Jelle Boomstra
Wouter Dhert
Ferry Melchels
Jos Malda

Biofabrication. 2013 Sep;5(3):035007

ABSTRACT

Additive manufacturing in the field of regenerative medicine aims to fabricate organized tissue-equivalents. However, the control over shape and composition of biofabricated constructs is still a challenge and needs to be improved. The current research aims to improve shape, by converging a number of biocompatible, quality construction materials into a single three-dimensional fiber deposition process. To demonstrate this, several models of complex anatomically shaped constructs were fabricated by combined deposition of poly(vinyl alcohol), poly(ϵ -caprolactone), gelatin methacrylamide/gellan gum and alginate hydrogel. Sacrificial components were co-deposited as temporary support for overhang geometries and were removed after fabrication by immersion in aqueous solutions. Embedding of chondrocytes in the gelatin methacrylamide/gellan component demonstrated that the fabrication and the sacrificing procedure did not affect cell viability. Further, it was shown that anatomically shaped constructs can be successfully fabricated, yielding advanced porous thermoplastic polymer scaffolds, layered porous hydrogel constructs, as well as reinforced cell-laden hydrogel structures. In conclusion, anatomically shaped tissue constructs of clinically relevant sizes can be generated when employing multiple building and sacrificial materials in a single biofabrication session. The current techniques offer improved control over both internal and external construct architecture underscoring its potential to generate customized implants for human tissue regeneration.

INTRODUCTION

Additive Manufacturing (AM) is the layer-by-layer construction of objects based on a three-dimensional (3D) model data set^{11,118}. In the field of regenerative medicine (RM), AM has the potential to produce customized tissue implants to replace damaged or eroded parts of the human body. In order to achieve this, a balanced combination of cells, growth factors, matrix and/or biomaterials needs to be processed into a 3D-construct with controlled architecture. Unlike conventional subtractive manufacturing, AM offers full control over internal and external architecture of the object and every deposited layer serves as a fundament for the next layer. Moreover, AM technologies, including 3D fiber deposition (3DF)^{11,118}, potentially allow for reproducibility and customization of complex tissue analogs with limited waste of the often expensive building biomaterials.

Scaffolds for tissue engineering have been fabricated with 3DF from biodegradable thermoplastic polymers, *e.g.* polycaprolactone (PCL)^{50,53,384} and PCL-derivatives³²⁷, polylactic acid (PLA)³⁸⁵ or PolyActive^{®386} allowing for direct implantation^{328,387} with the possibility of prior cell seeding⁸ or incorporation of growth factors⁵³. In addition, scaffolds have also been fabricated from hydrogels, where the hydrogel serves as a carrier for cells or bioactive factors, while simultaneously serving as a building block^{100,105,121,148,388}. Recently, the combined deposition of thermoplastic polymers and hydrogels was developed in order to reinforce hydrogel constructs with a thermoplastic polymer network^{65,75,76}.

For the translation of biofabrication to the clinic, tissue equivalents must be fabricated from digital blueprints of the anatomical structure that needs to be repaired or replaced^{11,179}. To this end, control over both shape and composition of implants needs to be improved^{11,116-118}, addressing complex internal and external architectures as well as multiple tissue types of the target structure. For example, when pursuing to fabricate a vascular network, the desired lumen diameter, branching pattern, vessel stiffness and possibly the different tissue types in the vessel wall need to be addressed. Similarly, when aiming to generate a construct with the shape of the external ear, the complex auricular shape, as well as the different tissue types (*i.e.* cartilage, skin and blood vessels) need to be put in place. In order to achieve this, better control over the deposition is needed, requiring novel construction biomaterials that facilitate tissue regeneration. In addition, in order to process these materials in three dimensions with high resolution, biofabrication techniques need to be optimized.

The current research aims to improve the shape of constructs by integrating several quality construction biomaterials into a single fabrication session. This includes materials that temporarily support overhang geometries in complex structures, as layer-by-layer fabrication will fail in the absence of a base layer. These support materials need to be sacrificed after fabrication, a principle that has already been applied in microfluid-

ics^{184,186,389}, but also for the casting of collagen scaffolds³⁹⁰ and for achieving internal porosity in tissue-engineered constructs^{391,392}. Moreover, sacrificial materials have been applied for realizing controlled internal architectures within hydrogel constructs, either by casting¹⁸⁸ or combining printing and casting^{158,185}. For the current 3DF approach, sacrificial materials were selected so that they can be processed layer-by-layer and removed from the target structure without compromising its shape. Furthermore, sacrificial materials should support, and form a stable interface with adjacent components, and should not compromise cellular survival.

Here, we demonstrate how several relevant-size models of complex anatomical structures, being a vascular network, an ear and a distal femur, can be fabricated by combining building and sacrificial materials in a multi-material 3DF setting. These include thermoplastic polymers and hydrogels that provide both mechanical support and a suitable environment for cells to regenerate tissue.

MATERIALS AND METHODS

Materials

Polyvinyl alcohol (PVA) filament (diameter 3 mm, melting point 160–170°C, density 1.25–1.35 g/cm³) (Kuraray USA, Houston, TX, USA) was obtained from Makerbot Industries, NY, USA. PCL (average M_n 45,000; M_w 48,000–90,000) was obtained from Sigma-Aldrich, Zwijndrecht, The Netherlands. Alginate hydrogel (10% w/v) was prepared by mixing sodium alginate powder (Sigma-Aldrich) overnight at 37°C in dH₂O. Gelatin methacrylamide (GelMA) was synthesized as described previously⁶³. GelMA-gellan hydrogel was prepared by dissolving GelMA (10% w/v) and gellan gum (Gelzantm CM, Sigma-Aldrich) (1.1% w/v) at 90°C for 20 minutes in dH₂O containing 0.1% w/v photoinitiator Irgacure 2959 (Ciba, BASF, Ludwigshafen am Rhein, Germany). In case cells were mixed in the hydrogel, D-mannose (5.4% w/v) was added to the mixture to obtain isotonic conditions⁶¹. GelMA-gellan hydrogels were stained with fast green (Merck, Whitehouse Station, NJ, USA) for visualization purposes when printing multi-layered constructs.

Experimental design

Several anatomically shaped constructs were designed using Rhinoceros computer aided design (CAD) software (McNeel, Seattle, WA, USA), including structures inspired by blood vessels, an ear and a distal femur (Table 1). Complementary structures were designed in order to temporarily support overhangs in the target structures on biofabrication. The CAD-files were loaded via computer-aided manufacturing (CAM) software (PrimCAM, Einsiedeln, Switzerland) in which a building material (PCL, GelMA-gellan hydrogel, or both) was assigned to the target structure and a specific sacrificial material

Target construct	Permanent material	Sacrificial material	Sacrificing procedure	Printed structures
Thermoplastic polymer	PCL	PVA	Wash in water	Models of a vascular branch, ear and DNA-helix
Hydrogel	GelMA-gellan	PCL	Manual removal	Model of a distal femur
		Alginate	Wash in citrate solution	Box with tubes
Fiber reinforced hydrogel	PCL + GelMA-gellan	Alginate	Wash in citrate solution	Single tube

Table 1. Printing of a thermoplastic polymer (PCL), a hydrogel (gelMA-gellan) or a combination of both in a fiber reinforced construct required specific sacrificial materials (PCL, PVA or alginate hydrogel) in order to achieve optimal shape fidelity. Different procedures were applied to sacrifice these materials.

(PVA, PCL or alginate hydrogel) was assigned to the support components. A stack of all these materials was fabricated, with subsequent removal of the sacrificial components, in order to evaluate the effects of the full fabrication process on the survival of cells embedded in the GelMA-gellan hydrogel component.

Cells: equine chondrocytes and mesenchymal stromal cells (MSCs)

Full-thickness cartilage was harvested (with consent of the owner) under sterile conditions from the stifle joint of a fresh equine cadaver ($n=1$; 7 years old) with macroscopically healthy cartilage that died of natural causes in the clinic. After overnight digestion in type II collagenase (Worthington Biochemical Corp) at 37°C the suspension was filtered and washed in PBS. The chondrocytes were seeded at a density of 5×10^3 cells/cm² and expanded for 10 days in a monolayer culture in chondrocyte expansion medium consisting of DMEM (Dulbecco's Modified Eagle Medium 41965, Invitrogen), 10% heat-inactivated fetal bovine serum (Biowhittaker), 100 units/ml penicillin and 100 $\mu\text{g}/\text{ml}$ streptomycin (Invitrogen), and 10 ng/ml FGF-2 (R&D Systems).

MSCs were obtained from a sternal bone marrow aspirate from a healthy, living equine donor ($n=1$), with approval of the institutional ethics committee. The mononuclear fraction (MNF) was isolated by centrifuging the sample on Ficoll-Paque. The MNF was seeded at a density of 2.5×10^5 cells/cm² and expanded in a monolayer culture till subconfluency in MSC expansion medium containing α -MEM (22561, Invitrogen) supplemented with 10% heat-inactivated fetal bovine serum, 0.2 mM L-ascorbic acid 2-phosphate (Sigma), 100 units/ml penicillin and 100 $\mu\text{g}/\text{ml}$ streptomycin, and 1 ng/ml FGF-2.

Histology

MSCs were suspended in gelatin hydrogel (from bovine skin, type B, Sigma-Aldrich) (10% w/v, 5×10^6 cells/ml), which was perfused through the lumen of a 3D-printed fiber reinforced tube. The tube was processed into cross-sectional 5 μ m paraffin slides and a triple-stained with hematoxylin, fast green, and Safranin-O (all from Sigma). To visualize the cells, gelatin and the GelMA-gellan (vessel wall) component, stained sections were examined using a light microscope (Olympus BX51).

Three-dimensional fiber deposition

Constructs were fabricated using the BioScaffolder 3DF system (SYS+ENG, Salzgitter-Bad, Germany), which can build three-dimensional objects by coordinated motion of several dispensing heads, depositing on a stationary platform. Four dispensing heads were used, employing different types of extrusion: piston-driven extrusion for GelMA-gellan and alginate hydrogel; auger screw driven melt extrusion for PCL, and filament extrusion for PVA. The filament extruder was custom-built, based on the commercially available open-source Ultimaker 3DF machine (Ultimaker LTD, Geldermalsen, The Netherlands) and was adapted for use within the BioScaffolder multiple-tool dispensing setting. The BioScaffolder was located at room temperature in a custom-built laminar flow cabinet to ensure sterile conditions and to facilitate rapid cooling of deposited thermoplastic materials. Fabrication parameters were set for each printing material, as detailed in Table 2. Strand spacing for both hydrogels ranged between 0.8 and 1.8 mm, in which the first setting yields a solid - at a given ratio of spindle speed and translational speed - and the second a porous construct. Both strand spacings were used in order to represent respectively the cartilage and bone component of a structure inspired by a distal femur.

	PVA	PCL	GelMA-gellan	Alginate
<i>Materials specifications</i>	Filament	Granules, m_n 45,000	Hydrogel, 10%-1.1% w/v	Hydrogel, 10% w/v
<i>Extrusion mechanism</i>	filament	auger screw	piston	piston
<i>Printing temperature</i>	185°C	90°C	35°C	25°C
<i>Needle type</i>	Ultimaker® Nozzle	DL Technology EZ-FLO™ (Haverhill, MA, USA)	Nordson EFD Precision Tips (East Providence, RI, USA)	Nordson EFD Precision Tips
<i>Needle internal diameter (mm, (Gauge))</i>	0.4 (22G)	0.32 (23G)	0.32 (23G)	0.5 (21G)
<i>Deposition speed (mm min⁻¹)</i>	350	150	1250	900
<i>Layer thickness (mm)</i>	0.20	0.17-0.20	0.17-0.20	0.19-0.20
<i>Strand spacing (mm)</i>	1.3-1.5	0.7-1.2	0.8-1.8	0.8-1.8

Table 2. Specifications of the BioScaffolder 3DF-system (SYS+ENG) for dispensing different materials in the current study.

To analyze internal shape fidelity, a four-strand-thick cross-section of the femoral condyle constructs was freeze-dried overnight and visualized with stereomicroscopy (SZ61/SZ2-ILST, Olympus, The Netherlands). Generated constructs were captured with a digital single lens reflex-camera (EOS 60D, Canon inc., Japan). Porosity of the fabricated PCL constructs was determined gravimetrically.

Sacrificing procedures

PVA, PCL and alginate hydrogel were used as sacrificial materials, each requiring a specific sacrificing procedure (Table 1). PVA served as a sacrificial support for PCL constructs. PVA dissolves easily in aqueous solutions and was, therefore, washed from the PCL construct with water on a rollerbank overnight. PCL and alginate hydrogel served as sacrificial materials to GelMA-gellan hydrogel constructs. The PCL was sacrificed by manually taking the hydrogel construct out of its PCL support structure. The alginate components were removed from the GelMA-gellan constructs by washing in a 130mmol sodium citrate solution on a rollerbank. The GelMA-gellan/alginate constructs were UV-cured for 5 minutes after printing (Superlite S-UV 2001AV lamp (Lumatec, Munchen, Germany) at 320–500 nm, intensity of 6 mW cm^{-2} at 365 nm) in order to irreversibly crosslink the GelMA component. Printing the fiber-reinforced construct involved a PCL/GelMA-gellan target structure with alginate support. Temporary PCL stands were designed at both ends of the construct in order to anchor PCL strands that were deposited on top of different hydrogels. After UV-crosslinking the anchoring blocks were sacrificed manually with a scalpel and the alginate was subsequently sacrificed by dissolving in sodium citrate solution.

Viability assay

The effects of the printing process, as well as the sacrificing procedure on cell viability in a printed construct were investigated. Hereto, a layered block ($L \times W \times H = 20 \times 20 \times 6 \text{ mm}$) was printed from PVA, PCL, GelMA-gellan (non-porous layer, containing 5×10^6 chondrocytes/ml) and alginate. The printed block was cut in half and both parts were washed on a rollerbank at 37°C in two different isotonic, pH7.4 trisodium citrate solutions (65 and 130mmol) in the absence of divalent ions to prevent the alginate from crosslinking. For both concentrations, cytocompatibility and the ability to dissolve the alginate component were analyzed. After washing for one hour, the GelMA-gellan-chondrocyte layer was cultured for 1 and 3 days in vitro at 37°C in chondrocyte expansion medium. A solid layer ($L \times W \times H = 20 \times 20 \times 1.5 \text{ mm}$) of GelMA-gellan containing chondrocytes was printed as a control to the washing procedure and a sheet ($L \times W \times H = 8 \times 8 \times 1.5 \text{ mm}$) was casted as a control to the printing process. All samples were UV crosslinked for 5 minutes. To visualize cell viability, a LIVE/DEAD Viability Assay (Molecular Probes MP03224, Eugene, USA) was performed according to the manufacturer's instructions. The samples were

examined using an Olympus BX51 light microscope and photomicrographs taken with an Olympus DP70 camera (both Olympus, United States). The excitation/emission filters were set at 488/530 nm to observe living (green) cells and at 530/580 nm to detect dead (red) cells. At least 300 live and dead cells per group were counted in at least four locations within the constructs.

RESULTS

Cell viability after printing and sacrifice of support components

In order to analyze whether the printing process and the sacrificing procedure of temporary support materials described here is cytocompatible, all building and sacrificial materials were printed in a square stack (Fig. 1a). By washing away the sacrificial layers, cells embedded in the GelMA-gellan hydrogel were exposed to low and high sodium citrate solutions containing an over-time increasing amount of dissolving PVA and alginate gel. After one hour the major part of the PVA and the alginate layers had dissolved in both solutions, resulting in separate PCL and GelMA-gellan sheets. From these

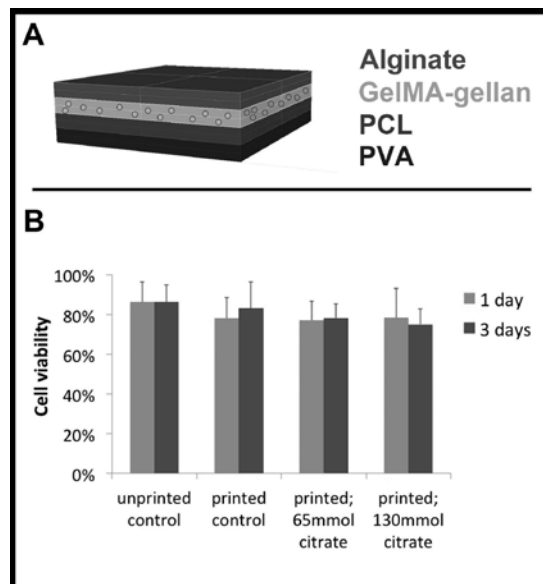


Figure 1. Viability of cells in multi-material constructs. (a) In order to analyze cell viability in a multiple-material construct a square stack was printed of the four materials used in the present research, from bottom to top PVA, PCL, GelMA-gellan (containing chondrocytes) and alginate. (b) Viability of chondrocytes in GelMA-gellan was not affected by the printing process after 1 and 3 days of *in vitro* culture, nor by the subsequent sacrificing procedure in 65 (low) and 130mmol (high) sodium citrate solutions. After one hour the alginate and PVA were considerably dissolved.

macroscopic findings, both citrate concentrations were equally potent in dissolving the alginate component. After 1 and 3 days *in vitro* culture, chondrocytes were found 75-86% viable in all groups (Fig. 1b). No significant difference in cell viability was observed for the printed group or for either the low or high citrate concentration as compared to the non-printed control.

Thermoplastic polymer scaffolds

Anatomically shaped PCL-based structures were successfully fabricated (Fig. 2). Overhangs in these constructs were supported by co-deposited PVA components, which were sacrificed without compromising the quality of the PCL target structure. High shape-fidelity was achieved as the structures matched the dimensions of the design files. A structure inspired by a vascular tree was fabricated with an open vessel lumen decreasing in diameter from 4 to 2 mm; the strand spacing of 0.7 mm resulted in a porosity of 61% (Figure 2A-C). Next, a structure resembling a right ear was fabricated with relevant human dimensions in which a strand spacing of 1.0 mm resulted in a porosity of 74% (Fig. 2d-f). PVA components were designed to support the tragus, located over

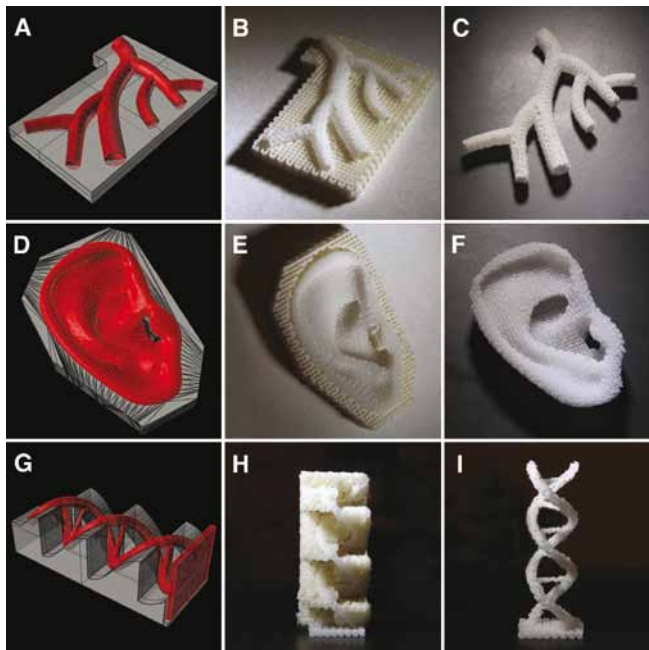


Figure 2. 3D-printed complex anatomical structures based on polycaprolactone (PCL) with polyvinyl alcohol (PVA) support. Vascular tree (a-c) (LxWxH = 67x42x8mm, vessel inner diameter 2-4mm); right ear (d-f) (LxWxH = 63x41x13mm); DNA helix (G-I) (LxWxH = 43x18x15mm). CAD designs (a,d,g) showing permanent (red) and sacrificial (gray) components; printed structures (b,e,h) showing PCL in bright white and PVA in off-white; PCL scaffold after sacrificing PVA support (c,f,i).

a cavity representing the auditory channel and for overhangs up to 60° in the outer contour of the ear. Additionally, the model of the DNA-helix is a powerful demonstration of the successful co-deposition of support material, since 0 to 90° overhangs are present in this complex structure (Fig. 2g-i).

Hydrogel constructs

A miniaturized model of a distal femur (Fig. 3) was printed including a solid layer (green) representing the cartilage component and a porous bone component (yellow) (Fig. 3b). GelMA-gellan hydrogel strands allowed for proper deposition onto the porous PCL support structure (Fig. 3c). Moreover, their stiffness after deposition was sufficient to retain shape and to support the overlying layers. The shape-fidelity of the internal architecture was shown in a cross-section of the femoral condyles (Fig. 3d, 3e). The hydrogel construct could be manually removed from the PCL support structure.

In a different approach, alginate hydrogel provided internal support for creating interconnected tubes within a GelMA-gellan hydrogel box (Fig. 4). Both hydrogels were compatible with the co-deposition process and the high-viscosity alginate was found to be stable enough to carry the overlying structures without crosslinking. By sacrificing

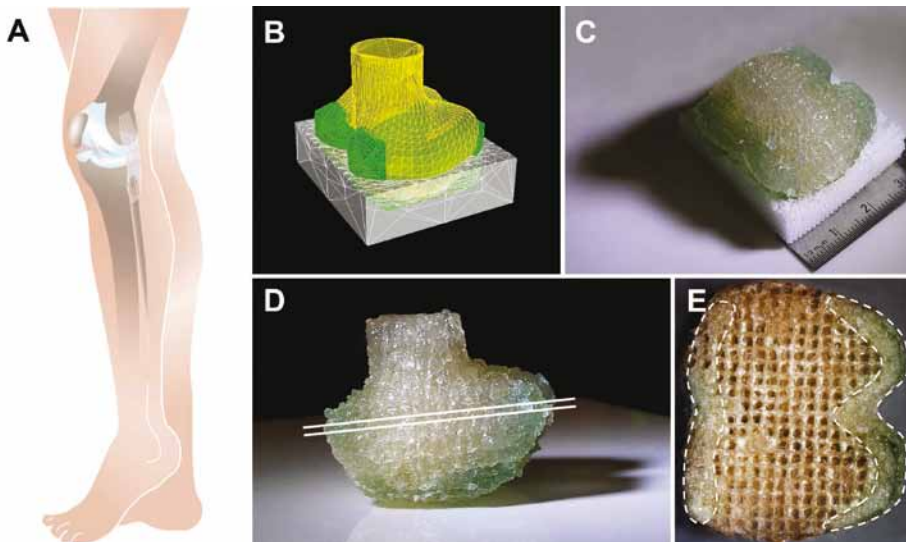


Figure 3. Multi-compartment hydrogel construct. **a)** Distal femur from a human knee **(b)** was designed in Rhino (LxWxH: 40x35x32mm) containing a bone component (yellow), a cartilage layer (green) and a support structure (white); **(c)** the distal femur printed in hydrogel including PCL support structure; **(d)** hydrogel component after manually removing support structure; **(e)** freeze-dried four-layer thick cross-section (level marked by white lines in fig. 3d) from the femoral condyles showing a solid cartilage component (marked by dashed boundary lines) and a porous bone component.

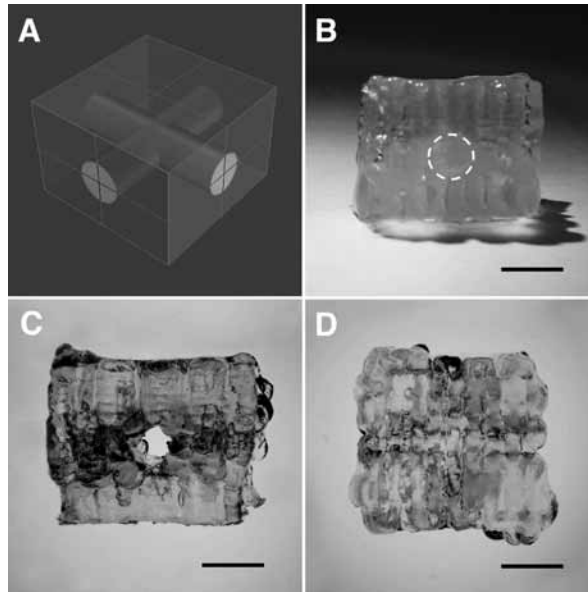


Figure 4. Formation of a tubular network using a sacrificial hydrogel. (a) Perspective view of a GelMA-gellan (red) hydrogel box design (LxWxH = 15x15x10mm) containing an internal tubular structure (gray, diameter 4mm); (b) a circular alginate component is marked by the dashed white line in a side-view of the GelMA-gellan box; (c) by sacrificing the alginate hydrogel an internal tubular network was created as visible in side-view and (d) top-view. All scale bars represent 5mm.

the alginate component, 4mm tubes were created within the box, matching the design geometry.

Fiber-reinforced hydrogel scaffold

A hollow tube was fabricated in a fiber-reinforced approach, inspired by a single blood vessel. Specific sacrificial components were integrated in supporting overhanging geometries of this hybrid construct (Fig. 5). The inner and outer curvatures of the tube were supported by high-viscosity alginate. PCL fibers were anchored in temporary PCL stands (Fig. 5a, b) that were successfully removed with a scalpel (Fig. 5c). By sacrificing the alginate components in a sodium citrate solution, a 4mm diameter lumen was created in the tube. The lumen was shown to be open and perfusable, by injection of an MSC-laden gelatin hydrogel (green on safranin-O staining (Fig. 5d and 5e)).

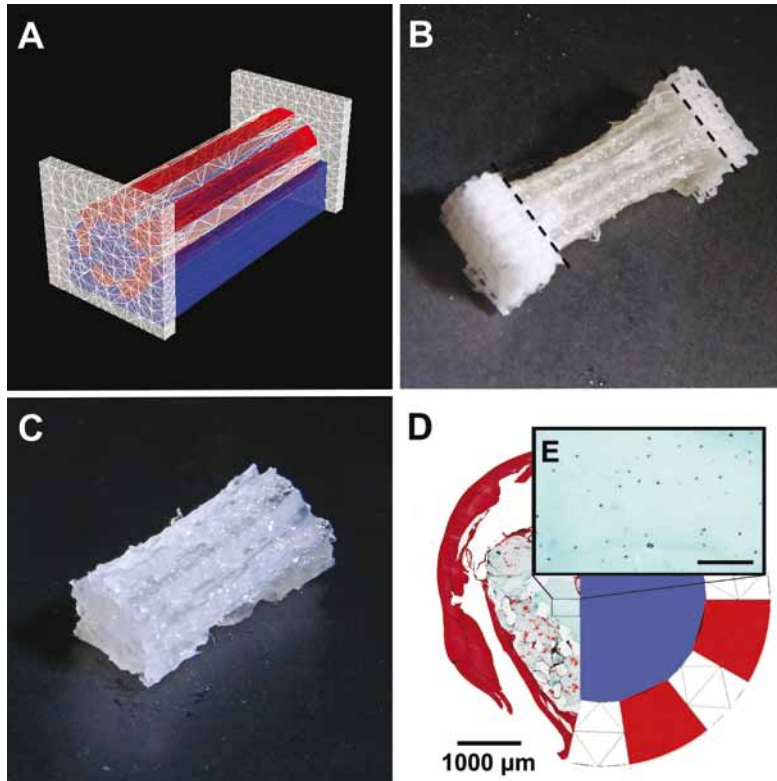


Figure 5. Complex fiber-reinforced construct. (a) Design of a fiber reinforced single tube (inner diameter 4mm, outer diameter 6mm, length 20mm) including anchoring stands (white: PCL, red: GelMA-gellan, blue: alginate); (b) construct directly after printing, scalpel cuts for removing stands represented by dashed lines; (c) tube after removing PCL stands; (d) cross-section of printed tube, right: design, left: after infusion with gelatin containing MSCs (safranin-O staining, red: GelMA-gellan tube wall; green: gelatin-MSC mixture). Reinforcing PCL fibers that were present in the tube wall were dissolved during the embedding process; (e) magnification from picture (d) of gelatin hydrogel containing MSCs (blue dots) (scale bar represents 200 μ m).

DISCUSSION

Anatomically shaped constructs were fabricated by integrating biocompatible thermoplastics, hydrogels and sacrificial materials into a single 3DF-based biofabrication approach. The application of specific sacrificial materials was essential in supporting internal and external overhang geometries in these constructs. Co-deposition of multiple materials and the sacrificing procedures did not adversely affect the shape of the target structure or viability of embedded cells.

Overhangs are inevitable in the internal and external geometry of most anatomical structures, although, for AM purposes, they can be minimized through optimal 3D rota-

tion of the digital blueprint. The remaining overhangs may require mechanical support components which need to be sacrificed by dissolving them in aqueous media or by manual removal from the target structure, as was recognized in a US patent in 1996³⁹³. This patent has mainly been applied for fabricating solid objects from thermoplastic polymers with commercial filament-based 3DF-machines. Obviously, when aiming to support constructs for biomedical applications, the range of suitable support materials will be smaller, since the material and its removal needs to be biocompatible. Therefore, in the current study, several specific biocompatible support materials were implemented.

In the first place, clinically relevant structures were realized by co-deposition of PVA as a soluble support material to PCL. Importantly, PCL is a biocompatible and degradable polymer that has gained FDA-approval in a range of devices, and PCL scaffolds have proven to facilitate abundant formation of neo-tissue at orthotopic locations in animal models^{53,40} and in humans^{387,394}. In order to achieve this, they can be loaded with growth factors⁵³ or cells^{394,395}, or can be functionalized by mixing in other components³⁸⁷. The current fabrication technique allow for customization of complex PCL-implants.

Printing complex structures from hydrogels is more challenging than printing them from thermoplastic polymers, since the large water fraction compromises the shape fidelity of hydrogel structures^{121,122}. This may explain why hydrogel printed structures so far mainly have been fabricated using relatively simple architectures^{11,118}. More complex, vessel-like constructs have been realized by co-printing hydrogels employing an ink-jet printer²³¹ or a Fab@home dispensing system²⁴¹. Hereby, channels were created in controlled hydrogel structures; even so, the complexity in 3D-geometry was limited²³¹ or the support component could not be sacrificed²⁴¹. Both issues were addressed in a combined approach of printing a sacrificial vascular structure as a framework for subsequent hydrogel casting¹⁸⁵. The carbohydrate glass vascular network was printed with high resolution, however casting offers limited control over the composition of the hydrogel construct, including gradients of different biomaterials, cell types or growth factors. For this reason, layer-by-layer assembly using multiple-materials, as demonstrated here, would be favorable for the fabrication of tissue equivalents.

Recently, GelMA-based hydrogels have shown to facilitate specific differentiation of different cell types^{63,64}. In addition, GelMA hydrogel platforms have been tailored for better shape fidelity whilst retaining their beneficial biological properties^{60,61}. With the addition of gellan gum to GelMA, a hydrogel was created with beneficial rheological properties improving shape-fidelity in 3DF⁶¹. By processing GelMA/gellan in combination with removable or soluble support materials the current research took a next step and the generated construct complexity goes beyond what has been achieved in 3DF with hydrogels so far^{60,105,121,133,148,179,232}. A miniaturized model of a distal femur was constructed employing two hydrogel printing heads realizing structures representing a bone and cartilage component that can potentially contain specific cells, growth factors

or bioactive peptides for tissue regeneration^{148,225,396}. The vertical porosity in the bone component facilitates diffusion of nutrients and oxygen⁸⁷, whereas chondrocytes are more likely to thrive under the relatively hypoxic conditions in the solid cartilage component³⁹⁷. The femoral condyles were supported during fabrication by a PCL component, which could be manually removed afterwards, possibly facilitated by the hydrophobic character of PCL. Nevertheless, the approach of creating a removable joint between the building and sacrificial component is not applicable when complexity of the target structure demands an internal or embracing support. Therefore, sacrificial materials have been introduced that can be washed away from the target structure^{158,184-186,188,389,390,398}. Still, there is a lack of support materials that are soluble and allow for deposition along with the hydrogel target structure. High-concentration alginate hydrogel meets both these requirements as was illustrated here with the realization of a tubular network in a GelMA-gellan hydrogel box. It should be noted however, that the resolution of the current tubes was lower compared to casting techniques^{185,188,399}.

Future 3DF constructs may increasingly consist of multiple types of materials. For example, methods have been introduced recently to improve the mechanical properties of hydrogel constructs by co-depositing a PCL network^{65,75,76}. An additional advantage of this fiber reinforcement approach would be increasing the complexity of printed structures, as PCL can be processed with high shape-fidelity and its fibers can form a rigid network⁵¹. Nevertheless, in contrast to earlier rectangle hybrid designs^{65,75,76}, integration of a reinforcing PCL network in complex structures may require deposition of PCL onto hydrogel in the absence of a fundamental PCL layer. As attachment of thermoplastic polymer strands onto hydrogel is poor, multiple-material designs should offer smart solutions. Therefore, in the present fiber-reinforced tube model, temporary PCL-stands were designed at both ends for anchoring the strands. Another solution could be implementation of a temporary support for PCL, as PVA was used in the current study. However, a material interface between PVA and hydrogel should be avoided, since the PVA would dissolve in contact with the hydrogel. This results in an unstable material interface compromising the shape fidelity of the target structure.

To increase the resolution of the fabrication technology, different technologies may need to be combined, as recently was achieved for solution electrospinning and inkjet printing²⁰¹. With inkjet printing, heterogeneous tissue constructs can be fabricated with high resolution²²¹. However, the droplet-driven technique may be less suitable for fabricating complex constructs of relevant size (particularly in height) as compared to 3DF. Moreover, for the fabrication of complex anatomical structures, melt electrospinning techniques may need to be integrated²⁰⁵, allowing for control over high-resolution fiber deposition⁵⁴, in contrast to traditional solution electrospinning where fibers are randomly deposited. In addition, interfacial bonding between the hydrogel and its

reinforcing fibers should be addressed, in order to further improve the integrity of the construct.

In line with earlier reports^{15,18, 22}, the present biofabrication process did not affect cell viability. Also, the sacrificing procedure of alginate in both low (65mmol) and high (130mmol) sodium citrate concentrations was not harmful to the cells. It was already known that cells are able to survive a 20-minute treatment with 55mmol citrate solutions for dissolving encapsulating alginate beads³⁹⁸. Based on the current results, higher sodium citrate concentrations also seem to be compatible with cells embedded in GelMA-gellan hydrogel. Still, the longer-term effect on cellular behavior and the question whether or not higher sodium citrate concentrations would result in shorter dissolving times of alginate hydrogel, needs to be investigated.

Future research still needs to be performed in order to optimize the translation of a digital blueprint of the target anatomical structure into a printable CAD-file including sacrificial and building components. In addition, software and hardware have to be integrated for reproducible fabrication with multiple tools. Complexity of constructs should be further increased and cells and bioactive components should be integrated.

To conclude, with the current research, an important step was made toward the biofabrication of anatomically shaped tissue constructs for application in the field of RM. High complexity of the constructs was achieved by the deposition of temporary mechanical support components in a multiple-tool biofabrication setting. Selection of the right polymer for the support component is crucial, since its fabrication or removal process can compromise the shape and viability of the target structures.

ACKNOWLEDGEMENTS

The research leading to these results has received funding from the European Community's Seventh Framework Programme (FP7/2007-2013) under grant agreements n°309962 (HydroZONES) and n°272286 (PrintCART). Jetze Visser was supported by a grant from the Dutch government to the Netherlands Institute for Regenerative Medicine (NIRM, grant n°FES0908) and Jos Malda was supported by the Dutch Arthritis Foundation.

Chapter 9

Biofabrication of Tissue Constructs by 3D Bioprinting of Cell-laden Microcarriers

Riccardo Levato

Jetze Visser

Josep A Planell

Elisabeth Engel

Jos Malda

Miguel A Mateos-Timoneda

Biofabrication. 2014 Sep;6(3):035020

ABSTRACT

Bioprinting allows the fabrication of living constructs with custom-made architectures by spatially controlled deposition of multiple bioinks. This is important for the generation of tissue, such as osteochondral tissue, which displays a zonal composition in the cartilage domain supported by the underlying subchondral bone. Challenges in fabricating functional grafts of clinically relevant size include the incorporation of cues to guide specific cell differentiation and the generation of sufficient cells, which is hard to obtain with conventional cell culture techniques. A novel strategy to address these demands is to combine bioprinting with microcarrier technology. This technology allows for the extensive expansion of cells, while they form multi-cellular aggregates, and their phenotype can be controlled. In this work, living constructs were fabricated via bioprinting of cell-laden microcarriers. Mesenchymal Stromal Cell (MSC)-laden polylactic acid microcarriers, obtained via static culture or spinner flask expansion, were encapsulated in gelatin methacrylamide-gellan gum bioinks, and the printability of the composite material was studied. This bioprinting approach allowed for the fabrication of constructs with high cell concentration and viability. Microcarrier encapsulation improved the compressive modulus of the hydrogel constructs, facilitated cell adhesion, and supported osteogenic differentiation and bone matrix deposition by MSCs. Bilayered osteochondral models were fabricated using microcarrier-laden bioink for the bone compartment. These findings underscore the potential of this new microcarrier-based biofabrication approach for bone and osteochondral constructs.

INTRODUCTION

Tissue engineering can yield three-dimensional (3D) tissue-like constructs that can serve as experimental platforms for biological studies and drug screening⁴⁰⁰, and as implants for clinical application. Recapitulating the complexity of living tissues, with regards to the variations in cell types, matrix components and organization, remains however a major challenge. Bioprinting is an innovative technology that allows for the generation of organized 3D tissue constructs via a layer-by-layer deposition process of cells and bio-materials^{58,126}. In this way, hydrogel matrices with embedded viable cells have already been produced, such as functional vascular-like networks with enhanced transfer of nutrients^{185,283}. In this fashion, bioprinting can potentially address the zonal organization of cartilage and osteochondronal constructs^{100,190,221}.

The building materials in biofabrication are generally cell-laden hydrogels - also known as bioinks. Bioinks are critical components in biofabrication, as they should possess the right rheological parameters required for the printing process and, simultaneously, offer an optimal environment for cell survival, proliferation, migration and biosynthetic activity^{115,246}. Among them, thermo- and photoresponsive gelatin methacrylamide (GelMA) has been proven as a versatile and promising platform for cartilage tissue engineering⁶³. At the same time, by blending GelMA with viscosity enhancers, such as hyaluronic acid⁶⁰ or gellan gum^{61,190}, it displays improved properties for printing of geometrically complex structures.

There are several challenges in the fabrication of hydrogel-based tissue constructs. For example, hydrogels provide a highly hydrophilic microenvironment in which suspended cells are constrained to a round shape, regardless their native morphology⁴⁰¹. Therefore, inclusion of cues to guide cell fate would be desired. Second, printing of large, clinically-relevant grafts requires the encapsulation of high amounts of cells, which are difficult to obtain from biopsies⁴⁰². For this reason, time-consuming 2D expansion steps are required, which reduces the therapeutic potential of the cultured cells by affecting their phenotype (e.g. dedifferentiation, loss of pluripotency)⁴⁰³. Moreover, hydrogels are too soft for application in load-bearing locations in the body²²¹. Consequently, strategies to enhance biological and mechanical properties of bioinks, and the high numbers of regenerative cells will have to be incorporated or attracted once implanted in the host in order to obtain functional tissue constructs.

A potential solution would be to produce composite printable materials by suspending particles with bioactive potential into the hydrogel matrix. Among particulate materials, microcarriers (MCs) are especially interesting, due to their versatility and wide array of applications. MCs are particles designed to promote attachment, homing and survival of adherent-dependent cells⁴⁰⁴. Due to their size that usually ranges from 60 to 400 μm ^{81,82}, MCs offer a very high specific surface area for cell proliferation. They usually

have a low density that facilitates their suspension in culture medium, and hence their application in stirred tanks bioreactors. Dynamic expansion on MCs is a well-established and scalable technology that allows for achieving high cell amounts. After the *in vitro* culture, cells can be either retrieved from the carriers, or be used for regenerative therapies as MC-cells complexes. These aggregates are rich in cell contacts and extracellular matrix (ECM). This resembles the *in vivo* microenvironment, which results in improved biological activity of cells⁴⁰⁵. Many cell types cultured on MCs, including chondrocytes⁸³, osteoblasts⁸³, keratinocytes⁴⁰⁶ and tenocytes⁴⁰⁷ have been found to better retain their phenotype and display greater potential to regenerate the tissue of their competence compared to 2D culture. Mesenchymal Stromal Cells (MSCs) from different sources (i.e. bone marrow, adipose tissue, placenta-derived) can be cultured on MCs to either preserve their pluripotency or to improve their differentiation^{404,408}. Moreover, MCs can be loaded with bioactive molecules as a cue to guide the differentiation of cells^{409,410}. Cultured MCs can be easily embedded in hydrogel matrices, and their encapsulation increases the mechanical strength of the gel, and offers a high cell-anchoring and spreading surface⁴¹¹. For example, encapsulation of cell-laden MCs has been investigated to promote attachment, viability and proliferation of MSCs in agarose and hyaluronic acid gels^{412,413}. In addition, osteoblastic cells have been shown to induce superior formation in a synthetic hydrogel when incorporated as complexes with MCs compared to suspended cells. This indicates that MC-loaded hydrogels are promising composite materials for bone regeneration⁴⁰¹. Thus, MCs are potential candidates to perform cell expansion, improve hydrogels mechanical properties and introduce cues to guide cell behavior.

The aim of this work is to generate living tissues constructs of clinically relevant sizes, by combining bioprinting and MC culture technologies. GelMA-based hydrogels were used as bioinks, and the effect of the incorporation of custom designed polylactic acid MCs⁸² was evaluated for the mechanical and printing properties. In addition, morphology and osteogenic potential of cells in MC-laden bioinks was assessed. Several methods were explored to obtain MC-enriched bioinks, including culture of MSCs on MCs in a spinner flask bioreactor, prior to biofabrication. To provide a proof of application of such an approach, biphasic scaffolds consisting of an osteogenic layer with MC-laden bioink, and a cartilage region composed by MC-free bioink were fabricated.

MATERIALS AND METHODS

Materials

Polylactic acid (PLA, Purasorb PLDL 7038, IV midpoint 3.8 dL g⁻¹, Mw ≈ 850000 Da) was purchased from Purac (The Netherlands). (-)-Ethyl-L-lactate (purity = 99.0%) and polyvi-

nyl alcohol (PVA, 30–70 kDa, 88% hydrolyzed) were obtained from Sigma-Aldrich (Spain). PLA MCs were fabricated using a green solvent-based method, which allows tuning of the particle size, as described in a previous report⁸². MCs with a mean diameter of 120 μm , and a surface area of $2\text{ cm}^2\text{ mg}^{-1}$ were used. GelMA was synthesized from gelatin derived from porcine skin (Sigma-Aldrich) as described elsewhere²²¹. GelMA hydrogels were obtained by dissolving GelMA (10% w/v) in deionized water supplemented with 5.4% w/v D-mannose (Sigma-Aldrich) and 0.1% w/v of Irgacure 2959 (Ciba, BASF, Germany) under magnetic stirring for 20 minutes at 90°C . In order to optimize GelMA as a bioink for 3D printing, 1% w/v gellan gum (Gelzantm CM, Sigma-Aldrich) was added. Cells and cell-laden MCs were mixed in the GelMA solutions. The other reagents were purchased from Sigma-Aldrich, unless specified otherwise.

Microcarrier surface modification

PLA MCs were functionalized with human recombinant collagen type I (FibroGen, USA), in order to improve cell response to the material, according to an established protocol⁴¹⁴. Briefly, MC surface was enriched in carboxyl group by controlled hydrolysis in 50 mM NaOH for 10 minutes. The generated groups were activated with ethyl(dimethylaminopropyl) carbodiimide (Acros Organics, Belgium) and N-hydroxysuccinimide. This allowed for the covalent binding between the free amines of the collagen and the activated COOH, after soaking the samples in a collagen type I solution ($100\text{ }\mu\text{g mL}^{-1}$, 24 hours). All reactions byproducts were water soluble and eliminated by washing the samples in Phosphate Buffered Saline (PBS).

Cells and culture conditions

MSCs were isolated from the long bones of 2–4 weeks old Lewis rats according to a previously published protocol⁴¹⁵. Briefly, rats were anesthetized using 5% isoflurane and sacrificed through CO_2 saturated atmosphere. Bone-marrow was obtained by flushing the bone with control medium -M199 supplemented with 20% Fetal Bovine Serum (FBS), 1% Pyr, 1% Pen/Strep, 1% L-glu and $22\text{ }\mu\text{g mL}^{-1}$ heparin-. The cellular fraction was resuspended in control medium, plated in Petri dishes and allowed to settle for 24 h. The adherent cell population was cultured in Advanced DMEM supplemented with 15% FBS, 1% Pen/Strep and 1% L-glu until reaching sub-confluency. Then, cells were expanded into T-flasks and cultured until passage 2. The acquired population of cells was highly enriched in Stro-1+, CD105+, CD44+, CD34⁻ and CD45⁻ MSCs. For all experiments, cells between passage 4 and 6 were used. These cells were retrieved from different rats and pooled together. The protocols concerning the animal care were previously approved by Committee on the Ethics and Animal Experiments of the Scientific Park of Barcelona (Permit number: 0006S/13393/2011). Cell expansion and experiments were carried out by

culturing MSCs in proliferation medium, consisting of Advanced DMEM, supplemented with 10% FBS, 1% Pen/Strep and 1% L-glu.

Microcarrier culture

MCs were prepared for cell culture by soaking them in 70% v/v ethanol, repeated washing with PBS under sterile conditions, and incubation in serum-free tissue culture medium. MSCs were cultured on PLA MCs both under static and dynamic conditions. For static culture, 3 mg of MCs were placed into an ultra-low attachment multiwell plate (Costar, Corning Inc., USA). The MSC suspension was seeded directly onto the particles, at a density between $1 \cdot 10^5 - 3 \cdot 10^5$ cells/well. For dynamic culture, a 250 mL spinner flask device was used (BellCo, USA). The bioreactor was filled with 100 mL of culture medium and with 2 g L^{-1} of MCs. The inoculum consisted of $2 \cdot 10^5$ cells mL^{-1} . An intermitted stirring regime was maintained for the first 6 hours of culture (30 rpm for 1 minute every 30 minutes). After this seeding period, the suspension was stirred continuously at 30-35 rpm. 2 mL samples were taken from the MCs suspension to estimate the number of cells in culture. The MC-MSCs complexes were lysed with M-PER solution (Thermo Scientific, Spain). The cell amount was calculated from a standard curve, by measuring lactate dehydrogenase (LDH) activity in the supernatant using the Cytotoxicity Detection KitPLUS (Roche, Switzerland).

Cell viability in MC-laden bioinks

30 mg mL^{-1} of MCs where either preseeded with MSCs and then suspended into GelMA-Gellan Gum solutions, or directly co-suspended with the cells into the hydrogels. The mixtures were then manually dispensed through a 20G conical needle (inner diameter = 0.61 mm, Nordson EFD, USA) into a multiwell plate and exposed to UV irradiation (intensity of 4 mWcm^{-2} , $\lambda = 365 \text{ nm}$ for 15 minutes) to induce an irreversible crosslinking of the hydrogel. At day 1 and 3 of culture, MSC viability was evaluated from microscopy images using a LIVE/DEAD Assay (calcein AM/ethidium homodimer, Life Sciences, USA). 5 random fields for each sample ($n=3$) were used to count living cells. A control group was prepared by dispensing MSC-laden MCs suspended in PBS and not exposed to UV light. To evaluate cell localization on MCs and into the hydrogel, samples were cultured for 4 hours, fixed in buffered paraformaldehyde, permeabilized with 0.5% v/v Triton X-100 and stained with phalloidin-FITC (Life Sciences, USA) and 4',6-diamidino-2-phenylindole (DAPI).

Mechanical properties of MC-laden bioink

The effect of MC concentration on the compressive modulus of GelMA-Gellan Gum hydrogels was assessed in an unconfined uniaxial compression test, using a dynamic mechanical analyzer (TA 2980 DMA, TA Instruments, USA). UV-crosslinked hydrogels

samples measuring 4x4x2 mm, containing increasing amounts of MCs (0, 30, 40 and 50 mg/mL) were subjected to a force ramp of 1 N/min up to 4 N and the related stress-strain curve was obtained. The slope of the curve in the elastic region was used as a representative value for the compression modulus. 5 replicates for each sample were tested. The assay was performed at room temperature.

Osteogenic differentiation

The role of MCs in the differentiation of MSCs towards the osteogenic lineage was investigated. First, MC culture was compared to standard culture on 2D polystyrene surfaces. After that, the differentiation capability of the cells encapsulated in GelMA based hydrogels was evaluated. To this end, 30 μ L of hydrogel mixture was placed into a poly(dimethyl siloxane) mold and UV-crosslinked. A preliminary test evaluating the effect of different MCs concentrations on osteogenic differentiation was also performed (data not shown). Since no consistent differences were found, we kept the concentration of MCs at 30 mg/mL for the differentiation assay. The volume of the gels samples used (30 μ L), the cells densities and MCs amount where chosen so that all the experimental group had approx. the same number of cells. The experimental groups are summarized in Table 1.

All samples were cultured for 21 days either in medium with or without supplemented osteogenic factors (10^{-8} M dexamethasone, 50 μ g mL⁻¹ ascorbic acid, 10 mM β -glycerol phosphate). Differentiation was studied by quantifying alkaline phosphatase (ALP) activity at day 7, 14 and 21 of culture; osteocalcin (OCN) secretion at day 14 and 21, and by alizarin red staining on cryostat sections at day 21 to assess the deposition of mineralized matrix. For ALP analysis, samples were washed with sterile PBS and the hydrogels were grinded using a pestle. Protein extracts were obtained inducing cell lysis with M-PER solution, followed by centrifugation for 15 minutes at 2500 rpm, to remove debris from cells, gels and MCs. ALP activity was measured using Sensolyte® pNPP Alkaline Phosphatase Assay Kit (AnaSpec, Inc., USA). OCN quantification was performed from cell culture

Experimental group	Description	MSCs density
TCPS	Culture on 2D tissue culture polystyrene surfaces	10^5 cm ⁻²
MCs	Static culture on MCs	10^5 cm ⁻²
GelMA	Cells encapsulated in GelMA	$8 \cdot 10^6$ mL ⁻¹
GelMA-GG	Cells encapsulated in GelMA-Gellan Gum	$8 \cdot 10^6$ mL ⁻¹
GelMA-GG MC-MSCs	Preseeding on 30 mg mL ⁻¹ MCs overnight and encapsulation in GelMA-Gellan Gum hydrogels	$8 \cdot 10^6$ mL ⁻¹
GelMA-GG MCs and MSCs	30 mg mL ⁻¹ MCs and the cell suspension are mixed together in GelMA-Gellan Gum hydrogels, with no preseeding	$8 \cdot 10^6$ mL ⁻¹

Table 1. Experimental groups analyzed in the osteogenic differentiation assay.

supernatant using an Enzyme-Linked ImmunoSorbent Assay kit (Demeditec Diagnostic GmbH, Germany), following the instructions of the manufacturer. OCN and ALP data were normalized against total cell number, as evaluated measuring LDH activity.

Bioprinting of MC-laden GelMA

Models of the constructs were obtained using Computer Aided Design (CAD) software (Rhinoceros, McNeel, Seattle, WA, USA). The CAD files were loaded in Computer Aided Manufacturing (CAM) software (PrimCAM, Einsiedeln, Switzerland), and printed with the Bioscaffolder system (SYS+ENG, Salzgitter-Bad, Germany), which has been described previously⁶³. GelMA-GG hydrogels loaded with MCs, tested for printability, and used as a bioink. While 50 mg mL^{-1} was the highest printable MC suspension, a concentration of 40 mg mL^{-1} MCs was chosen to maximize the amount of MCs and loaded cells, while simultaneously maintain a safety margin to prevent nozzle clogging by formation of MC-MSCs complexes during the pre-culture period. The optimal settings for printing were found to be an extrusion velocity of 2.40 (adimensional number) and a printing speed of 475 mm/min, at room temperature. The dispensing tip was a 20G conical nozzle. Distance between the hydrogel strands was set at 2.25 mm in the CAM model, while layer-to-layer spacing was set to 0.4 mm. Printed constructs were then UV cured for 5 minutes ($\lambda = 320\text{--}500 \text{ nm}$, intensity of 6 mWcm^2 at 365 nm, Superlite S-UV 2001AV lamp, Lumatec, Germany), and the immediately captured with an Olympus DP70 camera connected to a stereomicroscope. MC-MSCs complexes were introduced into the GelMA-GG hydrogels in order to assess the effect on cell viability and printability. MSCs were either pre-cultured on MCs under static conditions (12h) or in a spinner flask bioreactor for 5 days. For these assays, cylindrical, single-layered constructs were produced (diameter 16 mm, height 2.5 mm), using the settings described previously. To test cell viability, the constructs were cultured for 1 and 3 days in proliferation medium and then were analyzed using a LIVE/DEAD assay. To evaluate cell distribution in the printed constructs, cells were fluorescently stained for actin, and observed with a fluorescence microscope (Olympus BX51, Olympus, USA). In the samples, a total of $10 \cdot 10^6$ cells mL^{-1} was encapsulated, with or without 40 mg mL^{-1} of MCs.

Fabrication of bilayered osteochondral models

Cylindrical, bilayered constructs with anatomically relevant size (diameter 16 mm, height 5 + 5 mm) were fabricated, composed of two different bioinks. GelMA-GG encapsulating 40 mg mL^{-1} MCs was used to represent the bone compartment, while the cartilage layer was printed using the GelMA-GG without MCs. The optimal conditions to print the hydrogel without MCs were found to be an extrusion velocity of 3.80, a printing speed of 600 mm/min, and 34°C temperature.

Statistical analysis

Each experiment was performed in three or five replicates ($n=3$ or 5). Data are presented as mean and standard deviation of the replicates. Statistical significance was assessed performing Student's t-test using Origin 8.0 Software (OriginLab, USA).

RESULTS

Cell viability in MC-laden bioinks

Non-viscous suspensions of MSC-loaded microcarriers in PBS (30 mg mL^{-1}) were successfully dispensed without clogging of the syringe needle. After dispensing, 80% of the cells were viable 1 day and more than 90% after 3 days (Fig. 1a,b and e). MCs, cells and MC-MCS complexes suspended in GelMA-GG were homogeneously distributed in the gel matrix and showed good cell viability (Fig. 1c-g). Pre-seeded particles suspended in the gels had the lowest number of viable cells (60%) after 1 day of culture, which recovered to 90% after 3 days, indicating a high proliferation rate. Interestingly, MSCs that were separately mixed with MCs into GelMA-GG hydrogels, without a pre-seeding step, were found attached to the MCs surface. After 4h, in presence of GelMA, MSCs were found in an early stage of adhesion onto MCs, whereas they already expressed organized actin fibers if seeded directly on the MCs (Fig. 2a,b).

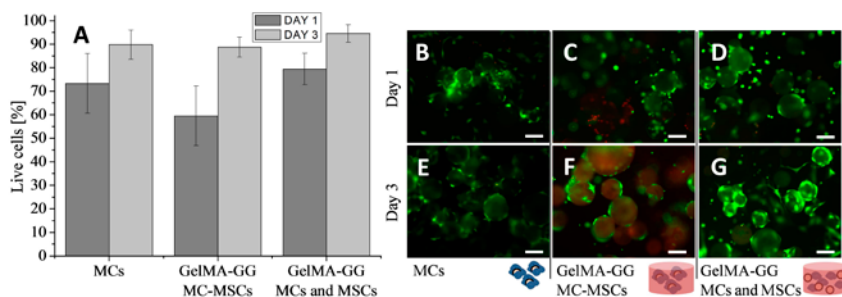


Figure 1. Viability and morphology of microcarriers (MCs) with MSCs after printing. (a) Viability of MSCs after dispensing; (b,e) Non-encapsulated cells cultured on MCs; (c,f) gels loaded with pre-cultured MC-MSC complexes and (d,g) with cells and MCs separately. Scale bar represents 50 μm.

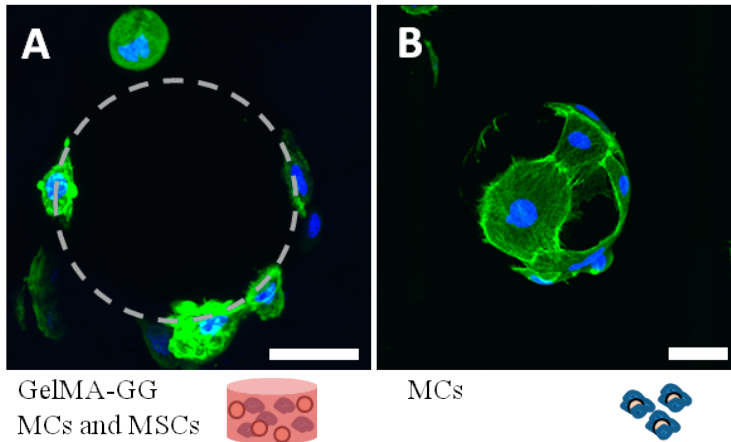


Figure 2. (a) Morphology of MSCs 4 hours after mixing with cell-free microcarriers in GelMA-GG (dashed circle indicates a MC) and (b) seeded directly on the MCs in absence of the gel. Scale bar is 40 μm . Cytoskeleton stained in green, nuclei in blue.

Mechanical properties of MC-laden GelMA

The incorporation of MCs into the GelMA-GG hydrogels resulted in an increment of the compressive modulus (Fig. 3). The stiff PLA MCs reinforced the softer hydrogel matrix, and the compression modulus increased along with the MC concentration. For the highest concentration tested, stiffness was 2-fold higher than for MC-free gels.

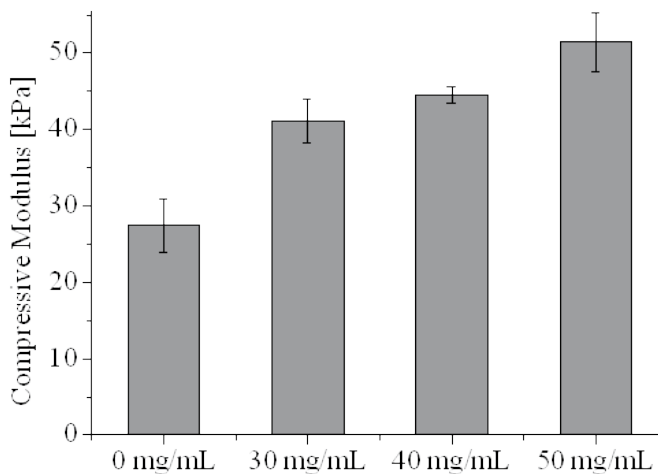


Figure 3. Compression modulus of GelMA-GG with different concentrations of MCs. The four samples show significantly different moduli ($p < 0.05$).

Osteogenic differentiation of MSCs

Cell number was monitored along the culture time (7, 14 and 21 days) using the LDH assay, and cell amounts were comparable between all the experimental groups, ranging between $2 \cdot 10^5$ and $2.5 \cdot 10^5$ cells/sample (data not shown). When MSCs were cultured in proliferation medium, no significant change in the expression of bone markers was observed during culture for all samples, suggesting the absence of spontaneous differentiation. In presence of osteogenic medium, ALP activity increased over time and was considerably higher for 2D monolayer cultures compared to 3D MC culture (Fig. 4a). However, MC-MSC complexes displayed enhanced OCN secretion, while histological analysis of both samples revealed the deposition of mineralized matrix, thus suggesting a consistent MSCs differentiation. MC culture also showed areas of alizarin red positive staining (Fig. 5), in case standard proliferation medium was used.

During long-term culture of hydrogel samples under osteogenic conditions, GelMA and GelMA-GG samples induced higher levels of active ALP, when compared to the gels with incorporated MCs (either pre-seeded with cells or not). On the other hand, encapsulated MC-MSC complexes secreted more OCN compared to the other experimental groups, indicating cell differentiation and a production of mature components of bone matrix. In all experimental samples cultured in osteogenic medium, MSCs deposited

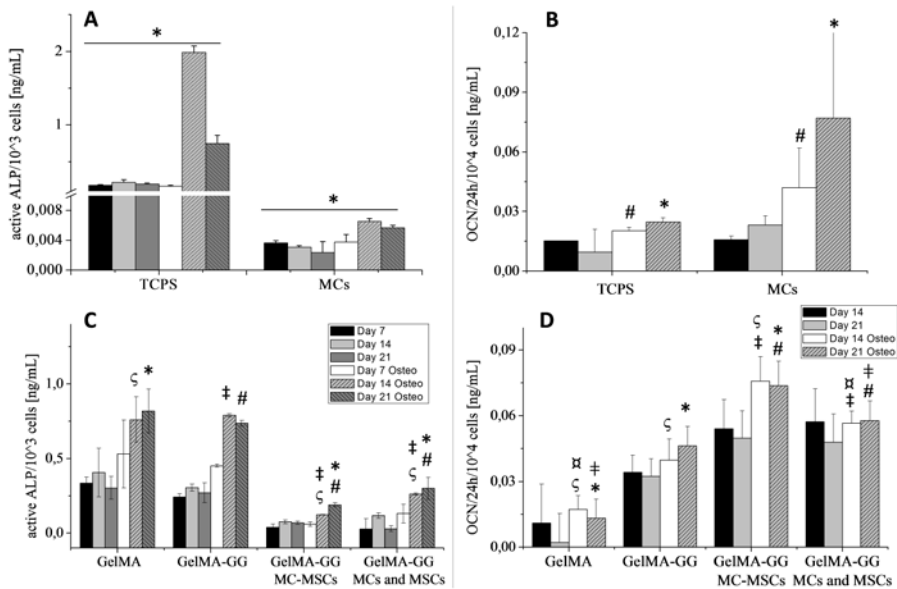


Figure 4. Osteogenic differentiation of MSCs in 2D culture (TCPS) compared to culture on MCs. (a) ALP and **(b)** OCN produced by MSCs in 2D culture and MCs. Quantification of **(c)** ALP and **(d)** OCN from GelMA-based hydrogels with or without MCs. The symbols group together samples that display statistically significant differences between them ($p < 0.05$).

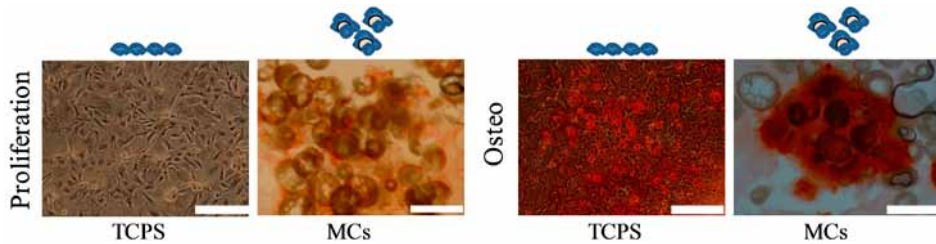


Figure 5. Alizarin red staining of monolayer cell cultures on TCPS and static MC culture after 21 days. Scale bar is 200 μm .

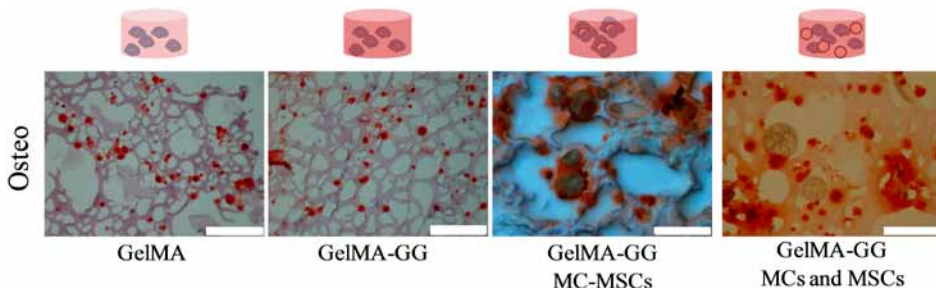


Figure 6. Alizarin red staining on hydrogel samples after 21 days of culture in osteogenic medium. Scale bar is 200 μm .

calcified matrix. However, both in GelMA and GelMA-GG samples, the mineralized ECM appeared as discrete and small alizarin red stained areas, more likely in the proximity of the cells suspended into the gel matrix (Fig. 6). Instead, GelMA-GG MC-MSCs samples displayed a diffuse staining surrounding the MCs.

Bioprinting of MC-MSC constructs

MC-MSC laden bioinks were printable, meaning that they formed strands upon extrusion able to retain their shape. Cell laden constructs were fabricated with a strand diameter of 715 ± 86 and pore width of 1006 ± 121 μm . MSCs and MC-MSC complexes displayed a high viability after the automated printing process, both following static seeding and dynamic MC culture (Fig. 7). MC-MSCs were cultured in a spinner flask, and excessive aggregation of the MCs was prevented. Viability values at day 1 and 3 after printing and photocrosslinking were comparable to those observed when MC-MSCs were dispensed manually. For all tested modalities, constructs were fabricated with homogeneous distribution of cells and MCs through the gel matrix, comparable geometry to the cell-free constructs (overall dimensions, strands orientation, struts and pore sizes), and a good fidelity to the original CAD design (Fig. 8).

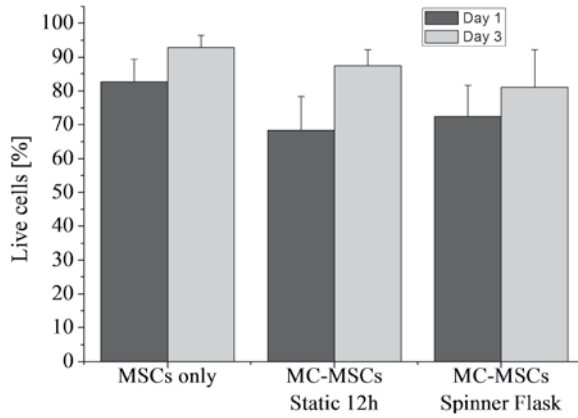


Figure 7. Viability of MSCs encapsulated in GelMA-GG hydrogels after printing.

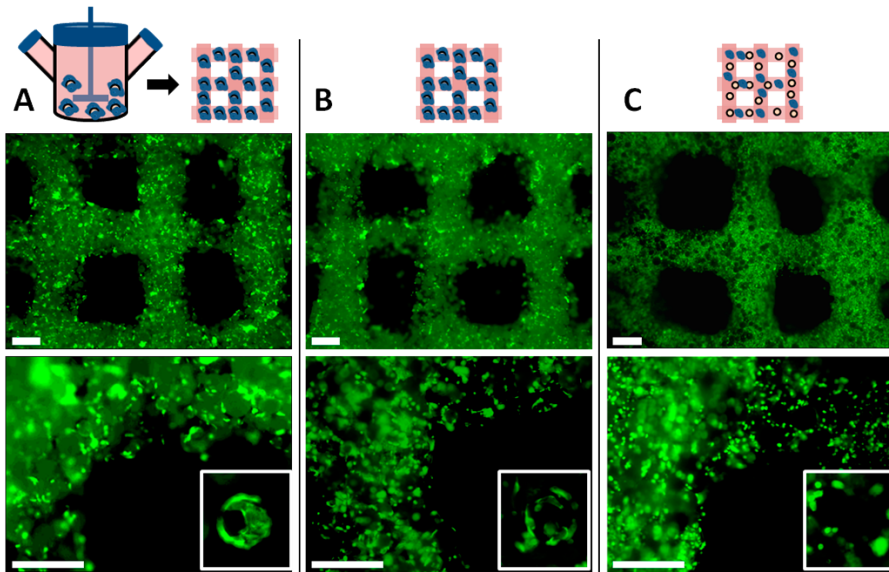


Figure 8. Immunofluorescence staining for actin cytoskeleton (green) on bioprinted GelMA-GG hydrogels with encapsulated cells and MCs. (a) MSCs were precultured on MCs either in a spinner flask bioreactor for 5 days; **(b)**, under static conditions for 12 h or **(c)** directly mixed together in the hydrogel solution without preculture. Lower panels and inserts show higher magnification of the constructs. Scale bar is 500 μm .

Printing of osteochondral models

Using the MC-based biofabrication approach, it was feasible to fabricate bilayered osteochondral graft model of clinically relevant size. The cartilage region was printed with GelMA-GG and the bone region was represented by GelMA-GG with encapsulated MCs. MC-laden gels flowed smoothly through the dispensing nozzle and strands retained their rounded shape better than the gel-only bioink, possibly due to the increased rigidity of the composite material. As a result, the constructs showed a strand diameter of $682 \pm 74 \mu\text{m}$ (with an average pore width of about $1226 \pm 83 \mu\text{m}$) for the MC-laden gel and $755 \pm 92 \mu\text{m}$ for the gel-only ink (with an average pore width of $1020 \pm 80 \mu\text{m}$). The two compartments were well aligned and no delamination was observed during the manipulation of the construct. There was a consistent axial porosity that can be observed in figure 9a and b. The MC-laden region showed a homogenous distribution of the PLA particles throughout the structure and appeared optically opaque (opposed to the translucent hydrogel-only section, Fig. 9a and 9c). As quite common with hydrogel printing, no significant lateral porosity was introduced into the construct, as the bioinks tend to lean on the underlying layer (Fig. 9d).

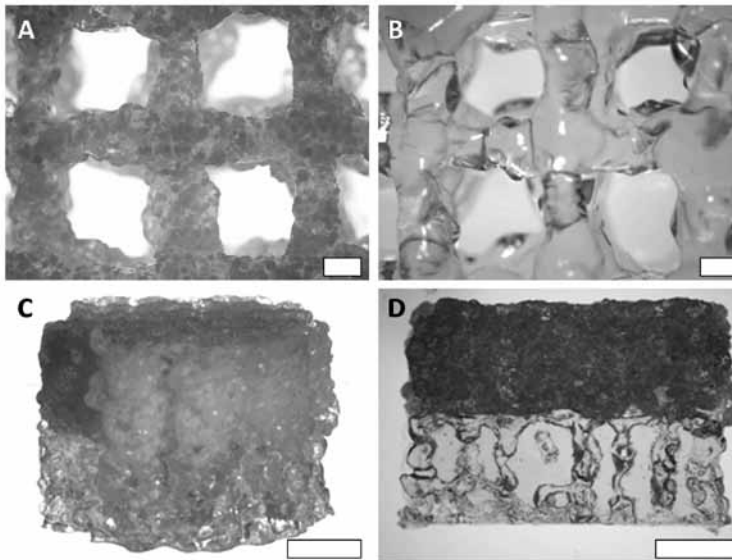


Figure 9. Bilayered GelMA-GG cylindrical osteochondral graft model (16 mm diameter, 1 cm height). (a) MC-laden layer top view, (b) GelMA-GG layer top view, (c) perspective, (d) cross-section. Scale bars are (a,b) $400 \mu\text{m}$ and (c,d) 4 mm.

DISCUSSION

In this study, living 3D structures containing MC-MSCs complexes were fabricated using bioprinting technology. MCs were found suitable substrates for cell adhesion and osteogenic differentiation and acted as reinforcing material to the hydrogel. Furthermore, high cells concentrations could be obtained by pre-culturing MSCs on MCs.

GelMA-GG was chosen as a bioink for bioprinting. Due to its shear-thinning behavior, it can be easily extruded into filaments, which then maintain their shape once deposited on the printing substrate, thus allowing the generation of 3D printed structures with good shape fidelity^{61,190}. Finally, the obtained scaffolds can be irreversibly crosslinked after mild UV-exposure. We found this procedure had little impact on cell viability, which is in line with previous research^{195,333,416}. It should be noted that human MSCs may show different survival rates compared to rat MSCs in response to mechanical stresses and UV radiation, although previous work reported reassuring results regarding MSCs differentiation (hence survival) after UV-encapsulation in collagenous hydrogels⁴¹⁷.

Another issue regarding the current crosslinking set-up, is that constructs were UV cured after the printing process, may limit the size of the constructs, since UV may not penetrate deeply into larger grafts. However, this can be solved by inducing photocross-linking during the printing process. Such technology has been recently described by Cui et al., and could be adapted to our system by a hardware modification⁹⁹.

In this work, cells and MCs were either suspended as precultured MC-MSCs complexes or mixed separately into the hydrogel. The first approach is preferable, since such aggregates have been shown to promote cell viability, biomolecules synthesis and differentiation⁴¹¹, due to the establishment of cell-cell contacts and actin cytoskeleton reorganization⁴¹⁸. However, since large aggregates can easily clog the injection nozzle, expansion periods under static culture should be limited. As an interesting alternative, MCs and MSCs can be separately mixed, without preculture steps. The current work showed that such suspensions can easily be dispensed, and once suspended in the bioink, cells were able to migrate through the hydrogel matrix to adhere, spread and proliferate on the MC surface. Although it could be possible to use this approach to tune MSCs adhesion and response, the amount of cells that could be loaded into the gel would be limited by standard 2D proliferation protocols. Therefore, 3D-expansion methods are required. To retain a printable bioink, cells should be expanded on individual MCs or small aggregates, a condition that can be achieved in a stirring bioreactor, as also shown in this study.

Composite bioinks were thus created, in which MCs, made of a mechanically stiff polymer, were dispersed in the softer hydrogel matrix. It is known that hydrogel stiffness can be improved increasing the polymer concentration or the crosslinking degree (UV exposure, temperature)⁶⁰. A high crosslink density however is less desirable, as it can hamper the migration of encapsulated cells and their ability to homogeneously colonize the

hydrogel with newly synthesized extracellular matrix⁷⁹. Instead, incorporation of MCs does not alter the nature of the hydrogel network, and construct stiffness was shown to increase along with the concentration of MCs. However, it should be considered that stress at failure may be reduced, although this was not evident in our mechanical assay. MC reinforcement of hydrogels does not lead to compressive moduli similar to hard tissues. When hydrogel-based constructs are implanted in load-bearing locations, external fixation will be required to reduce weight on the implant. Another strategy that can be implemented to improve the mechanical properties of hydrogel constructs, is co-printing of a supportive thermoplastic polymer network^{60,255}. Still, in all regenerative approaches, the final mechanical properties should be provided by the neo-tissue that is secreted by the embedded cells⁴¹⁹.

To further enhance the hydrogel compression modulus and match the stiffness of hard tissues, it may be feasible to encapsulate particles made of different materials (e.g. calcium phosphates)⁴²⁰, provided that they do not sediment over the time scale of the printing process and their size allows the extrusion of the bioink. However, an advantage of MCs encapsulation is to use them as devices to efficiently expand MSCs and then print MC-MSCs aggregates with improved biological behavior and bone forming potential⁴⁰⁸. For this reason, MCs with a highly porous core made from low density materials and suitable for spinner flask culture were chosen⁸².

The potential to improve the osteogenic differentiation of MSCs by encapsulating them with MCs into GelMA hydrogels was studied *in vitro*. All the samples cultured with differentiation medium displayed calcified matrix deposition, and MSC commitment towards osteogenic lineage, thus supporting the suitability to use GelMA-based gels for bone bioprinting. Alizarin red staining, which appeared as discrete spots surrounding cells without MCs, intensely marked diffused areas around MC-MSCs complexes. This indicates strongly mineralized regions, probably due to the fact that local cell density is higher on cell-colonized MCs, a factor affecting cell behavior and differentiation⁴⁰⁸. At a molecular level, MC-laden samples showed markedly reduced ALP activity compared to their respective controls. This was accompanied by a higher secretion of OCN, which is a late marker for maturation of osteoblasts, and key component of bone extracellular matrix⁴²¹. MC-MSCs gels gave the best results regarding the secretion of OCN, and at the same time induced matrix calcification, suggesting that they are able to form a mature bone-like tissue. This discrepancy of ALP levels *in vitro* and bone-forming capacity of MSCs was recently described by Goh et al. who compared the bone forming potential of human fetal MSCs cultured as monolayers with Cytodex 3 MCs. Despite a 45-fold reduction in ALP activity on MCs, MSCs cultured on MCs and MC-MSCs complexes induced better and more consistent bone formation *in vitro* and *in vivo* (in a rodent model), indicating that MC culture can improve the potential of MSCs in bone tissue engineering⁴²².

Eventually, it is worthwhile to underline that the addition of gellan gum to the bioink formulation did not have a relevant effect on osteogenic differentiation of MSCs. Gellan gum, may thus be safely mixed with GelMA for printing of bone tissue in order to increase the solution viscosity and improve the printability of the bioink⁶¹. The results of the differentiation assay also suggest that it is not advisable to use solely MSCs in GelMA-based hydrogels for the cartilage region, since they can easily differentiate towards osteoblastic lineage. For this reason, it would be preferable to use chondrocytes, which have shown capable of chondrogenic differentiation in GelMA *in vitro* and *in vivo*^{63,255}. MSCs can play an important role in maintaining chondrocyte phenotype in co-cultures^{381,423,424}, although the mechanism underlying this crosstalk is not fully understood, and cases of downregulation of chondrocytes differentiation have also been reported⁴²⁵. However, co-cultures of MSCs and chondrocytes in hydrogel systems have been reported, suggesting the beneficial effect of the combination of such cell types in generating bone and cartilage tissues. For instance, Mo et al. demonstrated that MSCs and chondrocytes each encapsulated in different compartment of an alginate matrix, interacted, possibly due to trophic factors secretion, determining an enhancement of GAGs secretion by chondrocytes and an initiation of osteogenesis of MSCs, which induced osteocalcin production⁴²⁶. These effects were found to be dependent on the MSC/chondrocyte ratio⁴²⁶.

Proven that MC-laden GelMA-GG can be a matrix for bone tissue engineering, the material was used as a bioink to construct model of an osteochondral graft. Recently, calcium phosphate particles (size 100-212 μm) have been introduced at low concentrations (up to 15 mg mL^{-1}) into alginate bioinks to promote bone regeneration¹⁴⁸. Poldervaart *et al.* also printed gelatin microparticles for controlled release of Bone Morphogenic Protein-2⁴²⁷. Both cases showed promising results in terms of *in vivo* osteoinduction, however low amounts of particles were encapsulated. We found that the addition of high concentrations of MCs to GelMA-GG hydrogels did not reduce the printability of the ink, nor did it affect the size of the extruded strands and the porosity. Living constructs were obtained by adding MC-MSCs to the bioink mixture, either after a short period of static culture (12h) or longer culture (5 days) in a spinner flask bioreactor. Both approaches generated viable MC-MSCs complexes, but the latter has a clear advantage, as dynamic culture allows cell proliferation while preventing formation of large, difficult to extrude, aggregates. Furthermore, spinner flask culture has the great potential to combine 3D printing with a well-established cell expansion technology. To date, bioprinting of cell aggregates was prevalently performed by producing tissue spheroids and using them as bioink components⁴²⁸. Despite of the interesting biological performance, spheroid generation methods are still time consuming and not suitable for mass production, thus limiting the size of printable tissues⁴²⁸. Conversely, microcarrier culture is a simple, industrially scalable technology to achieve large cell numbers, with precise control over

cell culture conditions⁴²⁹. MSCs aggregates have been demonstrated to improve cell proliferation, survival and multilineage differentiation, especially when the endogenous ECM produced in the aggregates is preserved⁴³⁰. Such matrix preservation is a characteristic of MC-MSCs complexes⁴⁰⁵ which are profitable to induce cell differentiation and build tissue engineered constructs⁴³¹. Additionally, to further exploit the advantage of 3D cell-cell connections, MCs with an open porous structure could be used, so that cells can colonize the inside of the carrier and display a 3D organization in it⁴⁰³. MC culture opens promising possibilities when combined with bioprinting technologies.

In tissue constructs fabricated from all MC-bioinks (short-term static culture, dynamic culture, and without preseeding), the complexes or the free cells and particles were homogeneously distributed in the printed graft with shape fidelity comparable to that of the cell-free constructs, thus proving the printability of MC-MSCs complexes. Under these conditions, zonal constructs composed of MC-laden and MC-free layers of gels with clinically relevant size were obtained. The size of the strand was not significantly affected by the presence of the MCs, thus allowing a good stacking and alignment of the two compartments, which generated a consistent and well-aligned axial porosity all through the construct. The high viability of MSCs, and the results of the multimaterial printing process demonstrates the feasibility of a combined MC culture-bioprinting strategy to generate large, living constructs, with potential applications in osteochondral tissue engineering and as 3D tissue models.

CONCLUSIONS AND FUTURE PERSPECTIVES

MC-laden GelMA-based bioink was shown to be a promising composite material for bioprinting. PLA MCs acted as a mechanical reinforcement to the soft GelMA matrix, without compromising the printability of GelMA bioinks. Additionally, encapsulation of MC-MSCs complexes - with improved cell adhesion and cell-cell contacts - supported bone matrix deposition, and hence is of great interest for the engineering of bone tissue. Finally, MC-MSC-rich living construct where obtained using bioprinting combined with microcarrier dynamic expansion. These are key findings to build advanced constructs for bone and cartilage tissue engineering. Furthermore, the printability of bioinks with high MC concentrations opens possibilities for the fabrication of biomedical screening models. Drug-encapsulating MCs could be used, adding an additional level of complexity in the bioprinting of living tissues. Co-delivery of cells and growth factors with control over the spatial and temporal distributions would be possible, and constitutes another promising trend that can be explored in the area of biofabrication.

ACKNOWLEDGMENTS

RL acknowledges the Spanish Ministry of Education, Culture and Sport (MECD) for its financial support through the FPU programme (grant reference AP2010-4827). JV was supported by a grant from the Dutch government to the Netherlands Institute for Regenerative Medicine (NIRM, grant n°FES0908) and JM was supported by the Dutch Arthritis Foundation.

Chapter 10

Preliminary results of a translational animal model

Biofabrication of Anatomically Shaped Implants for Regeneration of the Rabbit Humeral Head

Jetze Visser
Roel J.H. Custers
Paul D. Dalton
Razmara Nizak
Daniël B.F. Saris
Debby Gawlitta
Jos Malda

The results of the in vivo section of this study in rabbits are awaited before this manuscript will be submitted for publication.

ABSTRACT

In the present thesis, the state of the art of cartilage regeneration, biofabrication techniques for orthopaedic applications and mechanical reinforcement of hydrogels were explored. In this Chapter, these facets culminate to enter the next level in the form of a functional reconstruction of complex anatomical structures such as a shoulder joint. We aimed to biofabricate a customized, biphasic implant for the restoration of the humeral head. The implant was based on a CT-scan of a rabbit front leg identifying the bony and cartilaginous compartments. The bone component was printed from poly- ϵ -caprolactone (PCL) with fused deposition modelling (porosity 74%) and was coated with calcium phosphates. The cartilage component consisted of a gelatin-based hydrogel that was reinforced with organized PCL microfibers (porosity 92%) printed with melt electrospinning writing. Both components were manually fused prior to hydrogel infusion. Three variations of the cartilage compartment will be compared, *i.e.* fiber reinforced GelMA containing 1) expanded rabbit chondrocytes or 2) TGF- β and 3) a cell- and growth factor free control group. The complex biphasic scaffolds matched the anatomical dimensions of the rabbit humerus and were successfully implanted in cadaveric rabbits. The implants remained intact after abduction/adduction cycles of the rabbit shoulder. Chondrogenesis of expanded rabbit chondrocytes in GelMA was confirmed *in vitro*. A pilot study in three rabbits is ongoing to preliminarily assess construct behaviour in the three groups, and to monitor the rehabilitation of the animals. Thereafter, the scaffolds will be implanted in 18 rabbits ($n=6$) to study bone and cartilage regeneration and implant shape conservation. This approach for the regeneration of both cartilage and bone tissue in a customized implant potentially offers a biological solution for the replacement of (partially) degenerated joints.

INTRODUCTION

Tissue degeneration in articular joints can result from osteoarthritic processes, or can comprise osteochondral defects caused by trauma and/or genetic factors^{32,33}. The standard therapy for joint degeneration is replacement of the diseased tissue with a prosthesis^{7,18}. Regenerative medicine, however, seeks for solutions that regenerate degenerated tissue, rather than to replace it¹. In orthopedics, this strategy has been applied for the repair of focal articular cartilage defects⁶. Autologous chondrocyte implantation (ACI) is the most common of these regenerative treatments^{36,9}. Nevertheless, these therapies do not address the underlying bone and have an upper size limit for the defect to be repaired^{6,9}. Regenerative medicine thus has no solution yet for the regeneration of completely or partially degenerated joints.

A biphasic implant of a complex shape is likely required for the repair of large osteochondral joint defects, with specific biological and mechanical cues⁴³². In this context, numerous biphasic scaffolds were engineered in simple cylindrical shapes, with distinct matrix, cells and/or growth factor compositions for the cartilage and bone components^{35,36}. A few of these implants have found their way to clinical application, however, they do not address the complex architecture of large joint defects.

Additive manufacturing is a powerful approach to design and produce organized implants, and often use a fused deposition modeling (FDM) process to fabricate scaffolds¹¹. The most appealing approach so far of FDM and tissue repair with an large osteochondral implant was presented by Lee *et al*⁵³. In their study, the proximal humerus of rabbits was replaced with a porous implant from poly- ϵ -caprolactone (PCL) and hydroxyapatite, combined with transforming growth factor(TGF)- β_3 in a collagenous carrier in the cartilage layer. The articular surface of the shoulder was successfully regenerated through the activity of endogenous cells that were attracted or differentiated by the introduced growth factor. However, bone regeneration was not studied, and the biphasic nature of the scaffold was limited in terms of biological and mechanical properties.

Recent advancements in additive manufacturing in our group allow for the production of complex structures from PCL (Chapter 8)¹⁹⁰. Combined with cells and growth factors^{11,12}, in a process termed "biofabrication", such scaffolds can provide the sufficient morphological, mechanical and chemical cues to promote regeneration. PCL has been demonstrated a successful scaffold material for the regeneration of bone defects⁵⁰⁻⁵³, especially when the polymer material was coated with ceramics to improve bone conduction^{433,434}.

Organized scaffolds with thinner fibers that reinforce hydrogel structures are more suitable to produce the elastic cartilage component, when used as a reinforcement to hydrogels, as demonstrated in Chapter 6⁵⁴. The reinforcement of hydrogels with micro-fibers, which were produced by a melt electrospinning writing (MEW) process, resulted

in composite constructs with stiffnesses resembling those of native articular cartilage⁴³⁵. In these composites, cartilage matrix could be produced by chondrocytes *in vitro*, when cultured within reinforced gelatin methacrylamide / hyaluronic acid (GelMA/HA) hydrogels. The addition of a small amount of HA to GelMA is favorable for the chondrogenesis of embedded MSCs^{60,63,73}, hence this hydrogel composition was adopted in the current work.

This research project aims for the biofabrication of a biodegradable implant with a customized shape for the regeneration of the rabbit shoulder. Potentially, a combination of the thick, rigid PCL fibers and the microfibrinous hydrogel composite containing a clinically relevant cell composition results in a biphasic implant for the regeneration of bone and cartilage tissue. Such an implant could make the step from cell therapy for focal cartilage defects to the regeneration of partial or complete joint defects.

MATERIALS AND METHODS

Design of the implants

A humerus (upper arm) was harvested from a cadaveric New-Zealand White (NZW) rabbit and subsequently scanned with a Micro-CT (Voxel size 120 μm ; Quantum FX- Perkin Elmer). An osteochondral implant was designed using CAD-software, based on the shape of the humeral head. The cartilage component was separately segmented from the CT-scan and a stem was designed to press-fit the prosthesis in the humeral shaft. A sacrificial support structure was added in the design to facilitate the realization of the complex overhanging shapes during the printing process. The data set was then translated into standard tessellation language (.stl) for 3D printing.

Fabrication and coating of the bone component

The bone component of the implant was 3D-printed from PCL (Sigma-Aldrich; Mn 45.000) with the BioScaffolder (SYS+ENG, Salzgitter-Bad, Germany). Fibers with a diameter of 160 μm were deposited in a 0-90° orientation with 750 μm spacing. Polyvinyl alcohol (PVA) was printed as a temporary support structure along with the PCL to create the dome-shaped humeral head. After printing, the PVA was washed away in dH₂O on a rollerbank overnight at 37 °C. The implant was etched with 70% ethanol (1 h) and 5M NaOH (4 h), followed by coating with a five times concentrated simulated body fluid solution (NaCl (40 g), CaCl₂·2H₂O (1.84 g), MgCl₂·6H₂O (1.52 g), NaHCO₃ (1.72 g), and Na₂-HPO₄·2H₂O (0.9 g) salts in 1 L of dH₂O) for 24 hours at 37 °C under continuous gentle stirring. Following this coating step, the samples were immersed in a calcium phosphate solution (NaCl (8 g), CaCl₂·2H₂O (0.59 g), Na₂HPO₄·H₂O (0.36 g), and Tris (6.05 g) in 1 L dH₂O, pH 7.4) at 37

°C for 24 h on a roller plate. The coating procedure was based on a combination of two protocols^{433,434}. The coated samples were washed three times in dH₂O.

Fabrication of the cartilage component

The microfibers for the implant were fabricated from PCL (PURAC, Zwijndrecht, the Netherlands) using a custom-built melt electrospinning machine as previously described. The MEW fibers with a diameter of 14 µm were stacked with a spacing of 200 µm, with the overall scaffold dimensions of 60x60x0.4 mm (lxwxh). A defined pattern to cover the bone component was cut from the MEW scaffold and melted onto the coated bone component of the implant with a hot spatula. The cartilage component was infused with GelMA/HA hydrogel (stained with fast green for visualization purposes only in Fig. 1f). The gel was allowed to air-dry and was subsequently crosslinked for 70 seconds with a focused UV source with an intensity of 180 mW/cm² (350-450 nm, Höhle UV technology, Munich, Germany).

Preparation of GelMA/HA hydrogel

GelMA was synthesized by reaction of porcine type A gelatin (Sigma-Aldrich, St. Louis, Missouri, USA) with methacrylic anhydride at 50 °C for one hour as previously described⁶³. GelMA was dissolved in Phosphate Buffered Saline (PBS) at 60 °C at a concentration of 9.5% (w/v). Methacrylated hyaluronic acid in a concentration of 0.5% (w/v) was added to the GelMA solution to promote redifferentiation of embedded chondrocytes^{60,63,73}.

Measurement of the stiffness of the cartilage and bone component

Scaffolds representing the bone (FDM; thick fibers) and the cartilage (MEW; thin fibers) component with dimensions of 6 mm diameter and 2 mm height were punched from larger sheets for mechanical tests. The microfiber scaffolds for the cartilage components of the implant (stack of 5 to reach 2 mm height) were infused with GelMA hydrogel (at circa 37 °C) in a custom-made Teflon mold. After thermal gelation of the hydrogel (15 minutes), the samples were UV-crosslinked for 70 seconds on both sides with the focused UV source. Samples (n=5 per group) were subjected to single uniaxial unconfined compression in air at room temperature, after 1 hour of submersion in PBS from their preparation. Over a period of two minutes, a force ramp (axial strain rate ca. 10%/min) was applied to the samples employing a Dynamic Mechanical Analyser (DMA 2980, TA Instruments, New Castle, DE, USA). The stiffness was calculated from the linear derivative of the stress/strain curve between 3-10% strain.

Harvest and culture of rabbit chondrocytes for confirmation of chondrogenesis in GelMA/HA gels

Macroscopically healthy full-thickness cartilage was harvested under sterile conditions from the shoulder, hip and knee joints of fresh NZW rabbit cadavers (n=3, weight 4-5 kg). After fragmentation and overnight digestion in type II collagenase (Worthington Biochemical Corp) at 37°C, the suspension was filtered through a 100 µm cell strainer, washed in PBS and stored in liquid nitrogen at -196°C in culture medium (Dulbecco's Modified Eagle Medium (DMEM) 41965, Invitrogen) supplemented with 20% heat-inactivated fetal bovine serum (FBS, Biowhittaker) and 10% dimethylsulfoxide (DMSO (Merck, Darmstadt, Germany)). Upon thawing, the chondrocytes were seeded at a density of 5×10^3 cells/cm² and expanded for 10-12 days in a monolayer culture in chondrocyte expansion medium consisting of DMEM, 10% FBS, 100 units/ml penicillin and 100 µg/ml streptomycin (Invitrogen), and 10 ng/ml FGF-2 (R&D Systems) and embedded in GelMA/HA at passage 2 at a concentration of 20 million cells per mL gel.

The gel with cells was infused in a mold for samples with a diameter of 6 mm and height of 2 mm. The samples were UV-crosslinked for 70 seconds on both sides with the focused UV source. The samples (n=3) were cultured for four weeks *in vitro* in chondrogenic differentiation medium (DMEM (41965, Invitrogen), supplemented with 0.2 mM L-ascorbic acid 2-phosphate, 0.5% human serum albumin (SeraCare Life Sciences), 1x ITS-X (Invitrogen), 100 units/ml penicillin and 100 µg/ml streptomycin, 25 mM 4-(2-hydroxyethyl)-1-piperazineethanesulfonic acid (HEPES) (Invitrogen) and 5 ng/ml TGF-β2). Samples at day 1 of culture were taken as a control for the histology analysis. For the implantation of the cell-laden scaffold in rabbits, the rabbit chondrocytes will be infused in GelMA/HA into the cartilage component of the implant and UV-crosslinked for 70 seconds.

Histology and immunohistochemistry

The samples were processed for histology and immunohistochemistry by dehydration through a graded ethanol series, cleared in xylene and embedded in paraffin. The samples were sectioned into 5 µm slices and a triple stain of hematoxylin, fast green, and Safranin-O (all from Sigma) was applied to identify the presence of GAGs.

Collagen type II was stained by immunohistochemistry after deparaffinization and rehydration of the sections. The sections were blocked in 5% bovine serum albumin and 0.3% H₂O₂ following antigen retrieval. Antigen retrieval for collagen type II was performed by incubation with 1 mg/mL pronase (Sigma) and 10 mg/mL hyaluronidase (Sigma) at 37 degrees for half an hour each. Next, sections were incubated with the primary antibody for collagen type II (1:100, monoclonal mouse, II-II6B3, DSHB) at 4°C overnight, followed by incubation with GAM-HRP (1:200, Po447, Dako) at room temperature for an hour. Collagen type II was detected by a 10-minute conversion of 3,3'-diaminobenzidine solu-

tion (Sigma). Nuclei were counterstained with 50% Mayer's hematoxylin. The stained sections were examined using a light microscope (Olympus BX51).

Cadaver study

The prosthesis was implanted in the humerus of a cadaveric rabbit to establish the feasibility of the surgical procedure, to optimize the fit of the implant and to test its strength *in situ*. The shoulder joint was surgically opened through a craniolateral approach, according to a previously published protocol⁵³. In short, the acromial head of the deltoid muscle and the infraspinatus muscle were tenotomized at the insertion and retracted. The lateral joint capsule was opened to expose the humeral head by internal rotation and complete lateral luxation. Then the humeral head was excised through the metaphysis with an oscillating saw, preserving the greater and lesser tubercles and soft tissue attachments. An intramedullary tunnel was created with a hand-operated drill (diameter 6 mm). The scaffold was implanted, the deltoid and infraspinatus tendons were reattached and the wound was closed in layers. The shoulder was subjected to 50 abduction/adduction cycles under manual compression, to test the strength and fixation of the implant.

Outline of osteochondral tissue regeneration study in rabbits

Three experimental groups were designed for this study (Table 1). The bone component was similar in all groups, consisting of thick PCL fibers coated with calcium phosphates. The cartilage component consists of GelMA/HA reinforced with PCL microfibers, the gel containing: 1) expanded rabbit chondrocytes, 2) TGF- β 2 or 3) no additives. A pilot study is ongoing in three rabbits, in which one scaffold of each experimental group was implanted in the left shoulder of 26-months-old female NZW rabbits. The aim of the pilot study is to test scaffold strength and clinical recovery of the animals. The mobility

Group	Bone component	Cartilage component
1	Coated PCL scaffold	Reinforced GelMA/HA with <i>Expanded rabbit chondrocytes</i>
2	Coated PCL scaffold	Reinforced GelMA/HA with <i>Transforming Growth Factor β2</i>
3	Coated PCL scaffold	Reinforced GelMA/HA

Table 1. Experimental groups for study of osteochondral tissue restoration in the humeral head of rabbits. A pilot study is ongoing in 3 rabbits, including one construct of each group. A comparative study is scheduled for 18 rabbits ($n=6$ per group).

of the rabbits is monitored weekly. The animals will be euthanized after four weeks and the location and structure of the implant will be analyzed macroscopically and on cross-sections in the laboratory.

If the pilot study confirms feasibility of the current shoulder regeneration model in rabbits, the scaffolds will be implanted in 18 rabbits ($n=6$ per group), with a follow-up of 16 weeks, to study the regeneration of bone and cartilage. Fluorochromes will be administered at week 5 and 11 to monitor bone formation²⁹⁶. Additionally, a micro-CT scan will be made of the explanted shoulder joint and bone and cartilage formation is assessed biochemically, histologically and immunohistochemically.

RESULTS

Development and characteristics of the biofabricated implant

Cartilage and bone tissue were segmented from a CT-scan of the proximal humerus of a cadaveric rabbit (Fig. 1a,b). A construct with a porosity of 72% (28% PCL volume) was fabricated as the bone component of the implant, using PVA as a temporary support material (Fig. 1c,d). The cartilage component was fabricated from microfibers with a porosity of 92% (8% PCL volume), which was successfully molten onto the implant (Fig. 1e). Next, GelMA/HA hydrogel (ca. 100 μ l) was infused and crosslinked in the microfiber scaffold compartment (Fig. 1f). The microfiber scaffold absorbed the hydrogel and limited leakage to the bone component was observed (Fig. 1g).

The FDM fiber scaffolds had a stiffness of 18 ± 5 MPa; the stiffness of GelMA reinforced with MEW microfibers was 2.3 ± 0.4 MPa. The parameters of both components are summarized in Table 2.

	<i>Thick-fiber PCL scaffold</i>	<i>GelMA/HA reinforced with PCL microfibers</i>
Component in implant	bone	cartilage
Fabrication technique	Fused deposition modeling	Melt electrospinning writing
Filament thickness	160 μ m	14 μ m
Filament spacing	750 μ m	200 μ m
PCL volume fraction	26%	8%
Stiffness	18 ± 5 MPa	2.3 ± 0.4 MPa

Table 2 Properties of the bone and the cartilage component of the biofabricated implant.

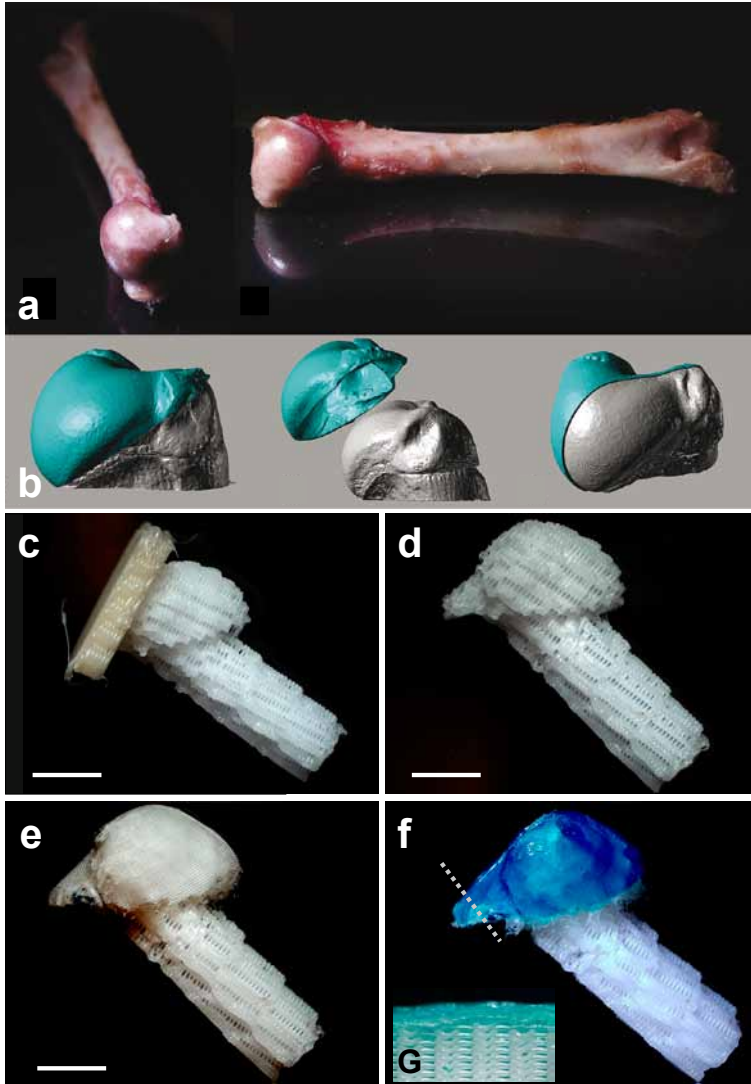


Figure 1. Biofabrication of a biphasic joint implant to replace the proximal humerus of a rabbit. (a) The humerus of a New-Zealand White rabbit; (b) The humerus from a) was scanned with micro-CT and the cartilage (green) and bone (grey) components were separately segmented; (c) the bone component was printed from poly- ϵ -caprolactone, with a temporary support structure of polyvinyl alcohol (yellow); (d) the support structure was dissolved in water and, (e) a microfiber scaffold was fused onto the humeral head; (f) GelMA (blue/green) was infused and UV-crosslinked in the microfiber scaffold, which (g) did not leak into the bone component (cross-section of the interface of both compartments). Scale bars represent 5 mm.

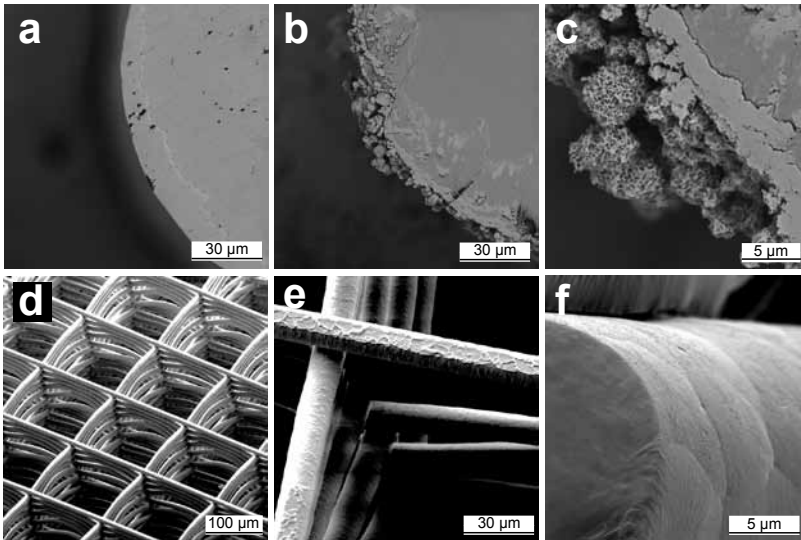


Figure 2. SEM imaging of scaffolds for the bone and the cartilage components of the implant. The bone component was from printed fibers (diameter 160 μm), of which cross-sections are shown (a) before coating and (b,c) after coating with calcium phosphates. (d,e) The scaffold for the cartilage component of the implant was fabricated from melt electrospun microfibers (diameter 14 μm) in a 0-90° orientation; (f) cross-section of a single PCL microfiber.

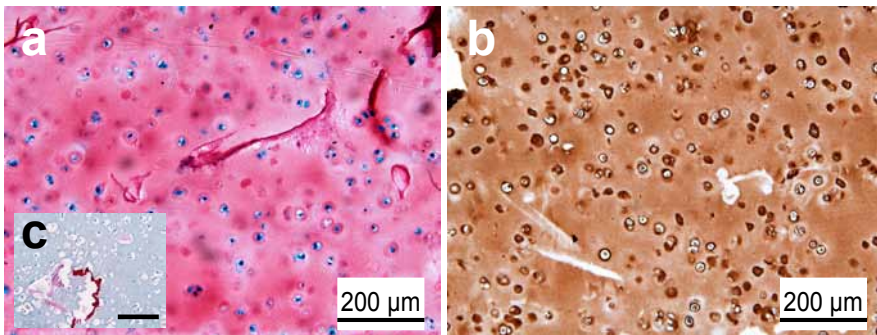


Figure 3. *In vitro* differentiation of rabbit chondrocytes in GelMA/HA hydrogel. Rabbit chondrocytes produced an interconnected cartilage matrix consisting of (a) glycosaminoglycans (safranin-O staining) and (b) collagen type II (brown), within the GelMA/HA hydrogel; (c) safranin-O staining of the sample at day 1 illustrates the basic level of GAG staining by the HA incorporation in the GelMA gel (scale bar represents 30 μm).

The fibers of the bone component initially had a smooth surface, as objectified with SEM scanning (Fig. 2a). The subsequent coating protocol resulted in sedimentation of calcium phosphate structures (Fig 2b,c). SEM scanning of the microfiber scaffold showed

a 0-90° orientation of the fibers (Fig. 2d-f). Next to the vertical pores, there was a horizontal porosity, formed by the space between the stacked fibers.

***In vitro* culture of rabbit chondrocytes in GelMA/HA**

Rabbit chondrocytes produced an interconnected cartilage matrix within the reinforced GelMA/HA hydrogel scaffold discs. Glycosaminoglycans (Fig. 3a) and collagen type II (Fig. 3b) were well distributed throughout the construct. As a control, minimal Safranin-O staining caused by the HA component in the hydrogel was observed in the sample taken at day 1 of the culture (Fig. 3c).

Implantation in cadaveric rabbits

First, upon implantation of the scaffolds in explanted humeri, the anatomical shape of the head was considered to be re-established by the implant (Fig. 4a,b). Second, the surgery on cadaveric rabbits could be performed in a reproducible manner. Removal of the humeral head through the metaphysis resulted in an angle of circa 40° between the sawed plane and the shaft of the humerus (Fig. 4c). The same angle was, therefore, designed in the implant. The internal diameter of the shaft and the stem of the implant

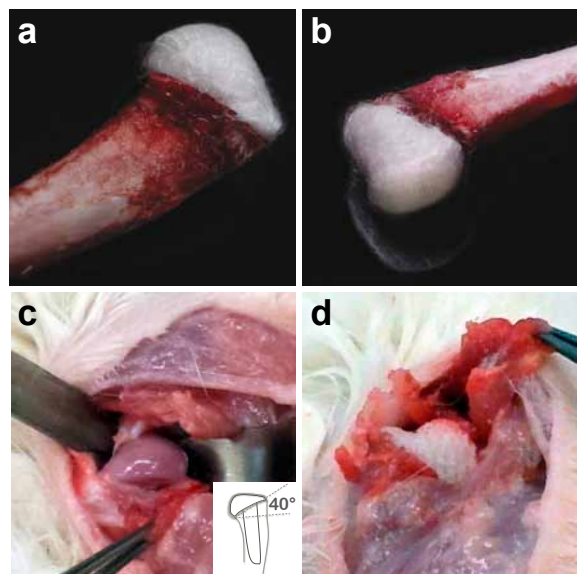


Figure 4. Cadaveric implantation of the biofabricated scaffold into the rabbit shoulder. (a,b) The anatomical shape of the humeral head was followed by the implant; (c,d) scaffolds (here only bone component) were implanted in cadaveric rabbits. The angle between the humeral head and the shaft of the humerus was 40 degrees (dashed line) in both the implant and the saw plane. The implant was press-fit into the humerus and did not dislocate or break after 50 abduction-adduction cycles of the cadaveric rabbit shoulder.

were circa 6 mm. Therefore, after removal of the proximal bone marrow with a 6 mm drill, there was a tight fit of the implant in the humerus (Fig. 4d). The implant was still macroscopically intact after 50 abduction/adduction cycles of the shoulder. The implantation of the biofabricated scaffolds into the shoulder of NZW rabbits was thus a feasible procedure.

DISCUSSION

Anatomically shaped, biphasic scaffolds were fabricated for the restoration of the humeral head in the rabbit shoulder. The complex design of the implant was based on a CT-scan of the proximal humerus, so that the cartilage and bone components matched the anatomical dimensions. The bone component consisted of PCL fibers with a porosity of 74%, which were coated with calcium phosphate. The cartilage component consisted of GelMA/HA hydrogel reinforced with PCL microfibers (92% porosity).

The biofabrication techniques FDM and MEW were combined for producing the biphasic implant. The bone component relied on a rigid FDM scaffold, which was previously shown to guide bone formation when ceramics were included or coated⁵¹⁻⁵³. The cartilage component separately was previously shown to support the formation of a cartilage matrix *in vitro*^{60,63,73,435}, which was reproduced here for rabbit chondrocytes. The two components were thermally fused by hand. A future biofabrication setup should allow for a single procedure, by direct MEW upon the FDM scaffold, in order to further customize the architecture of the implant²⁰⁵.

The current implant adds to the previously presented models that it consists of two components for bone and cartilage regeneration with distinct mechanical and biological properties^{53,436}. The difference between both components in the study by Lee *et al.* was only the administration of TGF- β to the top layer of the scaffold, which was absorbed in a rapidly degrading collagen gel⁵³. The new cartilage matrix was formed between the thick PCL/hydroxyapatite fibers, although these fibers form an unnatural environment for chondrocytes. Our implant aims for the cartilage matrix to be deposited within the reinforced GelMA/HA hydrogel, which better matches the stiffness and elasticity of articular cartilage than a FDM PCL scaffold^{360-362,435}, and which was proven a durable scaffold for cartilage matrix formation in other work in this thesis.

Both components of the current implant have an open connection to each other, through their vertical pores. Nevertheless, for osteochondral tissue engineering, the cartilage and bone component may need to be separated by an impermeable layer, like in native tissues^{432,437}, although this layer will prohibit migration of cells from the bone marrow to the cartilage component. Such a separation may, therefore, have a negative impact on the chondrogenic regeneration in the TGF- β group compared to

the expanded chondrocytes group. The interface between both compartments remains open in the current implants to facilitate migration of cells to the cartilage layer, which was shown the key to cartilage regeneration in the study by lee *et al.*

The follow-up of the presented work will evaluate bone and cartilage regeneration in the implants *in vivo*, comparing the presence and absence of chondrocytes and TGF- β in the cartilage component. In the human situation, the group with chondrocytes could potentially be translated as a matrix assisted ACI for osteochondral purposes. However, the outcomes of the outlined animal study should be interpreted with care, as rabbits are known for their huge regenerative capacity⁴³⁸, so tissue formation in humans will often be more challenging. Furthermore, the osteochondral scaffolds are here implanted in fresh defects, which are likely to heal better than osteochondral defects that present naturally. Also, the mechanical loading in the rabbit is lower than in weight-bearing joint in humans.

Altogether, implants with anatomical dimensions addressing both the biological and mechanical properties of bone and cartilage tissue were fabricated for the regeneration of large joint defects. The efficacy of these implants for joint repair remains to be demonstrated in the comparative study in rabbits that follows this work.

Chapter 11

General Discussion and Future Perspectives

The work presented in this thesis shows that constructs from biodegradable materials can be biofabricated with relevant dimensions for joint repair. In [Part I](#) the biological properties of gelatin methacrylamide (GelMA) gels are modified by the incorporation of tissue-derived matrices. [Part II](#) demonstrates that the strength and stiffness of GelMA gels is significantly improved by reinforcement with 3D-printed scaffolds. Such a composite scaffold is subsequently used *in vivo* in the equine stifle joint, first in a pilot study, then in a full-scale experimental that is ongoing at the moment of writing but of which study design and initial results are described in this thesis. In [Part III](#), complex shaped constructs for the repair of osteochondral defects are biofabricated and a model for the replacement of the entire shoulder joint of rabbits with 3D-printed implants is presented.

Biological improvement of GelMA with extracellular matrix components

The regeneration of tissue in the work presented in this thesis relies on cells encapsulated in a biodegradable GelMA hydrogel. Part I of this thesis aimed for the biological improvement of this hydrogel with help of tissue-derived matrices (TDMs). As TDMs are decellularized tissues, they form the ultimate substrate for tissue engineering based on biology. Both the structure and function (through adherence of bio-active substances to matrix components) of the tissue can be retained, forming an instructive scaffold for embedded, seeded or invading cells⁶⁶. TDMs have a potential in regenerative medicine, as demonstrated in several proof-of-concept studies for the regeneration of tissues such as liver, lung and trachea⁶⁸. In addition, several *in vitro* studies have reported positive stimulatory effects of TDMs on cells^{70,71,77,249}. Also, cartilage matrix production by *in vitro* cultured chondrocytes was stimulated when cultured on synthetic matrices consisting of collagen types I and II, which are common extracellular matrix components²⁶⁹⁻²⁷².

Nevertheless, as TDMs are derived from natural tissues with minimal processing steps⁶⁷, the matrix composition remains ill-defined and donor dependent. A standardized product is required for successful and predictable clinical application of TDMs. Therefore, many studies remain to be done on establishing the optimal biological and structural composition of TDMs for the regeneration of specific tissues, along with optimization of processing TDMs for use in biomaterials.

The TDMs used in Chapters 3 and 4 consisted predominantly of collagens in a dissolved or particulated state, without or with small amounts of glycosaminoglycans (GAGs), and an undefined panel of growth factors and signaling molecules^{244,273,274}. In contrast to the findings in previous reports, we found a neutral or negative effect of the addition of TDMs to GelMA on tissue formation by MSCs and chondrocytes, respectively. Earlier reports already pointed at the negative interaction of TDMs and chondrocytes, as collagen matrices appeared to induce catabolic pathways in cultured chondrocytes, which even led to degradation of the collagen matrix^{74,251,252}. More specifically, the matrix

degradation was a result of pro-inflammatory cytokines and matrix metalloproteinases (MMPs) that were produced by the chondrocytes^{251,252}. This response of chondrocytes to collagen matrix components may also be a mechanism of tissue degeneration in osteoarthritis.

As GelMA itself is based on a denatured collagen type I matrix, the addition of more collagens in the form of TDM may not lead to major changes to the biochemical composition of the gel. Instead, to present a more natural matrix composition to embedded chondrocytes, the addition of GAGs may be required. Indeed there is a body of literature that suggests that hyaluronic acid (HA) may have potential for stimulating chondrogenesis by chondrocytes^{63,73,439-441}. In particular, the dedifferentiation of chondrocytes in GelMA and other hydrogels was reduced by the presence of functionalized HA, which was evidenced by a lower expression of collagen type I and a more rounded cell morphology. The addition of only a small amount of HA to GelMA hydrogels resulted in more abundant chondrocyte differentiation compared to higher concentrations or the absence of HA⁷³. Therefore, a specific polymer composition (9.5/0.5% w/v GelMA/HA) was adopted in a number of studies in this thesis.

The matrices derived from cartilage, meniscus and tendon tissue used in this thesis may have a positive effect on chondrocytes when processed in a way that significantly more GAGs are retained. In order to achieve this, several modifications could be made to the series of chemical and mechanical treatments that are currently performed in the decellularization process, on the condition of course that this process is still effective and hence the tissues remain sufficiently decellularized⁶⁷. However, the realization of such changes in the decellularization process may not be easy and, given our results, addition of natural or synthetic HA to hydrogels seems a more straightforward approach, especially when the hydrogel (like GelMA) consists of denatured collagens. The HA is preferably covalently crosslinked to the GelMA, by methacrylation of the HA (HA-MA), for a sustained positive biological and mechanical effect on the tissue-engineered construct^{63,73}. Future biological optimization of GelMA should thus focus on the exploration of the effect of addition of defined matrix components (like HA) instead of TDMs.

Mechanical improvement of GelMA with 3D printed fibers

Hydrogels are soft due to the high water and low polymer content, which makes them suitable vehicles for matrix formation by embedded cells^{29,246}. Nevertheless, most hydrogels are too soft for tissue repair when used as large, unconfined implants in weight-bearing locations. Hydrogel stiffness can be improved by increasing the polymer concentration, however, a dense polymer network restricts cell-driven matrix formation^{79,104}. In finding ways to meet both the biological and the mechanical requirements of hydrogels for tissue engineering, researchers have been inspired by the fiber-reinforced extracellular matrix (ECM) structure of natural tissues^{55,56,77}. Like hydrogels, natural tissues have high

water content, but derive their strength and stiffness from an organized matrix of which the core is formed by fibrillar collagens. The configuration of the ECM is tissue-specific, resulting in differences in biomechanical characteristics of tissues. For example, the collagen meshwork interspersed with hydrophilic proteoglycan aggregates in cartilage results in a stiff and resilient tissue, and the strongly mineralized collagen skeleton in bone in very stiff, but more brittle, tissue.

In Parts II and III of this thesis, hydrogels were reinforced with printed polycaprolactone (PCL) fibers, in order to improve stiffness and shape stability. In these constructs, GelMA provided a suitable watery environment to embedded cells, and a secondary, reinforcing network was provided by the rigid thermoplastic polymer fibers, not unlike the composite structure of native cartilage. The stiffness of this network could be tailored by altering the fiber diameter or the spacing of the fibers³⁶³. Nevertheless, the 3D printed networks of PCL fibers applied in this thesis had a simple 0-90° orientation that did not mimic the complex structure of the natural ECM.

Scaffolds produced with this process of fused deposition modeling (FDM) typically have large intrinsic stiffness^{50,65} hydrogels reinforced with thick fibers (diameter ca. 200 μm) were shown to have high stiffness, yet these composites possessed low elasticity (Chapter 6). In line with these biomechanical properties, thick-fiber FDM scaffolds have shown promise to support the formation of bone matrix in orthotopic locations⁵². Nevertheless, FDM scaffolds have also been applied as a cell carrier for cartilage regeneration, *in vitro*^{442,443} and *in vivo*, and have successfully been translated to the clinic (*i.e.* in the "INSTRUCT" trial⁴⁴⁴).

The electrospun microfiber scaffolds (fiber diameter ca. 20 μm) presented in Chapter 6 may form a suitable alternative to the FDM scaffolds, as the biomechanical properties of hydrogels reinforced with these scaffolds better resemble the stiffness and elasticity of native articular cartilage. In addition, the porosity of microfiber scaffolds is significantly higher, resulting in more space for matrix production by embedded cells. The synergistic increase in stiffness when combining a soft hydrogel with a soft microfiber scaffold was also observed for other gels than GelMA. The mechanical properties of the hydrogel constructs were evaluated under compressive loading, however, future research is required to evaluate the performance under different loading regimes, for example tensile and shear testing, and combinations of different loads. It may well be that the 0-90° orientation of the fibers results in a poor resistance to combined compressive and shear loads, as the structure of vertical boxes that provides the stiffness to the PCL/hydrogel composite may be disrupted.

The elasticity of hydrogels reinforced with microfibers results in shape recovery after deformation by compression, and these deformation-reshaping cycles transfer mechanical stresses to the embedded cells. This cyclical stresses are advantageous, as repetitive compression of hydrogels can lead to improved synthesis of embedded chondrocytes⁴⁴⁵,

which are known to be sensitive to mechanic cues from their environment^{344,445,446}. In this thesis, chondrocytes in GelMA reinforced with microfiber scaffolds responded stronger to repetitive compression in a bioreactor in terms of gene expression than cells in GelMA alone; however, the formation of cartilage matrix was similar. As the hydrogel constructs in this work were subjected to a mechanical loading regime for only 2 weeks, a difference in ECM production may be expected after longer culture periods.

The newly formed ECM needs to gradually take over the mechanical resistance of the constructs that was initially provided by the thermoplastic polymer fibers, as these will degrade over the course of 2-3 years⁵⁰. This transition may need to be faster in microfiber-based compared to FDM scaffolds, since the fiber diameter is 10-fold smaller, resulting in faster degradation. In this context, recent studies are encouraging, as they showed increasing stiffness of GelMA-HA-MA constructs provided by the newly formed matrix of embedded chondrocytes over the course of 8 weeks of *in vitro* culture^{63,73}. The reinforcement of hydrogels with organized microfibers thus forms a promising approach for tissue-engineered constructs in terms of mechanical and biological compatibility.

The regenerative process of cartilage tissue in a focal defect

The mechanism of cartilage regeneration in a focal defect has not been fully elucidated, but follows most likely either a 'bottom-up' or substitutive pathway, for example within a biodegradable material. The regeneration of cartilage after an autologous chondrocyte implantation (ACI) procedure with fibrin glue is probably bottom-up, as cells will adhere to the bottom and the edges of the defect while the fibrin rapidly degrades. A comparable principle will apply after microfracturing of the subchondral plate: a hematoma forms in the defect and cells that migrate up from the bone marrow initiate a healing process¹⁷. In contrast, biomaterials that are designed for regenerative applications aim to serve as a supportive scaffold for matrix formation that is meant to generally substitute the artificial scaffold³⁶⁸. The formation of new matrix within the biomaterial should be balanced by degradation of the latter, hence retaining a constant volume of the implant⁵⁰.

The mechanism of tissue regeneration in a focal cartilage defect is most likely dependent on the shape stability and the degradation rate of the cell carrier. In Chapters 3, 4 and 6 and in other studies, GelMA was found to degrade over the course of months^{63,73,257}, which means the degradation rate is significantly lower than that of fibrin glue^{21,23,78}. Thus, when following processes in the petri dish, cells in fibrin glue would repair bottom-up, whereas cells in GelMA repair in the substitutive manner.

The process of matrix formation within GelMA gels was objectified *in vitro* (Chapters 3 and 4) and *in vivo* in rats (Chapters 4 and 6). Cells only invaded the periphery of GelMA samples after 8 weeks of culture in subcutaneous pockets in the immunocompromised rats. In contrast, the pilot study in a pony showed a massive infiltration of cells and deg-

radation of the GelMA after two weeks, but despite this infiltration, the GelMA retained its shape. Although this was a pilot study only, it lies at hand to conclude that the immune status of the host probably has a major influence on biomaterial degradation and tissue regeneration.

The follow-up study of cartilage repair in ponies, described in Chapter 7, aims to gain further insight in the biomaterial-dependency of the regenerative process after cell therapy for cartilage repair. To achieve this, the following four experimental groups were designed: 1) plain GelMA and 2) reinforced GelMA, both with a high concentration of embedded cells, and 3) 'GelMA cap' and 4) fibrin glue, both with a low concentration of cells. The high concentration of cells was based on standards in tissue engineering research, whereas the low concentration was based on clinical cell therapy standards. It can be conjectured that, when a low concentration of cells is suspended in a slowly degrading hydrogel, like GelMA, there is reduced cell-cell contact, which probably limits cartilage matrix formation⁴⁴⁷. To address this point without raising the number of cells to levels that are not feasible in the clinic, the GelMA cap group was introduced, where a low number of cells are deposited on the bottom of the defect, which is subsequently capped with a cell-free layer of GelMA. The hypothesis is that the GelMA cap configuration may result in controlled bottom-up regeneration of cartilage tissue. This controlled ingrowth of cells from the bone marrow has also been an aim of other recently developed therapies, in which the cartilage defect is covered with a cell-free biomaterial after microfracture^{372,373}.

In the long-term, both the substitutive and the bottom-up mechanisms of cartilage repair may lead to a comparable quality of repair tissue. Both approaches have not yet been directly compared in a clinical study. Most current cell therapies for cartilage repair are performed using rapidly degrading cell carriers, with some success. For example, ACI with fibrin glue has resulted in a good fill of the defect with fibrocartilaginous or hyaline-like tissue^{6,9}. Alternatively, cells seeded on a collagen type I/III matrix (matrix-induced autologous chondrocyte implantation, MACI), which degrades more slowly than fibrin, also initiated regeneration of cartilaginous tissue^{369,448}. Still, the quality of the repair tissue after two years of follow-up in patients treated with MACI was similar to that of microfracture⁴⁴⁸. The outcomes of the equine study may provide evidence whether the regenerative mechanism of cartilage in focal defects is really dependent on the type of the cell carrier, and if so, what is the effect of this process on the quality of the repair tissue after 1 year.

Biofabrication of osteochondral tissue

Organ or tissue defects often involve multiple tissue types, for which the repair may demand implants featuring a defined organization of multiple cell types. Therefore in Part III of this thesis biofabrication technology was used not only to reinforce hydrogels, but

also to impose an internal organization and an external architecture on the constructs. Large constructs were printed from a combination of various hydrogel bioinks, with separate layers for the regeneration of bone and cartilage tissue. However, these constructs were not selected for translation into animal models, as they were too soft to survive in the mechanically challenging orthotopic location without a reinforcing structure. Also, successful simultaneous regeneration of both bone and cartilage tissue has not yet been attained in these constructs. In particular, chondrocytes inhibited endochondral bone formation by MSCs in bilayered GelMA constructs in rats. Whereas the inhibition of endochondral bone formation is encouraging for engineering cartilage tissue with a co-culture of MSCs and chondrocytes²⁴, the engineering of osteochondral tissue may need another approach. For example, the bone and cartilage layer might be separated by an impermeable layer, preventing chondrocytes from inhibiting endochondral bone formation by MSCs. Alternatively, MSCs may be osteogenically differentiated via the intramembranous pathway, or the bone component of an osteochondral implant may be left cell-free.

It was the last approach that was chosen for the implants that were fabricated for the repair of osteochondral tissue in the shoulder joint of rabbits (Chapter 10), which contained a cell-free bone component. More specifically, they consisted of stiff PCL fibers coated with calcium phosphate, as these minerals have proven to improve the osteoconductivity of such scaffolds^{52,433}. The cartilage component relied on expanded chondrocytes in GelMA reinforced with PCL microfibers. A cell-free cartilage group containing only Transforming Growth Factor beta (TGF- β) was included in this study to be able to compare the outcome with a previous study on the regeneration of the articular surface in a similar rabbit model⁵³. That study focused only on cartilage formation (not on bone) and demonstrated the formation of a cartilage layer by cells that were attracted from the bone marrow by TGF- β into the porous scaffold that had been implanted in the rabbit shoulder. The osteochondral implant presented in Chapter 10 expanded on this previously published implant in the sense that it consisted of two components with distinct mechanical and biological characteristics for the repair of cartilage and bone tissue. The shoulder replacement model in rabbits can serve as a model for the repair of osteochondral defects, however with respect to translational aspects one should realize that a fresh defect in rabbits may have a larger regenerative capacity for both bone and cartilage compared to a natural defect in humans⁴³⁸.

Testing in cadaveric rabbits suggested that the implant is strong enough for immediate implantation. Nevertheless, the mechanical loading in unconfined defects is much larger in humans compared to rabbits. In order to ensure sufficient strength, the cartilage tissue may need to be matured in a bioreactor prior to implantation. Altogether, within Part III of this thesis, organized scaffolds with cartilage and bone components were developed for the regeneration of osteochondral or partial joint defects. Although

bone and cartilage were successfully regenerated separately *in vitro* and *in vivo*, the regeneration of osteochondral tissue through these scaffolds still needs to be established.

Biofabrication versus self-organization

Biofabrication has now been recognized as a promising technique for the engineering of tissue constructs that could ultimately be applied to treat damaged, diseased or degenerated tissue^{11,12}. Nevertheless, biofabrication should be considered a tool in a multidisciplinary research field and not as the independent solution for the generation of functional tissues. One may even question the need for biofabrication. For example, research in cell biology has already produced functional engineered tissues, without the need for imposing a cellular organization with biofabrication techniques. The large self-organizing capacity of stem cells resulted in organoids for tissue repair⁴⁴⁹: functional mini-guts were grown from single intestinal stem cells⁴⁵⁰. In fact, these 'guts' are epithelial structures, originating from a single stem cell that resides in the epithelium of the colon. Nevertheless, biofabrication may certainly add value to cell biology when the organization of the target tissue cannot be re-established by a single stem cell. In other words, biofabrication could help in the assembly and structuring of tissues originating from multiple cell types. First steps in this direction were made by the printing of multicellular spheroids, originating from a mixture of two cell types, which subsequently fused into defined patterns^{222,451,452}. Using this approach, mini-guts may not only be able to repair the epithelial cell layer, but also deeper layers of the colon. In addition, biofabrication may enable scaling up the size of these constructs, as shown in chapters 8 and 9, and may provide an integrated network of perfusable channels^{185,283}.

The balance between biofabrication and self-organization also applies to the generation of potential implants for repair of chondral tissue. Biofabrication was originally introduced as a tool to recreate all zones of articular cartilage¹⁰⁰. However, should all layers of cartilage tissue be recreated by the selective printing of cells, growth factors or ECM components⁴⁵³? Or is this strategy overcomplicated and should we better understand and make use of the intrinsic regenerative capacity of nature? For example, there is evidence that all zones may potentially be established from one cell type, by stimulation with the right differential mechanical and biochemical signals⁴⁵⁴.

In the case of osteochondral tissue engineering, distinct zones for bone and cartilage regeneration may at least need to be fabricated. These tissues are very close anatomically, and cartilage even transforms into bone during growth and development²⁷⁸, yet the properties and regenerative capacities of both tissues in their mature forms are very different²⁴⁵. In this context, most scaffolds that are developed for the repair of osteochondral tissue are biphasic^{35,432}. The two components may contain different cells or growth factors, or can be cell-free, with only differences in components and structure. In Chapters 8 and 9, bilayered hydrogel constructs were fabricated. This approach may

help in scaling up the size of cell-laden hydrogel implants that have been used successfully for the repair of osteochondral tissue⁴⁵⁵. The fabrication process may even include the construction of perfusable channels and an impermeable layer in between the two compartments, as discussed earlier^{185,283,432}. It can be concluded that the extent of organization and structure to be imposed with biofabrication thus depends on the self-organizing capacity of the cells used and the interaction between the different cell types in the tissue engineered constructs. The technique offers various options in regenerative medicine that have as yet not been fully explored.

Shape versus function

Once a construct is fabricated in a desired shape, what should be the required functionality before implantation? In Part III of this thesis it was shown that constructs with complex anatomical shapes could be created with biofabrication techniques. In addition, other studies have demonstrated excellent control over the printing of microvasculature in such constructs^{185,283}. Integration of biofabrication techniques that control micro- and macro-architecture will probably lead to constructs with the size of tissues and organs, in which the major cell and matrix types are in the correct anatomical locations. However, the proper functioning of such tissue-equivalents will remain a major challenge, as the communication mechanisms between cells and homeostasis in organs are complex and often poorly understood phenomena.

If immediate functionality of the tissue is not essential, cells could be given the opportunity to grow and produce matrix following implantation in orthotopic locations. This maturation *in situ* would apply to non-vital tissues such as cartilage or bone. The mechanical stability of the implants could in this case be temporarily provided by a reinforcing scaffold, as describe above. As an example, RM approaches for auricular reconstruction rely on a PCL scaffold to retain shape and on a cell/hydrogel component for the regeneration of auricular cartilage⁴⁵⁶. The regenerated tissue is expected, over the course of several months, to gradually take over the supporting role of the PCL scaffold⁵⁰. In contrast, a more immediate physiological function of the 3D-printed implant would be required for the repair of vital organs, such as the heart⁴⁵⁷ or liver⁴⁵⁸. Should tissue-engineered organs be ultimately implanted in future medicine, complete tissue function would in those cases need to be established unequivocally prior to implantation. To achieve this, tissue maturation is typically performed in a bioreactor or in ectopic locations in the body⁴⁵⁹.

Alternatively, shape and function could be integrated in a bionic approach. Artificial implants for the substitution of tissue function, like a hearing aid or pacemaker, have proven efficacy. In an attempt to combine these medical devices with regenerative solutions, the geometry of a human ear was printed from a cell-laden hydrogel, along with a conducting polymer consisting of infused silver nanoparticles⁴⁶⁰. This proof-of-concept

project resulted in a matrix for tissue regeneration of the outer ear, including a conductor for acoustic signals. This strategy could possibly be extended for the repair of vital organs, such as the heart or kidney, by simultaneous printing of myocardial tissue and a pacemaker or renal tissue and a dialysis membrane, respectively. An ethical framework for the advancement of these regenerative and bionic techniques should also be defined, as supernatural functions can potentially be engineered^{461,462}. Nevertheless, the replacement of tissues with devices and prostheses is well established and will remain for a long time, as the long-term efficacy of these therapies has been demonstrated. Still, the life expectancy of most traditional implants is limited, as their biological effect and mechanical function do not match with natural tissues. Therefore, tissue replacement on a biological level through regenerative strategies will ultimately result in the most durable restoration of its function.

Pitfalls and possible solutions in the translation from bench to bedside

Only very few biomaterials and tissues that are engineered in the laboratory find their way to clinical applications⁴⁶³⁻⁴⁶⁶. This situation is undesired, since developed potential solutions have limited value if they are not clinically applicable. The major challenges in translating tissue engineering to clinical application are discussed here.

Over the past years, research in biofabrication has predominantly focused on improving the printing process and its compatibility with cells. The first practical applications of biofabrication are acknowledged to be in the screening of cell-cell interactions, pharmaceuticals and patient specific disease models^{86,88}, as also outlined in Chapter 2. In the case of regenerative implants, biofabrication strategies should be focused on a clinical application, adjusted to patient needs. Once a promising therapy has been developed in the laboratory, its safety and efficacy should be demonstrated in relevant animal models.

The next step in translation comprises clinical trials in humans, for which regulatory hurdles apply. These regulations depend on the type of product that is to be applied. A 3D-printed implant without cells or growth factors could be considered a medical device⁴⁶⁵. A medical device has been defined by the US food and drug administration (FDA) as a health care product that does not achieve its purpose by chemical action or by being metabolized⁴⁶⁷. In Europe, medical devices should comply with a set of technical requirements, after which a conformity marking (CE mark) is granted. However, 3D-printed implants are usually customized for patient needs and are, therefore, categorized as custom made devices. Individual products in this group should still meet the technical requirements, but are exempt from a CE mark. For example, commercially available implants are fabricated from titanium in customized shapes with a GMP printing process^{46,468}. This process is standardized and meets the technical requirements, so that not every individual implant needs a CE mark.

Once biological components are included, the scaffold will be categorized as an advanced therapy medicinal product (ATMP)^{469,470}. ATMPs are medicines based on genes, cells or tissues. For example, ChondroCelect® (ACI) and MACI are authorized ATMPs for the repair of focal cartilage defects⁴⁷¹. The quality, safety and efficacy of the product must be scientifically demonstrated, before the ATMP grade may be granted⁴⁷¹. Implants should be fabricated according to good manufacturing practice (GMP), guaranteeing sterility and reproducibility⁴⁷⁰. This optimization and standardization is a critical stage in the development of an ATMP in which many candidates fail, and is therefore also termed 'the valley of death'⁴⁶⁴. In this stage, the help of industrial partners is required, although they have often not been involved in the development of the product.

The valley of death can best be crossed with a combination of a good product, sufficient funding and enthusiastic researchers and industrial partners. This could be organized better than is usually the case by the early teaming up of academy and industry in the start-up phase of the research, although admittedly academic progress may be delayed by the protection of intellectual property and patent requests by industrial partners. With such an approach, medical-grade materials and GMP could be used already in the laboratory phase and avoid backwards engineering from interesting findings with products and techniques that are hard to apply in a hospital⁴⁶⁶. In this way, industrial partners may be easier recruited for the production and doctors may be more interested in participating in the experimental work, as the translational approach is better feasible.

Translation of the presented biofabrication approaches to clinical applications

In addition to the general challenges in translation that apply for tissue engineering and biofabrication, there are specific challenges and opportunities in regard to the work presented in this thesis:

1) *Medical-grade biomaterials*. The biomaterials – PCL and GelMA – that formed the substrates for biofabrication in this thesis have potential for safe clinical application. PCL is available in medical grade, as used in a few of the presented studies, and PCL-based scaffolds have been approved and applied for bone regeneration in humans⁵¹. The GelMA used in this thesis was produced from gelatin with relatively high endotoxin levels that are not compliant with clinical application in humans. Only for the rabbit and equine studies, the GelMA was filtered to remove any bacteria that were either present in the gelatin at the start of the synthesis, or may have entered during some stage of the synthesis process. The removal of all pathogens and the elimination of batch-to-batch variations are still challenging, as gelatin is usually of bovine or porcine origin. Nevertheless, no adverse events, or inflammation other than related to the implantation surgery, were observed after implantation of GelMA constructs in ponies. This was in line with

findings of others in rodents⁴⁷². Future experimental work should be performed, however, with gelatins with low endotoxin levels, which are now commercially available⁴⁷³. Preferably, the endotoxin levels are further reduced to zero, which may be achieved with advanced sterilization methods during gelatin production combined with active endotoxin removal⁴⁷⁴ or through the synthesis of recombinant gelatin³⁷⁵. Once clinical-grade GelMA is developed, *in vitro* work should affirm comparable cellular differentiation in GelMA with high and low endotoxin levels, before proceeding to animal models. In cases in which GelMA is printed the sterility of the GelMA of the hydrogel should be re-evaluated after the printing process.

2) *Crosslinking the GelMA*. In the current work, GelMA was crosslinked with UV light or with a redox reaction. Both techniques have significant limitations, as they are cytotoxic when applied in high doses. UV crosslinking in the laboratory is performed with a low intensity source, to preserve the viability of cells and to minimize the DNA damage. However, this low-intensity source is only effective in an oxygen-deprived environment, as oxygen inhibits the photopolymerization process⁴⁷⁵. Since it is hard to remove oxygen from the articular joint area, a strong, focused UV source was used in the rabbit and equine studies. Although this UV beam did not affect cell viability when used for shorter than three minutes, as shown in Chapter 7, the lamp generated much heat when it was used repetitively during the equine surgeries. DNA damage is not unlikely to occur with such a powerful UV source, so there is a need for new crosslinking methods. In coming years, the crosslinking of GelMA with visible light will be developed⁴⁷⁶, and previous research has already shown that visible light photoinitiators can be used to crosslink hydrogels functionalized with acrylate groups⁴⁷⁷. However, the downside of photocrosslinking is the limited penetration of light in larger, reinforced constructs. As the fibers may block the light in these reinforced hydrogels, redox crosslinking with ammonium persulfate/tetramethylethylenediamide was selected in Chapter 6. However, high concentrations of these crosslinking agents are cytotoxic. Therefore, future studies should focus on the crosslinking of large, reinforced GelMA constructs with alternative redox agents⁴⁷⁸ or enzymes, such as transglutaminases⁴⁷⁹ or genipin⁴⁸⁰.

3) *GMP for the printing procedure*. The bioprinters that produced the implants presented in this thesis were located in university laboratories. Whereas an aseptic environment was facilitated by laminar air flow, the manufacturing standards were still far from GMP level. As the biofabrication hardware rapidly develops, and industrial partners are increasingly interested in the technique, biofabrication will become a more reproducible and sterile technique in coming years. The best physical location of the bioprinters still needs to be defined. The jury is still out whether printers can be best located in the surgical theatre or in cell therapy facilities outside or inside the hospital. The printer is required in the theatre in case of *in situ* repair, which has been developed for skin⁴⁸¹ and osteochondral tissue²²⁵. However, practical barriers were identified in these studies to

the presence of a 3D-printer in the surgical arena. A GMP facility close to the surgery theatre is probably preferable in the first clinical studies.

4) *Devices and ATMPs*. Should cartilage repair or osteochondral tissue repair with reinforced GelMA in the rabbit and equine studies prove to be effective, this cell/biomaterial product still requires approval as an ATMP. The first clinical therapies in which biofabrication will be used can most easily be based on existing devices and ATMPs. The cell component is best based on MACI, using expanded autologous chondrocytes⁴⁴⁸. When the biomaterials – GelMA and PCL – and the fabrication techniques are standardized to GMP level, an ATMP label could be requested. Nevertheless, a more feasible first step may be to label the biodegradable osteochondral implant that was developed for the rabbit shoulder as a medical device, provided no cells and growth factors are included. Such a strategy may pave the road for biofabricated ATMPs - including cells - that follow in the future.

Biofabrication in the hospital of the future

Biofabrication may still be in its infancy, but significant progress has been made over recent years. Extrapolation of the progress made thus far leads to speculations about the role of biofabrication for the repair of tissues in future health care^{45,482}. We may envision a collection of 3D printers close to the operating room, churning out customized spare body parts from a collection of bioinks and cells. However, for biofabrication to become an established and functional technique, its development has to pass the stages of the Gartners hype cycle (Gartner Inc.) for emerging technologies (see introduction, Fig. 5). First, the 'trough of disillusionment' must be crossed, which follows the 'peak of inflated expectations'. Then, the 'plateau of productivity' needs to be reached, by means of standardized and sterile biomaterials and fabrication methods, university-industry partnerships, and safe and efficient treatments. Achieving this progress of biofabrication demands a multidisciplinary approach, connecting chemists, biologists, engineers, doctors and entrepreneurs. A balanced group of colleagues with these backgrounds has been involved in the realization of the work presented in this thesis, and will be involved in moving biofabrication further from the laboratory setting to the operating theatre.

References

REFERENCES

- 1 DeWitt, N. Regenerative medicine. *Nature* 453, 301 (2008).
- 2 Passier, R., van Laake, L. W. & Mummery, C. L. Stem-cell-based therapy and lessons from the heart. *Nature* 453, 322-329 (2008).
- 3 Recknor, J. B. & Mallapragada, S. K. Nerve Regeneration: Tissue Engineering Strategies, in *The Biomedical Engineering Handbook: Tissue Engineering and Artificial Organs*, J.D. Bronzino, Editor. *Taylor & Francis: New York* (2006).
- 4 van Osch, G. J. *et al.* Cartilage repair: past and future--lessons for regenerative medicine. *Journal of cellular and molecular medicine* 13, 792-810 (2009).
- 5 Carnes, J., Stannus, O., Cicuttini, F., Ding, C. & Jones, G. Knee cartilage defects in a sample of older adults: natural history, clinical significance and factors influencing change over 2.9 years. *Osteoarthritis and cartilage / OARS, Osteoarthritis Research Society* 20, 1541-1547 (2012).
- 6 Mastbergen, S. C., Saris, D. B. & Lafeber, F. P. Functional articular cartilage repair: here, near, or is the best approach not yet clear? *Nature reviews. Rheumatology* 9, 277-290 (2013).
- 7 Felson, D. T. Clinical practice. Osteoarthritis of the knee. *The New England journal of medicine* 354, 841-848 (2006).
- 8 van Blitterswijk, C. A., Moroni, L., Rouwkema, J., Siddappa, R. & Sohier, J. Tissue engineering – an introduction, in *Tissue Engineering*. C.A. van Blitterswijk, Editor. *Elsevier* (2008).
- 9 Makris, E. A., Gomoll, A. H., Malizos, K. N., Hu, J. C. & Athanasiou, K. A. Repair and tissue engineering techniques for articular cartilage. *Nature reviews. Rheumatology* 11, 21-34 (2015).
- 10 Dimmeler, S., Ding, S., Rando, T. A. & Trounson, A. Translational strategies and challenges in regenerative medicine. *Nature medicine* 20, 814-821 (2014).
- 11 Melchels, F. P. W. *et al.* Additive manufacturing of tissues and organs. *Progress in Polymer Science* 37, 1079-1104 (2012).
- 12 Murphy, S. V. & Atala, A. 3D bioprinting of tissues and organs. *Nature biotechnology* 32, 773-785 (2014).
- 13 Martel-Pelletier, J., Boileau, C., Pelletier, J. P. & Roughley, P. J. Cartilage in normal and osteoarthritis conditions. *Best practice & research. Clinical rheumatology* 22, 351-384 (2008).
- 14 Coates, E. E. & Fisher, J. P. Phenotypic variations in chondrocyte subpopulations and their response to in vitro culture and external stimuli. *Annals of biomedical engineering* 38, 3371-3388 (2010).
- 15 Hayes, A. J., Hall, A., Brown, L., Tubo, R. & Caterson, B. Macromolecular organization and in vitro growth characteristics of scaffold-free neocartilage grafts. *The journal of histochemistry and cytochemistry: official journal of the Histochemistry Society* 55, 853-866 (2007).
- 16 Li, L. P. & Herzog, W. The role of viscoelasticity of collagen fibers in articular cartilage: theory and numerical formulation. *Biorheology* 41, 181-194 (2004).
- 17 Mandelbaum, B. R. *et al.* Articular cartilage lesions of the knee. *The American journal of sports medicine* 26, 853-861 (1998).
- 18 Bedi, A., Feeley, B. T. & Williams, R. J., 3rd. Management of articular cartilage defects of the knee. *The Journal of bone and joint surgery. American volume* 92, 994-1009 (2010).
- 19 Heir, S. *et al.* Focal cartilage defects in the knee impair quality of life as much as severe osteoarthritis: a comparison of knee injury and osteoarthritis outcome score in 4 patient categories scheduled for knee surgery. *The American journal of sports medicine* 38, 231-237 (2010).
- 20 Brittberg, M. *et al.* Treatment of deep cartilage defects in the knee with autologous chondrocyte transplantation. *The New England journal of medicine* 331, 889-895 (1994).

- 21 Saris, D. B. *et al.* Characterized chondrocyte implantation results in better structural repair when treating symptomatic cartilage defects of the knee in a randomized controlled trial versus microfracture. *The American journal of sports medicine* 36, 235-246 (2008).
- 22 Filardo, G. *et al.* Arthroscopic second generation autologous chondrocytes implantation associated with bone grafting for the treatment of knee osteochondritis dissecans: Results at 6 years. *The Knee* 19, 658-663 (2012).
- 23 Bekkers, J. E. *et al.* Single-stage cell-based cartilage regeneration using a combination of chondrons and mesenchymal stromal cells: comparison with microfracture. *The American journal of sports medicine* 41, 2158-2166 (2013).
- 24 de Windt, T. S. *et al.* Concise Review: Unraveling Stem Cell Cocultures in Regenerative Medicine: Which Cell Interactions Steer Cartilage Regeneration and How? *Stem cells translational medicine* 3, 723-733 (2014).
- 25 de Windt, T. *et al.* Allogeneic mesenchymal stem cells are safe and stimulate cartilage regeneration upon co-implantation with chondrons in the IMPACT trial. *Abstract no. 16.3.2 at the International Cartilage Repair Society conference, Chicago* (2015).
- 26 Deponti, D. *et al.* Fibrin-based model for cartilage regeneration: tissue maturation from in vitro to in vivo. *Tissue engineering. Part A* 18, 1109-1122 (2012).
- 27 Homminga, G. N., Buma, P., Koot, H. W., van der Kraan, P. M. & van den Berg, W. B. Chondrocyte behavior in fibrin glue in vitro. *Acta orthopaedica Scandinavica* 64, 441-445 (1993).
- 28 Ye, Q. *et al.* Fibrin gel as a three dimensional matrix in cardiovascular tissue engineering. *European journal of cardio-thoracic surgery : official journal of the European Association for Cardio-thoracic Surgery* 17, 587-591 (2000).
- 29 Hunt, N. C. & Grover, L. M. Cell encapsulation using biopolymer gels for regenerative medicine. *Biotechnology letters* 32, 733-742 (2010).
- 30 Spiller, K. L., Maher, S. A. & Lowman, A. M. Hydrogels for the repair of articular cartilage defects. *Tissue engineering. Part B, Reviews* 17, 281-299 (2011).
- 31 de Windt, T. S. *et al.* Arthroscopic airbrush assisted cell implantation for cartilage repair in the knee: a controlled laboratory and human cadaveric study. *Osteoarthritis and cartilage / OARS, Osteoarthritis Research Society* 23, 143-150 (2015).
- 32 Flynn, J. M., Kocher, M. S. & Ganley, T. J. Osteochondritis dissecans of the knee. *Journal of pediatric orthopedics* 24, 434-443 (2004).
- 33 Crawford, D. C. & Safran, M. R. Osteochondritis dissecans of the knee. *The Journal of the American Academy of Orthopaedic Surgeons* 14, 90-100 (2006).
- 34 Bartlett, W. *et al.* Autologous chondrocyte implantation at the knee using a bilayer collagen membrane with bone graft. A preliminary report. *The Journal of bone and joint surgery. British volume* 87, 330-332 (2005).
- 35 Panseri, S. *et al.* Osteochondral tissue engineering approaches for articular cartilage and subchondral bone regeneration. *Knee surgery, sports traumatology, arthroscopy : official journal of the ESSKA* 20, 1182-1191 (2012).
- 36 Hindle, P., Hendry, J. L., Keating, J. F. & Biant, L. C. Autologous osteochondral mosaicplasty or TruFit plugs for cartilage repair. *Knee surgery, sports traumatology, arthroscopy : official journal of the ESSKA* 22, 1235-1240 (2014).
- 37 Guermazi, A. *et al.* Prevalence of abnormalities in knees detected by MRI in adults without knee osteoarthritis: population based observational study (Framingham Osteoarthritis Study). *Bmj* 345, e5339 (2012).

- 38 Pelletier, J. P., Martel-Pelletier, J. & Abramson, S. B. Osteoarthritis, an inflammatory disease: potential implication for the selection of new therapeutic targets. *Arthritis and rheumatism* 44, 1237-1247 (2001).
- 39 Bijlsma, J. W., Berenbaum, F. & Lafeber, F. P. Osteoarthritis: an update with relevance for clinical practice. *Lancet* 377, 2115-2126 (2011).
- 40 Smith, J. O., Wilson, A. J. & Thomas, N. P. Osteotomy around the knee: evolution, principles and results. *Knee surgery, sports traumatology, arthroscopy: official journal of the ESSKA* 21, 3-22 (2013).
- 41 Wiegant, K. *et al.* Sustained clinical and structural benefit after joint distraction in the treatment of severe knee osteoarthritis. *Osteoarthritis and cartilage / OARS, Osteoarthritis Research Society* 21, 1660-1667 (2013).
- 42 Lohmander, L. S. & Roos, E. M. Clinical update: treating osteoarthritis. *Lancet* 370, 2082-2084 (2007).
- 43 Shan, L., Shan, B., Suzuki, A., Noh, F. & Saxena, A. Intermediate and long-term quality of life after total knee replacement: a systematic review and meta-analysis. *The Journal of bone and joint surgery. American volume* 97, 156-168 (2015).
- 44 Learmonth, I. D., Young, C. & Rorabeck, C. The operation of the century: total hip replacement. *Lancet* 370, 1508-1519 (2007).
- 45 The third industrial revolution. *The Economist* (2012).
- 46 Holzapfel, B. M. *et al.* Customised osteotomy guides and endoprosthesis reconstruction for periacetabular tumours. *International orthopaedics* 38, 1435-1442 (2014).
- 47 Spottiswoode, B. S. *et al.* Preoperative three-dimensional model creation of magnetic resonance brain images as a tool to assist neurosurgical planning. *Stereotactic and functional neurosurgery* 91, 162-169 (2013).
- 48 Noble, J. W., Jr., Moore, C. A. & Liu, N. The value of patient-matched instrumentation in total knee arthroplasty. *The Journal of arthroplasty* 27, 153-155 (2012).
- 49 Gagg, G., Ghassemieh, E. & Wiria, F. E. Effects of sintering temperature on morphology and mechanical characteristics of 3D printed porous titanium used as dental implant. *Materials science & engineering. C, Materials for biological applications* 33, 3858-3864 (2013).
- 50 Hutmacher, D. W. Scaffolds in tissue engineering bone and cartilage. *Biomaterials* 21, 2529-2543 (2000).
- 51 Woodruff, M. A. & Hutmacher, D. W. The return of a forgotten polymer-Polycaprolactone in the 21st century. *Progress in Polymer Science* 35, 1217-1256 (2010).
- 52 Reichert, J. C. *et al.* A tissue engineering solution for segmental defect regeneration in load-bearing long bones. *Science translational medicine* 4, 141ra193 (2012).
- 53 Lee, C. H. *et al.* Regeneration of the articular surface of the rabbit synovial joint by cell homing: a proof of concept study. *Lancet* 376, 440-448 (2010).
- 54 Brown, T. D., Dalton, P. D. & Hutmacher, D. W. Direct writing by way of melt electrospinning. *Advanced materials* 23, 5651-5657 (2011).
- 55 Coburn, J. *et al.* Biomimetics of the extracellular matrix: an integrated three-dimensional fiber-hydrogel composite for cartilage tissue engineering. *Smart Structures and Systems* 7, 213-222 (2011).
- 56 Coburn, J. M., Gibson, M., Monagle, S., Patterson, Z. & Elisseff, J. H. Bioinspired nanofibers support chondrogenesis for articular cartilage repair. *Proceedings of the National Academy of Sciences of the United States of America* 109, 10012-10017 (2012).
- 57 Calvert, P. Materials science. Printing cells. *Science* 318, 208-209 (2007).
- 58 Mironov, V. *et al.* Biofabrication: a 21st century manufacturing paradigm. *Biofabrication* 1, 022001 (2009).

- 59 Jakab, K., Damon, B., Neagu, A., Kachurin, A. & Forgacs, G. Three-dimensional tissue constructs built by bioprinting. *Biorheology* 43, 509-513 (2006).
- 60 Schuurman, W. *et al.* Gelatin-methacrylamide hydrogels as potential biomaterials for fabrication of tissue-engineered cartilage constructs. *Macromolecular Bioscience* 13, 551-561 (2013).
- 61 Melchels, F. P. W., Dhert, W. J. A., Hutmacher, D. W. & Malda, J. Development and characterisation of a new bioink for additive tissue manufacturing. *Journal of Materials Chemistry B* 2, 2282-2289 (2014).
- 62 Van Den Bulcke, A. I. *et al.* Structural and rheological properties of methacrylamide modified gelatin hydrogels. *Biomacromolecules* 1, 31-38 (2000).
- 63 Levett, P. A. *et al.* A biomimetic extracellular matrix for cartilage tissue engineering centered on photocurable gelatin, hyaluronic acid and chondroitin sulfate. *Acta biomaterialia* 10, 214-223 (2014).
- 64 Chen, Y. C. *et al.* Functional Human Vascular Network Generated in Photocrosslinkable Gelatin Methacrylate Hydrogels. *Advanced functional materials* 22, 2027-2039 (2012).
- 65 Schuurman, W. *et al.* Bioprinting of hybrid tissue constructs with tailorable mechanical properties. *Biofabrication* 3, 021001 (2011).
- 66 Badylak, S. F., Freytes, D. O. & Gilbert, T. W. Extracellular matrix as a biological scaffold material: Structure and function. *Acta biomaterialia* 5, 1-13 (2009).
- 67 Crapo, P. M., Gilbert, T. W. & Badylak, S. F. An overview of tissue and whole organ decellularization processes. *Biomaterials* 32, 3233-3243 (2011).
- 68 Badylak, S. F., Weiss, D. J., Caplan, A. & Macchiarini, P. Engineered whole organs and complex tissues. *Lancet* 379, 943-952 (2012).
- 69 Benders, K. E. M. *et al.* Extracellular matrix scaffolds for cartilage and bone regeneration. *Trends in biotechnology* 31, 169-176 (2013).
- 70 Medberry, C. J. *et al.* Hydrogels derived from central nervous system extracellular matrix. *Biomaterials* 34, 1033-1040 (2013).
- 71 Wolf, M. T. *et al.* A hydrogel derived from decellularized dermal extracellular matrix. *Biomaterials* 33, 7028-7038 (2012).
- 72 Billiet, T., Gevaert, E., De Schryver, T., Cornelissen, M. & Dubrue, P. The 3D printing of gelatin methacrylamide cell-laden tissue-engineered constructs with high cell viability. *Biomaterials* 35, 49-62 (2014).
- 73 Levett, P. A., Hutmacher, D. W., Malda, J. & Klein, T. J. Hyaluronic Acid enhances the mechanical properties of tissue-engineered cartilage constructs. *PLoS one* 9, e113216 (2014).
- 74 Benders, K. E. M. *et al.* Multipotent stromal cells outperform chondrocytes on cartilage-derived matrix scaffolds. *cartilage* 5, 221-230 (2014).
- 75 Shim, J. H., Lee, J. S., Kim, J. Y. & Cho, D. W. Bioprinting of a mechanically enhanced three-dimensional dual cell-laden construct for osteochondral tissue engineering using a multi-head tissue/organ building system. *Journal of Micromechanics and Microengineering* 22 (2012).
- 76 Lee, H., Ahn, S., Bonassar, L. J. & Kim, G. Cell(MC3T3-E1)-Printed Poly(ϵ -caprolactone)/Alginate Hybrid Scaffolds for Tissue Regeneration. *Macromolecular rapid communications* 34, 142-149 (2012).
- 77 Pati, F. *et al.* Printing three-dimensional tissue analogues with decellularized extracellular matrix bioink. *Nature communications* 5, 3935 (2014).
- 78 Lorentz, K. M., Kontos, S., Frey, P. & Hubbell, J. A. Engineered aprotinin for improved stability of fibrin biomaterials. *Biomaterials* 32, 430-438 (2011).
- 79 DeForest, C. A. & Anseth, K. S. Advances in bioactive hydrogels to probe and direct cell fate. *Annual review of chemical and biomolecular engineering* 3, 421-444 (2012).

- 80 Mcllwraight, C. W., Fortier, L. A., Frisbie, D. D. & Nixon, A. J. Equine Models of Articular Cartilage Repair. *Cartilage* 2, 317-326 (2011).
- 81 Ayyildiz-Tamis, D., Avci, K. & Deliloglu-Gurhan, S. I. Comparative investigation of the use of various commercial microcarriers as a substrate for culturing mammalian cells. *In vitro cellular & developmental biology. Animal* 50, 221-231 (2014).
- 82 Levato, R., Mateos-Timoneda, M. A. & Planell, J. A. Preparation of biodegradable polylactide microparticles via a biocompatible procedure. *Macromolecular Bioscience* 12, 557-566 (2012).
- 83 Malda, J. & Frondoza, C. G. Microcarriers in the engineering of cartilage and bone. *Trends in biotechnology* 24, 299-304 (2006).
- 84 James, C. B. & Uhl, T. L. A review of articular cartilage pathology and the use of glucosamine sulfate. *Journal of athletic training* 36, 413-419 (2001).
- 85 Mironov, V., Boland, T., Trusk, T., Forgacs, G. & Markwald, R. R. Organ printing: computer-aided jet-based 3D tissue engineering. *Trends Biotechnol.* 21, 157-161 (2003).
- 86 Guillemot, F., Mironov, V. & Nakamura, M. Bioprinting is coming of age: Report from the International Conference on Bioprinting and Biofabrication in Bordeaux (3B'09). *Biofabrication* 2, 010201 (2010).
- 87 Shipley, R. J. *et al.* Design criteria for a printed tissue engineering construct: a mathematical homogenization approach. *Journal of theoretical biology* 259, 489-502 (2009).
- 88 Catros, S. *et al.* Laser-assisted bioprinting for creating on-demand patterns of human osteoprogenitor cells and nano-hydroxyapatite. *Biofabrication* 3, 025001 (2011).
- 89 Hanson Shepherd, J. N. *et al.* 3D Microperiodic Hydrogel Scaffolds for Robust Neuronal Cultures. *Advanced functional materials* 21, 47-54 (2011).
- 90 Poellmann, M. J., Barton, K. L., Mishra, S. & Johnson, A. J. Patterned hydrogel substrates for cell culture with electrohydrodynamic jet printing. *Macromolecular Bioscience* 11, 1164-1168 (2011).
- 91 Choi, W. S., Ha, D., Park, S. & Kim, T. Synthetic multicellular cell-to-cell communication in inkjet printed bacterial cell systems. *Biomaterials* 32, 2500-2507 (2011).
- 92 Gruene, M. *et al.* Laser printing of three-dimensional multicellular arrays for studies of cell-cell and cell-environment interactions. *Tissue engineering. Part C, Methods* 17, 973-982 (2011).
- 93 Marga, F. *et al.* Toward engineering functional organ modules by additive manufacturing. *Biofabrication* 4, 022001 (2012).
- 94 Mironov, V., Kasyanov, V., Drake, C. & Markwald, R. R. Organ printing: promises and challenges. *Regen Med* 3, 93-103 (2008).
- 95 Lee, W. *et al.* Multi-layered culture of human skin fibroblasts and keratinocytes through three-dimensional freeform fabrication. *Biomaterials* 30, 1587-1595 (2009).
- 96 Murphy, S. V., Skardal, A. & Atala, A. Evaluation of hydrogels for bio-printing applications. *Journal of Biomedical Materials Research Part A* 101A, 272-284 (2013).
- 97 Cohen, D. L. *et al.* Increased mixing improves hydrogel homogeneity and quality of three-dimensional printed constructs. *Tissue Eng Part C Methods* 17, 239-248 (2011).
- 98 Duan, B., Hockaday, L. A., Kang, K. H. & Butcher, J. T. 3D Bioprinting of heterogeneous aortic valve conduits with alginate/gelatin hydrogels. *J Biomed Mater Res A* 101, 1255-1264 (2013).
- 99 Cui, X., Breitenkamp, K., Finn, M. G., Lotz, M. & D'Lima, D. D. Direct human cartilage repair using three-dimensional bioprinting technology. *Tissue engineering. Part A* 18, 1304-1312 (2012).
- 100 Klein, T. J. *et al.* Strategies for zonal cartilage repair using hydrogels. *Macromolecular Bioscience* 9, 1049-1058 (2009).
- 101 Fedorovich, N. E. *et al.* Hydrogels as extracellular matrices for skeletal tissue engineering: state-of-the-art and novel application in organ printing. *Tissue Eng.* 13, 1905-1925 (2007).

- 102 Visconti, R. P. *et al.* Towards organ printing: engineering an intra-organ branched vascular tree. *Expert Opin Biol Ther* 10, 409-420 (2010).
- 103 Dash, M., Chiellini, F., Ottenbrite, R. M. & Chiellini, E. Chitosan-A versatile semi-synthetic polymer in biomedical applications. *Prog Polym Sci* 36, 981-1014 (2011).
- 104 Seliktar, D. Designing cell-compatible hydrogels for biomedical applications. *Science* 336, 1124-1128 (2012).
- 105 Censi, R. *et al.* A Printable Photopolymerizable Thermosensitive p(HPMAm-lactate)-PEG Hydrogel for Tissue Engineering. *Advanced Functional Materials* 21, 1833-1842 (2011).
- 106 Fedorovich, N. E., De Wijn, J. R., Verbout, A. J., Alblas, J. & Dhert, W. J. Three-dimensional fiber deposition of cell-laden, viable, patterned constructs for bone tissue printing. *Tissue engineering. Part A* 14, 127-133 (2008).
- 107 Fedorovich, N. E. *et al.* Evaluation of photocrosslinked Lutrol hydrogel for tissue printing applications. *Biomacromolecules* 10, 1689-1696 (2009).
- 108 Smith, C. M. *et al.* Three-dimensional bioassembly tool for generating viable tissue-engineered constructs. *Tissue Eng.* 10, 1566-1576 (2004).
- 109 Bongio, M. *et al.* Biomimetic modification of synthetic hydrogels by incorporation of adhesive peptides and calcium phosphate nanoparticles: in vitro evaluation of cell behavior. *European cells & materials* 22, 359-376 (2011).
- 110 Lee, K. Y., Peters, M. C., Anderson, K. W. & Mooney, D. J. Controlled growth factor release from synthetic extracellular matrices. *Nature* 408, 998-1000 (2000).
- 111 Censi, R., Di Martino, P., Vermonden, T. & Hennink, W. E. Hydrogels for protein delivery in tissue engineering. *Journal of controlled release : official journal of the Controlled Release Society* 161, 680-692 (2012).
- 112 Hersel, U., Dahmen, C. & Kessler, H. RGD modified polymers: biomaterials for stimulated cell adhesion and beyond. *Biomaterials* 24, 4385-4415 (2003).
- 113 Kasko, A. M. & Wong, D. Y. Two-photon lithography in the future of cell-based therapeutics and regenerative medicine: a review of techniques for hydrogel patterning and controlled release. *Future medicinal chemistry* 2, 1669-1680 (2010).
- 114 Arcaute, K., Mann, B. K. & Wicker, R. B. Stereolithography of three-dimensional bioactive poly(ethylene glycol) constructs with encapsulated cells. *Ann Biomed Eng* 34, 1429-1441 (2006).
- 115 Billiet, T., Vandenhaute, M., Schelfhout, J., Van Vlierberghe, S. & Dubruel, P. A review of trends and limitations in hydrogel-rapid prototyping for tissue engineering. *Biomaterials* 33, 6020-6041 (2012).
- 116 Varghese, D. *et al.* Advances in tissue engineering: cell printing. *The Journal of thoracic and cardiovascular surgery* 129, 470-472 (2005).
- 117 Nakamura, M., Iwanaga, S., Henmi, C., Arai, K. & Nishiyama, Y. Biomatrices and biomaterials for future developments of bioprinting and biofabrication. *Biofabrication* 2, 014110 (2010).
- 118 Derby, B. Printing and prototyping of tissues and scaffolds. *Science* 338, 921-926 (2012).
- 119 Jakab, K., Neagu, A., Mironov, V. & Forgacs, G. Organ printing: fiction or science. *Biorheology* 41, 371-375 (2004).
- 120 Ferris, C. J., Gilmore, K. G., Wallace, G. G. & In het Panhuis, M. Biofabrication: an overview of the approaches used for printing of living cells. *Applied microbiology and biotechnology* 97, 4243-4258 (2013).
- 121 Khalil, S. & Sun, W. Bioprinting endothelial cells with alginate for 3D tissue constructs. *Journal of biomechanical engineering* 131, 111002 (2009).

- 122 Tirella, A., Orsini, A., Vozzi, G. & Ahluwalia, A. A phase diagram for microfabrication of geometrically controlled hydrogel scaffolds. *Biofabrication* 1, 045002 (2009).
- 123 Fardim, P. Paper and surface chemistry—Part 1: Fiber surface and wet end chemistry. *TAPPI Journal* 1 (2002).
- 124 Ballyns, J. J. *et al.* An optical method for evaluation of geometric fidelity for anatomically shaped tissue-engineered constructs. *Tissue Eng Part C Methods* 16, 693-703 (2010).
- 125 Butscher, A. *et al.* Printability of calcium phosphate powders for three-dimensional printing of tissue engineering scaffolds. *Acta Biomater* 8, 373-385 (2012).
- 126 Kang, K. H., Hockaday, L. A. & Butcher, J. T. Quantitative optimization of solid freeform deposition of aqueous hydrogels. *Biofabrication* 5, 035001 (2013).
- 127 Hockaday, L. A. *et al.* Rapid 3D printing of anatomically accurate and mechanically heterogeneous aortic valve hydrogel scaffolds. *Biofabrication* 4, 035005 (2012).
- 128 Koch, L., Gruene, M., Unger, C. & Chichkov, B. Laser assisted Cell Printing. *Curr Pharm Biotechnol* (2012).
- 129 Guillotin, B. & Guillemot, F. Cell patterning technologies for organotypic tissue fabrication. *Trends Biotechnol.* 29, 183-190 (2011).
- 130 Derby, B. Bioprinting: inkjet printing proteins and hybrid cell-containing materials and structures. *Journal of Materials Chemistry* 18, 5717-5721 (2008).
- 131 Cui, X., Dean, D., Ruggeri, Z. M. & Boland, T. Cell damage evaluation of thermal inkjet printed Chinese hamster ovary cells. *Biotechnol Bioeng* 106, 963-969 (2010).
- 132 Nakamura, M. *et al.* Biocompatible inkjet printing technique for designed seeding of individual living cells. *Tissue Eng.* 11, 1658-1666 (2005).
- 133 Arai, K. *et al.* Three-dimensional inkjet biofabrication based on designed images. *Biofabrication* 3, 034113 (2011).
- 134 Calvert, P. Inkjet printing for materials and devices. *Chem Mater* 13, 3299-3305 (2001).
- 135 Moon, S. *et al.* Layer by layer three-dimensional tissue epitaxy by cell-laden hydrogel droplets. *Tissue Eng Part C Methods* 16, 157-166 (2010).
- 136 Chahal, D., Ahmadi, A. & Cheung, K. C. Improving piezoelectric cell printing accuracy and reliability through neutral buoyancy of suspensions. *Biotechnol Bioeng* 109, 2932-2940 (2012).
- 137 Duarte Campos, D. F. *et al.* Three-dimensional printing of stem cell-laden hydrogels submerged in a hydrophobic high-density fluid. *Biofabrication* 5, 015003 (2013).
- 138 Maher, P. S., Keatch, R. P., Donnelly, K., Mackay, R. E. & Paxton, J. Z. Construction of 3D biological matrices using rapid prototyping technology. *Rapid Prototyping Journal* 15, 204-210 (2009).
- 139 Bryant, S. J. & Anseth, K. S. Hydrogel properties influence ECM production by chondrocytes photoencapsulated in poly(ethylene glycol) hydrogels. *J Biomed Mater Res* 59, 63-72 (2002).
- 140 Nicodemus, G. D. & Bryant, S. J. Cell encapsulation in biodegradable hydrogels for tissue engineering applications. *Tissue Eng Pt B-Rev* 14, 149-165 (2008).
- 141 Aguado, B. A., Mulyasmita, W., Su, J., Lampe, K. J. & Heilshorn, S. C. Improving viability of stem cells during syringe needle flow through the design of hydrogel cell carriers. *Tissue Eng Part A* 18, 806-815 (2012).
- 142 Feugier, P., Black, R. A., Hunt, J. A. & How, T. V. Attachment, morphology and adherence of human endothelial cells to vascular prosthesis materials under the action of shear stress. *Biomaterials* 26, 1457-1466 (2005).
- 143 Morigi, M. *et al.* Fluid shear-stress modulates surface expression of adhesion molecules by endothelial-cells. *Blood* 85, 1696-1703 (1995).

- 144 van der Meer, A. D., Poot, A. A., Feijen, J. & Vermes, I. Analyzing shear stress-induced alignment of actin filaments in endothelial cells with a microfluidic assay. *Biomicrofluidics* 4 (2010).
- 145 Macario, D. K., Entersz, I., Abboud, J. P. & Nackman, G. B. Inhibition of apoptosis prevents shear-induced detachment of endothelial cells. *J Surg Res* 147, 282-289 (2008).
- 146 Smith, R. L., Carter, D. R. & Schurman, D. J. Pressure and shear differentially alter human articular chondrocyte metabolism: a review. *Clin Orthop Relat Res*, S89-95 (2004).
- 147 Saunders, R. E., Gough, J. E. & Derby, B. Delivery of human fibroblast cells by piezoelectric drop-on-demand inkjet printing. *Biomaterials* 29, 193-203 (2008).
- 148 Fedorovich, N. E. *et al.* Biofabrication of Osteochondral Tissue Equivalents by Printing Topologically Defined, Cell-Laden Hydrogel Scaffolds. *Tissue engineering. Part C, Methods* (2011).
- 149 Guvendiren, M., Lu, H. D. & Burdick, J. A. Shear-thinning hydrogels for biomedical applications. *Soft Matter* 8, 260-272 (2012).
- 150 Rezende, R. A., Bartolo, P. J., Mendes, A. & Maciel, R. Rheological Behavior of Alginate Solutions for Biomanufacturing. *Journal of Applied Polymer Science* 113, 3866-3871 (2009).
- 151 Tang, J. M., Tung, M. A. & Zeng, Y. Y. Compression strength and deformation of gellan gels formed with mono- and divalent cations. *Carbohydrate polymers* 29, 11-16 (1996).
- 152 Mart, R. J., Osborne, R. D., Stevens, M. M. & Ulijn, R. V. Peptide-based stimuli-responsive biomaterials. *Soft Matter* 2, 822-835 (2006).
- 153 Banta, S., Wheeldon, I. R. & Blenner, M. Protein Engineering in the Development of Functional Hydrogels. *Annual Review of Biomedical Engineering* 12, 167-186 (2010).
- 154 Wang, Q., Wang, J., Lu, Q., Detamore, M. S. & Berkland, C. Injectable PLGA based colloidal gels for zero-order dexamethasone release in cranial defects. *Biomaterials* 31, 4980-4986 (2010).
- 155 Araki, J. & Ito, K. Recent advances in the preparation of cyclodextrin-based polyrotaxanes and their applications to soft materials. *Soft Matter* 3, 1456-1473 (2007).
- 156 Landers, R., Hubner, U., Schmelzeisen, R. & Mulhaupt, R. Rapid prototyping of scaffolds derived from thermoreversible hydrogels and tailored for applications in tissue engineering. *Biomaterials* 23, 4437-4447 (2002).
- 157 Pfister, A. *et al.* Biofunctional Rapid Prototyping for Tissue-Engineering Applications: 3D Bioplotting versus 3D Printing. *Journal of Polymer Science: Part A: Polymer Chemistry* 42, 624-638 (2004).
- 158 Chang, C. C., Boland, E. D., Williams, S. K. & Hoying, J. B. Direct-write bioprinting three-dimensional biohybrid systems for future regenerative therapies. *Journal of Biomedical Materials Research Part B-Applied Biomaterials* 98B, 160-170 (2011).
- 159 Dankers, P. Y. W., Harmsen, M. C., Brouwer, L. A., Van Luyn, M. J. A. & Meijer, E. W. A modular and supramolecular approach to bioactive scaffolds for tissue engineering. *Nature Materials* 4, 568-574 (2005).
- 160 Gacesa, P. Alginates. *Carbohydrate Polymers* 8, 162-181 (1988).
- 161 Wee, S. & Gombotz, W. R. Protein release from alginate matrices. *Adv Drug Deliv Rev* 31, 267-285 (1998).
- 162 Kolambkar, Y. M. *et al.* An alginate-based hybrid system for growth factor delivery in the functional repair of large bone defects. *Biomaterials* 32, 65-74 (2011).
- 163 Van Tomme, S. R., van Steenberghe, M. J., De Smedt, S. C., van Nostrum, C. F. & Hennink, W. E. Self-gelling hydrogels based on oppositely charged dextran microspheres. *Biomaterials* 26, 2129-2135 (2005).
- 164 Wang, Q., Wang, L., Detamore, M. S. & Berkland, C. Biodegradable colloidal gels as moldable tissue engineering scaffolds. *Adv Mater* 20, 236-239 (2008).

- 165 de Jong, S. J., van Dijk-Wolthuis, W. N. E., Kettenes-van den Bosch, J. J., Schuyl, P. J. W. & Hennink, W. E. Monodisperse enantiomeric lactic acid oligomers: Preparation, characterization, and stereocomplex formation. *Macromolecules* 31, 6397-6402 (1998).
- 166 Rashkov, I., Manolova, N., Li, S. M., Espartero, J. L. & Vert, M. Synthesis, characterization, and hydrolytic degradation of PLA/PEO/PLA triblock copolymers with short poly(L-lactic acid) chains. *Macromolecules* 29, 50-56 (1996).
- 167 Buwalda, S. J., Dijkstra, P. J., Calucci, L., Forte, C. & Feijen, J. Influence of amide versus ester linkages on the properties of eight-armed PEG-PLA star block copolymer hydrogels. *Biomacromolecules* 11, 224-232 (2010).
- 168 Li, L. *et al.* Polymer Networks Assembled by Host-Guest Inclusion between Adamantyl and β -Cyclodextrin Substituents on Poly(acrylic acid) in Aqueous Solution. *Macromolecules* 41, 8677-8681 (2008).
- 169 van de Manakker, F. *et al.* Protein-Release Behavior of Self-Assembled PEG- β -Cyclodextrin/PEG-Cholesterol Hydrogels. *Adv Funct Mater* 19, 2992-3001 (2009).
- 170 Kretschmann, O. *et al.* Switchable hydrogels obtained by supramolecular cross-linking of adamantyl-containing LCST copolymers with cyclodextrin dimers. *Angewandte Chemie* 45, 4361-4365 (2006).
- 171 Hennink, W. E. & van Nostrum, C. F. Novel crosslinking methods to design hydrogels. *Advanced drug delivery reviews* 54, 13-36 (2002).
- 172 Chaterji, S., Kwon, I. K. & Park, K. Smart Polymeric Gels: Redefining the Limits of Biomedical Devices. *Prog Polym Sci* 32, 1083-1122 (2007).
- 173 Peppas, N. A. & Leobandung, W. Stimuli-sensitive hydrogels: ideal carriers for chronobiology and chronotherapy. *J Biomater Sci Polym Ed* 15, 125-144 (2004).
- 174 Thomas, J. D., Fussell, G., Sarkar, S., Lowman, A. M. & Marcolongo, M. Synthesis and recovery characteristics of branched and grafted PNIPAAm-PEG hydrogels for the development of an injectable load-bearing nucleus pulposus replacement. *Acta Biomater* 6, 1319-1328 (2010).
- 175 Klouda, L. & Mikos, A. G. Thermoresponsive hydrogels in biomedical applications. *European journal of pharmaceuticals and biopharmaceutics : official journal of Arbeitsgemeinschaft fur Pharmazeutische Verfahrenstechnik e.V* 68, 34-45 (2008).
- 176 Joo, M. K., Park, M. H., Choi, B. G. & Jeong, B. Reverse thermogelling biodegradable polymer aqueous solutions. *J Mater Chem* 19, 5891-5905 (2009).
- 177 Park, M. H., Joo, M. K., Choi, B. G. & Jeong, B. Biodegradable thermogels. *Accounts of chemical research* 45, 424-433 (2012).
- 178 Skardal, A. *et al.* Photocrosslinkable hyaluronan-gelatin hydrogels for two-step bioprinting. *Tissue engineering. Part A* 16, 2675-2685 (2010).
- 179 Cohen, D. L., Malone, E., Lipson, H. & Bonassar, L. J. Direct freeform fabrication of seeded hydrogels in arbitrary geometries. *Tissue engineering* 12, 1325-1335 (2006).
- 180 Censi, R., Fieten, P. J., Di Martino, P., Hennink, W. E. & Vermonden, T. In-situ forming hydrogels by simultaneous thermal gelling and Michael addition reaction between methacrylate bearing thermosensitive triblock copolymers and thiolated hyaluronan. *Journal of controlled release : official journal of the Controlled Release Society* 148, e28-29 (2010).
- 181 Lallana, E., Sousa-Herves, A., Fernandez-Trillo, F., Riguera, R. & Fernandez-Megia, E. Click chemistry for drug delivery nanosystems. *Pharm Res* 29, 1-34 (2012).
- 182 Teixeira, L. S., Feijen, J., van Blitterswijk, C. A., Dijkstra, P. J. & Karperien, M. Enzyme-catalyzed crosslinkable hydrogels: emerging strategies for tissue engineering. *Biomaterials* 33, 1281-1290 (2012).

- 183 Pescosolido, L. *et al.* Hyaluronic acid and dextran-based semi-IPN hydrogels as biomaterials for bioprinting. *Biomacromolecules* 12, 1831-1838 (2011).
- 184 Dang, F. *et al.* Replica multichannel polymer chips with a network of sacrificial channels sealed by adhesive printing method. *Lab on a chip* 5, 472-478 (2005).
- 185 Miller, J. S. *et al.* Rapid casting of patterned vascular networks for perfusable engineered three-dimensional tissues. *Nature materials* 11, 768-774 (2012).
- 186 Gan, Z., Zhang, L. & Chen, G. Solvent bonding of poly(methyl methacrylate) microfluidic chip using phase-changing agar hydrogel as a sacrificial layer. *Electrophoresis* 32, 3319-3323 (2011).
- 187 Reed, H. A. *et al.* Fabrication of microchannels using polycarbonates as sacrificial materials. *Journal of Micromechanics and Microengineering* 11, 733-737 (2001).
- 188 Golden, A. P. & Tien, J. Fabrication of microfluidic hydrogels using molded gelatin as a sacrificial element. *Lab on a chip* 7, 720-725 (2007).
- 189 Ling, Y. *et al.* A cell-laden microfluidic hydrogel. *Lab on a chip* 7, 756-762 (2007).
- 190 Visser, J. *et al.* Biofabrication of multi-material anatomically shaped tissue constructs. *Biofabrication* 5, 035007 (2013).
- 191 Reiffel, A. J. *et al.* High-fidelity tissue engineering of patient-specific auricles for reconstruction of pediatric microtia and other auricular deformities. *PLoS One* 8, e56506 (2013).
- 192 Shin, S. R. *et al.* Carbon nanotube reinforced hybrid microgels as scaffold materials for cell encapsulation. *Acs Nano* 6, 362-372 (2012).
- 193 Erickson, I. E. *et al.* High mesenchymal stem cell seeding densities in hyaluronic acid hydrogels produce engineered cartilage with native tissue properties. *Acta biomaterialia* 8, 3027-3034 (2012).
- 194 Patel, P. N., Gobin, A. S., West, J. L. & Patrick, C. W., Jr. Poly(ethylene glycol) hydrogel system supports preadipocyte viability, adhesion, and proliferation. *Tissue engineering* 11, 1498-1505 (2005).
- 195 Shin, H., Olsen, B. D. & Khademhosseini, A. The mechanical properties and cytotoxicity of cell-laden double-network hydrogels based on photocrosslinkable gelatin and gellan gum biomacromolecules. *Biomaterials* 33, 3143-3152 (2012).
- 196 Myung, D. *et al.* Biomimetic strain hardening in interpenetrating polymer network hydrogels. *Polymer* 48, 5376-5387 (2007).
- 197 Suri, S. & Schmidt, C. E. Photopatterned collagen-hyaluronic acid interpenetrating polymer network hydrogels. *Acta biomaterialia* 5, 2385-2397 (2009).
- 198 Min Kyoon, S. *et al.* A tough nanofiber hydrogel incorporating ferritin. *Appl. Phys. Lett.* 93, 3 (2008).
- 199 Min Kyoon Shin, S. I. K., Seon Jeong Kim, Byung Joo Kim, Insuk So, Mikhail E. Kozlov, Jiyoung Oh, and Ray H. Baughman. A tough nanofiber hydrogel incorporating ferritin. *Appl. Phys. Lett.* 93, 3 (2008).
- 200 Saez-Martinez V, G.-G. S., Vera C, Olalde B, Madarieta I, Obieta I, Garagorri N. New Hybrid System: Poly(ethylene glycol) Hydrogel with Covalently Bonded Pegylated Nanotubes. *Journal of Applied Polymer Science* 120, 124-132 (2010).
- 201 Xu, T. *et al.* Hybrid printing of mechanically and biologically improved constructs for cartilage tissue engineering applications. *Biofabrication* 5, 015001 (2012).
- 202 Shim, J. H., Kim, J. Y., Park, M., Park, J. & Cho, D. W. Development of a hybrid scaffold with synthetic biomaterials and hydrogel using solid freeform fabrication technology. *Biofabrication* 3, 034102 (2011).
- 203 Catros, S. *et al.* Layer-by-layer tissue microfabrication supports cell proliferation in vitro and in vivo. *Tissue engineering. Part C, Methods* 18, 62-70 (2012).

- 204 Pham, Q. P., Sharma, U. & Mikos, A. G. Electrospun poly(epsilon-caprolactone) microfiber and multilayer nanofiber/microfiber scaffolds: characterization of scaffolds and measurement of cellular infiltration. *Biomacromolecules* 7, 2796-2805 (2006).
- 205 Dalton, P. D. *et al.* Electrospinning and additive manufacturing: converging technologies. *biomaterials science* 1, 171-185 (2013).
- 206 Farrugia, B. L. *et al.* Dermal fibroblast infiltration of poly(epsilon-caprolactone) scaffolds fabricated by melt electrospinning in a direct writing mode. *Biofabrication* 5, 025001 (2013).
- 207 Forgacs, G. Tissue engineering: Perfusable vascular networks. *Nat Mater* 11, 746-747 (2012).
- 208 Temenoff, J. S., Shin, H., Conway, D. E., Engel, P. S. & Mikos, A. G. In vitro cytotoxicity of redox radical initiators for cross-linking of oligo(poly(ethylene glycol) fumarate) macromers. *Biomacromolecules* 4, 1605-1613 (2003).
- 209 Williams, C. G., Malik, A. N., Kim, T. K., Manson, P. N. & Elisseeff, J. H. Variable cytocompatibility of six cell lines with photoinitiators used for polymerizing hydrogels and cell encapsulation. *Biomaterials* 26, 1211-1218 (2005).
- 210 Johnson, J. A., Turro, N. J., Koberstein, J. T. & Mark, J. E. Some hydrogels having novel molecular structures. *Prog Polym Sci* 35, 332-337 (2010).
- 211 Haque, M. A., Kurokawa, T. & Gong, J. P. Super tough double network hydrogels and their application as biomaterials. *Polymer* 53, 1805-1822 (2012).
- 212 Azuma, C. *et al.* Biodegradation of high-toughness double network hydrogels as potential materials for artificial cartilage. *J Biomed Mater Res A* 81, 373-380 (2007).
- 213 Harrass, K., Kruger, R., Moller, M., Albrecht, K. & Groll, J. Mechanically strong hydrogels with reversible behaviour under cyclic compression with MPa loading. *Soft Matter* 9, 2869-2877 (2013).
- 214 Gong, J. P. Why are double network hydrogels so tough? *Soft Matter* 6, 2583-2590 (2010).
- 215 Rivron, N. C. *et al.* Tissue assembly and organization: developmental mechanisms in microfabricated tissues. *Biomaterials* 30, 4851-4858 (2009).
- 216 Cohen, D. L. *et al.* Increased mixing improves hydrogel homogeneity and quality of three-dimensional printed constructs. *Tissue engineering. Part C, Methods* 17, 239-248 (2011).
- 217 Koch, L. *et al.* Skin tissue generation by laser cell printing. *Biotechnology and bioengineering* 109, 1855-1863 (2012).
- 218 Guillotin, B. *et al.* Laser assisted bioprinting of engineered tissue with high cell density and microscale organization. *Biomaterials* 31, 7250-7256 (2010).
- 219 Yan, J., Huang, Y. & Chrissey, D. B. Laser-assisted printing of alginate long tubes and annular constructs. *Biofabrication* 5, 015002 (2013).
- 220 Boland, T., Xu, T., Damon, B. & Cui, X. Application of inkjet printing to tissue engineering. *Biotechnology journal* 1, 910-917 (2006).
- 221 Xu, T. *et al.* Complex heterogeneous tissue constructs containing multiple cell types prepared by inkjet printing technology. *Biomaterials* 34, 130-139 (2013).
- 222 Jakab, K. *et al.* Tissue engineering by self-assembly of cells printed into topologically defined structures. *Tissue Engineering Part A* 14, 413-421 (2008).
- 223 Landers, R. *et al.* Fabrication of soft tissue engineering scaffolds by means of rapid prototyping techniques. *Journal of Materials Science* 37, 3107-3116 (2002).
- 224 Norotte, C., Marga, F. S., Niklason, L. E. & Forgacs, G. Scaffold-free vascular tissue engineering using bioprinting. *Biomaterials* 30, 5910-5917 (2009).
- 225 Cohen, D. L., Lipton, J. I., Bonassar, L. J. & Lipson, H. Additive manufacturing for in situ repair of osteochondral defects. *Biofabrication* 2, 035004 (2010).

- 226 Khalil, S., Nam, J. & Sun, W. Multi-nozzle deposition for construction of 3D biopolymer tissue scaffolds. *Rapid Prototyping Journal* 11, 9-17 (2005).
- 227 Song, S. J. *et al.* Sodium alginate hydrogel-based bioprinting using a novel multinozzle bioprinting system. *Artificial Organs* 35, 1132-1136 (2011).
- 228 Zhang, Y., Yu, Y., Chen, H. & Ozbolat, I. T. Characterization of printable cellular micro-fluidic channels for tissue engineering. *Biofabrication* 5, 025004 (2013).
- 229 Yan, Y. N. *et al.* Direct construction of a three-dimensional structure with cells and hydrogel. *Journal of Bioactive and Compatible Polymers* 20, 259-269 (2005).
- 230 Smith, C. M., Christian, J. J., Warren, W. L. & Williams, S. K. Characterizing environmental factors that impact the viability of tissue-engineered constructs fabricated by a direct-write bioassembly tool. *Tissue Engineering* 13, 373-383 (2007).
- 231 Lee, W. *et al.* On-demand three-dimensional freeform fabrication of multi-layered hydrogel scaffold with fluidic channels. *Biotechnology and Bioengineering* 105, 1178-1186 (2010).
- 232 Wang, X. *et al.* Generation of three-dimensional hepatocyte/gelatin structures with rapid prototyping system. *Tissue Engineering* 12, 83-90 (2006).
- 233 Zhang, T. *et al.* Three-dimensional gelatin and gelatin/hyaluronan hydrogel structures for traumatic brain injury. *Journal of Bioactive and Compatible Polymers* 22, 19-29 (2007).
- 234 Li, S. J. *et al.* Direct Fabrication of a Hybrid Cell/Hydrogel Construct by a Double-nozzle Assembling Technology. *Journal of Bioactive and Compatible Polymers* 24, 249-265 (2009).
- 235 Xu, M., Wang, X., Yan, Y., Yao, R. & Ge, Y. An cell-assembly derived physiological 3D model of the metabolic syndrome, based on adipose-derived stromal cells and a gelatin/alginate/fibrinogen matrix. *Biomaterials* 31, 3868-3877 (2010).
- 236 Yan, Y. *et al.* Fabrication of viable tissue-engineered constructs with 3D cell-assembly technique. *Biomaterials* 26, 5864-5871 (2005).
- 237 Cheng, J. *et al.* Rheological properties of cell-hydrogel composites extruding through small-diameter tips. *Journal of Manufacturing Science and Engineering-Transactions of the Asme* 130 (2008).
- 238 Xu, W. *et al.* Rapid prototyping three-dimensional cell/gelatin/fibrinogen constructs for medical regeneration. *Journal of Bioactive and Compatible Polymers* 22, 363-377 (2007).
- 239 Snyder, J. E. *et al.* Bioprinting cell-laden matrigel for radioprotection study of liver by pro-drug conversion in a dual-tissue microfluidic chip. *Biofabrication* 3, 034112 (2011).
- 240 Iwami, K. *et al.* Bio rapid prototyping by extruding/aspirating/refilling thermoreversible hydrogel. *Biofabrication* 2, 014108 (2010).
- 241 Skardal, A., Zhang, J. & Prestwich, G. D. Bioprinting vessel-like constructs using hyaluronan hydrogels crosslinked with tetrahedral polyethylene glycol tetracrylates. *Biomaterials* 31, 6173-6181 (2010).
- 242 Gonzalez-tello, P., Camacho, F. & Blazquez, G. Density and Viscosity of Concentrated Aqueous-Solutions of Polyethylene-Glycol. *J Chem Eng Data* 39, 611-614 (1994).
- 243 Knapp, D. M. *et al.* Rheology of reconstituted type I collagen gel in confined compression. *J Rheol* 41, 971-993 (1997).
- 244 Badylak, S. F. *et al.* Biologic scaffolds for constructive tissue remodeling. *Biomaterials* 32, 316-319 (2011).
- 245 Huey, D. J., Hu, J. C. & Athanasiou, K. A. Unlike bone, cartilage regeneration remains elusive. *Science* 338, 917-921 (2012).
- 246 Malda, J. *et al.* 25th anniversary article: engineering hydrogels for biofabrication. *Advanced materials* 25, 5011-5028 (2013).

- 247 Moreira Teixeira, L. S. *et al.* The effect of platelet lysate supplementation of a dextran-based hydrogel on cartilage formation. *Biomaterials* 33, 3651-3661 (2012).
- 248 Nguyen, L. H., Kudva, A. K., Guckert, N. L., Linse, K. D. & Roy, K. Unique biomaterial compositions direct bone marrow stem cells into specific chondrocytic phenotypes corresponding to the various zones of articular cartilage. *Biomaterials* 32, 1327-1338 (2011).
- 249 Freytes, D. O., Martin, J., Velankar, S. S., Lee, A. S. & Badylak, S. F. Preparation and rheological characterization of a gel form of the porcine urinary bladder matrix. *Biomaterials* 29, 1630-1637 (2008).
- 250 Mescher, A. L. Junqueira's basic histology: Text & atlas, 12th edition. *The McGraw-Hill Companies*.
- 251 Klatt, A. R. *et al.* A critical role for collagen II in cartilage matrix degradation: collagen II induces pro-inflammatory cytokines and MMPs in primary human chondrocytes. *Journal of orthopaedic research : official publication of the Orthopaedic Research Society* 27, 65-70 (2009).
- 252 Fichter, M. *et al.* Collagen degradation products modulate matrix metalloproteinase expression in cultured articular chondrocytes. *Journal of orthopaedic research : official publication of the Orthopaedic Research Society* 24, 63-70 (2006).
- 253 Delcogliano, M. *et al.* Use of innovative biomimetic scaffold in the treatment for large osteochondral lesions of the knee. *Knee surgery, sports traumatology, arthroscopy : official journal of the ESSKA* 22, 1260-1269 (2014).
- 254 Zheng, M. H. *et al.* Matrix-induced autologous chondrocyte implantation (MACI): biological and histological assessment. *Tissue engineering* 13, 737-746 (2007).
- 255 Boere, K. W. *et al.* Covalent attachment of a three-dimensionally printed thermoplast to a gelatin hydrogel for mechanically enhanced cartilage constructs. *Acta biomaterialia* 10, 2602-2611 (2014).
- 256 Nikkhah, M. *et al.* Directed endothelial cell morphogenesis in micropatterned gelatin methacrylate hydrogels. *Biomaterials* 33, 9009-9018 (2012).
- 257 Nichol, J. W. *et al.* Cell-laden microengineered gelatin methacrylate hydrogels. *Biomaterials* 31, 5536-5544 (2010).
- 258 Piper, D. W. & Fenton, B. H. Ph Stability and Activity Curves of Pepsin with Special Reference to Their Clinical Importance. *Gut* 6, 506-& (1965).
- 259 Gawlitta, D. *et al.* Modulating endochondral ossification of multipotent stromal cells for bone regeneration. *Tissue engineering. Part B, Reviews* 16, 385-395 (2010).
- 260 Pittenger, M. F. *et al.* Multilineage potential of adult human mesenchymal stem cells. *Science* 284, 143-147 (1999).
- 261 Chomczynski, P. & Mackey, K. Substitution of Chloroform by Bromochloropropane in the Single-Step Method of Rna Isolation. *Analytical Biochemistry* 225, 163-164 (1995).
- 262 Fujiwara, T. *et al.* Direct contact of fibroblasts with neuronal processes promotes differentiation to myofibroblasts and induces contraction of collagen matrix in vitro. *Wound repair and regeneration : official publication of the Wound Healing Society [and] the European Tissue Repair Society* 21, 588-594 (2013).
- 263 Yang, G. *et al.* Enhancement of tenogenic differentiation of human adipose stem cells by tendon-derived extracellular matrix. *Biomaterials* 34, 9295-9306 (2013).
- 264 Williams, C. G. *et al.* In vitro chondrogenesis of bone marrow-derived mesenchymal stem cells in a photopolymerizing hydrogel. *Tissue engineering* 9, 679-688 (2003).
- 265 Erickson, I. E. *et al.* Differential maturation and structure-function relationships in mesenchymal stem cell- and chondrocyte-seeded hydrogels. *Tissue engineering. Part A* 15, 1041-1052 (2009).
- 266 Carter-Arnold, J. L., Neilsen, N. L., Amelse, L. L., Odoi, A. & Dhar, M. S. In vitro analysis of equine, bone marrow-derived mesenchymal stem cells demonstrates differences within age- and gender-matched horses. *Equine veterinary journal* 46, 589-595 (2014).

- 267 Xu, L. *et al.* Increased expression of the collagen receptor discoidin domain receptor 2 in articular cartilage as a key event in the pathogenesis of osteoarthritis. *Arthritis and rheumatism* 56, 2663-2673 (2007).
- 268 Zhang, Y. *et al.* An essential role of discoidin domain receptor 2 (DDR2) in osteoblast differentiation and chondrocyte maturation via modulation of Runx2 activation. *Journal of bone and mineral research : the official journal of the American Society for Bone and Mineral Research* 26, 604-617 (2011).
- 269 Nehrer, S. *et al.* Canine chondrocytes seeded in type I and type II collagen implants investigated in vitro. *Journal of biomedical materials research* 38, 95-104 (1997).
- 270 Nehrer, S. *et al.* Matrix collagen type and pore size influence behaviour of seeded canine chondrocytes. *Biomaterials* 18, 769-776 (1997).
- 271 Rutgers, M. *et al.* Effect of collagen type I or type II on chondrogenesis by cultured human articular chondrocytes. *Tissue engineering. Part A* 19, 59-65 (2013).
- 272 Schwarz, S. *et al.* Processed xenogenic cartilage as innovative biomatrix for cartilage tissue engineering: effects on chondrocyte differentiation and function. *Journal of tissue engineering and regenerative medicine* (2012).
- 273 Chun, S. Y. *et al.* Identification and characterization of bioactive factors in bladder submucosa matrix. *Biomaterials* 28, 4251-4256 (2007).
- 274 Voytik-Harbin, S. L., Brightman, A. O., Kraine, M. R., Waisner, B. & Badylak, S. F. Identification of extractable growth factors from small intestinal submucosa. *Journal of cellular biochemistry* 67, 478-491 (1997).
- 275 Chen, C. C. *et al.* Cartilage fragments from osteoarthritic knee promote chondrogenesis of mesenchymal stem cells without exogenous growth factor induction. *Journal of orthopaedic research : official publication of the Orthopaedic Research Society* 30, 393-400 (2012).
- 276 Xue, J. X. *et al.* Chondrogenic differentiation of bone marrow-derived mesenchymal stem cells induced by acellular cartilage sheets. *Biomaterials* 33, 5832-5840 (2012).
- 277 Bosnakovski, D. *et al.* Chondrogenic differentiation of bovine bone marrow mesenchymal stem cells (MSCs) in different hydrogels: influence of collagen type II extracellular matrix on MSC chondrogenesis. *Biotechnology and bioengineering* 93, 1152-1163 (2006).
- 278 Kronenberg, H. M. Developmental regulation of the growth plate. *Nature* 423, 332-336 (2003).
- 279 Scammell, B. E. & Roach, H. I. A new role for the chondrocyte in fracture repair: endochondral ossification includes direct bone formation by former chondrocytes. *Journal of bone and mineral research : the official journal of the American Society for Bone and Mineral Research* 11, 737-745 (1996).
- 280 Mackie, E. J., Tatarczuch, L. & Mirams, M. The skeleton: a multi-functional complex organ: the growth plate chondrocyte and endochondral ossification. *The Journal of endocrinology* 211, 109-121 (2011).
- 281 Ma, J. *et al.* Concise review: cell-based strategies in bone tissue engineering and regenerative medicine. *Stem cells translational medicine* 3, 98-107 (2014).
- 282 Dawson, J. I., Kanczler, J., Tare, R., Kassem, M. & Oreffo, R. C. Bridging the gap: Bone regeneration using skeletal stem cell-based strategies - Where are we now? *Stem cells* 32, 35-44 (2013).
- 283 Kolesky, D. B. *et al.* 3D Bioprinting of Vascularized, Heterogeneous Cell-Laden Tissue Constructs. *Advanced materials* 26, 3124-3130 (2014).
- 284 Hirao, M., Tamai, N., Tsumaki, N., Yoshikawa, H. & Myoui, A. Oxygen tension regulates chondrocyte differentiation and function during endochondral ossification. *The Journal of biological chemistry* 281, 31079-31092 (2006).

- 285 Grimshaw, M. J. & Mason, R. M. Bovine articular chondrocyte function in vitro depends upon oxygen tension. *Osteoarthritis and cartilage / OARS, Osteoarthritis Research Society* 8, 386-392 (2000).
- 286 Scotti, C. *et al.* Recapitulation of endochondral bone formation using human adult mesenchymal stem cells as a paradigm for developmental engineering. *Proceedings of the National Academy of Sciences of the United States of America* 107, 7251-7256 (2010).
- 287 Pelttari, K. *et al.* Premature induction of hypertrophy during in vitro chondrogenesis of human mesenchymal stem cells correlates with calcification and vascular invasion after ectopic transplantation in SCID mice. *Arthritis and rheumatism* 54, 3254-3266 (2006).
- 288 Farrell, E. *et al.* In-vivo generation of bone via endochondral ossification by in-vitro chondrogenic priming of adult human and rat mesenchymal stem cells. *BMC musculoskeletal disorders* 12, 31 (2011).
- 289 van der Stok, J. *et al.* Chondrogenically differentiated mesenchymal stromal cell pellets stimulate endochondral bone regeneration in critical-sized bone defects. *European cells & materials* 27, 137-148 (2014).
- 290 Bahney, C. S. *et al.* Stem cell-derived endochondral cartilage stimulates bone healing by tissue transformation. *Journal of bone and mineral research : the official journal of the American Society for Bone and Mineral Research* 29, 1269-1282 (2014).
- 291 Harada, N. *et al.* Bone regeneration in a massive rat femur defect through endochondral ossification achieved with chondrogenically differentiated MSCs in a degradable scaffold. *Biomaterials* 35, 7800-7810 (2014).
- 292 Janicki, P., Kasten, P., Kleinschmidt, K., Luginbuehl, R. & Richter, W. Chondrogenic pre-induction of human mesenchymal stem cells on beta-TCP: enhanced bone quality by endochondral heterotopic bone formation. *Acta biomaterialia* 6, 3292-3301 (2010).
- 293 Sheehy, E. J., Vinardell, T., Buckley, C. T. & Kelly, D. J. Engineering osteochondral constructs through spatial regulation of endochondral ossification. *Acta biomaterialia* 9, 5484-5492 (2013).
- 294 Benton, J. A., DeForest, C. A., Vivekanandan, V. & Anseth, K. S. Photocrosslinking of gelatin macromers to synthesize porous hydrogels that promote valvular interstitial cell function. *Tissue engineering. Part A* 15, 3221-3230 (2009).
- 295 Gawlitta, D., van Rijen, M. H., Schrijver, E. J., Alblas, J. & Dhert, W. J. Hypoxia impedes hypertrophic chondrogenesis of human multipotent stromal cells. *Tissue engineering. Part A* 18, 1957-1966 (2012).
- 296 van Gaalen, S. M. *et al.* Use of fluorochrome labels in in vivo bone tissue engineering research. *Tissue engineering. Part B, Reviews* 16, 209-217 (2010).
- 297 Hildebrand, T., Laib, A., Muller, R., Dequeker, J. & Ruegsegger, P. Direct three-dimensional morphometric analysis of human cancellous bone: microstructural data from spine, femur, iliac crest, and calcaneus. *Journal of bone and mineral research : the official journal of the American Society for Bone and Mineral Research* 14, 1167-1174 (1999).
- 298 Kruyt, M. C. *et al.* Analysis of ectopic and orthotopic bone formation in cell-based tissue-engineered constructs in goats. *Biomaterials* 28, 1798-1805 (2007).
- 299 Kruyt, M. *et al.* Analysis of the dynamics of bone formation, effect of cell seeding density, and potential of allogeneic cells in cell-based bone tissue engineering in goats. *Tissue engineering. Part A* 14, 1081-1088 (2008).
- 300 Vonk, L. A. *et al.* Preservation of the chondrocyte's pericellular matrix improves cell-induced cartilage formation. *Journal of cellular biochemistry* 110, 260-271 (2010).

- 301 Fischer, J., Dickhut, A., Rickert, M. & Richter, W. Human articular chondrocytes secrete parathyroid hormone-related protein and inhibit hypertrophy of mesenchymal stem cells in coculture during chondrogenesis. *Arthritis and rheumatism* 62, 2696-2706 (2010).
- 302 Vermonden, T., Censi, R. & Hennink, W. E. Hydrogels for protein delivery. *Chem Rev* 112, 2853-2888 (2012).
- 303 Abbott, A. Cell culture: biology's new dimension. *Nature* 424, 870-872 (2003).
- 304 Bian, L. *et al.* Enhanced MSC chondrogenesis following delivery of TGF- β 3 from alginate microspheres within hyaluronic acid hydrogels in vitro and in vivo. *Biomaterials* 32, 6425-6434 (2011).
- 305 Rustad, K. C. *et al.* Enhancement of mesenchymal stem cell angiogenic capacity and stemness by a biomimetic hydrogel scaffold. *Biomaterials* 33, 80-90 (2012).
- 306 Klein, T. J. *et al.* Long-term effects of hydrogel properties on human chondrocyte behavior. *Soft Matter* 6, 5175-5183 (2010).
- 307 Anseth, K. S., Bowman, C. N. & Brannon-Peppas, L. Mechanical properties of hydrogels and their experimental determination. *Biomaterials* 17, 1647-1657 (1996).
- 308 Matricardi, P., Di Meo, C., Coviello, T., Hennink, W. E. & Alhaique, F. Interpenetrating Polymer Networks polysaccharide hydrogels for drug delivery and tissue engineering. *Advanced drug delivery reviews* (2013).
- 309 Krüger, R. & Groll, J. Fiber reinforced calcium phosphate cements - on the way to degradable load bearing bone substitutes? *Biomaterials* 33, 5887-5900 (2012).
- 310 Shin, M. K. *et al.* A tough nanofiber hydrogel incorporating ferritin. *Appl Phys Lett* 93, 163902 (2008).
- 311 Reza Nejadnik, M., Mikos, A. G., Jansen, J. A. & Leeuwenburgh, S. C. G. Facilitating the mineralization of oligo(poly(ethylene glycol) fumarate) hydrogel by incorporation of hydroxyapatite nanoparticles. *J Biomed Mater Res A*. 100, 1316-1323 (2012).
- 312 Ryon Shin, S. *et al.* Carbon nanotube reinforced hybrid microgels as scaffold materials for cell encapsulation. *ACS nano* 6, 362-372 (2012).
- 313 Saez-Martinez, V. *et al.* New hybrid system: Poly(ethylene glycol) hydrogel with covalently bonded pegylated nanotubes. *J Appl Polym Sci* 120, 124-132 (2011).
- 314 Kai, D. *et al.* Mechanical properties and in vitro behavior of nanofiber-hydrogel composites for tissue engineering applications. *Nanotechnology* 23, 95705 (2012).
- 315 Holloway, J. L., Lowman, A. M. & Palmese, G. R. Mechanical evaluation of poly(vinyl alcohol)-based fibrous composites as biomaterials for meniscal tissue replacement. *Acta biomaterialia* 6, 4716-4724 (2010).
- 316 Liao, I. C., Moutos, F. T., Estes, B. T., Zhao, X. & Guilak, F. Composite Three-Dimensional Woven Scaffolds with Interpenetrating Network Hydrogels to Create Functional Synthetic Articular Cartilage. *advanced functional materials* 23, 5833-5839 (2013).
- 317 Jang, J. *et al.* A cell-laden nanofiber/hydrogel composite structure with tough-soft mechanical property. *Appl Phys Lett* 102 (2013).
- 318 Caterson, E. J. *et al.* Three-dimensional cartilage formation by bone marrow-derived cells seeded in polylactide/alginate amalgam. *J Biomed Mater Res* 57, 394-403 (2001).
- 319 Wayne, J. S., McDowell, C. L., Shields, K. J. & Tuan, R. S. In vivo response of polylactic acid-alginate scaffolds and bone marrow-derived cells for cartilage tissue engineering. *Tissue Eng* 11, 953-963 (2005).
- 320 Ameer, G. A., Mahmood, T. A. & Langer, R. A biodegradable composite scaffold for cell transplantation. *J Orthop Res* 20, 16-19 (2002).
- 321 Kim, M. *et al.* Composite System of PLCL Scaffold and Heparin-Based Hydrogel for Regeneration of Partial-Thickness Cartilage Defects. *Biomacromolecules* 13, 2287-2298 (2012).

- 322 Bosworth, L. A., Turner, L. A. & Cartmell, S. H. State of the art composites comprising electrospun fibres coupled with hydrogels: a review. *Nanomedicine* 9, 322-335 (2013).
- 323 Kundu, J., Shim, J. H., Jang, J., Kim, S. W. & Cho, D. W. An additive manufacturing-based PCL-alginate-chondrocyte bioprinted scaffold for cartilage tissue engineering. *Journal of tissue engineering and regenerative medicine* (2013).
- 324 Dado, D. & Levenberg, S. Cell-scaffold mechanical interplay within engineered tissue. *Semin Cell Dev Biol* 20, 656-664 (2009).
- 325 Moutos, F. T. & Guilak, F. Composite scaffolds for cartilage tissue engineering. *Biorheology* 45, 501-512 (2008).
- 326 Seyednejad, H. *et al.* Synthesis and characterization of hydroxyl-functionalized caprolactone copolymers and their effect on adhesion, proliferation, and differentiation of human mesenchymal stem cells. *Biomacromolecules* 10, 3048-3054 (2009).
- 327 Seyednejad, H. *et al.* Preparation and characterization of a three-dimensional printed scaffold based on a functionalized polyester for bone tissue engineering applications. *Acta biomaterialia* 7, 1999-2006 (2011).
- 328 Seyednejad, H. *et al.* In vivo biocompatibility and biodegradation of 3D-printed porous scaffolds based on a hydroxyl-functionalized poly(epsilon-caprolactone). *Biomaterials* 33, 4309-4318 (2012).
- 329 Seyednejad, H. *et al.* Coaxially electrospun scaffolds based on hydroxyl-functionalized poly(epsilon-caprolactone) and loaded with VEGF for tissue engineering applications. *Biomacromolecules* 13, 3650-3660 (2012).
- 330 Seyednejad, H. *et al.* An electrospun degradable scaffold based on a novel hydrophilic polyester for tissue-engineering applications. *Macromol Bioscience* 11, 1684-1692 (2011).
- 331 Censi, R. *et al.* Photopolymerized Thermosensitive Poly(HPMA lactate)-PEG-Based Hydrogels: Effect of Network Design on Mechanical Properties, Degradation, and Release Behavior. *Biomacromolecules* 11, 2143-2151 (2010).
- 332 Vermonden, T. *et al.* Photopolymerized thermosensitive hydrogels: synthesis, degradation, and cytocompatibility. *Biomacromolecules* 9, 919-926 (2008).
- 333 Fedorovich, N. E. *et al.* The effect of photopolymerization on stem cells embedded in hydrogels. *Biomaterials* 30, 344-353 (2009).
- 334 Gawlitta, D., van Rijen, M. H. P., Schrijver, E. J. M., Alblas, J. & Dhert, W. J. A. Hypoxia Impedes Hypertrophic Chondrogenesis of Human Multipotent Stromal Cells. *Tissue Eng Part A* 18, 1957-1966 (2012).
- 335 Loontjens, C. A. M. *et al.* Synthesis and Characterization of Random and Triblock Copolymers of epsilon-Caprolactone and (Benzylated)hydroxymethyl glycolide. *Macromolecules* 40, 7208-7216 (2007).
- 336 Wu, C.-S. A comparison of the structure, thermal properties, and biodegradability of polycaprolactone/chitosan and acrylic acid grafted polycaprolactone/chitosan. *Polymer* 46, 147-155 (2005).
- 337 Kutzner, I. *et al.* Loading of the knee joint during activities of daily living measured in vivo in five subjects. *J Biomech* 43, 2164-2173 (2010).
- 338 Buckwalter, J. A. & Mankin, H. J. Instructional Course Lectures, The American Academy of Orthopaedic Surgeons-Articular Cartilage. Part I: Tissue Design and Chondrocyte-Matrix Interactions. *J Bone Jt Surg, Am Vol* 79-A, 600-614 (1997).
- 339 Samadi, N., van Nostrum, C. F., Vermonden, T., Amidi, M. & Hennink, W. E. Mechanistic studies on the degradation and protein release characteristics of poly(lactic-co-glycolic-co-hydroxymethylglycolic acid) nanospheres. *Biomacromolecules* 14, 1044-1053 (2013).
- 340 De Groot, C. J. *et al.* In vitro biocompatibility of biodegradable dextran-based hydrogels tested with human fibroblasts. *Biomaterials* 22, 1197-1203 (2001).

- 341 Cadée, J. A. *et al.* In vivo biocompatibility of dextran-based hydrogels. *J Biomed Mater Res* 50, 397-404 (2000).
- 342 Ben-David, D. *et al.* Low dose BMP-2 treatment for bone repair using a PEGylated fibrinogen hydrogel matrix. *Biomaterials* 34, 2902-2910 (2013).
- 343 Moutos, F. T., Freed, L. E. & Guilak, F. A biomimetic three-dimensional woven composite scaffold for functional tissue engineering of cartilage. *Nature materials* 6, 162-167 (2007).
- 344 Discher, D. E., Janmey, P. & Wang, Y. L. Tissue cells feel and respond to the stiffness of their substrate. *Science* 310, 1139-1143 (2005).
- 345 Kouwer, P. H. *et al.* Responsive biomimetic networks from polyisocyanopeptide hydrogels. *Nature* 493, 651-655 (2013).
- 346 Jeon, J. E. *et al.* Effect of preculture and loading on expression of matrix molecules, matrix metalloproteinases, and cytokines by expanded osteoarthritic chondrocytes. *Arthritis and rheumatism* 65, 2356-2367 (2013).
- 347 Nguyen, Q. T., Hwang, Y., Chen, A. C., Varghese, S. & Sah, R. L. Cartilage-like mechanical properties of poly (ethylene glycol)-diacrylate hydrogels. *Biomaterials* 33, 6682-6690 (2012).
- 348 Wan, L. Q. *et al.* Matrix deposition modulates the viscoelastic shear properties of hydrogel-based cartilage grafts. *Tissue engineering. Part A* 17, 1111-1122 (2011).
- 349 Maranchi, J. P., Trexler, M. M., Guo, Q. & Elisseff, J. Fibre-reinforced hydrogels with high optical transparency. *International Materials Reviews* 59, 264-296 (2014).
- 350 Yodmuang, S. *et al.* Silk microfiber-reinforced silk hydrogel composites for functional cartilage tissue repair. *Acta biomaterialia* 11, 27-36 (2015).
- 351 Moutos, F. T., Estes, B. T. & Guilak, F. Multifunctional hybrid three-dimensionally woven scaffolds for cartilage tissue engineering. *Macromolecular Bioscience* 10, 1355-1364 (2010).
- 352 Marijnissen, W. J. *et al.* Alginate as a chondrocyte-delivery substance in combination with a non-woven scaffold for cartilage tissue engineering. *Biomaterials* 23, 1511-1517 (2002).
- 353 Agrawal, A., Rahbar, N. & Calvert, P. D. Strong fiber-reinforced hydrogel. *Acta biomaterialia* 9, 5313-5318 (2013).
- 354 Cha, C. *et al.* Structural Reinforcement of Cell-Laden Hydrogels with Microfabricated Three Dimensional Scaffolds. *biomaterials science* 2, 703-709 (2014).
- 355 Malda, J. *et al.* Comparative study of depth-dependent characteristics of equine and human osteochondral tissue from the medial and lateral femoral condyles. *Osteoarthritis and cartilage / OARS, Osteoarthritis Research Society* 20, 1147-1151 (2012).
- 356 Mansour, J. M. & Welter, J. F. Multimodal evaluation of tissue-engineered cartilage. *J Med Biol Eng* 33, 1-16 (2013).
- 357 Pierce, D. M., Ricken, T. & Holzapfel, G. A. A hyperelastic biphasic fibre-reinforced model of articular cartilage considering distributed collagen fibre orientations: continuum basis, computational aspects and applications. *Computer Methods in Biomechanics and Biomedical Engineering* 16, 1344-1361 (2013).
- 358 Hosseini, S. M., Wilson, W., Ito, K. & van Donkelaar, C. C. How preconditioning affects the measurement of poro-viscoelastic mechanical properties in biological tissues. *Biomechanics and Modeling in Mechanobiology* 13, 503-513 (2014).
- 359 Hong, W., Zhao, X. H., Zhou, J. X. & Suo, Z. G. A theory of coupled diffusion and large deformation in polymeric gels. *Journal of the Mechanics and Physics of Solids* 56, 1779-1793 (2008).
- 360 Athanasiou, K. A., Agarwal, A. & Dzida, F. J. Comparative study of the intrinsic mechanical properties of the human acetabular and femoral head cartilage. *Journal of orthopaedic research : official publication of the Orthopaedic Research Society* 12, 340-349 (1994).

- 361 Jurvelin, J. S., Buschmann, M. D. & Hunziker, E. B. Optical and mechanical determination of Poisson's ratio of adult bovine humeral articular cartilage. *Journal of biomechanics* 30, 235-241 (1997).
- 362 Chen, A. C., Bae, W. C., Schinagl, R. M. & Sah, R. L. Depth- and strain-dependent mechanical and electromechanical properties of full-thickness bovine articular cartilage in confined compression. *Journal of biomechanics* 34, 1-12 (2001).
- 363 Moroni, L., de Wijn, J. R. & van Blitterswijk, C. A. 3D fiber-deposited scaffolds for tissue engineering: influence of pores geometry and architecture on dynamic mechanical properties. *Biomaterials* 27, 974-985 (2006).
- 364 Kwan, M. K., Lai, W. M. & Mow, V. C. Fundamentals of fluid transport through cartilage in compression. *Annals of biomedical engineering* 12, 537-558 (1984).
- 365 Grodzinsky, A. J., Levenston, M. E., Jin, M. & Frank, E. H. Cartilage tissue remodeling in response to mechanical forces. *Annual review of biomedical engineering* 2, 691-713 (2000).
- 366 Gefen, A. & Haberman, E. Viscoelastic properties of ovine adipose tissue covering the gluteus muscles. *Journal of biomechanical engineering* 129, 924-930 (2007).
- 367 Applied Solid Mechanics, Editor: Howell P. Cambridge University Press, UK. (2009).
- 368 Annabi, N. *et al.* 25th anniversary article: Rational design and applications of hydrogels in regenerative medicine. *Advanced materials* 26, 85-123 (2014).
- 369 Brittberg, M. Cell carriers as the next generation of cell therapy for cartilage repair: a review of the matrix-induced autologous chondrocyte implantation procedure. *The American journal of sports medicine* 38, 1259-1271 (2010).
- 370 Chu, C. R., Szczodry, M. & Bruno, S. Animal models for cartilage regeneration and repair. *Tissue engineering. Part B, Reviews* 16, 105-115 (2010).
- 371 Convery, F. R., Akesson, W. H. & Keown, G. H. The repair of large osteochondral defects. An experimental study in horses. *Clinical orthopaedics and related research* 82, 253-262 (1972).
- 372 Study to Evaluate the Safety and Performance of Treatment of Articular Cartilage Lesions Located on the Femoral Condyle With gelrinC. *ClinicalTrials.gov* NCT00989794.
- 373 Safety and Efficacy Study of HYTOP® in the Treatment of Focal Chondral Defects. *ClinicalTrials.gov* NCT01791062.
- 374 IMPACT: Safety and Feasibility of a Single-stage Procedure for Focal Cartilage Lesions of the Knee. *ClinicalTrials.gov* NCT02037204.
- 375 Sutter, M., Siepmann, J., Hennink, W. E. & Jiskoot, W. Recombinant gelatin hydrogels for the sustained release of proteins. *Journal of controlled release : official journal of the Controlled Release Society* 119, 301-312 (2007).
- 376 Poole, C. A. Articular cartilage chondrons: form, function and failure. *Journal of anatomy* 191 (Pt 1), 1-13 (1997).
- 377 Visser, J. *et al.* Endochondral bone formation in gelatin methacrylamide hydrogel with embedded cartilage-derived matrix particles. *Biomaterials* 37, 174-182 (2015).
- 378 Ortvad, K. F., Nixon, A. J., Mohammed, H. O. & Fortier, L. A. Treatment of subchondral cystic lesions of the medial femoral condyle of mature horses with growth factor enhanced chondrocyte grafts: a retrospective study of 49 cases. *Equine veterinary journal* 44, 606-613 (2012).
- 379 Ha, C. W., Noh, M. J., Choi, K. B. & Lee, K. H. Initial phase I safety of retrovirally transduced human chondrocytes expressing transforming growth factor-beta-1 in degenerative arthritis patients. *Cytotherapy* 14, 247-256 (2012).
- 380 Dhollander, A. A. *et al.* Midterm results of the treatment of cartilage defects in the knee using alginate beads containing human mature allogenic chondrocytes. *The American journal of sports medicine* 40, 75-82 (2012).

- 381 Wu, L., Prins, H. J., Helder, M. N., van Blitterswijk, C. A. & Karperien, M. Trophic effects of mesenchymal stem cells in chondrocyte co-cultures are independent of culture conditions and cell sources. *Tissue engineering. Part A* 18, 1542-1551 (2012).
- 382 Wu, L., Leijten, J., van Blitterswijk, C. A. & Karperien, M. Fibroblast growth factor-1 is a mesenchymal stromal cell-secreted factor stimulating proliferation of osteoarthritic chondrocytes in co-culture. *Stem cells and development* 22, 2356-2367 (2013).
- 383 Visser, J. *et al.* Crosslinkable Hydrogels Derived from Cartilage, Meniscus, and Tendon Tissue. *Tissue engineering. Part A* (2015).
- 384 De Santis, R. *et al.* A Basic Approach Toward the Development of Nanocomposite Magnetic Scaffolds for Advanced Bone Tissue Engineering. *Journal of Applied Polymer Science* 122, 3599-3605 (2011).
- 385 Serra, T., Planell, J. A. & Navarro, M. High-resolution PLA-based composite scaffolds via 3-D printing technology. *Acta biomaterialia* (2012).
- 386 Woodfield, T. B. *et al.* Design of porous scaffolds for cartilage tissue engineering using a three-dimensional fiber-deposition technique. *Biomaterials* 25, 4149-4161 (2004).
- 387 Probst, F. A., Hutmacher, D. W., Muller, D. F., Machens, H. G. & Schantz, J. T. [Calvarial reconstruction by customized bioactive implant]. *Handchirurgie, Mikrochirurgie, plastische Chirurgie : Organ der Deutschsprachigen Arbeitsgemeinschaft fur Handchirurgie : Organ der Deutschsprachigen Arbeitsgemeinschaft fur Mikrochirurgie der Peripheren Nerven und Gefasse : Organ der Vereinigung der Deutschen Plastischen Chirurgen* 42, 369-373 (2010).
- 388 Wang, X. H. *et al.* Generation of three-dimensional hepatocyte/gelatin structures with rapid prototyping system. *Tissue engineering* 12, 83-90 (2006).
- 389 Hamblin, M. N. *et al.* Capillary flow in sacrificially etched nanochannels. *Biomicrofluidics* 5, 21103 (2011).
- 390 Sachlos, E., Reis, N., Ainsley, C., Derby, B. & Czernuszka, J. T. Novel collagen scaffolds with pre-defined internal morphology made by solid freeform fabrication. *Biomaterials* 24, 1487-1497 (2003).
- 391 Hollister, S. J. Porous scaffold design for tissue engineering. *Nature materials* 4, 518-524 (2005).
- 392 Hwang, C. M. *et al.* Fabrication of three-dimensional porous cell-laden hydrogel for tissue engineering. *Biofabrication* 2, 035003 (2010).
- 393 Crump, S. S., Comb, J. W., Priedeman Jr, W. R. & Zinniel, R. L. Process of support removal for fused deposition modeling. *United States Patent 5503785* (1996).
- 394 Schantz, J. T. *et al.* Repair of calvarial defects with customized tissue-engineered bone grafts I. Evaluation of osteogenesis in a three-dimensional culture system. *Tissue engineering* 9 Suppl 1, S113-126 (2003).
- 395 Park, S. H., Kim, T. G., Kim, H. C., Yang, D. Y. & Park, T. G. Development of dual scale scaffolds via direct polymer melt deposition and electrospinning for applications in tissue regeneration. *Acta biomaterialia* 4, 1198-1207 (2008).
- 396 Guo, X. *et al.* Effects of TGF-beta3 and preculture period of osteogenic cells on the chondrogenic differentiation of rabbit marrow mesenchymal stem cells encapsulated in a bilayered hydrogel composite. *Acta biomaterialia* 6, 2920-2931 (2010).
- 397 Malda, J., Martens, D. E., Tramper, J., van Blitterswijk, C. A. & Riesle, J. Cartilage tissue engineering: controversy in the effect of oxygen. *Critical reviews in biotechnology* 23, 175-194 (2003).
- 398 Kitahara, S. *et al.* In vivo maturation of scaffold-free engineered articular cartilage on hydroxyapatite. *Tissue engineering. Part A* 14, 1905-1913 (2008).

- 399 Takei, T., Kishihara, N., Ijima, H. & Kawakami, K. Fabrication of capillary-like network in a matrix of water-soluble polymer using poly(methyl methacrylate) microfibers. *Artificial cells, blood substitutes, and immobilization biotechnology* 40, 66-69 (2012).
- 400 Rouwkema, J. *et al.* In vitro platforms for tissue engineering: implications for basic research and clinical translation. *Journal of tissue engineering and regenerative medicine* 5, e164-167 (2011).
- 401 Wang, C. *et al.* The control of anchorage-dependent cell behavior within a hydrogel/microcarrier system in an osteogenic model. *Biomaterials* 30, 2259-2269 (2009).
- 402 Zhu, Y. *et al.* Ex vivo expansion of adipose tissue-derived stem cells in spinner flasks. *Biotechnology journal* 4, 1198-1209 (2009).
- 403 Chang, J. *et al.* Optimization of culture of mesenchymal stem cells: a comparison of conventional plate and microcarrier cultures. *Cell proliferation* 45, 430-437 (2012).
- 404 Sart, S., Agathos, S. N. & Li, Y. Engineering stem cell fate with biochemical and biomechanical properties of microcarriers. *Biotechnology progress* 29, 1354-1366 (2013).
- 405 Urciuolo, F., Imparato, G., Palmiero, C., Trilli, A. & Netti, P. A. Effect of process conditions on the growth of three-dimensional dermal-equivalent tissue obtained by microtissue precursor assembly. *Tissue engineering. Part C, Methods* 17, 155-164 (2011).
- 406 Borg, D. J. *et al.* Functional and phenotypic characterization of human keratinocytes expanded in microcarrier culture. *Journal of biomedical materials research. Part A* 88, 184-194 (2009).
- 407 Stich, S. *et al.* Continuous cultivation of human hamstring tenocytes on microcarriers in a spinner flask bioreactor system. *Biotechnology progress* 30, 142-151 (2014).
- 408 Tseng, P. C. *et al.* Spontaneous osteogenesis of MSCs cultured on 3D microcarriers through alteration of cytoskeletal tension. *Biomaterials* 33, 556-564 (2012).
- 409 Bouffi, C. *et al.* The role of pharmacologically active microcarriers releasing TGF-beta3 in cartilage formation in vivo by mesenchymal stem cells. *Biomaterials* 31, 6485-6493 (2010).
- 410 Delcroix, G. J. *et al.* The therapeutic potential of human multipotent mesenchymal stromal cells combined with pharmacologically active microcarriers transplanted in hemi-parkinsonian rats. *Biomaterials* 32, 1560-1573 (2011).
- 411 Martin, Y., Eldardiri, M., Lawrence-Watt, D. J. & Sharpe, J. R. Microcarriers and their potential in tissue regeneration. *Tissue engineering. Part B, Reviews* 17, 71-80 (2011).
- 412 Zhang, Q. C. *et al.* Preparation of open porous polycaprolactone microspheres and their applications as effective cell carriers in hydrogel system. *Mat Sci Eng C-Mater* 32, 2589-2595 (2012).
- 413 Kim, B. S., Choi, J. S., Kim, J. D., Yeo, T. Y. & Cho, Y. W. Improvement of stem cell viability in hyaluronic acid hydrogels using dextran microspheres. *Journal of biomaterials science. Polymer edition* 21, 1701-1711 (2010).
- 414 Punet, X. *et al.* Enhanced cell-material interactions through the biofunctionalization of polymeric surfaces with engineered peptides. *Biomacromolecules* 14, 2690-2702 (2013).
- 415 Gonzalez-Vazquez, A., Planell, J. A. & Engel, E. Extracellular calcium and CaSR drive osteoinduction in mesenchymal stromal cells. *Acta biomaterialia* 10, 2824-2833 (2014).
- 416 Hwang, N. S., Varghese, S., Li, H. & Elisseeff, J. Regulation of osteogenic and chondrogenic differentiation of mesenchymal stem cells in PEG-ECM hydrogels. *Cell and tissue research* 344, 499-509 (2011).
- 417 Rowland, C. R., Lennon, D. P., Caplan, A. I. & Guilak, F. The effects of crosslinking of scaffolds engineered from cartilage ECM on the chondrogenic differentiation of MSCs. *Biomaterials* 34, 5802-5812 (2013).

- 418 Sart, S., Errachid, A., Schneider, Y. J. & Agathos, S. N. Modulation of mesenchymal stem cell actin organization on conventional microcarriers for proliferation and differentiation in stirred bioreactors. *Journal of tissue engineering and regenerative medicine* 7, 537-551 (2013).
- 419 Naito, H. *et al.* The effect of mesenchymal stem cell osteoblastic differentiation on the mechanical properties of engineered bone-like tissue. *Tissue engineering. Part A* 17, 2321-2329 (2011).
- 420 Marelli, B. *et al.* Accelerated mineralization of dense collagen-nano bioactive glass hybrid gels increases scaffold stiffness and regulates osteoblastic function. *Biomaterials* 32, 8915-8926 (2011).
- 421 Christenson, R. H. Biochemical markers of bone metabolism: an overview. *Clinical biochemistry* 30, 573-593 (1997).
- 422 Goh, T. K. *et al.* Microcarrier culture for efficient expansion and osteogenic differentiation of human fetal mesenchymal stem cells. *BioResearch open access* 2, 84-97 (2013).
- 423 Nakaoka, R., Hsiong, S. X. & Mooney, D. J. Regulation of chondrocyte differentiation level via co-culture with osteoblasts. *Tissue engineering* 12, 2425-2433 (2006).
- 424 Dahlin, R. L., Meretoja, V. V., Ni, M., Kasper, F. K. & Mikos, A. G. Chondrogenic phenotype of articular chondrocytes in monoculture and co-culture with mesenchymal stem cells in flow perfusion. *Tissue engineering. Part A* 20, 2883-2891 (2014).
- 425 Xu, L. *et al.* Mesenchymal stem cells downregulate articular chondrocyte differentiation in non-contact coculture systems: implications in cartilage tissue regeneration. *Stem cells and development* 22, 1657-1669 (2013).
- 426 Mo, X. T. *et al.* Variations in the ratios of co-cultured mesenchymal stem cells and chondrocytes regulate the expression of cartilaginous and osseous phenotype in alginate constructs. *Bone* 45, 42-51 (2009).
- 427 Poldervaart, M. T. *et al.* Sustained release of BMP-2 in bioprinted alginate for osteogenicity in mice and rats. *PLoS one* 8, e72610 (2013).
- 428 Mironov, V., Kasyanov, V., Drake, C. & Markwald, R. R. Organ printing: promises and challenges. *Regenerative medicine* 3, 93-103 (2008).
- 429 Rafiq, Q. A., Brosnan, K. M., Coopman, K., Nienow, A. W. & Hewitt, C. J. Culture of human mesenchymal stem cells on microcarriers in a 5 l stirred-tank bioreactor. *Biotechnology letters* 35, 1233-1245 (2013).
- 430 Kim, J. & Ma, T. Endogenous extracellular matrices enhance human mesenchymal stem cell aggregate formation and survival. *Biotechnology progress* 29, 441-451 (2013).
- 431 Chen, M. *et al.* A modular approach to the engineering of a centimeter-sized bone tissue construct with human amniotic mesenchymal stem cells-laden microcarriers. *Biomaterials* 32, 7532-7542 (2011).
- 432 Martin, I., Miot, S., Barbero, A., Jakob, M. & Wendt, D. Osteochondral tissue engineering. *Journal of biomechanics* 40, 750-765 (2007).
- 433 Nandakumar, A., Yang, L., Habibovic, P. & van Blitterswijk, C. Calcium Phosphate Coated Electrospun Fiber Matrices as Scaffolds for Bone Tissue Engineering. *Langmuir: the ACS journal of surfaces and colloids* 26, 7380-7387 (2010).
- 434 Luickx, N. *et al.* Optimization of the activation and nucleation steps in the precipitation of a calcium phosphate primer layer on electrospun poly(varepsilon-caprolactone). *Journal of biomedical materials research. Part A* (2014).
- 435 Visser, J. *et al.* Reinforcement of hydrogels using three-dimensionally printed microfibrils. *Nature Communications* 6, doi: 10.1038/ncomms7933 (2015).
- 436 Woodfield, T. B. *et al.* Rapid prototyping of anatomically shaped, tissue-engineered implants for restoring congruent articulating surfaces in small joints. *Cell proliferation* 42, 485-497 (2009).

- 437 Buckwalter, J. A. & Mankin, H. J. Articular cartilage: tissue design and chondrocyte-matrix interactions. *Instructional course lectures* 47, 477-486 (1998).
- 438 Wei, X., Gao, J. & Messner, K. Maturation-dependent repair of untreated osteochondral defects in the rabbit knee joint. *Journal of biomedical materials research* 34, 63-72 (1997).
- 439 Akmal, M. *et al.* The effects of hyaluronic acid on articular chondrocytes. *The Journal of bone and joint surgery. British volume* 87, 1143-1149 (2005).
- 440 Allemann, F. *et al.* Effects of hyaluronan on engineered articular cartilage extracellular matrix gene expression in 3-dimensional collagen scaffolds. *Journal of biomedical materials research* 55, 13-19 (2001).
- 441 Kawasaki, K., Ochi, M., Uchio, Y., Adachi, N. & Matsusaki, M. Hyaluronic acid enhances proliferation and chondroitin sulfate synthesis in cultured chondrocytes embedded in collagen gels. *Journal of cellular physiology* 179, 142-148 (1999).
- 442 Hendriks, J. A., Moroni, L., Riesle, J., de Wijn, J. R. & van Blitterswijk, C. A. The effect of scaffold-cell entrapment capacity and physico-chemical properties on cartilage regeneration. *Biomaterials* 34, 4259-4265 (2013).
- 443 Moroni, L., Hendriks, J. A., Schotel, R., de Wijn, J. R. & van Blitterswijk, C. A. Design of biphasic polymeric 3-dimensional fiber deposited scaffolds for cartilage tissue engineering applications. *Tissue engineering* 13, 361-371 (2007).
- 444 INSTRUCT for Repair of Knee Cartilage Defects. *ClinicalTrials.gov* NCT01041885.
- 445 Jeon, J. E., Schrobback, K., Hutmacher, D. W. & Klein, T. J. Dynamic compression improves biosynthesis of human zonal chondrocytes from osteoarthritis patients. *Osteoarthritis and cartilage / OARS, Osteoarthritis Research Society* 20, 906-915 (2012).
- 446 Ahearne, M. Introduction to cell-hydrogel mechanosensing. *Interface focus* 4, 20130038 (2014).
- 447 de Windt, T. *et al.* unraveling chondrocyte and MSC cocultures: direct cell-cell contact and chondroinduction are key mechanisms for cartilage regeneration. *Abstract no. 16.3.4 at the International Cartilage Repair Society conference, Chicago* (2015).
- 448 Saris, D. *et al.* Matrix-Applied Characterized Autologous Cultured Chondrocytes Versus Microfracture: Two-Year Follow-up of a Prospective Randomized Trial. *The American journal of sports medicine* 42, 1384-1394 (2014).
- 449 Lancaster, M. A. & Knoblich, J. A. Organogenesis in a dish: modeling development and disease using organoid technologies. *Science* 345, 1247-1255 (2014).
- 450 Sato, T. & Clevers, H. Growing self-organizing mini-guts from a single intestinal stem cell: mechanism and applications. *Science* 340, 1190-1194 (2013).
- 451 Jakab, K. *et al.* Tissue engineering by self-assembly and bio-printing of living cells. *Biofabrication* 2 (2010).
- 452 Jakab, K., Neagu, A., Mironov, V., Markwald, R. R. & Forgacs, G. Engineering biological structures of prescribed shape using self-assembling multicellular systems. *Proceedings of the National Academy of Sciences of the United States of America* 101, 2864-2869 (2004).
- 453 Schuurman, W. *et al.* Cartilage regeneration using zonal chondrocyte subpopulations: a promising approach or an overcomplicated strategy? *Journal of tissue engineering and regenerative medicine* (2012).
- 454 Karimi, T., Barati, D., Karaman, O., Moeinzadeh, S. & Jabbari, E. A developmentally inspired combined mechanical and biochemical signaling approach on zonal lineage commitment of mesenchymal stem cells in articular cartilage regeneration. *Integrative biology : quantitative biosciences from nano to macro* 7, 112-127 (2015).

- 455 Lam, J. *et al.* Osteochondral defect repair using bilayered hydrogels encapsulating both chondrogenically and osteogenically pre-differentiated mesenchymal stem cells in a rabbit model. *Osteoarthritis and cartilage / OARS, Osteoarthritis Research Society* 22, 1291-1300 (2014).
- 456 Otto, I. A. *et al.* Auricular reconstruction using biofabrication-based tissue engineering strategies. *Biofabrication (accepted pending minor revisions)*.
- 457 Gaetani, R. *et al.* Cardiac tissue engineering using tissue printing technology and human cardiac progenitor cells. *Biomaterials* 33, 1782-1790 (2012).
- 458 Struecker, B., Raschzok, N. & Sauer, I. M. Liver support strategies: cutting-edge technologies. *Nature reviews. Gastroenterology & hepatology* 11, 166-176 (2014).
- 459 Martin, I., Wendt, D. & Heberer, M. The role of bioreactors in tissue engineering. *Trends in biotechnology* 22, 80-86 (2004).
- 460 Mannoor, M. S. *et al.* 3D printed bionic ears. *Nano letters* 13, 2634-2639 (2013).
- 461 Niemansburg, S. L., van Delden, J. J., Oner, F. C., Dhert, W. J. & Bredenoord, A. L. Ethical implications of regenerative medicine in orthopedics: an empirical study with surgeons and scientists in the field. *The spine journal : official journal of the North American Spine Society* 14, 1029-1035 (2014).
- 462 Gilbert, F. Nano-Bionic Devices for the Purpose of Cognitive Enhancement: Toward a Preliminary Ethical Framework. *Trends in Augmentation of Human Performance* 1, 125-138 (2013).
- 463 Hollister, S. J. & Murphy, W. L. Scaffold translation: barriers between concept and clinic. *Tissue engineering. Part B, Reviews* 17, 459-474 (2011).
- 464 Hollister, S. J. Scaffold engineering: a bridge to where? *Biofabrication* 1, 012001 (2009).
- 465 Webber, M. J., Khan, O. F., Sydlik, S. A., Tang, B. C. & Langer, R. A perspective on the clinical translation of scaffolds for tissue engineering. *Annals of biomedical engineering* 43, 641-656 (2015).
- 466 Evans, C. H. Barriers to the clinical translation of orthopedic tissue engineering. *Tissue engineering. Part B, Reviews* 17, 437-441 (2011).
- 467 Bergsland, J., Elle, O. J. & Fosse, E. Barriers to medical device innovation. *Medical devices* 7, 205-209 (2014).
- 468 <http://www.materialise.com>.
- 469 Pearce, K. F. *et al.* Regulation of advanced therapy medicinal products in Europe and the role of academia. *Cytotherapy* 16, 289-297 (2014).
- 470 Abou-El-Enein, M. *et al.* Good Manufacturing Practices (GMP) manufacturing of advanced therapy medicinal products: a novel tailored model for optimizing performance and estimating costs. *Cytotherapy* 15, 362-383 (2013).
- 471 Regulation (EC) No. 1394/2007 of the European Parliament and of the Council of 13 November 2007 on advanced therapy medicinal products and amending Directive 2001/83/EC and Regulation (EC) No. 726/2004. . *Official Journal of the European Union*. 324, 121-131 (2007).
- 472 Sirova, M. *et al.* Immunocompatibility evaluation of hydrogel-coated polyimide implants for applications in regenerative medicine. *Journal of biomedical materials research. Part A* 102, 1982-1990 (2014).
- 473 Matsui, M. & Tabata, Y. Enhanced angiogenesis by multiple release of platelet-rich plasma contents and basic fibroblast growth factor from gelatin hydrogels. *Acta biomaterialia* 8, 1792-1801 (2012).
- 474 Magalhaes, P. O. *et al.* Methods of endotoxin removal from biological preparations: a review. *J Pharm Pharm Sci* 10, 388-404 (2007).
- 475 Ligon, S. C., Husar, B., Wutzel, H., Holman, R. & Liska, R. Strategies to reduce oxygen inhibition in photoinduced polymerization. *Chemical reviews* 114, 557-589 (2014).

- 476 Mazaki, T. *et al.* A novel, visible light-induced, rapidly cross-linkable gelatin scaffold for osteo-
chondral tissue engineering. *Scientific reports* 4, 4457 (2014).
- 477 Fairbanks, B. D., Schwartz, M. P., Bowman, C. N. & Anseth, K. S. Photoinitiated polymerization of
PEG-diacrylate with lithium phenyl-2,4,6-trimethylbenzoylphosphinate: polymerization rate and
cytocompatibility. *Biomaterials* 30, 6702-6707 (2009).
- 478 Temenoff, J. S. & Mikos, A. G. Review: tissue engineering for regeneration of articular cartilage.
Biomaterials 21, 431-440 (2000).
- 479 Chen, P. Y. *et al.* Fabrication of large perfusable macroporous cell-laden hydrogel scaffolds using
microbial transglutaminase. *Acta biomaterialia* 10, 912-920 (2014).
- 480 Cui, L., Jia, J., Guo, Y., Liu, Y. & Zhu, P. Preparation and characterization of IPN hydrogels composed
of chitosan and gelatin cross-linked by genipin. *Carbohydrate polymers* 99, 31-38 (2014).
- 481 Campbell, P. G. & Weiss, L. E. Tissue engineering with the aid of inkjet printers. *Expert Opin Biol Th*
7, 1123-1127 (2007).
- 482 The coming revolution in knee repair. *Scientific American* (2015).

List of Abbreviations

LIST OF ABBREVIATIONS

2D	Two-dimensional
3D	Three-dimensional
3DF	Three-dimensional fiber deposition
α -MEM	Minimal essential medium α
ACI	Autologous chondrocyte implantation
ALP	Alkaline phosphatase
AM	Additive manufacturing
ANOVA	Analysis of variance
APS	Ammonium persulphate
ATMP	Advanced therapy medicinal product
CAD	Computer-aided design
CAM	Computer-aided manufacturing
CartMA	Methacrylated cartilage matrix
CDM	Cartilage-derived matrix
Col	Collagen
CT	Computed tomography
DAPI	4',6-diamidino-2- phenylindole
DCM	Dichloromethane
DMA	Dynamic mechanical analyzer
DMAP	<i>N,N'</i> -dimethyl amino pyridine
DMEM	Dulbecco's modified eagle medium
DMSO	Dimethylsulphoxide
DN	Double network
DNA	Deoxyribonucleic acid
DSC	Differential scanning calorimetry
DSHB	Developmental studies hybridoma bank
ECM	Extracellular matrix
EDTA	Ethylenediaminetetraacetic acid
FBS	Fetal bovine serum
FDM	Fused deposition modeling
FGF	Fibroblast growth factor
GAGs	Glycosaminoglycans
GelMA	Gelatin methacrylamide
GG	Gellan gum
GMP	Good manufacturing practice
GPC	Gel permeation chromatography
H&E	Hematoxylin and Eosin
HA	Hyaluronic acid
HCl	Hydrochloric acid
HEPES	4-(2-hydroxyethyl)-1-piperazineethanesulfonic acid
Ig	Immunoglobulin
IHC	Immunohistochemistry
IPN	Interpenetrating polymer network

ITS-X	Insulin-transferrin-selenium-ethanolamine
LDH	Lactate dehydrogenase
MA	Methacrylate
MACI	Matrix-induced autologous chondrocyte implantation
MC	Microcarrier
MenMA	Methacrylated meniscus matrix
MEW	Melt electrospinning writing
MMA	Polymethylmethacryate
MMP	Matrix metalloproteinase
MNF	Mononuclear fraction
MRI	Magnetic resonance imaging
MSC	Mesenchymal stromal cell / multipotent stem cell
NaOH	Sodiumhydroxide
NMR	Nuclear Magnetic Resonance
NSAIDs	Nonsteroidal anti-inflammatory drugs
NZW	New zealand white
OCN	Osteocalcin
OCT	Optical coherence tomography
<i>P</i>	Statistical significance
pBMGCL	Poly(benzyloxymethylglycolide-co- ϵ -caprolactone)
PBS	Phosphate-buffered saline
PCL	poly(ϵ -caprolactone)
PCR	Polymerase chain reaction
pHMGL/PCL	Poly(hydroxymethylglycolide-co- ϵ -caprolactone)/poly(ϵ -caprolactone)
PLA	Poly(lactid acid)
pMHMGL/PCL	Poly(hydroxymethylglycolide-co- ϵ -caprolactone)/poly(ϵ -caprolactone) functionalized with methacrylate groups
RM	Regenerative medicine
RNA	Ribonucleic acid
SI	Supporting information
STL	Standard tessellation language
TCP	Tricalcium phosphate
TCPS	Culture on 2D tissue culture polystyrene surface s
TDM	Tissue derived matrix
TE	Tissue engineering
TEA	Triethylamine
TEMED	Tetramethylethylenediamide
TendMA	Methacrylated tendon matrix
TGF	Transforming growth factor
THF	Tetrahydrofuran
TRAP	Tartrate-resistant acid phosphatase
US	Ultrasound
UV	Ultraviolet

Summary and Answers to Research Questions

In this thesis, implants were biofabricated for the repair of chondral and osteochondral articular joint defects. The implants were based on gelatin methacrylamide (GelMA) hydrogels combined with printed fibers from polycaprolactone (PCL) for mechanical reinforcement. In Part I of this thesis, biological modifications of GelMA by the addition of matrix derived from cartilage, meniscus or tendon tissue did show a neutral or negative effect on cartilage matrix production by encapsulated MSCs and chondrocytes, respectively. Furthermore, MSCs in GelMA in a subcutaneous rat model could not be locked in their chondrogenic state, considering the evident process of endochondral bone formation in these constructs. Both the quantity and quality of bone formed by MSCs in GelMA are nonetheless encouraging for bone tissue engineers. In Part II, hydrogels were successfully reinforced with microfibers. These hydrogel/microfiber composites approached the stiffness and elasticity of articular cartilage and permitted the formation of cartilage matrix by embedded chondrocytes. In Part III, reinforced GelMA was applied for the biofabrication of larger, osteochondral constructs. Orthotopic animal models were established for evaluating the efficacy of reinforced GelMA for the repair of focal cartilage defects (in ponies) and for total joint replacement (in rabbits). The preparation of the biofabricated implants was described, as well as the implantation and preliminary outcomes of both animal models.

Engineering hydrogels for biofabrication

Hydrogels with low polymer content are beneficial for tissue formation by embedded cells. However, these gels are poor bioinks for the fabrication of three-dimensional (3D) structures with high mechanical integrity, because of their watery nature. Hydrogels with high polymer content have better shape-stability and stiffness and, hence, are better building blocks for biofabrication. Unfortunately, these gels limit the formation of an interconnected tissue by embedded cells. **Chapter 2** outlines *the current status of hydrogels as a bioink for biofabrication and the opportunities in this field*.

We highlighted how the biology vs. fabrication dilemma in the development of bioinks could be resolved by smart chemistry and engineering. Changing the polymer structure of bioinks, while retaining an open microporosity for tissue regeneration, could optimize its rheological properties for printing. One example is to combine polymers with different properties in one bioink, such as GelMA

Alternatively, the biofabrication process itself can be tailored to produce 3D constructs from 'watery' hydrogels. The hydrogel could be crosslinked more effectively and earlier in the biofabrication process, *e.g.* by cooling the collector platform, UV-crosslinking in the nozzle or with dual extrusion systems. Also, co-deposited sacrificial materials can temporarily support watery gels by printing with multiple materials (Chapter 8).

PART I) BIOLOGICAL IMPROVEMENT OF GELMA HYDROGEL WITH TISSUE-DERIVED MATRICES

Crosslinkable hydrogels derived from cartilage, meniscus and tendon tissue

Gelatin is a polymer derived from the porcine skin. The denatured collagen type I matrix contains a wide variety of adhesion sites and biochemical cues to embedded cells. The gelatin in the work presented in this thesis was methacrylated (into GelMA) in order to covalently crosslink the polymers. Chondrocytes embedded in GelMA gels were previously shown capable of forming a cartilage matrix within the gel *in vitro*. In **Chapter 3** we aimed to further improve the biological properties of the GelMA gel by the addition of tissue-derived matrices (TDM). The positive effect of several decellularized tissues on cell differentiation was yet demonstrated. Moreover, tissue-derived matrices served as a substrate for tissue engineering in clinical proof-of-concept studies. The following research questions were posed here: *Can stable hydrogels be derived from natural tissues, such as cartilage, meniscus and tendon? Does the addition of such tissue-derived matrices to GelMA hydrogel enhance chondrogenic differentiation of chondrocytes and MSCs in vitro?*

Cartilage, meniscus and tendon tissue were successfully decellularized, digested into a collagenous gels and functionalized with methacrylate groups. This process resulted in crosslinked tissue-derived hydrogels with a reasonable stiffness. Unfortunately, chondrocytes embedded in GelMA that was functionalized with these matrices performed worse than chondrocytes in GelMA alone. MSCs produced more matrix than chondrocytes, but there was no added value of the tissue-derived matrices.

Endochondral bone formation in gelatin methacrylamide hydrogel with embedded cartilage-derived matrix particles

In previous work, porous scaffolds from cartilage-derived matrix (CDM) were shown to be effective substrates for the deposition of cartilage matrix by seeded mesenchymal stem cells (MSCs) *in vitro*. On the contrary, chondrocytes did not form a cartilage matrix and eventually degraded the scaffold. The aim of **Chapter 4** was to study *what is the effect of cartilage-derived matrix particles in GelMA on the differentiation of chondrocytes and MSCs, and whether endochondral tissue can be regenerated in bilayered hydrogel constructs with chondrocytes and MSCs.*

CDM particles suspended in GelMA were found to have a negative effect on *in vitro* cartilage matrix formation by chondrocytes and a mildly positive effect of matrix formation by embedded MSCs. In a subcutaneous, immunocompromized rat model, chondrocytes produced a small amount of cartilage matrix, whereas MSCs formed an interconnected cartilage matrix. Moreover, MSCs hypertrophied and abundant endochondral bone was formed. The calcified area in the constructs was comparable to the mineral content in native bone (circa 40%), irrespective of the presence of CDM particles. In bilayered hy-

drogels with separate layers of chondrocytes and MSCs, cartilage was formed predominantly by MSCs, but no endochondral ossification occurred. As chondrocytes prevent MSCs from endochondral bone formation, the current approach is not appropriate for the regeneration of osteochondral tissue.

PART II) MECHANICAL IMPROVEMENT OF GELMA HYDROGEL CONSTRUCTS WITH 3D-PRINTED SCAFFOLDS

Covalent attachment of a three-dimensionally printed thermoplast to a gelatin hydrogel for mechanically enhanced cartilage constructs

Hydrogels are soft, due to the high water content. To withstand the challenging environment in articular joints, hydrogels have been reinforced with 3D-printed scaffolds from thermoplastic polymers, such as poly(ϵ -caprolactone) (PCL). Biofabrication techniques have been optimized to print PCL and the hydrogel in one session to create organized constructs with high stiffness. Nevertheless, both components of the constructs have a poor physical connection. Therefore, in **Chapter 5** it was investigated *whether the covalent attachment of a 3D-printed scaffold as reinforcement to GelMA gel leads to stronger constructs.*

It was demonstrated that GelMA hydrogel could be crosslinked to a thermoplastic polymer (poly(hydroxymethylglycolide-co- ϵ -caprolactone)/poly(ϵ -caprolactone) that was functionalized with methacrylate groups. Covalent grafting of both materials led to increased interface-binding strength. In addition, GelMA reinforced with a 3D-printed scaffold of the methacrylated polymer was stiffer and stronger than the gel reinforced with the non-methacrylated polymer. In these reinforced gels, Human chondrocytes produced cartilage matrix in the GelMA component *in vitro* and *in vivo*, subcutaneously in immunocompromized rats.

Reinforcement of hydrogels with three-dimensionally printed microfibres

Hydrogels have been reinforced through scaffolds fabricated with fused deposition modeling (FDM) (chapter 5) and with solution electrospun meshes. The FDM scaffolds are typically constructed from fibers with a thickness of circa 200 μm and provided a stiff reinforcement to the hydrogels. Nevertheless, these scaffolds have a relatively large polymer mass, are stiffer than articular cartilage, and have low elasticity. On the other hand, solution electrospun meshes consist of thin fibers, but fiber organization and relevant scaffold dimensions are hard to achieve with this technique. Melt electrospinning was therefore introduced as a 3D-printing technique to produce well-organized scaffolds from microfibers. In **Chapter 6**, the following questions were addressed: *could the mechanical properties of articular cartilage be approached with composite constructs*

consisting of a hydrogel reinforced with 3D-printed microfibers? How do chondrocytes embedded in these constructs respond to dynamic loading in an in vitro bioreactor culture?

Scaffolds with a fiber diameter of circa 20 μm and a high porosity (93-98%) were fabricated with melt electrospinning. The stiffness and elasticity of hydrogels reinforced with these microfiber scaffolds approached values of native articular cartilage, while both the hydrogel and the microfiber scaffold were soft. The soft microfiber scaffolds achieved this synergistic degree of reinforcement through confining the hydrogel upon axial compression and by stretching of the fibers, as was demonstrated with video imaging. Modeling affirmed that reinforcement with defined microfiber scaffolds is applicable to numerous hydrogels. Human chondrocytes embedded in reinforced GelMA responded positively to a dynamic loading regime in terms of chondrogenic differentiation; the reinforcing scaffold did not limit this process.

Cartilage repair with a co-culture of chondrons and MSCs in gelatin methacrylamide hydrogel: the establishment of an equine model

Cell therapies for the repair of focal cartilage defects currently rely on rapidly degrading cell carriers, such as fibrin glue. In contrast, hydrogels that have been specifically engineered for the use in regenerative medicine, have a lower degradation rate to balance with new tissue formation by embedded cells *within* the gel. GelMA has proven to support the formation of cartilage matrix by embedded chondrocytes *in vitro*. Chapter 4 demonstrated a slow degradation rate in immunocompromised rats, but also showed extensive endochondral bone formation when only MSCs were embedded. In order to translate reinforced GelMA to clinical applications, in **Chapter 7**, it was investigated *how (reinforced) GelMA hydrogel can be applied in an equine model for the repair of focal cartilage defects*. A co-culture of allogeneic chondrons and MSCs was used to prevent bone formation and to allow a one-step implantation procedure.

Reinforced GelMA gels were successfully UV-crosslinked into cartilage defects in the stifle joint of Shetland ponies. The constructs stayed in place after flexion-extension cycles of cadaveric stifles and after two weeks of implantation in a weight-bearing pony. The Shetland pony was found a feasible cartilage repair model, as these animals have a resilient nature and permit easier logistics compared to horses, while still approaching the cartilage thickness and biomechanics of humans. A long-term study to the regeneration of focal cartilage defects in Shetland ponies is ongoing, comparing (reinforced) GelMA to fibrin glue as a carrier of a mixture of allogeneic equine chondrons and MSCs. Baseline images of the implants were acquired with ultrasound and optical coherence tomography. All animals recovered well from surgery and showed normal gait within two weeks.

PART III) BIOFABRICATION OF COMPLEX SHAPED CONSTRUCTS FOR OSTEOCHONDRAL TISSUE REPAIR

Biofabrication of multi-material anatomically shaped tissue constructs

The work presented in this thesis so far addressed biological modifications of GelMA gels with tissue-derived matrices (part I) and the mechanical improvement of GelMA gels with 3D-printed scaffolds (part II). In Part III, we aimed to fabricate constructs for the repair of large osteochondral joint defects, or ultimately, for the biological restoration of partial or complete joints. In the introduction of this thesis, a few approaches were introduced for the biofabrication of constructs with relevant sizes and a well-defined internal and external architecture. One approach is modification of the bioink itself, as shown in Chapter 9; another is the implementation of a temporary support to overhanging structures in the printed construct. To this end, in **Chapter 8**, it was explored *which support and construction materials can best be combined to establish the complex geometry of anatomical structures in a multi-material 3D-printing setting*.

Specific support materials were designed for biofabrication with hydrogels and PCL. Prerequisites for support materials were found its printability, sufficient stiffness, it should not react with the construction material and the process of washing away the support material should be compatible with cell survival. Polyvinyl alcohol was found a suitable support material for the fabrication of PCL scaffolds, and a high concentration of alginate gel was a proper support material for creating GelMA/Gellan Gum hydrogel constructs. Printing of multiple materials in one session resulted in anatomically shaped constructs for the engineering of tissues with relevant sizes.

Biofabrication of tissue constructs by 3D bioprinting of cell-laden microcarriers

Microcarriers (MCs) are used in tissue engineering as an expansion vehicle for cells. MCs may form a solution for obtaining the high cell numbers that are usually required to create a functional new tissue. Cells are cultured and form matrix on the round surface of the MCs, in which biochemical substances could be incorporated for the controlled differentiation of these cells, *e.g.* for differentiation into the bone or cartilage lineages. In order to fabricate osteochondral grafts, in **Chapter 9** it was investigated whether *GelMA bioinks can be improved for bone regeneration by the incorporation of microcarriers*.

MSCs formed a calcified matrix in a GelMA/Gellan Gum bioink, when precultured on MCs under osteogenic conditions and incorporated in the ink. The bioink with MC/MS complex was printable and had a higher initial stiffness than the bioink without MCs. Hydrogel constructs with two components were printed with relevant sizes for osteochondral grafts. However, the regeneration of both bone and cartilage tissue in such a construct remains to be established.

3D-printed biodegradable shoulder replacement in a rabbit model: a pilot study on osteochondral tissue regeneration

The biological restoration of whole articular joints based on 3D-printed implants has previously been explored in proof-of concept studies in rabbit models. However, the regeneration of both bone and cartilage in these implants has not been established yet. The work in **Chapter 10** aimed to fabricate and implant the next generation of this 3D-printed osteochondral implant, with a distinct cartilage and bone component. In a pilot study in rabbits, it was investigated whether *both bone and cartilage tissue could be regenerated in a shoulder replacement model in rabbits with a single 3D-printed biodegradable implant*.

A porous, degradable shoulder replacement for rabbits was biofabricated from PCL, consisting of a bone and a cartilage component. The bone component had a porosity of 74% and was coated with calcium phosphate. The cartilage component consisted of GelMA reinforced with a melt electrospun PCL network with a porosity of 92%. The implant design was improved based on implantations in three cadaveric rabbits, resulting in strong implants, with the right anatomical dimensions. The content of the cartilage component varied in three experimental groups: 1) with allogeneic chondrocytes; 2) with Transforming Growth Factor β , and 3) cell-free. The model is currently tested in a pilot study in three rabbits (each group $n=1$). When the fixation and preliminary tissue formation suffice, a study to bone and cartilage formation will commence with $n=6$ per group with a follow-up of 20 weeks.

Altogether, the work in this thesis resulted in implants for articular joint regeneration, consisting of gelatin-based hydrogels that were reinforced with 3D-printed fibers. The shape and content of the implants could be tailored with biofabrication techniques, based on 3D-scans of the joint defect. Animal models were initiated to evaluate the repair capacities of the implants for a focal cartilage defect and for a complete joint. With tissue regeneration in reinforced hydrogels, larger articular joint defects in patients can potentially be repaired on a biological level.

Nederlandse Samenvatting

NEDERLANDSE SAMENVATTING

Het werk in dit proefschrift laat zien hoe stevige en biologisch actieve implantaten worden gemaakt en toegepast voor het herstel van defecten in een gewricht. Deze defecten komen meestal voor bij jonge mensen als gevolg van een groeistoornis of door een trauma. Momenteel kunnen kleine kraakbeendefecten al worden gerepareerd middels celtherapie. Omvangrijke schade in het gewricht wordt nu nog vervangen door een prothese van kunststof of metaal. In dit proefschrift is een stevige, nieuwe dragerstructuur voor de celtherapie ontwikkeld, zodat ook grotere defecten op een biologisch niveau kunnen worden hersteld. De implantaten worden op maat gemaakt met een 3D-printer en zijn gebaseerd op een gecrosslinkte gelatine hydrogel (GelMA), welke is versterkt met vezels van een afbreekbaar plastic (polycaprolactone (PCL)). Omdat ook cellen en/of groeifactoren kunnen worden geprint in het implantaat wordt het proces *biofabrication* genoemd.

Het eerste deel van het proefschrift beschrijft hoe de GelMA gel biologisch is aangepast door de toevoeging van extracellulaire matrices verkregen van kraakbeen-, meniscus-, en peesweefsel. Deze toevoeging blijkt een neutraal effect te hebben op volwassen stamcellen (MSCs) in de GelMA en een negatief effect op matrix productie van kraakbeencellen. Tevens zien we dat er bot werd gevormd in een implantaat van GelMA met MSCs, wanneer deze onder de huid was geïmplantéerd in ratten. Dit bot wordt gevormd via de endochondrale route, waarbij mineralisatie van een kraakbeenmatrix plaatsvindt, zoals ook gebeurt bij de groei van lange pijpbeenderen. De graad van mineralisatie is vergelijkbaar met natuurlijk botweefsel en hiertussen zijn gebieden lijkend op beenmerg aanwezig. Dit is een veelbelovende bevinding voor het regenereren van bot, echter, wanneer MSCs gebruikt worden voor kraakbeenherstel in GelMA hydrogelen hebben deze dus een andere chondrogene stimulatie nodig dan die van de huidige extracellulaire matrices, om botvorming te voorkomen.

In het tweede deel laten we zien dat GelMA gel sterker en stijver wordt wanneer deze gecombineerd wordt met een netwerk van 3D-geprinte vezels van PCL. Een chemische binding van deze vezels aan de hydrogel leidt tot sterkere constructen, bovendien lijkt de stijfheid en elasticiteit van hydrogelen versterkt met microvezels (ca. 20 μm) op die van kraakbeen uit de knie. Kraakbeencellen in deze constructen produceren een kraakbeenspecifieke matrix zowel *in vitro* als onder de huid in ratten. Deze versterkte GelMA is vervolgens geïmplantéerd in kraakbeendefecten in de knieën van acht Shetland pony's om de regeneratie van kraakbeen te bestuderen in een relevante omgeving. Pony's vormen een goed model voor de mens gezien de dikte van het kraakbeen en de belasting van de gewrichten. Een mix van chondronen (kraakbeencellen met hun pericellulaire matrix intact) en MSCs is geïmplantéerd in GelMA, in vezelversterkte GelMA en in fibrinelijm (de klinische standaard). Het proces van de groei van nieuw kraakbeen in

de defecten wordt momenteel een jaar lang gevolgd met verscheidene beeldvormende technieken, waaronder kijkoperaties.

In het derde deel van het proefschrift gebruiken we verschillende *biofabrication* technieken om grotere implantaten te maken met anatomische vormen. Controle over architectuur van het implantaat is namelijk nodig om een groter defect van het gewricht te repareren, dat vaak een unieke vorm heeft en zowel kraakbeen als botweefsel betreft. Na aanpassing van de reologische eigenschappen van GelMA hydrogel met een verdikker (Gellan Gum), konden grote en gelaagde constructen worden geprint. Overhangende delen in anatomische gevormde structuren werden tijdelijk ondersteund door een ander printbaar materiaal, die vervolgens kon worden weggewassen in een celvriendelijke procedure. Microcarriers werden gebruikt in de 'botlaag' van deze constructen om grote hoeveelheden MSCs te kunnen expanderen en om hun osteogene differentiatie te stimuleren. Het meest veelbelovende en haalbare construct is doorontwikkeld voor de vervanging van de gehele schouderkop in konijnen. Het implantaat werd ontworpen en geprint op basis van een CT-scan van de schouderkop met daarin een bot- en kraakbeencomponent. De botcomponent bestaat uit dikke PCL filamenten gecoat met hydroxyapatiet en de kraakbeencomponent bestaat uit GelMA versterkt met PCL microvezels en daarin kraakbeencellen of een groeifactor. Een pilot studie naar de stevigheid en fixatie van het implantaat is gaande in drie konijnen.

Het werk in dit proefschrift heeft dus geleid tot sterkere en biologisch actieve implantaten voor het herstel van schade aan gewrichten. Door *biofabrication* technieken kan de inhoud en vorm van het implantaat worden afgestemd op de patiënt. Met deze benadering kunnen mogelijk grotere delen van het gewricht van patiënten op een biologisch niveau worden hersteld.

**Papers not included
in this thesis**

Acknowledgements/Dankwoord

Curriculum Vitae

PAPERS NOT INCLUDED IN THIS THESIS

Gawlitta D, Benders KE, Visser J, van der Sar AS, Kempen DH, Theyse LF, Malda J, Dhert WJA. Decellularized Cartilage-Derived Matrix as Substrate for Endochondral Bone Regeneration.

Tissue Eng Part A. 2015 Feb;21(3-4):694-703.

de Windt TS, Vonk LA, Buskermolen JK, Visser J, Karperien M, Bleys RL, Dhert WJ, Saris DB. Arthroscopic airbrush assisted cell implantation for cartilage repair in the knee: a controlled laboratory and human cadaveric study.

Osteoarthritis Cartilage. 2015 Jan;23(1):143-50.

Visser J, Verra WC, Kuijlen JM, Horsting PP, Journée HL. Recovery of TES-MEPs during surgical decompression of the spine: a case series of eight patients.

Journal of Clinical Neurophysiology. 2014 Dec;31(6):568-74.

Hellegering J, Visser J, Kloke HJ, D'Ancona FCH, Hoitsma AJ, van der Vliet JA, Warlé MC. Poor early graft function impairs long-term outcome in living donor kidney transplantation.

World Journal of Urology. 2013 Aug;31(4):901-6.

Visser J, Brinkman JM, Bleys RL, Castelein RM, van Heerwaarden RJ. The safety and feasibility of a less invasive distal femur closing wedge osteotomy technique: a cadaveric dissection study of the medial aspect of the distal femur.

Knee Surgery, Sports Traumatology, Arthroscopy. 2013 Jan;21(1):220-7.

Visser J, Busch VJJF, de Kievit- van der Heijden I, ten Ham AM. Non-Hodgkin's Lymphoma of the synovium discovered in total knee arthroplasty: a case report.

BMC Research Notes. 2012 Aug 20;5:449.

Hellegering J, Visser J, Kloke HJ, D'Ancona FCH, Hoitsma AJ, van der Vliet JA, Warlé MC. Influence of prolonged warm ischemia in living donor kidney transplantation.

Transplantation Proceedings 2012 Jun;44(5):1222-6.

Visser J, Tienen van TG, Hoogeveen AR, Diercks RL. Het compartimentsyndroom van de diepe achterste loge van het onderbeen: diagnostische en therapeutische problemen.

Sport en Geneeskunde 2010 Oct;43(4):28-33

Parastatidis I, Thomson L, Burke A, Chernysh I, Nagaswami C, Visser J, Stamer S, Liebler DC, Koliakos G, Heijnen HF, Fitzgerald GA, Weisel JW, Ischiropoulos H. Fibrinogen beta-chain tyrosine nitration is a prothrombotic risk factor.

The Journal of Biological Chemistry. 2008 Dec 5;283(49):33846-53.

Mouser VHM, Melchels FP, Visser J, Gawlitta D, Dhert WJA, Malda J. Tailoring a gelatin methacrylamide and gellan hydrogel for cartilage biofabrication.

In preparation

Zhao X, Erali R, Otto IA, Visser J, Melchels FP, Saris DBF, Malda J, Randolph MA. Cartilage regeneration using different chondrocyte sources and photochemically crosslinked gelatin-methacrylamide (GelMA) hydrogel.

In preparation

Boere KWM, van den Dikkenberg J, Gao Y, Visser J, Hennink WE, Vermonden T. Thermogelling and chemoselectively cross-linked hydrogels with controlled mechanical properties and degradation behavior.

In preparation

ACKNOWLEDGEMENTS/DANKWOORD

Promotor en copromotoren

Geachte prof. dr. Dhert, beste Wouter,

Vier jaar geleden diende ik me per email aan voor een promotieplek. Wat ben ik blij dat ik langs mocht komen en dat je het vertrouwen in me had na dit gesprek. Ik heb ook onze latere gesprekken - veelal op borrels – erg gewaardeerd. We zaten op een lijn over de toekomst van biofabrication, een lijn die we voor verscheidene gezelschappen hebben gepresenteerd. Hoe ongemakkelijk voelde ik me op jouw kamer een dag voor zo'n presentatie, toen mijn verklaring van goed gedrag niet op orde leek te zijn, juist toen er een lid van het koninklijk huis langs zou komen. Het werd een unieke 1 april grap die je erg sportief hebt opgevat! Veel plezier en succes als decaan.

Geachte dr. ir. Malda, beste Jos,

Mede door jouw enthousiasme en harde werken is biofabrication in Utrecht als een speer gegaan de afgelopen jaren. Het was fijn en vanzelfsprekend om als PhD student mee te gaan in deze flow; ik betwijfel of ik ooit nog zoveel mediaoptredens zal hebben. Ik heb geleerd van je vermogen om de juiste mensen bij elkaar te brengen, zowel binnen de afdeling als internationaal. Bedankt dat je me mee nam naar Australië met Annelie en de kinderen. Ik zal de Aussie koffies, BBQs en hikes niet snel vergeten.

Geachte dr. ir. Gawlitta, beste Debby,

Je was de side-kick vanuit de kaakchirurgie bij wie ik altijd terecht kon voor een praktische vraag. Ik heb geleerd van je geduld om studenten te begeleiden. Het zou erg gaaf zijn als het je lukt om iets van het huidige werk klinisch toe te passen.

Collegae

Geachte dr. ir. Melchels, beste Ferry,

Toen ik in Brisbane aan kwam was jij al een halve Aussie. Terug in Nederland heb je die vibe niet meer verloren en je hunkerde nog wel eens terug. Ik hoop dat jij en de dames in Schotland een vergelijkbaar avontuur tegemoet gaan. Zonder jouw logica en kennis over polymeren en engineering was dit proefschrift zeker van mindere kwaliteit geweest. Doordat je deze kennis met geduld over kan brengen was je een consultant voor vele PhD studenten; de afdeling gaat dit missen!

Geachte prof. dr. Saris, beste Daan,

Bedankt dat ik altijd mijn werk kon toetsen aan je scherpe klinische blik. Ik heb bewondering voor je pragmatisme en je strakke, translationele onderzoekslijn.

Geachte prof. dr. van Weeren, beste René,
 Bedankt voor het kritisch nakijken van mijn stukken, inclusief de algemene discussie.
 Deze stroomlijning is zeker terug te zien in dit proefschrift!

Dear prof. dr. Hutmacher, dear Dietmar,
 Thanks for having me in Australia and for your great hospitality to dine at your place not
 only once.

Loek, zonder jou aan mijn rechterzijde was Q zoveel saaier geweest. Het filosoferen over
 het leven, de wereld en changing the face of science zal ik missen. Onze gedeelde passie
 voor de natuur en bergen bracht ons zelfs in Nepal en we komen elkaar in de toekomst
 zeker nog tegen.

Dino, man van de Tiramisu & Radler, wat was het mooi wonen op de Jeremiestraat.

Mattie, bedankt dat je me op weg hebt geholpen in en rondom het lab, voor de koffie
 en de borrels.

Willemijn, bedankt voor alle achterklap als moeder van de afdeling en voor je hulp aan
 vele willekeurige aspecten van dit proefschrift.

Orthopedie: Tom, Beeki (we staan gelijk op de Mt. Ventoux), Anika & Kim, Rhandy, Croes,
 Maaïke, Anita, Vivian, Maarten, Behdad, Parisa, Imke, Razmara, Maurits, Anne, Huub (be-
 dankt voor de stoelen op de middenlijn van de Kuip), Riccardo, Marianne, Said, Barbara,
 Michelle, Lucienne, Joris, Schuurman, Fiona, Hsiao-Yin, Saskia, Mechteld, Linda, Angela,
 Yvonne, Kim, dank voor een prachtige tijd in Utrecht!

Diergeneeskunde: Harold, Irina, Janneke, Filipe, Nikae, Stefan, Annemiek, Jannie, Thijs,
 professor van Barneveld, Pia, Juha, Jaimy, Bert, Peter, Henk, Henk en het hele equine
 cartilage repair team, bedankt voor de soepele samenwerking!

Farmacie: Kristel, fijn dat we gelijk zijn opgestart, bedankt voor je trouwe hulp, onder de
 gepassioneerde begeleiding van Tina, Mies, Sima en professor Hennink.

Australia: Patrina, Mohid, Tomasz, Marco, Urip, Paul (I really appreciated our talks and
 dinners all over the world), Travis, Pete (great person for an exchange and I am honoured
 to be your paranimf) & Libby, thanks for the introduction in Brisbane and its surround-
 ings – including New Zealand.

Studenten: Ben, Erik, Jeremy, Selynda, Twan, Karin, Marco, Trudy, Bram, Lydia, Ali, Britta en Elder, jullie zijn een belangrijk fundament onder dit proefschrift, dank!

Anderen: professor Öner, Jelle Boomstra, Laura Creemers, Jacqueline Alblas, bedankt voor jullie input.

Martijn Brinkman, Ronald van Heerwaarden en professor Castelein, bedankt dat jullie mijn kruiwagen waren middels de femur osteotomie studie, die mij naar Utrecht bracht.

Paranimfen

Bram, vaste maat vanaf het begin in Groningen, fijn dat ik aan je zijde mocht staan bij jouw verdediging in Amsterdam, ik heb alle vertrouwen in je wederdienst in Utrecht.

Tommy, ik ben blij dat wij al snel elkaars respect en vriendschap vonden. Bedankt voor het sparren over de inhoud van ons werk en je gezelschap op vele congressen.

Vrienden en familie

Thijs, veel bergtoppen hebben we al gezien, veel kilometers gefietst, beiden uit de klei getrokken, bedankt dat ik altijd op je vriendschap kan rekenen.

Dre, een vriend vanaf de eerste zeildag en tot de laatste. Iedereen van de P.J., met name ook de Jonge Honden, Helly, de Goeroe en Paul, bedankt voor 18 onvergetelijke zomers op het water.

Mannen van de Whiskey en K.V. Rumpite atque Vomate, onze activiteiten zijn belangrijk en zullen blijven.

Jongens uit Dronten, fijn dat we nog steeds vrienden van het eerste uur zijn.

Lieve Frans en Gerda, bedankt voor de vaste uitvalsbasis aan de Perzikgaarde, waar het eten altijd goed smaakt en altijd een logeerplek is. FW, daar samen naar 'de Belg' kijken is erg inspirerend.

Lieve Sietske, jouw werk is eigenlijk veel belangrijker dan wat ik de afgelopen vier jaar heb gedaan. Fijn om al 28 jaar getuige te zijn van jouw eigen wil, je nuchterheid, praktisch inzicht en avonturisme.

Lieve papa en mama, klassieke piano op zondag, spreuken op het toilet, eten aan de ronde tafel, rode wijn uit Frankrijk, toch beide benen aan de grond, tussen de Friese meren en altijd interesse. Bedankt voor dit veilige nest, om altijd naar terug te keren.

Elisa, gelukkig is onze liefde is veel sterker dan twee proefschriften. Tegelijk een promotietraject was een fantastische tijd met veel vrijheid. Je leerde me box-plotjes, keek stukken na, zocht me op waar ik ook was, begreep de missie. Na zeven jaar op afstand nu eindelijk samen, van mij mag dat voor altijd duren.

CURRICULUM VITAE



Jetze Visser was born in Gaasterland, the Netherlands, on the 6th of January 1985. He graduated from high school (Gymnasium, Ichthus College, Kampen) in 2003 and did his medical studies at the University of Groningen. During his study, he participated in a research project on the fundamentals of blood coagulation at the University of Pennsylvania (Philadelphia, USA) and he did his clinical rotations at the UMC Groningen, Isala Klinieken (Zwolle), Same District Hospital (Same, Tanzania) and the Radboudumc. After graduating in 2010 he worked as a non-training resident in orthopaedics at the Sint Maartenskliniek in Nijmegen. In 2011 he started as a PhD candidate on the subject of biofabrication for cartilage regeneration at the UMC Utrecht, the department of orthopaedics, under supervision of prof. dr. W.J.A. Dhert, dr. ir. J. Malda and dr. ir. D. Gawlitta. He performed part of the work of this thesis at the Queensland University of Technology (Brisbane, Australia) under supervision of prof. dr. D.W. Hutmacher. In July 2015 he started his clinical training at the department of general surgery at the Rijnstate ziekenhuis in Arnhem, after which he will continue in orthopaedic surgery at the Radboudumc and Sint Maartenskliniek in Nijmegen, and the Rijnstate ziekenhuis. Jetze currently lives in Arnhem together with Elisa Hamer.

